

NORTHWESTERN UNIVERSITY

Investigating Basalt Chemical Weathering in Iceland and its Role in Climate Regulation with  
Stable Calcium Isotopes

A DISSERTATION

SUBMITTED TO THE GRADUATE SCHOOL IN PARTIAL FULFILLMENT OF THE  
REQUIREMENTS

for the degree

DOCTOR OF PHILOSOPHY

Field of Earth and Planetary Sciences

By Claire Juliet Nelson

EVANSTON, ILLINOIS

December 2021

© Copyright by Claire Juliet Nelson 2021

All Rights Reserved

## Abstract

This dissertation investigates processes controlling the Ca isotope geochemistry ( $\delta^{44/40}\text{Ca}$ ) of Icelandic samples, from an atomic to island-wide scale. These studies embody the range of applications for which the Ca isotope proxy can apply in surficial environments, and I offer novel  $\delta^{44/40}\text{Ca}$  data for Icelandic rivers, rocks, minerals, soil, and vegetation. By characterizing the  $\delta^{44/40}\text{Ca}$  values of mineralogical end members (Chapter 2) and identifying mechanisms that control the transport, distribution, and fate of Ca isotopes (Chapter 3), I use Ca isotopes of Icelandic rivers to evaluate the chemistry of basalt-draining rivers, which has previously been taken to reflect rapid basalt weathering rates and disproportionate atmospheric  $\text{CO}_2$  drawdown (Chapter 4). The studies combined provide key new insights into processes that control Ca isotope cycling, thereby advancing the tracer and broadening its potential applications.

Only one study has reported Ca isotope compositions of zeolite minerals, and this dissertation is the first to specifically investigate controls on the Ca isotope geochemistry of the minerals. Icelandic zeolites show a  $\delta^{44/40}\text{Ca}$  range of 1.4‰, which is on the order of the range observed for all igneous rocks thus far measured. Zeolite  $\delta^{44/40}\text{Ca}$  values strongly correlate with average mineral Ca-O bond lengths, which appears most consistent with equilibrium isotope partitioning. Equilibrium controlled fractionation of Ca isotopes by zeolites elevates the  $\delta^{44/40}\text{Ca}$  of coexisting groundwaters, from which calcite then precipitates at or near equilibrium. This study reports novel Ca isotope data for zeolites and offers a new perspective on the mechanisms controlling Ca isotope fractionation during mineral precipitation in general, which has implications for the carbonate  $\delta^{44/40}\text{Ca}$  paleoclimate proxy. The results also have significance for using Ca isotopes to trace basalt weathering and its role in long-term climate regulation, as zeolites pervasively form in basaltic settings.

Through a high-resolution field study of the Skagafjörður region in North Iceland, I characterize key reservoirs hypothesized to control the Ca isotope composition of surface and groundwaters including vegetation, soil, clays, and colloidal and suspended particulates. While these reservoirs display some  $\delta^{44/40}\text{Ca}$  variability, the primary control on river  $\delta^{44/40}\text{Ca}$  appears to be mixing with isotopically heavy Ca sourced from groundwater and calcite weathering. Groundwaters show trends between  $\delta^{44/40}\text{Ca}$  and pH, temperature, distance from the coast, and Sr/Ca ratios, indicating that geochemical evolution controls groundwater  $\delta^{44/40}\text{Ca}$  values due to fractionation by zeolites. Only direct-runoff tributaries draining minimally altered, crystalline basalt show Ca isotope ratios indicative of basalt weathering by atmospheric  $\text{CO}_2$ , and solute fluxes in these rivers are much lower than those employed in previous attempts to estimate basalt weathering rates.

Finally, I studied the Ca isotope geochemistry of rivers draining the Icelandic highlands to investigate the relative mineral stability hypothesis, which predicts that mafic minerals should weather faster than felsic minerals at the Earth's surface. In the highlands, subglacial basaltic eruptions generate breccias bearing crystalline clasts and highly reactive basaltic glass. The highlands also support vigorous hydrothermal activity that results in the precipitation of secondary minerals, including calcite. Glacial highland rivers display the highest  $\delta^{44/40}\text{Ca}$  values of all rivers measured in Iceland, clearly indicating that basalt weathering by atmospheric  $\text{CO}_2$  does not control riverine solute fluxes. High solute fluxes in basalt-draining rivers globally have been interpreted as evidence for rapid basalt weathering, and for decades, Earth scientists have hypothesized that basalt weathering disproportionately consumes atmospheric  $\text{CO}_2$ . Results from this study challenge the underlying assumptions regarding the role of basalt weathering on long-

term climate regulation and indicate that solute fluxes used to assess basalt weathering rates have likely resulted in significant overestimates.

## Acknowledgements

There are so many people whose effort, support, and presence have made this work possible. My parents, Jim and Lorraine, and my sister Monica have supported me so endlessly such that I am tempted to put their names on the title page. They are my coaches, teammates, and biggest fans all in one. I am incredibly grateful for them. Not many people's moms would volunteer to be their field assistant and trek around Iceland carrying rocks and water. I also thank all of my friends, you all have been there to celebrate with me, commiserate with me, and all around ride the PhD rollercoaster by my side. Thank you.

I never would have thought it possible to switch my major to Geology as a senior if it weren't for my undergraduate advisor, Dr. John Garver, who believed in me, inspired me, and sparked my passion for Earth science. I also would like to thank Dr. Holli Frey, who introduced me to Andy, as well as the rest of the Geology Department at Union College, I would not be where I am without any of you.

Thank you to all EPS department members, especially the staff who made my field trips possible, as well as my first field assistant, Grace Schellinger. Thank you to the Jacobson Lab Group members, past and present. Thank you to Dr. Matt Hurtgen and Dr. Brad Sageman, my committee members, who have supported and inspired me throughout this whole adventure. I deeply appreciate you all.

And finally, to Dr. Andrew Jacobson. Andy, you are a brilliant scientist who taught me so much more than I could ever put onto paper, and for that I give a resounding thank you. You gave me the incredible gift that was this experience, and handed me the most amazing project that I could possibly imagine. Thank you for sharing your immeasurable knowledge and expertise with me. I am profoundly grateful to call you my advisor, mentor, and friend.

## **Dedication**

For Iceland

we will never truly understand your beauty, immensity, and mystery.

## Table of Contents

Abstract.....	3
Acknowledgements.....	6
Dedication.....	7
List of Tables.....	11
List of Figures.....	13
Chapter 1. Introduction and Overview.....	15
1.1 Introduction.....	15
1.2 Chapter 2: Large calcium isotope fractionations by zeolite minerals from Iceland.....	20
1.3 Chapter 3: Controls on riverine calcium isotope ratios during basalt weathering in the Skagafjörður watershed, Iceland.....	22
1.4 Chapter 4: Basalt weathering in the Icelandic highlands: reassessing the role of basalt weathering on long term climate regulation with Ca isotope geochemistry.....	24
Chapter 2. Large calcium isotope fractionations by zeolite minerals from Iceland. ....	26
2.1 Introduction.....	26
2.2 Geologic Setting.....	32
2.3 Methods.....	33
2.4 Results.....	37
2.5 Discussion.....	40
2.6 Conclusions.....	58
Chapter 3. Controls on riverine calcium isotope ratios during basalt weathering in the Skagafjörður watershed, Iceland .....	60

	9
3.1 Introduction.....	60
3.2 Geologic and Climatic Setting.....	62
3.3 Methods.....	66
3.4 Results.....	71
3.5 Discussion.....	84
3.6 Conclusions.....	103
 Chapter 4. Basalt weathering in the Icelandic highlands: reassessing the role of basalt weathering on long term climate regulation with Ca isotope geochemistry.....	105
4.1 Introduction.....	105
4.2 Geologic and Climatic Setting.....	107
4.3 Methods.....	109
4.4 Results.....	114
4.5 Discussion.....	120
4.5 Conclusions.....	133
 Chapter 5: Conclusions.....	135
References.....	137
Appendix A. Zeolite statistical analyses and experiments.....	163
A.1 Zeolite statistical analyses .....	163
A.2 Zeolite sequential leaching and digestion experiment.....	166
Appendix B. Sample location and field data.....	172
Appendix C. Colloid separation methods and experiments.....	177
C.1 Methods and experimental procedures.....	177

	10
C.2 Sample results and discussion .....	182
Appendix D. Field photos of palagonites and hyaloclastites.....	189

## List of Tables

<b>Table 2.1:</b> Elemental and Ca isotope data for bulk basalt, primary mineral separates, and calcite.....	37
<b>Table 2.2:</b> Elemental and Ca isotope data for zeolite minerals.....	39
<b>Table 2.3:</b> Data for estimated average zeolite Ca-O bond lengths.....	48
<b>Table 3.1:</b> Elemental and Ca isotope data of Skagafjörður river and groundwaters, and other river samples from throughout Iceland.....	73
<b>Table 3.2:</b> Elemental and isotopic data of Skagafjörður rocks, calcites, and Hvanná river travertines.....	78
<b>Table 3.3:</b> Elemental and Ca isotope data of Skagafjörður sediment and soil leachates and digests, and bulk vegetation digests.....	79
<b>Table 4.1:</b> Geochemical and isotopic data of river and snow samples from the highlands.....	115
<b>Table 4.2:</b> Geochemical and isotopic data of hyaloclastite, palagonite and glass.....	116
<b>Table 4.3:</b> Suspended sediment leachate and digest elemental and Ca isotope data.....	117
<b>Table 4.4:</b> Ratio of suspended sediment exchangeable Ca to dissolved riverine Ca.....	119
<b>Table A1:</b> Zeolite Ca-O bond length data and sources.....	164
<b>Table A2:</b> Results of alternate linear regression models.....	165
<b>Table A3:</b> Elemental and Ca isotope data for zeolite leachate and residual digests.....	167
<b>Table B1:</b> Field data for samples included in Chapter 3.....	172
<b>Table B2:</b> Field data for samples included in Chapter 4.....	175
<b>Table C1:</b> Ca concentration and isotope data for samples and standards processed by TFF ultrafiltration methods.....	179

<b>Table C2:</b> Major cation and Si concentrations for samples processed through the ultrafiltration and colloidal separation method.....	187
--	-----

## List of Figures

<b>Figure 1.1:</b> CO <sub>2</sub> consumption rates versus runoff for global rivers.....	18
<b>Figure 2.1:</b> Map of sample locations and zeolite zones in the Berufjörður-Breiðdalur region of East Iceland.....	31
<b>Figure 2.2:</b> δ <sup>44/40</sup> Ca versus approximate burial depth for Icelandic zeolites.....	41
<b>Figure 2.3:</b> δ <sup>44/40</sup> Ca versus Sr/Ca ratios for Icelandic zeolites, calcite, basalt, and primary mineral separates .....	42
<b>Figure 2.4:</b> Zeolite, calcite, and average groundwater δ <sup>44/40</sup> Ca versus average Ca-O bond length.....	49
<b>Figure 3.1:</b> Map of samples from Iceland, showing Skagafjörður study region.....	65
<b>Figure 3.2:</b> δ <sup>44/40</sup> Ca versus Sr/Ca for river, groundwater, basalt, and calcite samples.....	85
<b>Figure 3.3:</b> δ <sup>44/40</sup> Ca versus saturation index of calcite for river and groundwater.....	88
<b>Figure 3.4:</b> δ <sup>44/40</sup> Ca versus Na/Ca for river, basalt, and calcite.....	89
<b>Figure 3.5:</b> δ <sup>44/40</sup> Ca versus Mg/Ca and K/Ca for river, groundwater, basalt, and calcite.....	92
<b>Figure 3.6:</b> δ <sup>44/40</sup> Ca of Skagafjörður soil exchangeable leachates versus mol percent of total Ca leached by NH <sub>4</sub> Cl.....	94
<b>Figure 3.7:</b> δ <sup>44/40</sup> Ca versus temperature, pH, and Sr/Ca for thermal and non-thermal Skagafjörður groundwaters.....	99
<b>Figure 3.8:</b> δ <sup>13</sup> C versus the saturation index of calcite for rivers and groundwaters.....	101
<b>Figure 4.1:</b> Map of highland sample locations and non-highland palagonite ridges.....	109
<b>Figure 4.2:</b> δ <sup>44/40</sup> Ca versus Sr/Ca for all highland samples and palagonite samples.....	121
<b>Figure 4.3:</b> δ <sup>44/40</sup> Ca versus Na/Ca, Mg/Ca, and K/Ca.....	123

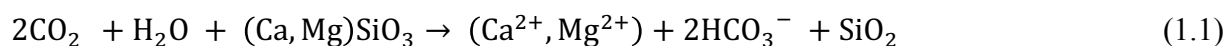
<b>Figure 4.4:</b> $\delta^{44/40}\text{Ca}$ versus $\delta^{13}\text{C}$ for highland river samples, Berufjörður-Breiðdalur calcites, and Skagafjörður groundwater samples.....	131
<b>Figure 4.5:</b> Saturation index of calcite versus $\delta^{13}\text{C}$ for highland river samples.....	132
<b>Figure A1:</b> $\delta^{44/40}\text{Ca}$ versus Si/Al molar ratio for bulk zeolites.....	165
<b>Figure A2:</b> $\delta^{44/40}\text{Ca}$ versus Sr/Ca for zeolite leachates and residual digests.....	169
<b>Figure A3:</b> $\delta^{44/40}\text{Ca}$ of leachate, residual digest, and bulk zeolite versus Na/Ca.....	170
<b>Figure A4:</b> Zeolite $\delta^{44/40}\text{Ca}$ versus mole fraction of Ca leached.....	172
<b>Figure C1:</b> Results of the TFF experiments.....	182
<b>Figure C2:</b> $\Delta^{44/40}\text{Ca}$ of ultrafiltered and dissolved fractions.....	184
<b>Figure C3:</b> Elemental ratios of ultrafiltered, colloidal, and dissolved fractions.....	185
<b>Figure C4:</b> $\delta^{44/40}\text{Ca}$ versus Sr/Ca ratio of dissolved, ultrafiltered, and colloidal fractions.....	188
<b>Figure D1:</b> Photos of highland hyaloclastite and glass.....	189
<b>Figure D2:</b> Photos of Helgafell palagonites.....	190
<b>Figure D3:</b> Photos of palagonitized outcrop in the Vesturdalur canyon.....	190

## Chapter 1

### Introduction and Overview

#### 1.1 Introduction

The long-term carbon (C) cycle describes exchanges of C between the atmosphere, hydrosphere, and lithosphere. Because carbon dioxide (CO<sub>2</sub>) is a greenhouse gas, the balance between inflows and outflows of atmospheric CO<sub>2</sub> regulates global temperatures and thus determines the evolution and stability of Earth's climate (Urey, 1952; Berner et al., 1983). Over geologic (million-year) timescales, C is removed from the atmosphere through silicate weathering, buried in oceans during carbonate precipitation, and ultimately returned to the atmosphere during plate subduction and volcanic degassing. The primary mechanism removing CO<sub>2</sub> from the atmosphere is silicate chemical weathering, where the dissolution of silicate minerals transforms CO<sub>2</sub> to bicarbonate (HCO<sub>3</sub><sup>-</sup>), as described by the following generalized reaction:

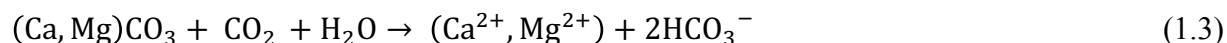


In this reaction, atmospheric CO<sub>2</sub> and water dissolve silicate minerals and release the solutes into rivers. Of the cations released during silicate weathering, Ca<sup>2+</sup> and Mg<sup>2+</sup> are of key importance because they are required for carbonate precipitation in the oceans, which proceeds as follows:



These equations describe how the chemical weathering of silicate minerals removes CO<sub>2</sub> from the atmosphere and transforms it into riverine bicarbonate, which then enters oceans and precipitates as solid carbonate rock over geologic timescales. Riverine HCO<sub>3</sub><sup>-</sup> produced from the

weathering of Na- and K- silicate minerals is not considered in traditional models of the long-term carbon cycle, as reverse weathering reactions in oceans return CO<sub>2</sub> to the atmosphere (Mackenzie and Garrels, 1966). The weathering of carbonate minerals also removes CO<sub>2</sub> from the atmosphere and adds HCO<sub>3</sub><sup>-</sup> to rivers:



However, this reaction is simply the reverse of Equation 1.2, thus carbonate weathering has no net effect on long-term climate. Only the weathering of Ca- and Mg- bearing silicate minerals controls long-term climate. As increasing atmospheric CO<sub>2</sub> levels accelerates the reaction given by Equation 1.1, silicate weathering is a key negative feedback that is responsible for maintaining a stable and habitable climate on Earth (Walker et al., 1981; Zeebe and Caldeira, 2008).

The weathering of mafic rocks, such as basalt, is of particular interest. Mafic rocks are predicted to weather faster than felsic because mafic minerals are less stable at the Earth's surface (Goldich, 1938). Basalt contains high proportions of Ca- and Mg- bearing silicate minerals, which are major constituents of the long-term C cycle (Equation 1.1). Additionally, basaltic rock generally hosts appreciable quantities of volcanic glass, which weathers even faster than crystalline mafic minerals (Gislason and Eugster, 1987a; Gislason and Oelkers, 2003). High solute fluxes in basalt-draining rivers globally have been interpreted as evidence of the relative mineral stability prediction (Gislason et al., 1996; Gaillardet et al., 1999; Dessert et al., 2001; Ibarra et al., 2016). It has been suggested that basalt weathering accounts for 30-35% of modern CO<sub>2</sub> consumption by silicate weathering (Dessert et al., 2003) despite only comprising ~5% of exposed continental area (Suchet et al., 2003). Thus, the weathering of basalt is generally

accepted to have a disproportionate role in climate regulation. The rapid weathering of basaltic rock has been invoked to explain changes in global climate throughout geologic history (Dessert et al., 2001; Jagoutz et al., 2016; Cox et al., 2016), and it forms the basis for many burgeoning geoengineering strategies to mitigate the effects of anthropogenic climate change (Snæbjörnsdóttir et al., 2020; Beerling et al., 2020).

Solute fluxes in basalt-draining rivers have been used to assess the controls on weathering rates, such as temperature, runoff, and vegetation (Berner et al., 1983; Nesbitt and Wilson, 1992; Bluth and Kump, 1994; Gislason et al., 1996; Dessert et al., 2003; Das et al., 2005b; West et al., 2005; Tipper et al., 2006a; Schopka et al., 2011; Moon et al., 2014; Li et al., 2016). Additionally, studies have used solute flux data to evaluate the strength of the silicate weathering-climate feedback (Berner et al., 1983; Berner, 1992; Gislason et al., 2009; Eiriksdottir et al., 2013; Torres et al., 2017), which has crucial implications not only for understanding the evolution of Earth's climate, but also for predicting how the Earth will respond to future C cycle perturbations. Interestingly,  $\text{HCO}_3^-$  fluxes in basalt-draining rivers overlap with the range for carbonate draining rivers, despite the fact that carbonate minerals dissolve orders of magnitude faster than basalt (Figure 1.1). Relative mineral stability cannot explain this pattern, thus, a paradox emerges: either basalt weathers as fast as carbonate, despite vast differences in weathering rates, or trace carbonate mineral weathering dominates the chemistry of basalt-draining rivers. Further investigation of solute sources in basalt-draining rivers is paramount for understanding the role of basalt weathering in the evolution and stability of Earth's climate, as well as for assessing the potential application of basalt weathering for climate change mitigation strategies.

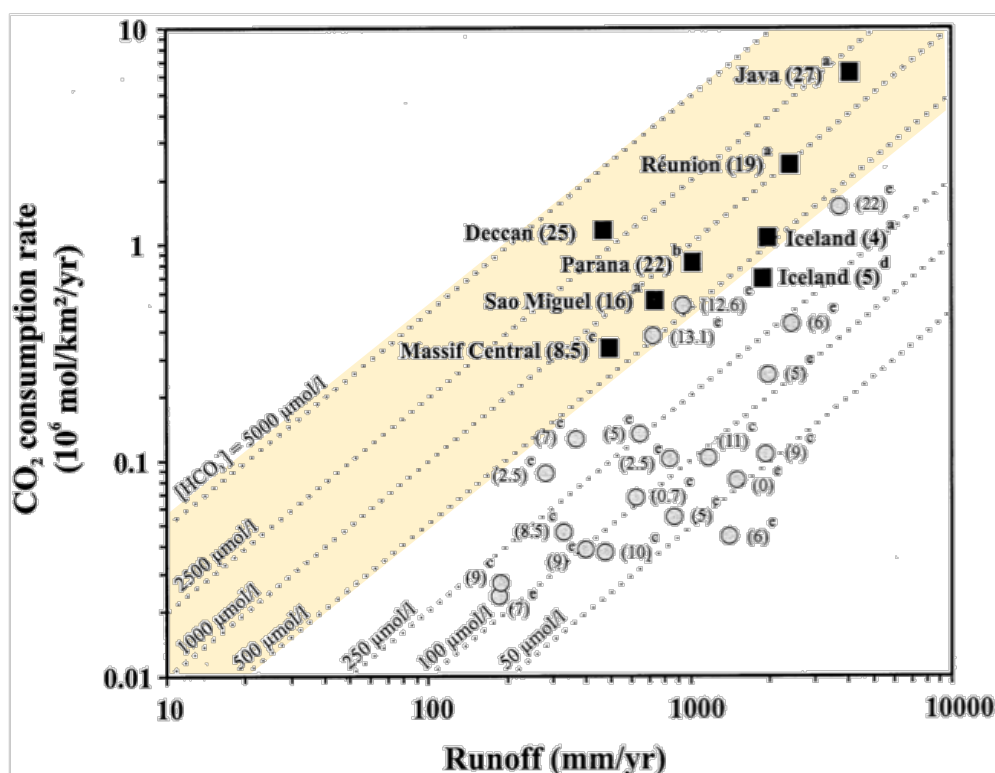


**Figure 1.1.** CO<sub>2</sub> consumption rates calculated from HCO<sub>3</sub><sup>-</sup> concentrations in basalt-draining rivers (black squares) and felsic draining rivers (grey circles) versus runoff (Dessert et al., 2001). Mean annual temperatures of each region are given in parentheses. The shaded region corresponds to the range of riverine HCO<sub>3</sub><sup>-</sup> fluxes for global carbonate draining rivers (Meybeck, 1987; Suchet et al., 2003; Cai et al., 2008).

Stable calcium (Ca) isotopes are a useful tool for investigating basalt weathering, as Ca directly participates in long-term climate regulation. Ca isotope analyses can be employed to trace mineralogical sources of Ca and processes controlling Ca cycling through the weathering environment (Griffith et al., 2020 and references therein). Ca has six naturally occurring stable isotopes (<sup>40</sup>Ca, <sup>42</sup>Ca, <sup>43</sup>Ca, <sup>44</sup>Ca, <sup>46</sup>Ca, <sup>48</sup>Ca), and recent advances in mass spectrometry allow for

high-precision measurements of Ca isotope ratios (Lehn et al., 2013), which are reported in delta notation ( $\delta^{44/40}\text{Ca}$ ) calculated from the following equation:

$$\delta^{44/40}\text{Ca}_{\text{sample}}(\text{‰}) = \left( \frac{(^{44}\text{Ca}/^{40}\text{Ca})_{\text{sample}}}{(^{44}\text{Ca}/^{40}\text{Ca})_{\text{standard}}} - 1 \right) \times 1000 \quad (1.4)$$

The standard in this dissertation refers to Atlantic Seawater (ASW).

Studies in Iceland have used stable Ca isotopes to differentiate between basalt weathering and trace calcite weathering as controls on river geochemistry (Hindshaw et al., 2013; Jacobson et al., 2015). Iceland is an ideal location to investigate basalt weathering with Ca isotopes, as basalt composes ~90% of the bedrock (Gislason et al., 1996), and Icelandic basalt and calcite have distinct  $\delta^{44/40}\text{Ca}$  values (Jacobson et al., 2015). A recent Ca isotope study indicated that calcite weathering could supply significant proportions of Ca (25% - 90%) in Icelandic rivers could be sourced from calcite weathering (Jacobson et al., 2015), implying that  $\text{HCO}_3^-$  fluxes do not accurately reflect basalt weathering by atmospheric  $\text{CO}_2$ . This result implies that the role of basalt weathering in climate regulation may be vastly overestimated. Moreover, if factors other than basalt weathering contribute to river geochemistry, solute fluxes cannot be used to assess the controls on basalt weathering rates. Further investigation of Ca cycling during basalt weathering is paramount for constraining the role of basalt weathering on climate regulation, quantifying parameters that influence atmospheric  $\text{CO}_2$  drawdown rates, investigating the strength of the silicate weathering-climate feedback, and optimizing strategies that exploit basalt for climate change mitigation.

Ca isotopes may prove to be a key tool for examining basalt weathering; however, controls on the Ca isotope geochemistry of basalt-draining rivers are debated (Hindshaw et al., 2013; Jacobson et al., 2015). This dissertation is focused on resolving this debate by studying

controls on the Ca isotope geochemistry of rivers in Iceland. I present three studies that characterize the  $\delta^{44/40}\text{Ca}$  of key Ca reservoirs in Iceland and address prime questions about processes controlling Ca isotope mixing and fractionation within and between reservoirs. Together, these studies vastly improve our ability to interpret riverine  $\delta^{44/40}\text{Ca}$  values and provide significant advancements to the Ca isotope geochemistry toolbox. The dissertation begins by examining the atomic-level behavior of Ca isotopes by zeolite minerals that form in the subsurface during the hydrothermal alteration of basalt (Chapter 2). In Chapter 3, I investigate Ca cycling at the watershed-scale through a high-resolution study of the Skagafjörður region in North Iceland. And finally, in Chapter 4, I employ the Ca isotope proxy to understand regional-scale weathering processes occurring in the Icelandic Highlands and test longstanding assumptions regarding whether rapid basaltic glass weathering contributes to long-term climate regulation.

## **1.2 Chapter 2: Large calcium isotope fractionations by zeolite minerals from Iceland**

In Iceland, basalt represents the initial reservoir of Ca, and basalts have a narrow range of  $\delta^{44/40}\text{Ca}$  values (Jacobson et al., 2015). Curiously, hydrothermal waters and calcites throughout Iceland have much higher  $\delta^{44/40}\text{Ca}$  values than basalt. “Heavy” calcite is highly unusual because most carbonate minerals form kinetically and incorporate lighter isotopes relative to the Ca source reservoir (Lemarchand et al., 2004; Gussone et al., 2005; Tang et al., 2008a). This study explores the hypothesis that Ca isotope fractionation by zeolites drives hydrothermal waters and calcites to high  $\delta^{44/40}\text{Ca}$  values in Icelandic hydrothermal systems.

Zeolites are secondary minerals with structures that comprise frameworks of linked Si- or Al-O tetrahedra, creating voids and channels that contain  $\text{H}_2\text{O}$ , Ca, and other cations that are

readily exchangeable (Passaglia and Sheppard, 2001; Armbruster and Gunter, 2001; Pabalan and Bertetti, 2001). The minerals serve as significant  $\text{Ca}^{2+}$  sinks during the low-grade burial metamorphism of Icelandic basalt (Wood et al., 1976; Kristmannsdóttir and Tómasson, 1978; Neuhoff et al., 1999, 2000; Franzson, 2000; Weisenberger and Selbekk, 2009; Weisenberger et al., 2014). In this study, I used a high-precision Thermal Ionization Mass Spectrometry (TIMS) method to measure  $\delta^{44/40}\text{Ca}$  values of six zeolite mineral species collected from a type-locality in the Berufjörður-Breiðdalur region of East Iceland. I also analyzed bulk basalt, primary mineral separates, and calcite to characterize key mineralogical reservoirs of Ca in basaltic environments. Zeolite minerals display a  $\delta^{44/40}\text{Ca}$  range of  $\sim 1.4\%$ , which is comparable to the range exhibited by all igneous rocks thus far measured (Fantle and Tipper, 2014; Antonelli and Simon, 2020). Curiously, zeolite  $\delta^{44/40}\text{Ca}$  values vary widely, where minerals that form under identical conditions show  $\delta^{44/40}\text{Ca}$  values that bracket the value of bulk basalt, with one mineral isotopically heavier than basalt and the other isotopically lighter. I discovered that zeolite  $\delta^{44/40}\text{Ca}$  values strongly correlate with the average Ca-O bond length per mineral, which indicates that equilibrium isotope partitioning determines the variability and large range of zeolite  $\delta^{44/40}\text{Ca}$  values. The results of this study confirm previous hypotheses that fractionation of Ca isotopes during zeolite ion-exchange elevates the  $\delta^{44/40}\text{Ca}$  values of hydrothermal water from which calcite then precipitates, thus resolving the “heavy calcite” problem.

This study reports novel Ca isotope data necessary for interpretations offered in subsequent chapters of this dissertation. Most Ca isotope studies of mineral fractionation have focused either on low temperature ( $<40^\circ\text{C}$ ) calcite formation or high temperature ( $>200^\circ\text{C}$ ) silicate mineral crystallization. The study presented in Chapter 2 fills a crucial data gap for minerals that form at “intermediate” temperatures ( $\sim 30^\circ\text{C} - 200^\circ\text{C}$ ) and is one of few studies to

identify a system that appears to be equilibrium-controlled with respect to Ca isotopes. As equilibrium isotope fractionation factors strongly depend on temperature (Urey, 1947), my findings suggest that the Ca isotope geochemistry of zeolite minerals could be developed into an entirely new “geothermometer” for investigating low-grade basalt metamorphism.

### **1.3 Chapter 3: Controls on riverine calcium isotope ratios during basalt weathering in the Skagafjörður watershed, Iceland**

Rivers in Iceland show elevated  $\delta^{44/40}\text{Ca}$  values relative to basalt (Hindshaw et al., 2013; Jacobson et al., 2015), but the cause remains debated. Hindshaw et al. (2013) suggested that fractionation of light Ca isotopes by secondary minerals, such as clays or zeolites, elevates riverine  $\delta^{44/40}\text{Ca}$  values. Uptake of lighter Ca isotopes by vegetation and adsorption onto particulate surfaces also fractionate Ca isotopes in the weathering environment (Cenki-Tok et al., 2009; Schmitt et al., 2012; Fantle and Tipper, 2014; Brazier et al., 2019; Griffith et al., 2020). A more recent study in Iceland concluded that the weathering of isotopically heavy calcite elevates riverine  $\delta^{44/40}\text{Ca}$  values (Jacobson et al., 2015). To test these and other hypotheses, I investigated the Ca isotope geochemistry of the Skagafjörður region of North Iceland. The Skagafjörður valley encompasses an area of 3,650 km<sup>2</sup> with bedrock that consists mostly of well-crystallized, Tertiary tholeiitic flood basalts. Skagafjörður is characterized by glacial erosion, sediment-laden rivers, peat soil, and fairly dense vegetation, thus making it an ideal setting to investigate fractionation controls on river chemistry. In the summer of 2017, I collected various samples to characterize key reservoirs, such as rivers, groundwater, soil, vegetation, colloids, suspended sediments, and stream sediments. I studied the chemistry of both main stem valley rivers, which

receive significant inputs from the barren, glaciated highlands, as well as small, direct-runoff tributaries draining unaltered, crystalline basalt in the surrounding mountains.

Riverine  $\delta^{44/40}\text{Ca}$  values correlate with Sr/Ca and Na/Ca ratios, as well as the saturation index (SI) of calcite. Stable carbon isotope ratios ( $\delta^{13}\text{C}$ ) of riverine dissolved inorganic carbon also correlate with SI calcite. The combined patterns largely reflect three-component mixing between basalt weathering, calcite weathering, and hydrothermal water inputs. Only the small tributaries on the flanks of the valley show signals indicative of basalt weathering by atmospheric  $\text{CO}_2$ . Skagafjörður groundwater  $\delta^{44/40}\text{Ca}$  values correlate with pH, temperature, distance from the coast, and Sr/Ca ratios, all consistent with fractionation control yielding varying degrees of geochemical evolution. This further confirms that fractionation of Ca isotopes by zeolites dictates the  $\delta^{44/40}\text{Ca}$  values of Icelandic groundwaters. This study highlights the significance of hydrothermal water inputs to Icelandic rivers, which have been previously underestimated. Fractionation by soils is negligible because soils are mainly Ca-poor material with basaltic  $\delta^{44/40}\text{Ca}$  values. Soil exchangeable  $\text{Ca}^{2+}$  and vegetation both show low  $\delta^{44/40}\text{Ca}$  values, however rivers entering Skagafjörður from the soil and vegetation-free highlands show the highest  $\delta^{44/40}\text{Ca}$ , inconsistent with a soil-related fractionation mechanism as the primary control on river  $\delta^{44/40}\text{Ca}$  values. Attempts to analyze the Ca isotope geochemistry of colloids suggest that colloids have lower  $\delta^{44/40}\text{Ca}$  values than truly dissolved  $\text{Ca}^{2+}$  and that the proxy could be developed as a tracer for colloidal inputs to rivers; however, some evidence also exists that method for separating colloids could introduce artifacts, thus pointing to a need for further refinement. Results from this study suggest that water mass mixing offers the best explanation for the dataset, implying that surficial basalt weathering rates are likely much lower than previously appreciated.

## **1.4 Chapter 4: Basalt weathering in the Icelandic highlands: reassessing the role of basalt weathering on long term climate regulation with Ca isotope geochemistry**

Particular interest has been placed on rivers draining young and glassy volcanic rocks (Gislason et al., 1996; Stefansson and Gislason, 2001) because basaltic glass dissolves faster than crystalline silicate minerals (Gislason and Eugster, 1987a; Oelkers and Gislason, 2001), which implies that glass weathering could represent a significant sink for atmospheric CO<sub>2</sub>. Moreover, glaciers accelerate mechanical erosion rates, thereby increasing reactive surface area and accelerating dissolution rates (Gislason et al., 2009). This study investigates “rapid” volcanic glass weathering in the glacial plains of the Icelandic highlands. The Icelandic highlands are characterized by large and sediment-laden rivers draining young, glassy volcanic rock. Because the region is devoid of soil and vegetation, mechanisms potentially contributing to fractionation of Ca isotopes are minimal. The highlands are therefore an ideal location to investigate the relative mineral stability paradigm and assess the role that basalt weathering plays in regulating long-term global climate.

River samples from the central highlands have the heaviest  $\delta^{44/40}\text{Ca}$  values of nearly all river samples measured to date in Iceland (Hindshaw et al., 2013; Jacobson et al., 2015). The distinct Ca isotope ratios of highland rocks and rivers indicates that weathering of highland rocks and glass are not major factors controlling riverine  $\delta^{44/40}\text{Ca}$  values. This study investigates two possible fractionation mechanisms that may elevate highland river  $\delta^{44/40}\text{Ca}$  values. The adsorption of Ca<sup>2+</sup> onto suspended material does not appear to control riverine  $\delta^{44/40}\text{Ca}$  values because sediment laden and non-sediment laden rivers similarly high  $\delta^{44/40}\text{Ca}$  values. Alteration of volcanic glasses to clay material (palagonitization) does not appear to fractionate Ca isotopes on a scale that could affect rivers. Riverine  $\delta^{44/40}\text{Ca}$  and  $\delta^{13}\text{C}$  values generally correlate, which is

best explained by mixing between calcite weathering and groundwater inputs. This result indicates that very little Ca in highland rivers is sourced from rapid weathering of basaltic glass and primary minerals by atmospheric CO<sub>2</sub>. High solute fluxes in young volcanic regions do not reflect rapid weathering caused by parameters, such as rock age and glacial activity. Thus, these solute sources must be accounted for when using riverine dissolved loads to estimate atmospheric CO<sub>2</sub> drawdown or approximate the strength of the silicate weathering feedback under Earth surface conditions.

## Chapter 2

### Large calcium isotope fractionations by zeolite minerals from Iceland

#### 2.1 Introduction

Calcium, the fifth most abundant element in the crust (Fleischer, 1954), plays a key role in regulating climate over geologic timescales (Urey, 1952; Berner et al., 1983) and is essential for biological processes, such as biomineralization, plant growth, and cellular regulation (DePaolo, 2004; Gussone et al., 2016). Due to the ubiquitous occurrence of Ca in Earth and extraterrestrial materials, as well as major geochemical cycles, stable Ca isotope ratios have emerged as a promising tool for investigating processes in geochemistry, cosmochemistry, biology, and archaeology (Fantle and Tipper, 2014; Griffith and Fantle, 2020). Calcium isotope ratios are reported in delta notation as  $\delta^{44/40}\text{Ca}_{\text{smp}} (\text{‰}) = [({}^{44}\text{Ca}/{}^{40}\text{Ca})_{\text{smp}}/({}^{44}\text{Ca}/{}^{40}\text{Ca})_{\text{std}} - 1] \times 1000$ , where *smp* refers to the sample and *std* refers to the normalizing standard, which in this study is OSIL Atlantic Seawater or *ASW* ( $\delta^{44/40}\text{Ca}_{\text{ASW}} = 0\text{‰}$ ).

In the ongoing effort to develop and apply the  $\delta^{44/40}\text{Ca}$  tracer, research has focused on quantifying mechanisms that fractionate isotopes according to their masses and produce isotopic offsets ( $\Delta$ ) between related Ca-bearing reservoirs, i.e.,  $\Delta^{44/40}\text{Ca}_{\text{a-b}} = \delta^{44/40}\text{Ca}_{\text{a}} - \delta^{44/40}\text{Ca}_{\text{b}}$ . Differentiating between kinetic and equilibrium isotope effects during mineral formation is particularly essential for implementing Ca isotopes as paleoenvironmental or temperature proxies (Urey, 1947; Bigeleisen and Mayer, 1947; Schauble, 2004). Most studies aimed at understanding Ca isotope fractionation during mineral precipitation have focused on calcite ( $\text{CaCO}_3$ ) formation at low temperatures ( $<30^\circ\text{C}$ ) characterizing the Earth's surface. Here, kinetic isotope effects (Lemarchand et al., 2004; Tang et al., 2008a; DePaolo, 2011; Nielsen et al., 2012; AlKhatib and

Eisenhauer, 2017; Wang et al., 2021; Blättler et al., 2021) cause calcite to preferentially incorporate lighter Ca isotopes from solution with  $\Delta^{44/40}\text{Ca}_{\text{cal-sol}}$  on the order of  $-1$  to  $-2\text{‰}$  (Fantle and Tipper, 2014). Theory predicts that higher temperatures should promote equilibrium effects and minimize isotopic offsets ( $\Delta^{44/40}\text{Ca}_{\text{cal-sol}} \approx 0\text{‰}$ ) during calcite formation (Marriott et al., 2004; Tang et al., 2008a; AlKhatib and Eisenhauer, 2017); however, only a handful of natural calcites precipitated at elevated temperatures have been measured (Amini et al., 2008; John et al., 2012; Brown et al., 2013; Jacobson et al., 2015). In parallel, some studies examining silicate mineral formation at high temperatures characterizing the solid Earth have attributed  $\delta^{44/40}\text{Ca}$  variability to equilibrium isotope partitioning (Huang et al., 2010; Feng et al., 2014), driven by differences in Ca-O bonding conditions (Urey, 1947; Schauble, 2004). However, discrepancies between measured inter-mineral  $\Delta^{44/40}\text{Ca}$  of high-temperature silicates and *ab initio* model predictions of equilibrium Ca isotope offsets have been interpreted as evidence for mostly kinetic control (Antonelli et al., 2019b; Antonelli and Simon, 2020).

Missing from Ca isotope fractionation theory is an understanding of mechanisms that produce  $\delta^{44/40}\text{Ca}$  variability during mineral formation at temperatures bridging the surface and solid Earth. “Intermediate” temperatures in the range of  $\sim 30^\circ\text{C}$  to  $200^\circ\text{C}$  characterize many hydrothermal systems, which represent key interfaces linking surficial geochemical cycles and solid Earth processes. Studies have used Ca isotopes to examine mid-ocean ridge hydrothermal systems (Amini et al., 2008; Brown et al., 2020; Gussone et al., 2020b), seafloor weathering and oceanic lithosphere subduction (John et al., 2012), continental hydrothermal systems (Brown et al., 2013), and water-rock interactions in pilot studies of mineral carbonation of basalt, a leading carbon capture and storage (CCS) strategy (Pogge von Strandmann et al., 2019a; Snæbjörnsdóttir

et al., 2020). Application of the Ca isotope tracer to these and other intermediate temperature systems requires a thorough examination of all secondary minerals that may fractionate Ca isotopes and contribute to the  $\delta^{44/40}\text{Ca}$  values of circulating waters. Additionally, a better understanding of both equilibrium and kinetic effects on Ca isotope fractionation at intermediate temperatures is essential for improving knowledge about Ca isotope cycling and identifying novel applications for the  $\delta^{44/40}\text{Ca}$  tracer.

Hydrothermal alteration commonly leads to the formation of zeolites (Coombs et al., 1959; Chipera and Apps, 2001). Zeolite mineral structures comprise frameworks of linked Si- or Al-O tetrahedra, creating voids and channels that contain  $\text{H}_2\text{O}$ , Ca, and other cations, which are readily exchangeable (Passaglia and Sheppard, 2001; Armbruster and Gunter, 2001; Pabalan and Bertetti, 2001). The minerals serve as significant  $\text{Ca}^{2+}$  sinks during low-grade metamorphism (Wood et al., 1976; Kristmannsdóttir and Tómasson, 1978; Neuhoff et al., 1999, 2000; Franzson, 2000; Weisenberger and Selbekk, 2009; Weisenberger et al., 2014). In basaltic settings such as Iceland, equilibrium-controlled ion-exchange reactions with zeolites strongly regulate  $\text{Ca}^{2+}$  concentrations in natural hydrothermal waters (Fridriksson, 2004; Fridriksson et al., 2009), as well as those produced in field-scale CCS experiments (Gysi and Stefánsson, 2012b; Aradóttir et al., 2012; Matter et al., 2016; Snæbjörnsdóttir et al., 2017). Calcium cycling during basalt weathering in subsurface hydrothermal systems also plays a major role in regulating Earth's long-term carbon cycle (Dessert et al., 2003; Rad et al., 2007; Andrews and Jacobson, 2017). Moreover, owing to their properties as ion-exchangers, absorbents, molecular sieves, and catalysts (Li et al., 2011), zeolites have numerous environmental, industrial, and medical applications, including drinking water purification (Mumpton, 1999; Li et al., 2017; Jiang et al.,

2018), nuclear waste management (Borai et al., 2009; Lonin et al., 2015), contaminant transport mitigation (Kallo, 2001; Leyva-Ramos et al., 2010; Baek et al., 2018), automotive emission reduction (Sarshar et al., 2009), and cancer treatment (Bacakova et al., 2018).

Nonetheless, despite the widespread occurrence and applicability of zeolites, their Ca isotope geochemistry has been neglected. Only one study has reported Ca isotope data for zeolites (Jacobson et al., 2015). Coexisting heulandite and stilbite from Iceland are isotopically lighter and heavier, respectively, relative to basalt. Icelandic hydrothermal water and calcite also have  $\delta^{44/40}\text{Ca}$  values higher than basalt (Jacobson et al., 2015). “Heavy” calcite is highly unusual because most carbonate minerals form kinetically and incorporate lighter isotopes relative to the Ca source reservoir (Lemarchand et al., 2004; Gussone et al., 2005; Tang et al., 2008a). Uptake of lighter Ca isotopes during zeolitization may elevate the relative abundance of heavier Ca isotopes in hydrothermal waters from which calcite precipitates (Jacobson et al., 2015), but no systematic understanding has been established.

To better understand the Ca isotope geochemistry of zeolites, I used a high-precision Thermal Ionization Mass Spectrometry (TIMS) method to measure  $\delta^{44/40}\text{Ca}$  values of six zeolite mineral species. I also analyzed bulk basalt, primary mineral separates, and calcite. Specimens were collected from the Berufjörður-Breiðdalur region of East Iceland, which is a type-locality for the zeolitization of basaltic lava flows due to burial metamorphism (Walker, 1960). Here, increasing temperature with depth below the surface of the lava pile has generated distinct “zeolite zones” where two zeolite mineral types, referred to as “coindex mineral pairs” (Walker, 1960), distinctly form and thus are diagnostic of each depth zone (Figure 2.1). Depth-controlled zeolite zones have been identified worldwide in active geothermal systems (Kristmannsdóttir and

Tómasson, 1978; Fridriksson et al., 2009; Alfredsson et al., 2013), as well as extinct systems now exposed at the surface (Coombs et al., 1959; Neuhoff et al., 1999; Fridriksson et al., 2001; Weisenberger and Selbekk, 2009; Kousehlar et al., 2012). I report a large range in zeolite  $\delta^{44/40}\text{Ca}$  values, which is best explained by equilibrium isotope partitioning, given a strong observed correlation with Ca-O bond lengths. Our findings point the way for developing entirely new tools for investigating low-grade basalt alteration. They also broadly illustrate how future efforts focused on the Ca isotope geochemistry of zeolites could have implications for numerous other topics, such as understanding the compositional evolution of hydrothermal waters, quantifying elemental cycling in the oceans, and improving CCS strategies.

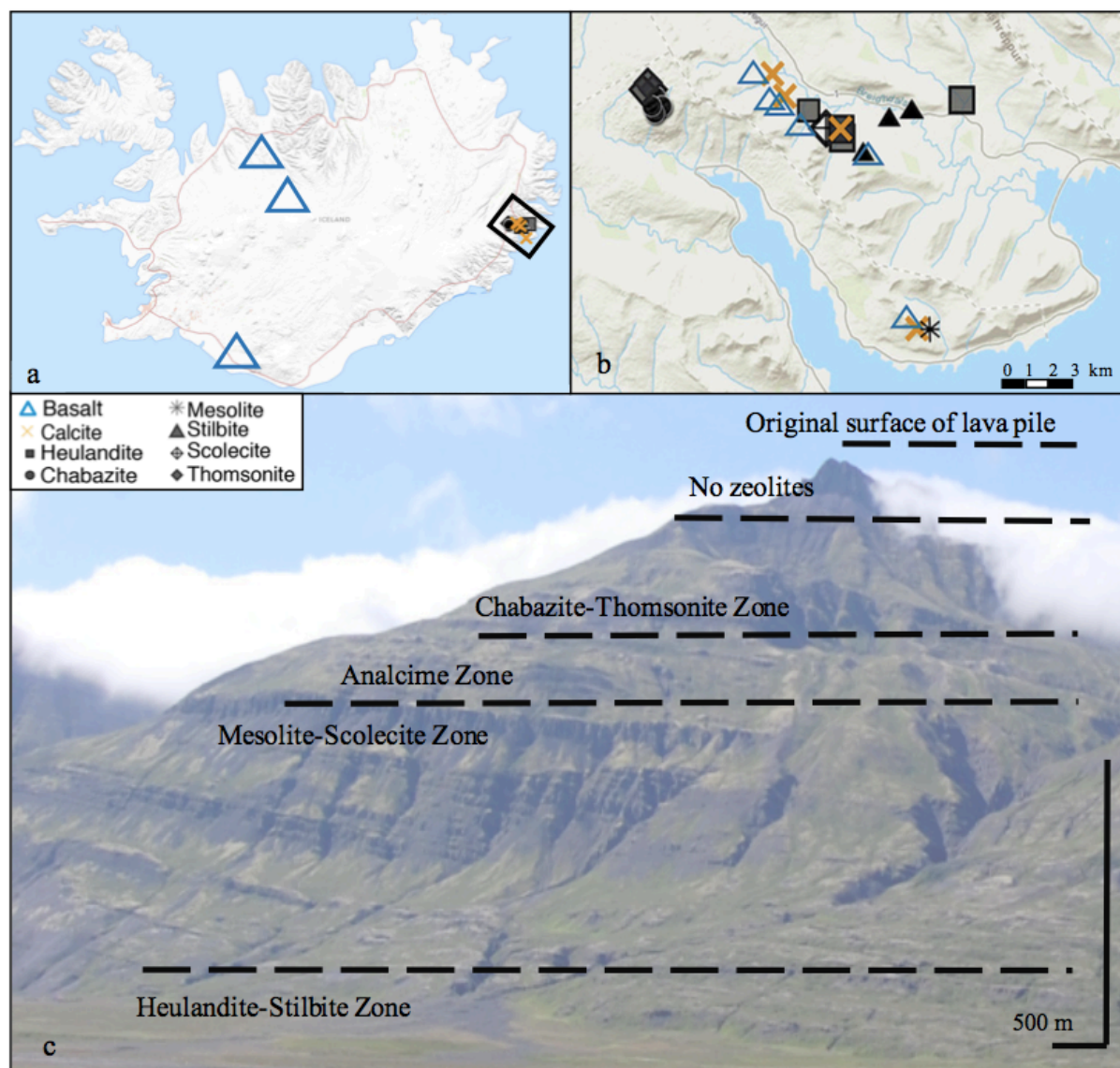


**Figure 2.1:** Map of Iceland showing sample locations. (a) Mineral separates were obtained from basalts sampled throughout Iceland. The Berufjörður-Breiðdalur region of East Iceland is outlined. (b) Sampling locations of bulk rocks, calcite, and zeolites collected from the main region of study. (c) Zeolite sampling locations correspond to different elevations, or “depths” below the original surface of the lava pile. Depth-controlled zeolite zones, adapted from Walker (1960), are overlain on a photograph of the Berufjörður volcanic sequence taken from the north.

## 2.2 Geologic Setting

Iceland is an exposed section of the Atlantic mid-ocean ridge overlying a mantle plume, which has caused extensive rifting and volcanism over the past 50-60 Myr (White and McKenzie, 1989). Rocks increase in age away from the active rift zone, with the oldest rocks at the edges of Iceland dating to ~16 Ma (Moorbath et al., 1968). Samples analyzed in this study were collected from Berufjörður-Breiðdalur region described in detail by Walker (1960) (Figure 2.1). Successive eruptions of a Tertiary volcano supplied lava that piled to a minimum total thickness of ~2,000 m at the eastern end (Walker, 1960, 1964; Robinson et al., 1982). The central volcano comprises highly altered rhyolite, while the flows are predominantly tholeiitic basalt, with lesser amounts of olivine-basalt (Walker, 1960, 1964). Within ~1 Myr after the eruptions ceased, heat from burial, as well as the volcanic center and associated dike swarms, extensively zeolitized the lava pile, filling up to 90% of primary porosity (Walker, 1960; Robinson et al., 1982; Mehegan et al., 1982; Neuhoff et al., 1999). Pleistocene glacial erosion carved deep valleys and fjords into the lava pile and exposed the top ~1,000 m of the altered sequence, where the depth-controlled “zeolite zones” are clearly delineated and accessible above sea level (Figure 2.1). The shallowest zone studied here is the chabazite-thomsonite zone (~30°C – 70°C), followed by the mesolite-scolecite zone (~70°C – 90°C) and the stilbite-heulandite zone (~90°C – 150°C), which reaches a maximum depth of ~1,500 m below the top of the lava pile (Walker, 1960; Neuhoff et al., 2000; Chipera and Apps, 2001; Thien et al., 2015).

## 2.3 Methods

### 2.3.1 Field Collection

During the summer of 2017, zeolites, bulk basalt, and calcite were collected from various outcrops in the Berufjörður-Breiðdalur region of East Iceland. Mineral types were identified in the field and later confirmed by X-ray Diffraction, as described below. Where possible, coindex zeolite pairs were collected from a single outcrop for every “depth-zone” described by Walker (1960), and calcite samples were collected from all zones. Rock samples for primary mineral separates were collected from basaltic flows throughout Iceland (Figure 2.1).

### 2.3.2 Sample Preparation

Heavy liquids (Apatite-to-Zircon Inc; Viola, ID, USA) were used to separate mostly pure fractions of plagioclase, clinopyroxene, olivine, and apatite from three basalt samples with different ages and geologic histories. Intergrown zeolite samples from the same amygdule were physically separated. All basalt and mineral specimens, including primary minerals, calcite, and zeolites, were washed with MilliQ water and sonicated to remove excess sediment and impurities. Samples were dried in an oven at 50°C and powdered by hand using a diamondite mortar and pestle. Zeolites fundamentally differ from typical rock-forming silicate minerals, as their frameworks only comprise Al, Si, and O, i.e., the minerals do not contain structurally bound Ca. All Ca is extra-framework, as it occurs in voids and channels created by the frameworks. Therefore, bulk measurements are most appropriate for characterizing the Ca isotope geochemistry of zeolites. Sub-samples of basalt, primary mineral, and zeolite powders were completely digested using HF and HNO<sub>3</sub> acids. No insoluble residues were observed. Calcite powders were completely dissolved in 5% HNO<sub>3</sub>. To further interrogate the Ca isotope

geochemistry of zeolites, a sequential leaching and digestion procedure was applied, see Appendix A.

### 2.3.3 X-ray Diffraction

The identities of zeolite specimens collected in the field were confirmed by X-ray Diffraction (XRD) in the Integrated Molecular Structure Education and Research Center (IMSERC) at Northwestern University. Powder XRD data were collected at room temperature on a STOE-STADI-P powder diffractometer equipped with an asymmetric curved Germanium monochromator (CuK $\alpha$ 1 radiation,  $\lambda = 1.54056 \text{ \AA}$ ) and a one-dimensional silicon strip detector (MYTHEN2 1K from DECTRIS). The line focused Cu X-ray tube was operated at 40 kV and 40 mA. Intensity data from  $2\theta$  ranges of  $1^\circ$  to  $100^\circ$  were collected over a period of 30 mins. The instrument was calibrated against a NIST Si standard (640d) prior to measurement.

### 2.3.4 Elemental Analysis

Sample solutions were diluted with 5% HNO<sub>3</sub> and analyzed for concentrations of Ca, Na, Mg, K, and Sr using a Thermo Scientific iCAP 6500 ICP-OES at Northwestern University. The concentrations have an uncertainty of  $\pm 10\%$  (RSD), as determined by repeated analyses of NIST SRM 1643f. Concentrations of Si and Al were measured using a lithium metaborate fusion procedure and an Enviro II ICP-AES (Activation Laboratories, Ancaster, Ontario). These data have an uncertainty of  $\pm 5\%$ .

### 2.3.5 Ca isotope ratios

Calcium isotope ratios ( $^{44}\text{Ca}/^{40}\text{Ca}$ ) were measured with a Thermo-Fisher Triton MC-TIMS in the Radiogenic Isotope Laboratory at Northwestern University, using an optimized  $^{43}\text{Ca}$ - $^{42}\text{Ca}$  double-spike procedure (Lehn et al., 2013). Samples containing 50  $\mu\text{g}$  of Ca were

equilibrated with the spike, and the solutions were eluted through Teflon columns packed with Bio-Rad AG MP-50 cation exchange resin. Approximately 12.5  $\mu\text{g}$  of purified Ca was loaded onto outgassed, single Ta filament assemblies together with 0.5  $\mu\text{L}$  of 10%  $\text{H}_3\text{PO}_4$ . Total procedural blanks ( $n = 4$ ) determined with a  $^{42}\text{Ca}$  isotope dilution method were negligible (65 – 117 ng). Reported  $\delta^{44/40}\text{Ca}$  have an internal precision of  $\pm 0.02\text{--}0.03\text{‰}$  ( $2\sigma_{\text{SEM}}$ ). The double-spike was frequently recalibrated by analyzing at least 8 OSIL ASW standards and 2 NIST 915b standards every 30 or fewer samples. During the period of study, repeated analyses of the standards yielded  $\delta^{44/40}\text{Ca}_{\text{ASW}} = 0.000 \pm 0.005\text{‰}$  ( $2\sigma_{\text{SEM}}$ ,  $n = 68$ ) and  $\delta^{44/40}\text{Ca}_{915b} = -1.147 \pm 0.012\text{‰}$  ( $2\sigma_{\text{SEM}}$ ,  $n = 17$ ). These data correspond to a short-term external reproducibility ( $2\sigma_{\text{SD}}$ ) of  $\pm 0.045\text{‰}$  for OSIL ASW and  $\pm 0.049\text{‰}$  for NIST 915b. Long-term records for the laboratory yield  $\delta^{44/40}\text{Ca}_{\text{ASW}} = 0.000 \pm 0.002\text{‰}$  ( $2\sigma_{\text{SEM}}$ ,  $n = 661$ ) and  $\delta^{44/40}\text{Ca}_{915b} = -1.135 \pm 0.003\text{‰}$  ( $2\sigma_{\text{SEM}}$ ,  $n = 263$ ). These data point to a  $2\sigma_{\text{SD}}$  of  $\pm 0.044\text{‰}$  for OSIL ASW and  $\pm 0.048\text{‰}$  for NIST 915b. Based on all standard measurements, I adopt a  $2\sigma_{\text{SD}}$  of  $\pm 0.05\text{‰}$  for the present dataset. As shown in the data tables, duplicate analyses of sample unknowns are better than  $\pm 0.02\text{‰}$ . Long-term records for the laboratory yield a SRM915a value of  $\delta^{44/40}\text{Ca}_{915a} = -1.86 \pm 0.01\text{‰}$  ( $2\sigma_{\text{SEM}}$ ,  $n = 68$ ) relative to ASW, therefore data reported here can be converted to the SRM915a scale using the following equation:  $\delta^{44/40}\text{Ca} (\text{‰}, \text{SRM915a}) = \delta^{44/40}\text{Ca} (\text{‰}, \text{ASW}) + 1.86\text{‰}$ .

### 2.3.6 Bond length calculation

The weighted average bond length per zeolite mineral ( $L$ ) was approximated by compiling published data on lengths for the two types of bonds (either  $\text{Ca-O}_w$  or  $\text{Ca-O}_{\text{fmwk}}$ ) specific to each exchange site containing Ca (Table A1). For some zeolites, Ca occupying a

given exchange site can coordinate to both water O atoms and framework O atoms (Table 2.3).

Because, in general, bond lengths differ depending on whether Ca coordinates to water O or framework O atoms, I calculated weighted average, site-specific bond lengths ( $l_s$ ), which account for differences in Ca-O<sub>w</sub> bond lengths ( $l_w$ ) and Ca-O<sub>fmwk</sub> bond lengths ( $l_{fmwk}$ ) according to the number of water O atoms ( $N_w$ ) and framework O atoms ( $N_{fmwk}$ ) available for coordination.

The equations are:

$$L = (f_{Ca_1} \times l_{s_1}) + (f_{Ca_2} \times l_{s_2}) \dots + (f_{Ca_i} \times l_{s_i}) \quad (2.1)$$

$$l_s = \left( l_w \times \frac{N_w}{CN_s} \right) + \left( l_{fmwk} \times \frac{N_{fmwk}}{CN_s} \right) \quad (2.2)$$

$$CN_s = N_w + N_{fmwk} \quad (2.3)$$

$L$  = estimated bond length per mineral (Å)

$f_{Ca}$  = fraction of Ca occupying each site (1, 2, ...i)

$l_s$  = weighted average site-specific bond length (Å)

$l_w$  = average Ca-O<sub>w</sub> bond length in a given site (Å)

$l_{fmwk}$  = average Ca-O<sub>fmwk</sub> bond length in a given site (Å)

$N_w$  = number of Ca-O<sub>w</sub> bonds in a given site

$N_{fmwk}$  = number of Ca-O<sub>fmwk</sub> bonds in a given site

$CN_s$  = total coordination number of Ca in a given site

The calculations adopted for Figure 2.4 assume even distribution of Ca across all potential Ca-bearing sites (Table 2.3). Sensitivity to this assumption was tested by changing  $f_{Ca}$  to values that produce the minimum and maximum possible estimates of  $L$  for each mineral. The correlation remains significant for all scenarios ( $R^2 > 0.80$ ,  $p < 0.001$ ). See Appendix A for more details on statistical analysis.

## 2.4 Results

### 2.4.1 Bulk Basalt and Primary Minerals

Table 2.1 presents elemental and Ca isotope data for bulk basalt and primary mineral separates. Bulk basalt samples from the Berufjörður-Breiðdalur region yield an average  $\delta^{44/40}\text{Ca}$  of  $-1.04 \pm 0.08\text{‰}$  ( $2\sigma_{\text{SD}}$ ,  $n = 5$ ), which agrees well with the average of  $-1.06 \pm 0.02\text{‰}$  ( $2\sigma_{\text{SD}}$ ,  $n = 6$ ) for basalt sampled from other regions throughout Iceland (Jacobson et al., 2015). The primary minerals have a narrow range of  $\delta^{44/40}\text{Ca}$  values, which bracket those for bulk basalt. Olivine has the highest average  $\delta^{44/40}\text{Ca}$  ( $-1.02 \pm 0.14\text{‰}$ ,  $2\sigma_{\text{SD}}$ ,  $n = 3$ ), followed by clinopyroxene ( $-1.05 \pm 0.06\text{‰}$ ,  $2\sigma_{\text{SD}}$ ,  $n = 3$ ), apatite ( $-1.12 \pm 0.06\text{‰}$ ,  $2\sigma_{\text{SD}}$ ,  $n = 3$ ), and plagioclase ( $-1.14 \pm 0.04\text{‰}$ ,  $2\sigma_{\text{SD}}$ ,  $n = 3$ ).

**Table 2.1.** Elemental and Ca isotope data for bulk basalt, primary mineral separates, and calcite. Duplicate analyses are shown in “()”. Elements not detected are marked with “-”.

Sample ID	Ca ( $\mu\text{mol/g}$ )	Na ( $\mu\text{mol/g}$ )	Sr ( $\text{nmol/g}$ )	Mg ( $\mu\text{mol/g}$ )	$\delta^{44/40}\text{Ca}$ ( $\text{‰}$ )
<i>Bulk Basalt</i>					
ILR_D_6	1997	701	2845	1582	-1.00
ILR_D_13	1833	656	3168	1275	-1.10
ILR_12_f	1280	792	3145	1008	-1.02
ILR_12_l	1748	668	3049	1371	-1.02
ILR_12_m	1723	759	2894	1201	-1.05

*Plagioclase*

ILR_PL_16	3206	437	2139	69.1	-1.12
ILR_SJ_22	2800	753	8084	47.5	-1.15
ILR_SV_2	3212	460	2293	62.7	-1.16

*Clinopyroxene*

ILR_PL_16	3405	134	299	3633	-1.03
ILR_SJ_22	4023	141	560	3369	-1.05
ILR_SV_2	3873	94.7	189	3260	-1.08

*Apatite*

ILR_PL_16	3162	448	2384	158	-1.09
ILR_SJ_22	2390	811	7883	56.5	-1.14
ILR_SV_2	3105	539	2589	185	-1.14

*Olivine*

ILR_PL_16	344	51.9	119	9269	-0.95
ILR_SJ_22	2416	127	497	4605	-1.08
ILR_SV_2	900	51.4	104	6878	-1.03

*Calcite*

ILM_C_15	9182	-	140	0.72	-0.66
ILM_C_35	9120	-	2428	3.37	-0.89
ILM_C_44	8802	-	1916	23.6	-0.86 (-0.87)
ILM_C_49	8710	-	174	1.04	-0.80

*2.4.2 Calcite*

Table 2.1 presents elemental and Ca isotope data for calcite samples. The average  $\delta^{44/40}\text{Ca}$  equals  $-0.80 \pm 0.20\text{‰}$  ( $2\sigma_{\text{SD}}$ ,  $n = 4$ ), which is similar to the average of  $-0.79 \pm 0.34\text{‰}$  ( $2\sigma_{\text{SD}}$ ,  $n = 13$ ) for “zeolite zone” calcite reported in Jacobson et al. (2015). Calcite consistently has higher  $\delta^{44/40}\text{Ca}$  than basalt and primary minerals.

### 2.4.3 Zeolites

Table 2.2 provides elemental and Ca isotope data for bulk zeolites. Stilbite has the highest average  $\delta^{44/40}\text{Ca}$  ( $-0.72 \pm 0.24\text{‰}$ ,  $2\sigma_{\text{SD}}$ ,  $n = 3$ ), followed by scolecite ( $-0.84\text{‰}$ ,  $n = 1$ ), thomsonite ( $-0.94 \pm 0.18\text{‰}$ ,  $2\sigma_{\text{SD}}$ ,  $n = 3$ ), chabazite ( $-1.58 \pm 0.22\text{‰}$ ,  $2\sigma_{\text{SD}}$ ,  $n = 4$ ), mesolite ( $-1.78\text{‰}$ ,  $n = 1$ ), and heulandite ( $-1.81 \pm 0.28\text{‰}$ ,  $2\sigma_{\text{SD}}$ ,  $n = 5$ ).  $\delta^{44/40}\text{Ca}$  for stilbite and heulandite agree with previously reported values (Jacobson et al., 2015).

**Table 2.2.** Elemental and Ca isotope data for bulk zeolite minerals. Analyses not made due to limited sample sizes are marked with “-”.

Sample ID	Ca ( $\mu\text{mol/g}$ )	Na ( $\mu\text{mol/g}$ )	Sr ( $\text{nmol/g}$ )	Si ( $\mu\text{mol/g}$ )	Al ( $\mu\text{mol/g}$ )	$\delta^{44/40}\text{Ca}$ ( $\text{‰}$ )
<i>Heulandite</i>						
HD_1	1243	426	23551	9706	3130	-1.74
HD_11	1350	468	26254	9713	3209	-1.72
HD_18	1219	456	24593	9753	3062	-1.69
HD_23	1280	447	26143	9674	3107	-1.90
HD_28	1305	429	21123	-	-	-2.00
<i>Chabazite</i>						

CZ_54	1698	163	17815	7995	3662	-1.72
CZ_56b	1644	216	11681	8211	3550	-1.48
CZ_61	1640	317	12881	8240	3621	-1.49
CZ_62	1734	199	18117	8003	3729	-1.62
<i>Thomsonite</i>						
TM_57	1368	328	51.5	9293	3240	-0.91
TM_58	1415	474	38.1	9263	3211	-0.87
TM_63	1412	680	120	8960	3483	-1.04
<i>Stilbite</i>						
SB_17	1417	161	41.1	9796	2946	-0.62
SB_69	1401	157	95.5	9543	2750	-0.68
SB_73	1462	209	535	9651	3015	-0.85
<i>Mesolite</i>						
MS_50	1786	1689	3951	7183	5604	-1.78
<i>Scolecite</i>						
SC_3	1857	80.2	53.7	7940	4907	-0.84

## 2.5 Discussion

### 2.5.1 Controls on zeolite $\delta^{44/40}\text{Ca}$ .

#### 2.5.1.1 Kinetic Isotope Effects

A striking observation is that for each “zeolite zone” (Walker, 1960), coindex pairs have contrasting  $\delta^{44/40}\text{Ca}$  that bracket basalt, with one mineral lower and the other higher (Figure 2.2). Relative to basalt, the zeolites chabazite, mesolite, and heulandite have low  $\delta^{44/40}\text{Ca}$ , while their

respective pairs (thomsonite, scolecite, and stilbite) have high  $\delta^{44/40}\text{Ca}$ . Neglecting those that host significant  $^{40}\text{Ca}$  additions from the radioactive decay of  $^{40}\text{K}$  (Ryu et al., 2011), chabazite, mesolite, and heulandite represent some of the isotopically lightest minerals thus far measured (Fantle and Tipper, 2014; Gussone et al., 2020a; Antonelli and Simon, 2020). The data provide good evidence that zeolites fractionate Ca isotopes, as bulk basalt and primary mineral separates show effectively no isotopic variability (Figure 2.3).

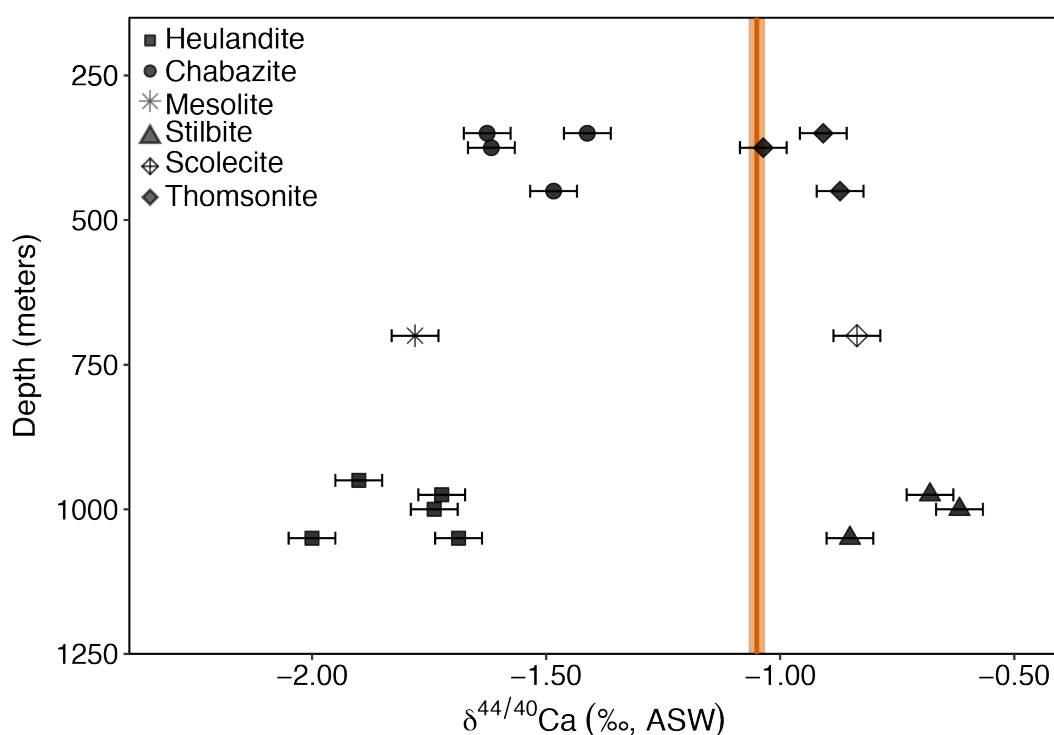


**Figure 2.2:**  $\delta^{44/40}\text{Ca}$  of bulk zeolites versus approximate burial depth in the Berufjörður-Breiðdalur region (Walker, 1960). Orange line shows the average value for all basalts analyzed here and by Jacobson et al. (2015), with the width encompassing the standard deviation ( $-1.05 \pm 0.03\text{‰}$ ,  $1\sigma_{\text{SD}}$ ,  $n = 11$ ). Error bars show external reproducibility ( $\pm 0.05\text{‰}$ ,  $2\sigma_{\text{SD}}$ ).

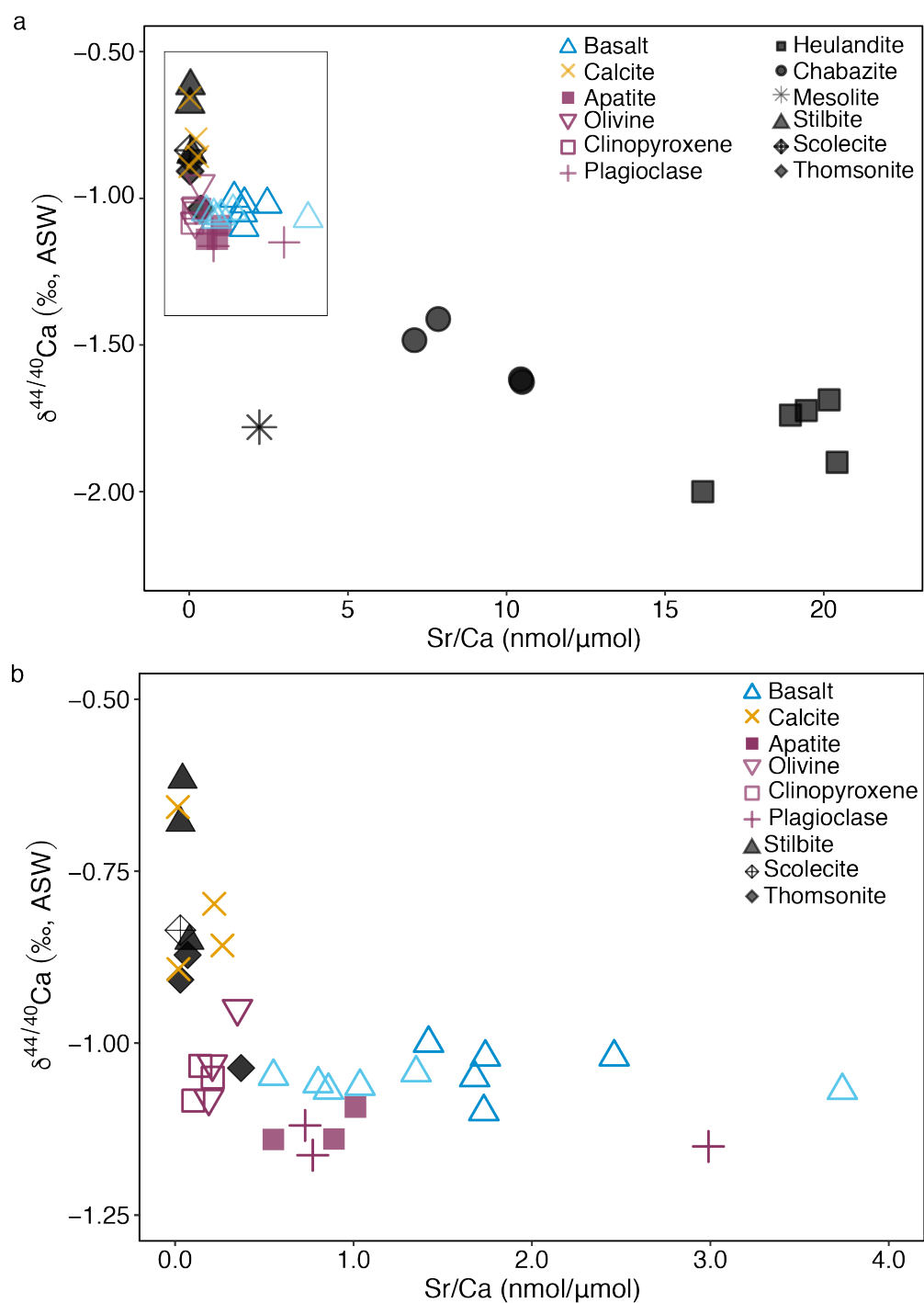


**Figure 2.3:**  $\delta^{44/40}\text{Ca}$  versus Sr/Ca for primary minerals, bulk basalt, calcite, and zeolites. (b) Inset from panel (a) includes basalt from the Berufjörður-Breiðdalur region (dark blue triangles), as well as basalt from previous studies (light blue triangles) (Jacobson et al., 2015). Symbol size is larger than external reproducibility ( $\pm 0.05\text{‰}$ ,  $2\sigma_{\text{SD}}$ ).

Many studies have shown that kinetic fractionation during mineral precipitation causes preferential uptake of lighter Ca isotopes relative to the main Ca reservoir (DePaolo, 2011; Gussone et al., 2020a). Other minerals measured thus far with low  $\delta^{44/40}\text{Ca}$  values similar to zeolites are mainly carbonates, which have experienced kinetic fractionation due to either variable precipitation rates (Tang et al., 2008a; Wang et al., 2021) or biogenic vital effects during mineral growth (Gussone et al., 2020a). Kinetic effects resulting in low  $\delta^{44/40}\text{Ca}$  have also been observed in some high-temperature silicate minerals (Zhao et al., 2017; Antonelli et al., 2019b, 2019a). However, unlike carbonates and primary rock-forming silicate minerals, all Ca in zeolites is exchangeable (Pabalan and Bertetti, 2001); therefore it cannot be assumed that kinetic fractionation mechanisms identified for the former minerals readily apply to zeolites. Kinetic isotope fractionation during mineral precipitation from solution mainly occurs due to incomplete exchange of ions or molecules, when transfer from solution to the solid proceeds more quickly than the reverse reaction (Schauble, 2004; DePaolo, 2011; Oelkers et al., 2019). Calcium ion-exchange in zeolite minerals is equilibrium controlled (Pabalan and Bertetti, 2001; Fridriksson, 2004), thus implying that forward and backward reaction rates are equal and proceed quickly. Nevertheless, I consider below potential transport-related kinetic isotope effects.

Zeolites consist of an aluminosilicate tetrahedral framework, where cations occupy specific exchange sites within void channels (Armbruster and Gunter, 2001). Isomorphic substitution of  $\text{Al}^{3+}$  for  $\text{Si}^{4+}$  in the tetrahedra creates a net negative charge in the zeolite framework, which is balanced by the uptake of mono- and divalent cations, including  $\text{Ca}^{2+}$ , from the coexisting solution (Armbruster and Gunter, 2001). Thus, coulombic forces related to charge density could in theory kinetically fractionate Ca isotopes due to variable mass-dependent

diffusion rates or other rate-dependent phenomena occurring at the mineral-fluid interface, or within the zeolite framework itself (Richter et al., 2009; Bourg et al., 2010; DePaolo, 2011; Hofmann et al., 2012). Charge density and distribution, as well as framework topology, control the ease and rate of Ca uptake and diffusion through zeolite frameworks (Pabalan and Bertetti, 2001; Kirov and Filizova, 2012; Baek et al., 2018). Commonly a proxy for charge density, and thus cation-exchange capacity, zeolite Si/Al ratios reflect the anionic field strength that attracts cations into the structure. In general, zeolites with lower Si/Al ratios have higher charge densities and more readily take up cations relative to those with higher Si/Al ratios and lower charge densities (Pabalan and Bertetti, 2001; Nakamura et al., 2014). If kinetic effects related to rates of Ca uptake or diffusion fractionated Ca isotopes, then a trend between zeolite Si/Al ratios and  $\delta^{44/40}\text{Ca}$  values should exist. However, I observe no trend for the present dataset, suggesting that charge density does not elicit kinetic isotope effects for these minerals (Figure A1).

One key point is that basalt represents the initial source of Ca in this system (Kristmannsdóttir and Tómasson, 1978; Neuhoff et al., 1999). If the occurrence of zeolites with  $\delta^{44/40}\text{Ca}$  higher than basalt was the result of a kinetic fractionation mechanism during mineral formation, this would require that zeolites with lower  $\delta^{44/40}\text{Ca}$  either precipitate faster or form first, thereby creating an isotopically enriched solution from which zeolites with higher  $\delta^{44/40}\text{Ca}$  later precipitate, as no kinetic fractionation mechanism could result in the preferential uptake of heavier Ca isotopes. Calculations and experiments employing solution chemistry and thermodynamic conditions have been used to predict the progression of zeolitization (Iijima, 1980; Donahoe and Liou, 1985; Liou et al., 1991; Kiseleva et al., 2001), and while petrographic evidence in some locations points to possible chronologic sequences of zeolites (Coombs et al.,

1959; Liou et al., 1985; Weisenberger and Bucher, 2011; Weisenberger et al., 2014), studies in Iceland indicate that the coindex pairs form simultaneously under similar conditions (Neuhoff et al., 1999; Weisenberger and Selbekk, 2009; Clark et al., 2019; Kristmannsdóttir and Tómasson, 1978). Furthermore, some coindex zeolite pairs analyzed here were intergrown and collected from a single amygdale, indicating simultaneous precipitation. Absence of clear evidence for kinetically-controlled “reservoir” effects is unsurprising, as all zeolite-bound Ca is “extra-framework,” with ion-exchange reactions between zeolites and fluids continuing long after initial growth of the aluminosilicate frameworks (Fridriksson et al., 2001; Fridriksson, 2004). Calculated equilibrium elemental compositions of zeolites, as well as those produced experimentally under equilibrium conditions, agree with geochemical analyses of natural Icelandic zeolites, which strongly indicates that the ion-exchange reactions are equilibrium-controlled (Fridriksson et al., 2001, 2009; Fridriksson, 2004). Because zeolites with identical formation conditions have contrasting  $\delta^{44/40}\text{Ca}$  and the ion-exchange processes governing Ca uptake are equilibrium-controlled, kinetic effects unlikely contribute to the  $\delta^{44/40}\text{Ca}$  variations observed here.

Another interesting observation is that zeolites with lower  $\delta^{44/40}\text{Ca}$  also have higher Sr/Ca (Figure 2.3). During calcite precipitation, rate-dependent shifts in Ca isotope fractionation and Sr partitioning produce linear correlations between  $\delta^{44/40}\text{Ca}$  values and Sr/Ca ratios (Tang et al., 2008a); however, the pattern observed in Figure 2.3 for zeolites is non-linear. In general, the understanding achieved for simple ionic solids does not immediately apply to more complex minerals, such as zeolites. Each zeolite studied here has a unique aluminosilicate framework. Incorporation of Sr into chabazite and heulandite, for example, is widely documented to reflect

underlying structural characteristics, where zeolite framework topology and local bonding conditions give rise to exchange sites that prefer Sr relative to Ca (Barrer and Klinowski, 1972; Armbruster, 1993; Gunter et al., 1994; Armbruster and Gunter, 2001; Fridriksson, 2004). The trend shown in Figure 2.3 provides evidence that structural properties known to control Sr incorporation may also discriminate Ca isotopes as well.

### *2.5.1.2 Equilibrium Isotope Effects*

I deduce that a fractionation mechanism related to mineral-specific Ca bonding conditions likely explains zeolite  $\delta^{44/40}\text{Ca}$  variability. Previous research has shown that Ca isotope fractionation significantly varies as a function of coordination number (CN) (Zhang et al., 1988; Gussone et al., 2005; Rustad et al., 2010; Colla et al., 2013; Moynier and Fujii, 2017), and relationships between  $\delta^{44/40}\text{Ca}$  and Ca-O bond length have been identified for carbonates, phosphates, hydrous minerals, silicates, and aqueous calcium (Rustad et al., 2010; Colla et al., 2013; Moynier and Fujii, 2017; Wenzhong et al., 2017; Antonelli et al., 2019b). Both a function of bond length and CN, bond strength (stiffness) determines isotope fractionation, where stronger bonds preferentially concentrate heavier isotopes (Chacko et al., 2001; Schauble, 2004).

The CN of Ca in zeolites can vary widely within each mineral because the minerals support a variety of exchange sites with unique Ca-O bonding conditions (Armbruster and Gunter, 2001). For example, Ca in chabazite could have a CN of 6 or 12 depending on which exchange site Ca occupies (Table 2.3) (Alberti et al., 1982). Moreover, within a given zeolite exchange site, Ca can coordinate to either framework oxygens ( $\text{O}_{\text{fmwk}}$ ), those composing molecular water also contained within the framework ( $\text{O}_{\text{w}}$ ), or some combination thereof. In

general,  $\text{Ca-O}_{\text{fmwk}}$  bonds are considerably longer than  $\text{Ca-O}_w$  bonds at a given site; thus, Ca-O bond lengths can vary greatly within one individual site, as well as between sites within a single mineral (Table 2.3). The effect of CN on bond strength is documented for mineral systems where most of the bonds contributing to the CN of Ca have nearly equal length, relative to zeolites, which support highly different Ca-O bond lengths (Rustad et al., 2010; Colla et al., 2013; Moynier and Fujii, 2017; Antonelli et al., 2019b). As the average CN of Ca per zeolite cannot take into account non-uniform bond lengths, the average Ca-O bond length per zeolite likely better approximates bond strength for this particular mineralogical system. Therefore, I calculated an average Ca-O bond length for each unique Ca site and used this as a proxy for the average Ca-O bond length per mineral, assuming Ca is evenly distributed across all potential sites (Table 2.3).

**Table 2.3.** Compilation of mineral data used for estimating average mineral Ca-O bond lengths. The calculation accounts for different cation bonding sites within tetrahedral frameworks specific to each zeolite, as well as different lengths of Ca-O bonds that vary with the type of O atom participating in the bond. See Methods section for equations and Table A1 for data sources.

Mineral Type	Site	Number of Ca-O <sub>w</sub> bonds, $N_w$	Number of Ca-O <sub>fmwk</sub> bonds, $N_{fmwk}$	Coordination Number for site, $CN_s$	Average Ca-O <sub>w</sub> bond length, $l_w$ (Å)	Average Ca-O <sub>fmwk</sub> bond length, $l_{fmwk}$ (Å)	Average site Ca-O bond length, $l_s$ (Å)	$f_{Ca}$ in each site	Weighted average mineral Ca-O bond length, $L$ (Å)
<i>Stilbite</i>	Ca-only	8	0	8	2.45		2.45	1	2.45
<i>Mesolite</i>	Ca-only channel	3	4	7	2.34	2.51	2.44	1	2.44
	Na-only channel	2	4	6				0	
<i>Scolecite</i>	Ca-only channel	3	4	7	2.34	2.53	2.45	1	2.45
<i>Thomsonite</i>	Ca-only	2	4	6	2.39	2.52	2.48	0.5	
	Ca or Na	4	4	8	2.56	2.57	2.57	0.5	2.52
<i>Chabazite</i>	C1- Ca-only	0	6	6		3.05	3.05	0.25	
	C2	0	6	6		2.80	2.80	0.25	
	C3	8	4	12	2.36	2.82	2.51	0.25	2.76
	C4- Ca-only	0	8	8		2.67	2.67	0.25	
<i>Heulandite</i>	Ca2	5	3	8	2.63	2.85	2.71	0.333	
	Ca or Na	4	5	9	2.65	2.81	2.74	0.333	2.79
	K3	2	6	8	2.92	2.93	2.93	0.333	

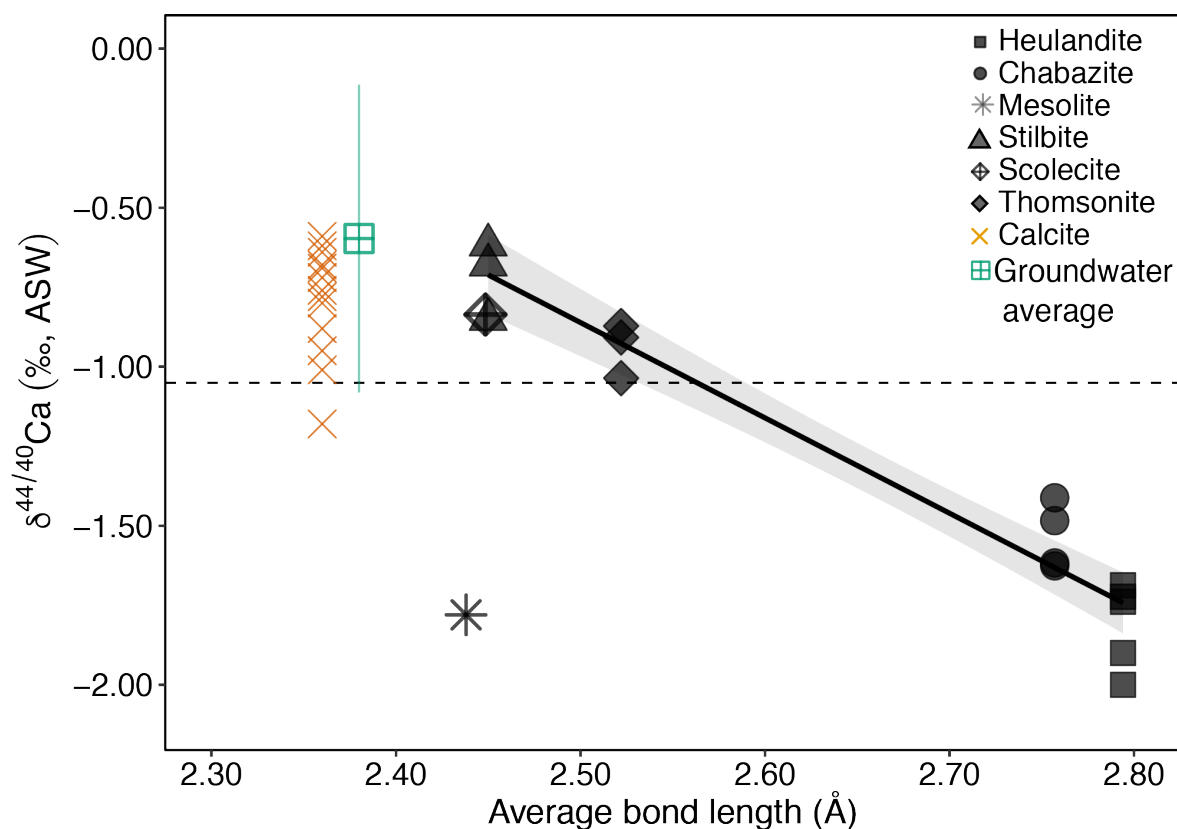


**Figure 2.4:** Zeolite  $\delta^{44/40}\text{Ca}$  versus estimated average Ca-O bond length for each mineral. Also shown are data for calcite from this study, “zeolite zone” calcite from Jacobson et al. (2015). The average of natural groundwaters (Jacobson et al., 2015) and pre-injection groundwaters from the CarbFix1 site (Pogge von Strandmann et al., 2019a), which circulate through active zeolite zones analogous to the extinct system studied here (Alfredsson et al., 2013), is also shown. The black dashed line shows the average value for Icelandic basalt ( $-1.05\text{‰}$ ) determined from this study and Jacobson et al. (2015). Average Ca-O bond length and  $\delta^{44/40}\text{Ca}$  of bulk zeolites strongly correlate ( $R^2 = 0.93$ ,  $p < 0.001$ ), when mesolite is excluded from the regression. The grey shading represents the confidence interval of this regression (see Appendix A for details of the statistical model).

When zeolite  $\delta^{44/40}\text{Ca}$  values are plotted versus average Ca-O bond length per mineral (Figure 2.4), five of the six zeolites studied generate a significant correlation ( $R^2 = 0.93$ ,  $p < 0.001$ ). In general, zeolites with lower  $\delta^{44/40}\text{Ca}$  have longer approximate Ca-O bond lengths,

while zeolites with higher  $\delta^{44/40}\text{Ca}$  have shorter approximate Ca-O bond lengths, consistent with equilibrium isotope fractionation theory (Urey, 1947; Schauble, 2004). While CN can adequately predict bond strength for many mineral systems (Zhang et al., 1988; Gussone et al., 2005, 2020a; Rustad et al., 2010; Colla et al., 2013; Antonelli and Simon, 2020), the observation that stilbite (CN = 8) and scolecite (CN = 7) have nearly identical average Ca-O bond lengths and  $\delta^{44/40}\text{Ca}$  values supports our assumption that bond length better approximates the effect of bond strength on Ca isotope fractionation for zeolites. I suggest that differences in zeolite Ca-O bond energies underlie the trend between  $\delta^{44/40}\text{Ca}$  and bond length shown in Figure 2.4, which I interpret as evidence for equilibrium isotope partitioning.

In the context of isotope fractionation between solution and mineral, it is important to consider Ca-O bonding dynamics in the surrounding fluid. Aqueous  $\text{Ca}^{2+}$  coordinates to water O atoms in “coordination spheres” or “hydration spheres”, which have shorter Ca-O bond lengths than zeolites (Moynier and Fujii, 2017). Icelandic groundwater has higher  $\delta^{44/40}\text{Ca}$  values than zeolites (Figure 2.4), consistent with predictions from equilibrium fractionation theory that stronger bonds preferentially concentrate heavier isotopes (Urey, 1947; Bigeleisen and Mayer, 1947; Schauble, 2004). The exchange of Ca between groundwater and zeolite frameworks involves breaking a certain number of Ca-O<sub>w</sub> bonds in the hydration spheres (“desolvation”) to create Ca-O<sub>fmwk</sub> bonds (Kirov and Filizova, 2012). Theoretical studies focusing on calcite have argued that desolvation can elicit kinetic isotope effects due to faster bond breaking of hydration spheres containing lighter Ca isotopes (Hofmann et al., 2012; Lammers et al., 2020). If such a mechanism applied here, then minerals requiring more bond breaking of hydration spheres (i.e., those comprising fewer Ca-O<sub>w</sub> bonds) should preferentially incorporate lighter Ca isotopes.

However, this pattern is not observed. For example, heulandite and thomsonite only need to break three to four hydration sphere bonds but show greater apparent fractionations than calcite, which must break at least six hydration sphere bonds, as the mineral supports no Ca-O<sub>w</sub> bonds. Stilbite has only Ca-O<sub>w</sub> bonds (Table 2.3), implying an absence of desolvation, yet Icelandic calcite and stilbite have similar  $\delta^{44/40}\text{Ca}$  (Figure 2.3). Additionally, chabazite has the least Ca-O<sub>w</sub> bonds of all zeolites studied here, but shows higher  $\delta^{44/40}\text{Ca}$  than heulandite. In parallel, heulandite and thomsonite have the same proportions of Ca-O<sub>w</sub> bonds relative to total Ca-O bonds, suggesting that these two minerals should desolvate hydration spheres identically, but heulandite has much lower  $\delta^{44/40}\text{Ca}$  values than thomsonite. While more research is needed to constrain relationships between zeolite structural characteristics, desolvation kinetics, and Ca isotope fractionation, our present observations better support an equilibrium isotope effect related to mineral Ca-O bond lengths.

Mesolite is the only exception to the relationship shown in Figure 2.4. This zeolite and scolecite support identical Ca-site structures, but the mesolite framework also comprises alternating channels of Ca- and Na- sites (Artioli et al., 1986; Kol'tsova, 2010). Our bond length estimate assumes that all Ca in mesolite resides in the Ca channel; however, Ca can substitute into the Na channel, where it coordinates to O<sub>fmwk</sub> with much longer bonds than in the Ca channel (Ståhl and Thomasson, 1994; Kirfel and Gibbs, 2000). For this particular sample, it is possible that a substantial proportion of the Ca occupies the Na channel, where Ca-O<sub>fmwk</sub> bond lengths are longer than our calculation estimates. Thus, accumulation of lighter Ca isotopes in the Na channel could explain the sample's lower  $\delta^{44/40}\text{Ca}$  value. Similar observations of bond lengths varying with elemental substitutions have been made for calcite and other silicates,

where Mg/Ca ratios discernably correlate with  $\delta^{44/40}\text{Ca}$  (Feng et al., 2014; Antonelli and Simon, 2020).

An alternative explanation is that mesolite experienced kinetic isotope effects. The Ca sites in mesolite and scolecite have identical framework topologies, Ca-O bond lengths, and CNs. Theory for this scenario dictates that contrasting Ca isotope ratios could reflect kinetic isotope effects (Antonelli and Simon, 2020). However, because precipitation rate effects observed for other types of minerals do not apply to zeolites, which participate in equilibrium-controlled ion-exchange after initial precipitation, the exact mechanism that would produce kinetic isotope effects is uncertain. Nevertheless, the data imply that mesolite is the most likely candidate of all zeolites examined here to have experienced kinetic fractionation. If correct, then our observation that mesolite plots “off” the line in Figure 2.4 only supports equilibrium isotope partitioning for the other minerals.

Barring the one mesolite sample, bulk zeolite  $\delta^{44/40}\text{Ca}$  values inversely vary with approximate Ca-O bond lengths. While I interpret this pattern to reflect inter-mineral equilibrium isotope partitioning, more research is needed to better constrain zeolite fractionation mechanisms. The correlation between zeolite Ca-O bond lengths and  $\delta^{44/40}\text{Ca}$  reported here is consistent with theoretical (Rustad et al., 2010; Feng et al., 2014; Moynier and Fujii, 2017; Wenzhong et al., 2017; Aufort et al., 2017), laboratory (Gussone et al., 2005; Griffith et al., 2008; Colla et al., 2013), and field studies of other mineral types (Huang et al., 2010; Antonelli et al., 2019b; Chen et al., 2020; Gussone et al., 2020b; Antonelli and Simon, 2020). Our study is the first to report such effects in zeolites, as few studies have investigated  $\delta^{44/40}\text{Ca}$  variability in minerals that form in nature at intermediate temperatures. Our interpretation is also consistent

with an early investigation reporting that fractionation of Li and K isotopes by zeolites during ion-exchange is largely equilibrium-controlled (Taylor and Urey, 1938).

While structural differences between zeolite frameworks adequately explains  $\delta^{44/40}\text{Ca}$  variability, I do note that the Ca isotope offsets between the coindex pairs increases with depth (Figure 2.2), which counters the expectation that higher temperatures diminish equilibrium isotope fractionation (Urey, 1947). This only underscores the first order control of mineral structure, where a positive correlation exists between degree of isotopic offset and Ca-O bond-length difference between pairs. Whereas zeolite Si and Al framework structures are “set” during initial crystallization and offer a diagnostic tool for identifying temperature-dependent depth zones (Walker, 1960; Neuhoff et al., 1999), the Ca isotope geochemistry of the structures could more relate to the temperature of groundwater, as zeolites participate in equilibrium-controlled ion-exchange reactions later in time (Neuhoff et al., 1999; Fridriksson, 2004; Fridriksson et al., 2009). Calcium isotopes could be developed into a proxy for circulating fluid temperature; however, more studies are needed to better elucidate equilibrium versus kinetic controls on fractionation and fully quantify fractionation factors for each mineral relative to solution. Nevertheless, our present findings illustrate potential for developing an entirely new “geothermometer” for investigating low-grade basalt metamorphism, as well as probing a diverse range of other environments where zeolites form (Lisitzina and Butuzova, 1982; Hay and Sheppard, 2001).

### 5.2.2 Controls on hydrothermal water $\delta^{44/40}\text{Ca}$ .

Primary minerals display limited Ca isotope contrast and bracket  $\delta^{44/40}\text{Ca}$  values of bulk basalt (Figure 2.3). This confirms previous suggestions that the limited Ca isotope variability of Icelandic basalt is due to a narrow range of primary mineral  $\delta^{44/40}\text{Ca}$  (Jacobson et al., 2015). The source of fluid in the system studied here is meteoric (Kristmannsdóttir and Tómasson, 1978; Mehegan et al., 1982; Fridriksson, 2004), which implies that its initial  $\delta^{44/40}\text{Ca}$  value is rock-dominated ( $\sim -1\text{‰}$ ). No evidence exists for preferential Ca isotope release during primary silicate mineral dissolution for any silicate rock type. Therefore, hydrothermal waters and calcite in Iceland must be driven heavy as a byproduct of secondary light Ca sinks. During hydrothermal alteration of basalt, Ca-bearing zeolites and calcite are the two main sinks of aqueous  $\text{Ca}^{2+}$  (Gysi and Stefánsson, 2012c; Aradóttir et al., 2012), with zeolites forming distinctly prior to calcite (Neuhoff et al., 1999; Gysi and Stefánsson, 2008; Aradóttir et al., 2012; Snæbjörnsdóttir et al., 2017; Clark et al., 2019). Smectite and mixed layer clays form before zeolites, but they incorporate little Ca by comparison (Neuhoff et al., 1999; Weisenberger and Selbekk, 2009; Aradóttir et al., 2012; Alfredsson et al., 2013; Weisenberger et al., 2020). The low  $\delta^{44/40}\text{Ca}$  values of chabazite, mesolite, and heulandite indicate that fractionation by zeolites overshadows any effects due to  $\text{Ca}^{2+}$  adsorption onto clays. If a significant amount of clay with low  $\delta^{44/40}\text{Ca}$  values formed prior to zeolites, then all zeolites would have elevated  $\delta^{44/40}\text{Ca}$  values, due to a reservoir effect, which is not the observed pattern. Thus, either clays are negligible Ca sinks or they have negligible Ca isotope fractionation factors. Recent research has attributed elevated  $\delta^{44/40}\text{Ca}$  in CCS waters to the formation of isotopically light calcite (Pogge von Strandmann et al., 2019a), but no such calcite, whether anthropogenic or natural, has been measured in the

Icelandic system. However, similar to natural hydrothermal waters (Gislason and Arnórsson, 1993; Flaathen et al., 2009; Alfredsson et al., 2013; Pogge von Strandmann et al., 2016; Thomas et al., 2016), CCS waters are supersaturated with respect to zeolites after periods of CO<sub>2</sub> injection (Aradóttir et al., 2012; Snæbjörnsdóttir et al., 2017; Clark et al., 2019). While some zeolites do show higher  $\delta^{44/40}\text{Ca}$  than basalt, the depth trend presented here is clearly asymmetric, where negative fractionations are larger (Figure 2.2). Thus, it follows that progressive ion-exchange with zeolites would elevate groundwater  $\delta^{44/40}\text{Ca}$ , supporting previous suggestions that uptake of lighter Ca isotopes by zeolites enriches hydrothermal waters in heavier isotopes (Hindshaw et al., 2013; Jacobson et al., 2015; Andrews and Jacobson, 2017).

Studies of other groundwater systems have suggested that preferential uptake of light Ca by anhydrite or calcite elevates water  $\delta^{44/40}\text{Ca}$  values relative to source rocks (Amini et al., 2008; Druhan et al., 2013; Brown et al., 2013; Syverson et al., 2018). Zeolites form ubiquitously at temperatures ranging from  $\sim 30^\circ\text{C} - 150^\circ\text{C}$  during the hydrous alteration of silicates in many diverse environments (Chipera and Apps, 2001; Utada, 2001). Our results emphasize a need to consider Ca uptake by zeolites in studies aimed at understanding the geochemical evolution of natural groundwater, as well as CCS waters monitored during mineral carbonation of basalt (Syverson et al., 2018; Pogge von Strandmann et al., 2019a; Antonelli and Simon, 2020; Mayfield et al., 2021).

### 2.5.3 Controls on calcite $\delta^{44/40}\text{Ca}$

The overlapping range of calcite and hydrothermal water  $\delta^{44/40}\text{Ca}$  in Iceland suggests that  $\Delta^{44/40}\text{Ca}_{\text{cal-sol}}$  is close to 0‰ (Jacobson et al., 2015), similar to patterns documented in other natural systems, where calcite slowly forms about the state of chemical equilibrium (Fantle and

DePaolo, 2007; Jacobson and Holmden, 2008). Equilibrium isotope effects appear to control the Ca isotope composition of zeolites, given the strong linear correlation between zeolite Ca-O bond lengths and  $\delta^{44/40}\text{Ca}$  (Figure 2.4). Many hydrothermal calcite samples also have  $\delta^{44/40}\text{Ca}$  values that closely approach this line, suggesting a similar control by Ca-O bond length. I therefore propose that the unusually high  $\delta^{44/40}\text{Ca}$  of Icelandic hydrothermal calcite reflects the influence of zeolites on hydrothermal water  $\delta^{44/40}\text{Ca}$ . Because calcite samples display a range of  $\delta^{44/40}\text{Ca}$  (Figure 2.4), it is possible that the lighter calcite samples may have precipitated from hydrothermal waters that isotopically evolved to differing degrees. Alternatively, kinetic isotope effects due to variable precipitation rates may have contributed to the lower  $\delta^{44/40}\text{Ca}$  of some calcites relative to hydrothermal water. Regardless, it is likely that many Icelandic hydrothermal calcites have  $\delta^{44/40}\text{Ca}$  values consistent with equilibrium isotope control.

While several studies have identified how variable Ca coordination controls *inter-mineral* equilibrium isotope partitioning (Gussone et al., 2005; Griffith et al., 2008), few have determined the effects of CN on *mineral-fluid* Ca isotope partitioning during natural calcite growth (Mills et al., 2021). Calcite supports only one Ca site having Ca-O bonds of uniform length (Reeder, 1983; Skinner and Jansen, 1994; Smyth and Ahrens, 1997; Rustad et al., 2010); therefore, unlike zeolites, the CN for calcite adequately approximates bond strength and subsequent isotopic effects. Calcium in calcite coordinates to six O atoms (Reeder, 1983). Thus, calcite has a lower CN than any of the zeolites examined in this study (Table 2.3). It follows that calcite should have higher  $\delta^{44/40}\text{Ca}$  than zeolites, which is the relationship observed in Figure 2.4. Experimental results and calculations have demonstrated that Ca isotope fractionation during mineral precipitation depends on the CN of mineral Ca, as well as the CN of aqueous  $\text{Ca}^{2+}$ , which can

range from six to ten (Hewish et al., 1982; Rustad et al., 2010; Hofmann et al., 2012; Colla et al., 2013; Moynier and Fujii, 2017). Because Icelandic calcite appear to imprint the  $\delta^{44/40}\text{Ca}$  of hydrothermal waters and plot near the equilibrium-controlled zeolite Ca-O bond-length line, I suggest that aqueous  $\text{Ca}^{2+}$  in this system likely has a CN of six. Calcite, which has a known CN and a well constrained Ca-O bond length, shows similar  $\delta^{44/40}\text{Ca}$  and bond length to Icelandic groundwater; thus, it follows that these reservoirs likely have similar CN. The isotopic offset between water and zeolites further implies that the CN of aqueous  $\text{Ca}^{2+}$  must be lower than those of zeolites (lowest CN = 7) and more similar to that of calcite (CN = 6). The apparent offset between Ca-O bond lengths for calcite and hydrothermal water (Figure 2.4) is likely a consequence of our assumptions, as bond lengths in calcite vary with impurities (Rustad et al., 2010; Wenzhong et al., 2017), and bond lengths for sixfold coordinated aqueous  $\text{Ca}^{2+}$  vary with temperature, ion-pairing, and fluid ionic strength among other factors (Hewish et al., 1982; Todorova et al., 2008; Hofmann et al., 2012; Colla et al., 2013; Moynier and Fujii, 2017).

Our results suggest that equilibrium-controlled calcite  $\delta^{44/40}\text{Ca}$  values could be used to identify the CN of aqueous  $\text{Ca}^{2+}$ , and that laboratory studies able to control the CN of aqueous  $\text{Ca}^{2+}$  could better constrain equilibrium isotope effects in synthesized calcites. In this context, the equilibrium isotopic offset between calcite and water ( $\Delta^{44/40}\text{Ca}_{\text{cal-sol}}$ ), which is generally accepted to be  $\sim 0\text{‰}$  given small  $\Delta^{44/40}\text{Ca}_{\text{cal-sol}}$  observed in natural settings where calcite precipitates near chemical equilibrium (Jacobson and Holmden, 2008; Blättler et al., 2021), could be interpreted not only as an absence of kinetic isotope effects, but also as an indication that aqueous  $\text{Ca}^{2+}$  and calcite Ca both have a CN of six. This potentially has significant implications for various applications of the Ca isotope tracer, as the CN of aqueous  $\text{Ca}^{2+}$  can vary with ionic strength and

temperature (Hewish et al., 1982; Lim et al., 2009), which could theoretically impact the equilibrium isotope fractionation factor between calcite and water. For example, if fluid  $\text{Ca}^{2+}$  was coordinated to eight oxygens instead of six (likely resulting in longer bond lengths in the hydration sphere (Katz et al., 1996)),  $\Delta^{44/40}\text{Ca}_{\text{cal-sol}}$  at equilibrium would be nonzero and positive, resulting in calcite that is enriched in heavier Ca isotopes (Rustad et al., 2010; Colla et al., 2013; Moynier and Fujii, 2017). Further work is needed to explore these ideas; however, our findings provide a valuable perspective on mineral-fluid isotope equilibrium, which could have implications for interpreting the  $\delta^{44/40}\text{Ca}$  values of marine carbonates deposited throughout geologic history.

## 2.6 Conclusions

This study reports novel Ca isotope data for natural zeolite minerals from Iceland, as well as hydrothermal calcite, bulk basalt, and primary mineral separates. Zeolite minerals display a  $\delta^{44/40}\text{Ca}$  range of  $\sim 1.4\%$ , which is on the order of the range exhibited by all igneous rocks thus far measured (Fantle and Tipper, 2014; Antonelli and Simon, 2020). Zeolite  $\delta^{44/40}\text{Ca}$  values strongly correlate with average Ca-O bond lengths, which I interpret to reflect equilibrium isotope partitioning. The bond length hypothesis presented here also provides some evidence that equilibrium isotope effects control  $\Delta^{44/40}\text{Ca}$  between hydrothermal calcite and waters, given that these reservoirs support similar Ca-O bond lengths and display small isotopic offsets. As equilibrium isotope fractionation factors strongly depend on temperature (Urey, 1947), our findings suggest that the Ca isotope geochemistry of zeolite minerals could be developed into an entirely new “geothermometer” for investigating low-grade basalt metamorphism. Moreover,

zeolites should be considered in Ca isotope studies of other continental and oceanic hydrothermal systems where the minerals pervasively occur. Calcium isotopes hold particular promise for quantifying the mineralization of injected CO<sub>2</sub> during mineral carbonation of basalt, which is a leading carbon capture and storage (CCS) strategy (Pogge von Strandmann et al., 2019a; Snæbjörnsdóttir et al., 2020). Our study characterizes the composition of key mineral reservoirs necessary for interpreting and modeling Ca isotope variations in both field and theoretical CCS studies. Lastly, more research dedicated to the Ca isotope geochemistry of zeolites could help improve numerous environmental, industrial, and medical applications of the minerals.

## Chapter 3

### Controls on riverine calcium isotope ratios during basalt weathering in the Skagafjörður watershed, Iceland

#### 3.1 Introduction

Calcium (Ca) is the fifth most abundant element in Earth's crust and plays a key role in the long-term carbon cycle (Urey, 1952; Fleischer, 1954; Berner, 1992). The weathering of Ca-bearing silicate minerals and subsequent precipitation of carbonate minerals in the oceans sequesters atmospheric CO<sub>2</sub> and thus regulates Earth's climate over geologic timescales (Walker et al., 1981; Berner et al., 1983; Ridgwell, 2003). Investigating parameters that influence riverine Ca fluxes to the oceans is therefore central to understanding the role of silicate weathering in long-term climate regulation.

Stable Ca isotope ratios offer a powerful tool for study of chemical weathering processes (Griffith et al., 2020). Calcium isotope ratios are reported in delta notation as  $\delta^{44/40}\text{Ca}_{smp} (\text{‰}) = [({}^{44}\text{Ca}/{}^{40}\text{Ca})_{smp}/({}^{44}\text{Ca}/{}^{40}\text{Ca})_{std} - 1] \times 1000$ , where *smp* refers to the sample and *std* refers to the normalizing standard, which in this study is OSIL Atlantic Seawater or ASW. Many processes influence the Ca isotope geochemistry of rivers. Riverine  $\delta^{44/40}\text{Ca}$  values can identify mineralogical sources of Ca to rivers (Ryu et al., 2011; Moore et al., 2013; Jacobson et al., 2015; Lehn et al., 2017; Pogge von Strandmann et al., 2019b). Other processes that influence Ca cycling can fractionate Ca isotopes and alter riverine  $\delta^{44/40}\text{Ca}$  values, such as secondary mineral precipitation (Tipper et al., 2006b, 2008; Hindshaw et al., 2013; Yan et al., 2016), vegetation uptake (Cenki-Tok et al., 2009; Schmitt et al., 2012; Moore et al., 2013; Bagard et al., 2013) and

adsorption onto clay mineral surfaces (Teichert et al., 2009; Hindshaw et al., 2011; Fantle et al., 2012; Brazier et al., 2019).

Basalt weathering has been implicated as having a disproportionate role in long-term climate regulation (Dessert et al., 2003), as basalt comprises mafic minerals that are inferred to weather more readily than felsic minerals (Goldich, 1938), and high solute fluxes from basaltic settings, such as Iceland (Gislason et al., 1996, 2009; Stefansson and Gislason, 2001; Georg et al., 2007; Louvat et al., 2008; Eiriksdottir et al., 2013), the Deccan traps (Dessert et al., 2001; Das et al., 2005b, 2005a, 2006; Gupta et al., 2011; Babechuk et al., 2014), and Réunion Island (Louvat and Allègre, 1997; Rad et al., 2007), have been interpreted as evidence for rapid CO<sub>2</sub> consumption (Dessert et al., 2003; Hartmann et al., 2014; Ibarra et al., 2016). In Iceland, Ca isotopes can potentially be utilized to apportion riverine solute fluxes among basalt and calcite weathering because Icelandic basalt and calcite have contrasting  $\delta^{44/40}\text{Ca}$  values (Hindshaw et al., 2013; Jacobson et al., 2015; Nelson et al., 2021). Since the weathering of carbonate minerals has no net effect on long-term climate (Berner et al., 1983), riverine Ca fluxes from carbonate minerals must be constrained prior to using riverine solute fluxes to quantify the role of silicate weathering on climate. Icelandic rivers show elevated  $\delta^{44/40}\text{Ca}$  values, similar to the  $\delta^{44/40}\text{Ca}$  values of calcite (Jacobson et al., 2015). However, uptake of lighter Ca isotopes may also elevate Icelandic riverine  $\delta^{44/40}\text{Ca}$  values (Hindshaw et al., 2013). Thus, potential fractionation mechanisms must be identified and quantified prior to employing riverine  $\delta^{44/40}\text{Ca}$  values to apportion Ca sources.

This contribution presents a high-resolution study of the Skagafjörður region in North Iceland. Aimed at characterizing processes that may fractionate Ca isotopes and elevate riverine

$\delta^{44/40}\text{Ca}$  values, I use a high-precision Thermal Ionization Mass Spectrometry (TIMS) method (Lehn et al., 2013) to measure a variety of samples that serve as reservoirs of Ca, including rocks, rivers, soil, vegetation, calcite, and suspended sediments. I also investigate the controls on groundwater  $\delta^{44/40}\text{Ca}$  values from thermal and non-thermal springs. I consider the relative impacts of both fractionation and source mixing control on the  $\delta^{44/40}\text{Ca}$  values of Skagafjörður rivers. Results from this study demonstrate the ability of Ca isotopes to trace mineralogical sources of riverine Ca, which has key implications for understanding the nature of the basalt weathering feedback on long-term global climate.

### **3.2 Geologic and Climatic Setting**

Iceland is an exposed section of the North Atlantic Mid Ocean Ridge overlying a mantle plume, which has caused extensive rifting and volcanism over the past 50-60 Myr (White and McKenzie, 1989). Iceland mainly comprises basalt (80-85%) (Gislason et al., 1996), which generally increases in age from the center of the island outward, where some rocks date to ~16 Myr (Moorbath et al., 1968). This study primarily focused on the Skagafjörður valley in North Iceland (Figure 3.1), although, as noted below, additional samples were collected from other locations.

The Skagafjörður valley encompasses an area of 3,650 km<sup>2</sup>, extending from the Hofsjökull ice cap in the central highland region to the north coastline. The mean annual temperature and precipitation are 3.1°C and 514 mm. Arnórsson et al. (2002) presents an in-depth description of the regional geology. In brief, well-crystallized, Tertiary tholeiitic flood basalts form most of the bedrock in the Skagafjörður valley. The succession is ~ 7 km thick, and

the oldest rocks have an age of ~12 Myr. Mountains on either side of the valley have a maximum elevation of ~1,300 m and generally comprise unaltered rocks, whereas vesicles in rocks in the valley host secondary minerals, namely calcite and chalcedony, but also lesser amounts of low-temperature (~30°C to 100°C) zeolites, such as chabazite, thomsonite, and analcime (Saemundsson et al., 1980). Drill core data from the neighboring Eyjafjörður valley to the east suggest that depth-dependent zeolite zones, similar to those documented elsewhere in Iceland (Walker, 1960, 1964; Neuhoff et al., 1999; Weisenberger and Selbekk, 2009), extend beneath the central Skagafjörður valley floor to a depth of ~2000 m (Saemundsson et al., 1980; Fridriksson et al., 2009).

Main stem Skagafjörður rivers are largely fed by the Hofsjökull ice cap in the highland region of Hofsafrétt, where basalt is much younger (middle Pleistocene-modern) and has a higher (~80%) glass content (Franzson et al., 2011; Hjartarson and Saemundsson, 2014). The Austari-Jökulsá and Vestari-Jökulsá rivers are sediment-laden, relatively steep gradient glacial rivers that flow northward from the highland region and converge at lower elevations in the Skagafjörður valley. The Hofsa and Svartá rivers are also main stem rivers with headwaters in the highlands. The largest and most central lowland Skagafjörður river is the Héraðsvötn, which is formed by the confluence of the Austari-Jökulsá and Vestari-Jökulsá rivers. The valley floor is initially ~7 km wide at the southern end of the Skagafjörður valley and gradually widens to ~11 km at the mouth of the Héraðsvötn. The Héraðsvötn also receives inputs from tributaries draining the surrounding mountains on the eastern and western flanks of the valley, most of which can be categorized as direct-runoff rivers. Numerous cold and hot groundwater springs emerge along the Héraðsvötn river, with temperatures generally decreasing northward away from

the active rift zone (Arnórsson et al., 2002; Arnórsson and Sveinbjörnsdóttir, 2004; Fridriksson et al., 2009). All Skagafjörður valley rivers, including tributaries, support andosol soils covered by grass, small shrubs and groundcover, but few trees. The soils are brown andosols and mainly comprise basaltic and rhyolitic tephra, aeolian material, and some (~10 – 30%) secondary weathering products, which mainly include poorly crystalline allophane and ferrihydrite but not pedogenic carbonate (Stefansson and Gislason, 2001; Arnalds, 2004, 2015a). The Héraðsvötn river floodplain contains thick (~1 - 3 m) peat soils and wetlands, where the Héraðsvötn river approaches the fjord. In contrast, the glaciated highland region is devoid of soil and vegetation.

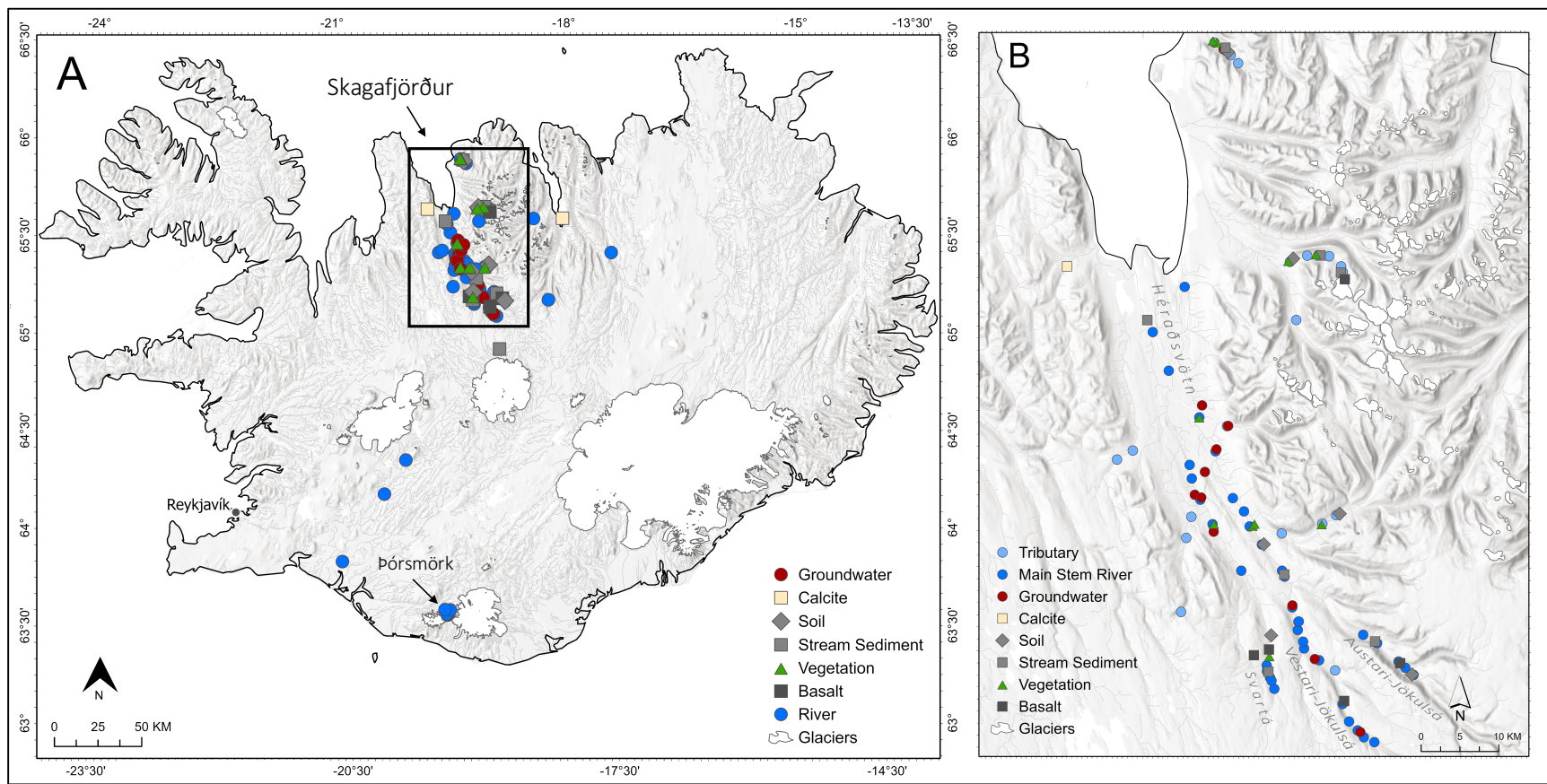


**Figure 3.1:** (A) Map of Iceland showing sample locations for all samples included in this study, where the box in “A” outlines the Skagafjörður region, shown in higher resolution in panel “B”. (B) Details of locations of samples collected from the Skagafjörður region.

### 3.3 Methods

#### 3.3.1 Sample collection

Figure 3.1 shows locations for all samples collected in this study. At each sample location, GPS data was recorded with a Garmin 60Csx handheld GPS meter (Appendix B). All rivers are categorized as either “tributary,” which refers to smaller, clear, direct-runoff streams that exclusively drain non-glacial lowland watersheds or “main stem,” which refers to larger, sediment-laden, glacial rivers that receive inputs from both highland and lowland watersheds. In July of 2017 and 2019, river water samples, as well as groundwater samples from springs and wells, were collected from locations throughout the Skagafjörður valley. Additional main stem lowland samples were taken from the Eyjafjörður, Hvítá, Þjórsá, and Skjálfandafljót, which drain other regions in Iceland, and two rivers from the southern region of Þórsmörk, the Krossá and Hvanná rivers (Figure 1). The Hvanná river is mostly fed by a CO<sub>2</sub>-rich spring that emerges from beneath the Eyjafjallajökull ice cap (Olsson et al., 2014). In total, I collected 75 river water samples and 11 groundwater samples.

Water pH and temperature were measured on-site using a Thermo-Scientific Orion 3-Star Portable pH Meter equipped with a temperature probe and a glass-body Orion 8104BNUWP ROSS rugged bulb pH electrode. The electrode was calibrated daily with pH 4, 7, and 10 buffers. Water samples were collected using a peristaltic pump and filtered through Geotech 0.45 µm filters containing Versapor membranes. Samples for cation, Si, and Ca isotope analyses were collected into I-CHEM HDPE bottles and acidified to pH <2 with ultrapure, concentrated HNO<sub>3</sub>. Samples for anion and alkalinity analyses were filtered into LDPE bottles. Total carbonate alkalinity ( $A_T = [\text{HCO}_3^-] + 2[\text{CO}_3^{2-}]$ ) in µeq/L was measured by Gran Titration with 0.02N HCl.

Uncertainty of this method was determined to be  $\pm 5\%$  by repeated measurements of a gravimetric  $\text{Na}_2\text{CO}_3$  standard. Given the pH range of water samples, alkalinity is assumed to equal bicarbonate anion concentration. Water samples for  $\delta^{13}\text{C}_{\text{DIC}}$  analyses were collected using BD 5 mL sterile syringes equipped with Precision Glide 23-gauge needles, and samples were filtered through Whatman Puradisc 25 mm polypropylene 0.45  $\mu\text{m}$  filters into white-cap 12 mL round-bottom Exetainers.

Rock, bedload sediment, calcite, soil, and vegetation samples were collected into LDPE bags. Calcite samples were collected from an outcrop that was partially submerged by river water. In addition, calcite samples intergrown with zeolites were collected from the chabazite-thomsonite zone exposed in the adjacent Eyjafjörður valley, and travertine samples were taken from the Hvanná river. Soil pits were dug on convex hilltops, and visible horizons were sampled after measuring depths. Suspended sediment samples were collected on pre-weighed glass-microfiber filters by vacuum-pumping water through a porcelain Buchner funnel into an Erlenmeyer flask. Water collected in the flask was then poured into a graduated cylinder, and the total volume of water passed through the filter was recorded. This study also included an attempt to analyze the Ca isotope geochemistry of colloids. Methods, results, and supporting experiments related to the collection of these samples are described in Appendix C.

### *3.3.2 Sample preparation*

Whole rock samples were cut with a rock saw to remove any weathering rinds, and the inner portions were cut into cubes. Rock cubes were then crushed to chips with a hammer and subsequently powdered in a shatterbox using a tungsten-carbide grinding container. Sediment, (bedload and filters containing suspended material), soil, and vegetation samples were dried in

an oven at 50°C. Dried filters containing suspended sediment were weighed. Bedload sediment and soil samples were then sieved using a <2 mm nylon mesh, and subsamples of this fraction were powdered. Bedload sediment and soil powders were processed through a standard sequential leaching and digestion procedure (Moore et al., 2013) designed to isolate the exchangeable, carbonate, and silicate fractions. Powders (~1 g) weighed into LDPE centrifuge tubes were reacted with ~10 mL of 1M NH<sub>4</sub>Cl (adjusted to pH 8) on a rocker table for ~6 hrs. Samples were centrifuged, and the supernatants were filtered through Whatman Puradisc polypropylene 0.45 μm syringe filters into Teflon vials. These samples, defined here as the “exchangeable fraction,” were dried and redissolved in 5% HNO<sub>3</sub>. The residue was then reacted with ~10 mL of 4 M acetic acid (HAc) for ~6 – 8 hours, centrifuged, and the supernatants were collected using the same procedure. The HAc leaching step was repeated until the supernatant reached a constant pH of <2. For each repetition, the supernatant, here assumed to represent the “carbonate fraction,” was collected into the same Teflon vial, dried, and redissolved in 5% HNO<sub>3</sub>. Finally, centrifuge tubes containing the reacted residues, here termed the “silicate fraction,” were dried in the oven at 50°C, and ~0.8 g subsamples were weighed into Teflon vials and digested with a combined HF-HNO<sub>3</sub> mixture at 130°C for several days until no visible material remained. Samples were dried, refluxed in concentrated HNO<sub>3</sub>, dried again, and refluxed in 6N HCl to ensure complete dissolution. The solutions were dried and redissolved in 5% HNO<sub>3</sub>. Bulk rock powders were digested using the same procedure. Roots, stems, and leaves of vegetation samples were dried, homogenized, powdered with a mortar and pestle, and then dissolved in concentrated HNO<sub>3</sub>. When visible residue remained, solutions were placed in a UV

box for several days to break down organic matter until solutions were clear. Calcite was completely dissolved in 5% HNO<sub>3</sub>.

#### 3.3.4 Elemental Analysis

All solutions were analyzed for major and minor cation concentrations using a Thermo Scientific iCAP 6500 ICP-OES in the Aqueous Geochemistry Laboratory at Northwestern University. For some water samples with Al concentrations below detection limit, Al was analyzed using a Thermo iCapQ quadrupole ICP-MS in the Quantitative Bio-element Imaging Center at Northwestern University. Cation concentrations determined by repeated analyses of NIST SRM 1643f standard were within  $\pm 10\%$  of certified values. Anion concentrations in water samples were analyzed using a Dionex DX-120 IC equipped with an AS15 exchange column and an ASRS-300 suppressor. Repeated analyses of a NIST-traceable standard were within  $\pm 10\%$  of reported concentrations. The average charge balance error [CBE =  $(TZ^+ - TZ^-)/(TZ^+ + TZ^-)$ ], where  $TZ^+$  is the sum of all cations and  $TZ^-$  is the sum of all anions (in equivalents), for all river water samples equals 5.17%. Six samples have CBEs  $> 10\%$ , which broadly correlate with their extremely low alkalinities ( $< 80 \mu\text{eq/L}$ ). Ion activities were computed using PHREEQC (Parkhurst and Appelo, 1999) implemented with the llnl.dat database. Calcite saturation indices ( $SI_{\text{cal}}$ ) were calculated using the ion activity output and calculated temperature-dependent equilibrium constants (Plummer and Busenberg, 1982).

### 3.3.5 Ca and C isotope ratios

Calcium isotope ratios ( $^{44}\text{Ca}/^{40}\text{Ca}$ ) were measured with a Thermo-Fisher Triton MC-TIMS in the Radiogenic Isotope Laboratory at Northwestern University, using an optimized  $^{43}\text{Ca}$ - $^{42}\text{Ca}$  double-spike procedure (Lehn et al., 2013). Samples containing 50  $\mu\text{g}$  of Ca were equilibrated with the spike, and the solutions were eluted through Teflon columns packed with Bio-Rad AG MP-50 cation exchange resin. Approximately 12.5  $\mu\text{g}$  of purified Ca was loaded onto outgassed, single Ta filament assemblies together with 0.5  $\mu\text{L}$  of 10%  $\text{H}_3\text{PO}_4$ . Total procedural blanks ( $n = 6$ ) determined with a  $^{42}\text{Ca}$  isotope dilution method were negligible (65 – 196 n g). Calcium isotope ratios are reported in delta notation as  $\delta^{44/40}\text{Ca}_{\text{smp}} (\text{‰}) = [({}^{44}\text{Ca}/{}^{40}\text{Ca})_{\text{smp}}/({}^{44}\text{Ca}/{}^{40}\text{Ca})_{\text{std}} - 1] \times 1000$ , where *smp* refers to the sample and *std* refers to the normalizing standard, which in this study is OSIL Atlantic Seawater or *ASW* ( $\delta^{44/40}\text{Ca}_{\text{ASW}} = 0\text{‰}$ ). Reported  $\delta^{44/40}\text{Ca}$  have an internal precision of  $\pm 0.02$ - $0.03\text{‰}$  ( $2\sigma_{\text{SEM}}$ ). The double-spike was frequently recalibrated by analyzing at least 8 OSIL ASW standards and 2 NIST 915b standards every 30 or fewer samples. During the period of study, repeated analyses of the standards yielded  $\delta^{44/40}\text{Ca}_{\text{ASW}} = 0.000 \pm 0.001\text{‰}$  ( $2\sigma_{\text{SEM}}$ ,  $n = 156$ ) and  $\delta^{44/40}\text{Ca}_{915\text{b}} = -1.136 \pm 0.010\text{‰}$  ( $2\sigma_{\text{SEM}}$ ,  $n = 42$ ). Long-term records for the laboratory yield  $\delta^{44/40}\text{Ca}_{\text{ASW}} = 0.000 \pm 0.002\text{‰}$  ( $2\sigma_{\text{SEM}}$ ,  $n = 785$ ) and  $\delta^{44/40}\text{Ca}_{915\text{b}} = -1.134 \pm 0.003\text{‰}$  ( $2\sigma_{\text{SEM}}$ ,  $n = 296$ ). These data point to a  $2\sigma_{\text{SD}}$  of  $\pm 0.044\text{‰}$  for OSIL ASW and  $\pm 0.050\text{‰}$  for NIST 915b. Based on all standard measurements, I adopt a  $2\sigma_{\text{SD}}$  of  $\pm 0.05\text{‰}$  for the present dataset. Duplicate analyses of sample unknowns are better than  $\pm 0.04\text{‰}$ .

The carbon isotope composition of total dissolved inorganic carbon ( $\delta^{13}\text{C}_{\text{DIC}}$ ) was analyzed using a Thermo Gasbench II mated to a Delta V Plus Isotope Ratio Mass Spectrometer (IRMS) at the Northwestern University Stable Isotope Biogeochemistry Laboratory. Filtered

samples (0.45  $\mu\text{m}$ ), collected in airtight glass Exetainers, were acidified using 103%  $\text{H}_3\text{PO}_4$  so that all of the DIC was converted to  $\text{CO}_2$  for measurement by IRMS.  $\delta^{13}\text{C}_{\text{DIC}}$  values are reported relative to VPDB. Replicates of in-house standards ( $\text{NaHCO}_3$ ) indicate a precision of  $\pm 0.09\text{‰}$  ( $1\sigma_{\text{SD}}$ ) for  $\delta^{13}\text{C}$ .

### 3.4 Results

#### 3.4.1 Waters

Table 3.1 presents elemental and Ca isotope data for river and groundwater samples. In tributaries,  $\text{Ca}^{2+}$  dominates the cationic charge ( $\sim 40\%$ ), closely followed by  $\text{Na}^+$  and  $\text{K}^+$  ( $\sim 35\%$ ), with smaller contributions from  $\text{Mg}^{2+}$  ( $\sim 25\%$ ). The proportions of cationic charge in main stem rivers varies more widely, but in general  $\text{Na}^+$  and  $\text{K}^+$  dominate ( $\sim 31\% - 52\%$ ), followed by  $\text{Ca}^{2+}$  ( $\sim 19\% - 42\%$ ) and  $\text{Mg}^{2+}$  ( $\sim 12\% - 48\%$ ). In groundwaters,  $\text{Na}^+$  and  $\text{K}^+$  dominate the cationic charge ( $\sim 89\%$ ), followed by  $\text{Ca}^{2+}$  ( $\sim 10\%$ ) and  $\text{Mg}^{2+}$  ( $< 1\%$ ). In both tributary and main stem rivers,  $\text{HCO}_3^-$  dominates the anionic charge ( $> 75\%$ ), with lesser contributions from  $\text{Cl}^-$  ( $\sim 11 - 19\%$ ) and little influence from  $\text{SO}_4^{2-}$  ( $< 5\%$ ). In groundwaters,  $\text{HCO}_3^-$  also dominates the anionic charge ( $\sim 65\%$ ), but these waters show higher contributions from  $\text{Cl}^-$  ( $22\%$ ) and  $\text{SO}_4^{2-}$  ( $\sim 13\%$ ) relative to surface waters. River water pH ranges from 6.72-8.68. All rivers are undersaturated with respect to calcite, with the exception of one sample from the  $\text{CO}_2$ -rich Hvanná river in southern Iceland. Groundwaters show a higher pH range from 7.10-10.34 and are either at equilibrium or slightly oversaturated with respect to calcite.

Main stem rivers have a higher average  $\delta^{44/40}\text{Ca}$  value ( $-0.72 \pm 0.09\text{‰}$ ,  $1\sigma_{\text{SD}}$ ,  $n = 32$ ) than tributaries ( $-0.95 \pm 0.06\text{‰}$ ,  $1\sigma_{\text{SD}}$ ,  $n = 17$ ). The Ca isotope ratios of Skagafjörður rivers correlate

with Sr/Ca and Na/Ca ratios, as well as the saturation index (SI) of calcite (Figures 3.2-3.4).

Groundwaters have the highest average  $\delta^{44/40}\text{Ca}$  ( $-0.64 \pm 0.22\text{‰}$ ,  $1\sigma_{\text{SD}}$ ,  $n = 9$ ), with values ranging from  $-1.03\text{‰}$  for a hot spring far inland to a very high value of  $-0.28\text{‰}$  for one cold spring close to the coast.

Main stem rivers have a higher average  $\delta^{13}\text{C}$  value ( $-4.12 \pm 0.77\text{‰}$ ,  $1\sigma_{\text{SD}}$ ,  $n = 39$ ) than tributaries ( $-5.77 \pm 0.96\text{‰}$ ,  $1\sigma_{\text{SD}}$ ,  $n = 17$ ). The average  $\text{HCO}_3^-/\text{DIC}$  ratio for all rivers is 0.95, indicating that the tracer is conservative. Most riverine  $\delta^{13}\text{C}$  values correlate with  $\text{SI}_{\text{cal}}$ .

Groundwaters define a much lower average  $\delta^{13}\text{C}$  value ( $-10.58 \pm 1.34\text{‰}$ ,  $1\sigma_{\text{SD}}$ ,  $n = 9$ ) and no correlation is observed with  $\text{SI}_{\text{cal}}$ .

**Table 3.1.** Elemental and isotopic data for all water samples. “SS” indicates suspended sediment concentrations in rivers. “-” indicates values below detection limit, “nd” denotes no data, and duplicate analyses are given in “()”.

Sample ID	T (°C)	pH	Ca (μmol/L)	K (μmol/L)	Mg (μmol/L)	Na (μmol/L)	Al (nmol/L)	Si (μmol/L)	Sr (nmol/L)	Cl (μmol/L)	SO <sub>4</sub> (μmol/L)	HCO <sub>3</sub> <sup>-</sup> (μmol/L)	SI <sub>cal</sub>	δ <sup>44/40</sup> Ca (‰, ASW)	SS (mg/L)	δ <sup>13</sup> C <sub>DIC</sub> (‰, VPDB)
<i>Non-glacial, Skagafjörður tributaries</i>																
BNG_1	8.9	7.33	52.9	6.3	31.4	151	108	152	60.5	148	7.6	394	-2.82	nd	-	-5.61
BNG_2	9	7.35	58.2	6.6	34.1	161	101	166	61.7	151	11.3	194	-2.75	nd	4.26	-5.71
BNG_3	10	7.51	70.2	7.7	41.7	185	95.2	184	65.1	179	9.8	288	-2.41	nd	-	-5.11
BNG_5	10.6	7.39	69.0	7.9	41.3	183	112	181	62.8	170	12.1	283	-2.58	nd	-	-5.89
Y_1	11.7	7.94	171	23.9	106	209	297	405	177	91.8	15.1	704	-1.13	-0.94	-	-4.80
MF_1	10.2	7.81	145	14.8	79.7	183	122	324	137	97.2	11.1	560	-1.44	-0.87	-	nd
MF_2	11.7	7.85	147	14.7	82.2	189	125	326	130	100	11.8	598	-1.35	-0.87 (-0.87)	-	-4.61
VT_1	13.6	8.02	189	24.0	135	253	178	372	196	150	13.2	774	-0.95	-1.01	-	-7.56
VT_2	12.1	8.04	191	23.2	140	263	339	338	194	151	12.7	808	-0.93	nd	-	nd
ND_1	7.5	7.55	54.9	11.9	35.0	70.6	192	194	67.3	39.4	7.6	267	-2.48	-0.95	-	-4.76
ND_2	8.5	7.58	55.8	12.4	35.5	72.8	105	198	67.3	40.6	7.6	254	-2.43	nd	-	nd
ND_3	9.1	7.60	59.4	12.7	36.9	78.2	139	206	69.6	45.8	7.7	263	-2.36	-0.99	-	-4.75
BT_1	8.3	7.66	64.5	16.2	36.6	101	462	229	81.0	53.3	8.7	283	-2.25	-0.89 (-0.93)	-	nd
BG_1	3.7	6.72	25.6	4.6	17.2	42.3	3029	97.4	36.5	32.6	5.6	154	-4.22	-1.02	8.66	-6.74
BG_2	4.3	6.77	26.0	4.6	17.6	42.9	3810	100	38.8	32.4	6.4	140	-4.48	-1.02	4.30	-7.36
BG_3	4.2	6.77	31.5	5.8	20.5	47.5	3264	114	44.5	33.9	6.6	158	-4.20	-0.99	4.25	-6.73
BG_4	5.3	7.25	36.2	6.0	22.4	53.0	1511	132	52.6	33.6	6.5	312	-3.56	-1.01	4.24	-6.19
BG_5	5.6	7.36	43.2	7.1	25.9	60.5	1156	148	59.4	33.3	7.0	174	-2.96	-1.00	4.25	-5.53
BG_6	5.8	7.33	46.3	7.6	27.8	64.8	1357	157	60.5	35.5	7.2	177	-2.95	-1.00	4.26	-5.35
BG_7	5.8	7.40	50.0	8.3	30.1	69.0	1445	163	62.8	36.7	7.3	220	-2.76	-0.98	2.12	-5.79

BG_8	10.2	7.59	46.4	9.2	26.9	87.3	nd	186	58.2	66.6	9.7	166	-2.69	nd	-	-4.70
WT_1	13.5	8.00	229	6.5	73.3	284	nd	235	147	205	45.5	620	-0.98	-0.88 (-0.89)	-	-5.87
MF_3	11	7.88	173	22.7	88.4	234	nd	363	183	116	14.5	636	-1.24	-0.89	-	-8.70
HG_1	12	7.59	57.0	11.3	35.2	90.5	nd	193	61.6	57.9	10.1	204	-2.50	-0.97	-	-3.60

*Main Stem Skagafjörður Rivers*

*Hofsá*

HF_a	10.2	7.93	129	20.0	95.6	358	400	255	51.4	74.8	16.1	749	-1.26	-0.72	-	-4.24
HF_b	9.6	8.13	119	30.6	87.5	409	496	281	54.8	81.1	15.2	802	-1.07	-0.68	4.22	-6.91
HF_d	10.9	7.95	113	20.6	95.4	328	568	247	46.8	69.8	14.5	699	-1.31	-0.76	-	-3.99
HF_e	11	7.99	114	20.9	97.9	336	570	252	47.9	72.2	14.7	737	-1.25	-0.62	4.26	-4.01
HF_g	12.9	8.04	129	23.6	107.6	330	477	276	67.3	75.4	15.0	763	-1.10	nd	-	-4.50
HF_i	9.9	7.68	124	21.9	103.3	359	nd	260	49.1	90.2	17.5	707	-1.55	nd	-	-3.11

*Svartá*

SV_1	6.9	8.10	115	45.5	295	354	324	364	91.4	104	21.0	1237	-0.99	-0.57	-	-4.32
SV_2	7.1	8.13	115	45.7	295	354	261	363	89.1	104	20.5	1240	-0.95	-0.51	-	-4.21
SV_3	7.9	8.16	117	45.1	285	346	250	357	93.7	103	19.9	1165	-0.93	-0.58	-	-4.11
SV_4	9.8	8.07	135	38.6	251	340	387	350	112	108	18.3	1046	-0.98	-0.68	-	-3.47
SV_5	12	8.09	142	38.2	248	347	390	352	114	113	18.7	1058	-0.90	-0.70	-	-3.65
SV_6	11.5	8.29	142	33.3	215	341	312	358	115	117	18.7	981	-0.74	-0.71	-	-3.90
SV_7	5.7	8.18	121	48.6	322	387	nd	370	92.4	141	24.5	1130	-0.94	nd	-	-3.66
SV_8	6.2	8.23	120	48.3	317	382	nd	364	92.4	142	25.2	1140	-0.89	-0.51	-	-3.40
SV_9	12.3	8.40	154	39.4	257	421	nd	372	115	158	26.9	1042	-0.57	nd	-	-3.74
SV_10	15.1	8.68	156	39.6	252	418	nd	370	119	157	26.5	1068	-0.25	nd	-	-3.97

*Austari-Jökulsá*

AJ_a	7.3	7.72	78.8	8.9	27.9	205	2165	198	19.4	55.5	10.2	431	-1.97	-0.77	51.0	-5.14
AJ_b	7.7	7.68	73.4	8.3	25.5	189	3072	194	22.8	49.4	9.5	381	-2.06	-0.73	34.1	-4.71
AJ_c	8	7.70	73.6	8.0	26.1	188	3076	196	22.8	49.3	9.3	422	-2.10	-0.73	30.2	-4.66
AJ_d	8.2	7.68	71.1	7.7	26.8	173	2953	191	25.1	48.6	9.4	373	-2.12	-0.73	25.4	-4.44

AJ_j	10	7.71	78.6	5.4	21.1	173	nd	161	13.7	67.2	11.0	318	-2.05	nd	99.0	-4.32
<i>Vestari-Jökulsá</i>																
VJ_a	6.6	7.80	87.8	18.1	153	201	2904	210	52.5	64.3	16.7	658	-1.66	-0.68	243. 6	-3.51
VJ_b	8.2	7.81	87.8	18.1	153	199	4285	212	53.6	64.5	16.8	390	-1.64	-0.81	241. 4	-3.27
VJ_c	11.9	7.97	124.8	22.4	119	306	2496	270	67.3	82.1	15.8	715	-1.23	nd	34.3	-4.38
VJ_d	10.1	7.85	95.4	20.2	152	217	4365	223	58.2	69.6	17.2	646	-1.54	-0.75	175. 0	-3.75
VJ_e	11	7.87	104.3	20.3	144	242	4782	238	59.3	72.3	17.0	675	-1.45	-0.78	120. 9	-4.02
VJ_m	8.1	7.76	72.1	11.9	99.0	152		147	37.7	59.7	15.0	406	-1.96	nd	390. 5	-3.61
<i>Héraðsvötn</i>																
HR_1	8.3	7.79	83.4	12.1	66.2	199	4490	199	35.4	58.2	12.1	470	-1.81	-0.76	95.0	-4.84
HR_2	8.2	7.78	82.5	12.3	65.7	197	5165	198	36.6	60.6	12.3	472	-1.82	nd	nd	nd
HR_3	9.1	7.81	81.9	11.7	64.7	197	2477	194	34.3	59.6	12.2	456	-1.79	-0.74	83.7	-4.33
HR_4	13.2	7.68	67.2	12.9	45.0	114	1837	208	58.3	49.7	8.9	332	-2.08	nd	nd	nd
HR_5	11.1	7.81	76.8	13.1	56.8	163	2730	203	45.7	53.6	10.7	376	-1.88	-0.79	53.1	-4.30
HR_6	12.7	7.91	87.9	12.7	68.0	192	4133	217	46.8	63.0	12.9	452	-1.62	nd	nd	nd
HR_7	12.5	7.72	92.9	14.1	75.4	197	3205	219	54.8	61.3	11.9	458	-1.78	-0.81	37.8	-5.85
HR_8	15.8	7.88	88.2	14.2	66.9	186	4058	214	37.7	59.1	11.7	464	-1.60	nd	nd	nd
HR_9	13.8	7.83	82.8	14.4	62.7	184	3439	212	36.6	57.4	12.1	431	-1.73	-0.79 (-0.83)	25.4	-4.58
HR_10	11.1	7.72	82.8	13.5	62.0	172	2456	223	49.1	62.4	11.4	436	-1.87	nd	nd	nd
HR_11	10	7.16	65.1	9.3	45.5	130	nd	175	32.0	68.6	11.7	310	-2.69	-0.78	178. 8	-4.28
HR_12	11.4	7.72	79.1	9.3	56.0	165	nd	175	28.5	73.2	12.9	368	-1.98	-0.66	232. 4	-3.90
<i>Other main stem rivers</i>																
<i>Hvítá</i>	10.8	8.35	113.6	9.0	52.8	289	-	202	36.5	109	35.1	458	-1.12	nd	nd	-4.25
<i>Hvítá</i>	12.1	7.77	107.0	8.4	51.6	236	-	180	36.5	102	33.2	395	-1.76	nd	nd	-3.07
<i>Þjórsá</i>	12.8	7.76	107.7	9.4	52.5	287	-	175	36.5	81.8	40.1	436	-1.71	nd	nd	-4.45
<i>Skjálfandafljót</i>	13.9	8.31	128.1	10.2	77.7	337	-	273	51.4	76.3	39.1	601	-0.93	-0.81 (-0.84)	nd	-3.10
<i>Eyjafljóður</i>	9	7.67	61.4	5.2	27.5	121	-	203	21.7	54.7	10.0	232	-2.33	-0.79	nd	-2.56

*Dórsmörk rivers, Southern Iceland**Hvanná*

HV_1	2.7	7.57	782	57.1	533	765	nd	291	844	540	341	2380	-0.53	-0.83	nd	-0.73
HV_2	3	7.80	820	60.5	566	824	nd	300	905	565	371	2528	-0.26	nd	nd	-0.33
HV_3	3.3	7.96	808	61.2	570	820	nd	299	891	559	368	2521	-0.10	-0.85	nd	-0.3
HV_4	3.8	8.01	816	64.2	682	977	nd	302	925	563	383	2940	0.02	nd	nd	-0.69
HV_5	4.1	7.97	728	61.7	687	1011	nd	297	857	480	336	2948	-0.06	-0.82	nd	-1.33

*Krossá*

KR_1	3.3	7.76	135	9.8	78.5	275	nd	136	186	131	45.7	500	-1.69	-0.70	nd	-3.07
KR_2	3.9	7.87	153	10.6	87.1	301	nd	147	208	140	49.2	552	-1.47	nd	nd	-2.97

*Groundwater*

HS_1	79.8	8.69	120	62.3	0.2	5183	1935	1903	126	2571	956	1203	0.17	-1.03	-	-8.16
HS_2	60.9	9.18	68.8	19.9	0.6	2898	3366	1156	21.7	1388	288	1259	0.19	-0.66	-	-10.52
HS_3	22.2	10.34	54.5	5.5	0.8	1601	2187	858	-	221	132	1252	0.18	-0.5	-	-10.14
HS_4	45.8	9.81	38.1	9.0	0.2	2035	5393	1232	13.7	264	114	1724	0.15	-0.48	-	-10.15
HS_5	49.6	9.66	44.8	18.9	1.6	2466	5592	nd	19.4	619	244	1799	0.14	nd	-	-12.97
HS_6	63.0	9.47	42.3	16.4	0.1	2477	5319	1522	18.3	522	227	1776	0.45	-0.66	-	-10.88
HS_7	35.2	9.82	90.1	73.8	15.6	1923	2049	1243	66.3	294	151	1529	0.08	-0.72	-	-11.48
HS_8	40.8	9.96	31.6	8.4	0.2	1767	3663	1174	-	133	58	1694	0.17	-0.84	-	-9.38
GW_1	3.9	7.10	83.7	8.7	50.5	220	35	213	44.6	248	17	341	nd	nd	-	-10.17
GW_2	7.3	9.16	134	56.6	67.3	619	335	384	67.4	144	19	1034	0.01	-0.59	-	-11.9
GW_3	12.4	10.01	48.1	2.1	1.2	860	836	383	4.6	138	32	853	0.06	-0.28	-	nd

### 3.4.2 Rocks and Minerals

Table 3.2 presents elemental and Ca isotope data for basalt and calcite. Basalt samples yield an average  $\delta^{44/40}\text{Ca}$  value of  $-1.04 \pm 0.05\text{‰}$ ,  $1\sigma_{\text{SD}}$ ,  $n = 6$ . Calcite samples from the Skagafjörður valley define an average  $\delta^{44/40}\text{Ca}$  of  $-0.87 \pm 0.05\text{‰}$ ,  $1\sigma_{\text{SD}}$ ,  $n = 2$ . Travertine samples collected from the streambed of the Hvanná river produce a much lower average  $\delta^{44/40}\text{Ca}$  value of  $-2.12 \pm 0.19\text{‰}$ ,  $1\sigma_{\text{SD}}$ ,  $n = 3$ .

Three calcite samples previously studied by Nelson et al. (2021) were analyzed for carbon isotopes in this study. The calcite  $\delta^{13}\text{C}$  values, along with previously published elemental and Ca isotope data, are reported in Table 3.2.

### 3.4.3 Sediment, Soil, and Vegetation

Table 3.3 presents elemental and Ca isotope data for bedload sediments, soil leachates and digests, and vegetation. Bedload sediment  $\text{NH}_4\text{Cl}$  leachates had lower average  $\delta^{44/40}\text{Ca}$  ( $-1.24 \pm 0.18\text{‰}$ ,  $1\sigma_{\text{SD}}$ ,  $n = 5$ ) than basalt, however  $\text{NH}_4\text{Cl}$  leached only 2% of sediment Ca on average. The average  $\delta^{44/40}\text{Ca}$  for the residual sediment HF- $\text{HNO}_3$  digest ( $-1.04 \pm 0.02\text{‰}$ ,  $1\sigma_{\text{SD}}$ ,  $n = 5$ ) is identical to the average  $\delta^{44/40}\text{Ca}$  of bulk basalt. The acetic acid leached substantial amounts of Al, Fe, and Si, and had identical Sr/Ca to  $\text{NH}_4\text{Cl}$  leachates. Acetic acid and  $\delta^{44/40}\text{Ca}$  was not measured.

Soil  $\text{NH}_4\text{Cl}$  leachate  $\delta^{44/40}\text{Ca}$  values range from  $-0.91\text{‰}$  to  $-1.44\text{‰}$ , with an average of  $-1.20\text{‰} \pm 0.17\text{‰}$  ( $1\sigma_{\text{SD}}$ ,  $n = 17$ ). The  $\text{NH}_4\text{Cl}$  solution leached an average of  $5.2\% \pm 6.5\%$  ( $1\sigma_{\text{SD}}$ ,  $n = 18$ ) of the total Ca (relative to the HF- $\text{HNO}_3$  digests), but the average drops to  $2.9\% \pm 1.4\%$  ( $1\sigma_{\text{SD}}$ ,  $n = 16$ ) when two outliers from a single pit in the Svarta watershed yielding higher proportions (21% and 24%) are excluded.

**Table 3.2.** Elemental and Ca isotope data for basalt and calcite from North Iceland, and travertine from the hyperalkaline Hvanná river in South Iceland. “-” indicates values below detection limit, “nd” denotes no data collected, and duplicate analyses are given in “()”. “\*” denotes samples previously analyzed by Nelson et al. (2021).

Sample ID	Sample type	Ca ( $\mu\text{mol/g}$ )	K ( $\mu\text{mol/g}$ )	Mg ( $\mu\text{mol/g}$ )	Na ( $\mu\text{mol/g}$ )	Sr (nmol/g)	$\delta^{44/40}\text{Ca}$ (‰, ASW)	$\delta^{13}\text{C}_{\text{DIC}}$ (‰, VPDB)
<i>Skagafjörður basalt</i>								
BG_1	Neogene tholeiite	1838	83.2	1469	799	3105	-1.01	nd
SV_2	Plio-Pleistocene porphyritic basalt	2170	59.9	1792	660	1648	-1.02	nd
AJ_3a	Neogene tholeiite	1769	57.9	1410	799	3280	-1.03	nd
SV_16a	Plio-Pleistocene porphyritic basalt	1506	153	1088	986	2967	-1.12	nd
X_19	Plio-Pleistocene basaltic andesite	1135	382	786	1394	2442	-1.00	nd
<i>Skagafjörður calcite</i>								
WT_19	Greenschist calcite	6162	-	1.6	-	1006	-0.90	nd
WT_20	Greenschist calcite	10456	-	-	-	1670	-0.83	nd
<i>Eyjafjörður calcite</i>								
AK1	Chabazite-thomsonite zone calcite	10505	-	10.3	-	8508	nd	nd
AK4	Chabazite-thomsonite zone calcite	6643	-	-	-	3495	nd	nd
<i>Hvanná River</i>								
HV_4	Travertine	39902	-	459	-	3283	-1.95	nd
HV_5	Travertine	10574	-	110	-	2901	-2.09	nd
HV_9	Travertine	10473	-	102	-	4223	-2.32	nd
<i>*Berufjörður-Breiðdalur calcite</i>								

C_35	Heulandite-stilbite zone calcite	9120	-	3.37	-	2428	-0.89	-3.86
C_44	Mesolite-scolecite zone calcite	8802	-	23.6	-	1916	-0.86 (-0.87)	-1.22
C_49	Heulandite-stilbite zone calcite	8710	-	1.04	-	174	-0.80	-3.84

**Table 3.3.** Elemental and Ca isotope data for sediment and soil leachates and digests, and bulk vegetation digests. “-” indicates values below detection limit, “nd” denotes no data, and duplicate analyses are given in “()”.

Sample ID	Depth (cm)	Ca ( $\mu\text{mol/g}$ )	Sr (nmol/g)	Al (nmol/g)	Fe ( $\mu\text{mol/g}$ )	K ( $\mu\text{mol/g}$ )	Mg ( $\mu\text{mol/g}$ )	Na ( $\mu\text{mol/g}$ )	Si ( $\mu\text{mol/g}$ )	$\delta^{44/40}\text{Ca}$ (‰, ASW)	% Ca leached relative to total soil Ca	
<i>Stream Sediment</i>												
ILS_BG_1												
		NH <sub>4</sub> Cl	75.5	201	-	-	9.62	37.4	-	-	nd	5
		HF-HNO <sub>3</sub>	1436	2927	2471	2087	35.4	1162	691	-	nd	nd
ILS_BG_2												
		NH <sub>4</sub> Cl	30.4	80.2	-	-	2.44	11.3	-	-	nd	1.8
		HF-HNO <sub>3</sub>	1669	2809	2657	1975	39.5	1380	720	1669	nd	nd
ILS_BNG_3												
		NH <sub>4</sub> Cl	33.6	207	-	-	2.37	13.5	-	-	nd	2.0
		HAc	33.3	214	140	94.7	0.55	24.5	2.0	6.7	nd	2.0
		HF-HNO <sub>3</sub>	1632	2124	2663	1940	34.2	1467	642	-	nd	
ILS_SV_4												
		NH <sub>4</sub> Cl	31.8	87.7	-	-	7.04	37.0	3.00	-	-0.93	1.8
		HAc	40.6	85.1	186	192	1.21	204	6.9	10.4	nd	2.3
		HF-HNO <sub>3</sub>	1709	2068	2651	1607	53.3	1474	653	-	-1.03	

ILS_AJ_5											
	NH <sub>4</sub> Cl	23.4	37.6	-	-	1.79	3.52	-	-	-1.33	.97
	HAc	57.0	98.6	112	187	0.54	327	12.1	37.0	nd	2.4
	HF-HNO <sub>3</sub>	2324	2121	3438	1291	2.22	1531	670	-	-1.03	
ILS_HR_6											
	NH <sub>4</sub> Cl	38.9	45.5	-	-	3.32	10.3	3.18	-	-1.27	1.9
	HAc	76.1	88.8	234	149	0.68	170	18.4	31.2	nd	3.7
	HF-HNO <sub>3</sub>	1923	1840	2855	1439	29.5	1787	645	-	-1.04	
ILS_HR_7											
	NH <sub>4</sub> Cl	32.6	50.2	-	-	3.30	9.50	2.54	-	-1.32	1.6
	HAc	95.3	148	197	183	1.22	244	24.0	27.8	nd	4.8
	HF-HNO <sub>3</sub>	1871	1975	2827	1514	63.6	1568	688	-	-1.07	
ILS_FS_8											
	NH <sub>4</sub> Cl	21.7	23.5	-	-	1.26	6.39	-	-	-1.35	1.0
	HAc	67.3	80.0	141	194	0.77	310	15.6	18.1	nd	3.1
	HF-HNO <sub>3</sub>	2091	1851	3008	1373	18.8	1683	622	-	-1.04	
<i>Soil</i>											
ILO_BG_1 40											
	NH <sub>4</sub> Cl	35.1	179.5	-	-	-	16.9	3.8	-	-1.17	2.3
	HAc	51.3	150.6	344	117	-	26.4	-	48.5	nd	3.3
	HF-HNO <sub>3</sub>	1468	2462	2535	1923	89.7	1149	700	-	nd	
ILO_AJ_3a 22											
	NH <sub>4</sub> Cl	47.1	102	-	-	10.0	20.7	1.9	-	-1.09	2.9
	HAc	107	206	355	229	-	149	21.4	15.6	-1.26	6.5
	HF-HNO <sub>3</sub>	1498	1800	2475	1373	86.1	1298	651	-	-1.04 (-1.06)	
ILO_AJ_3b 37											
	NH <sub>4</sub> Cl	46.3	109	-	-	3.3	18.8	2.9	-	-1.22	2.7
	HAc	131	222	405.2	260	-	176	30.4	21.4	-1.16	7.5
	HF-HNO <sub>3</sub>	1560	1893	2582	1426	88.8	1344	674	-	-1.08 (-1.08)	

ILO_AJ_3c	45										
NH <sub>4</sub> Cl		27.7	62.9	-	-	-	18.2	1.7	-	-1.11	3.2
HAc		37.6	61.1	104	91.3	-	36.1	8.4	30.6		4.3
HF-HNO <sub>3</sub>		802	1513	2682	834	363.3	537	1104	-	-1.07	
ILO_AJ_3d	60										
NH <sub>4</sub> Cl		31.5	77.2	-	-	-	19.1	3.1	-	-1.44 (-1.44)	2.1
HAc		61.6	145.8	420	263	-	70.9	8.4	7.0	-1.28	4.2
HF-HNO <sub>3</sub>		1385	1798	2543	1420	99.3	1120	658	-	-1.07	
ILO_ND_4a	16										
NH <sub>4</sub> Cl		28.4	56.4	-	-	2.2	-	1.6	-	-1.47	2.2
HAc		48.6	127.0	88.1	1369	-	13.3		12.0	nd	3.7
HF-HNO <sub>3</sub>		1230	2048	2150	1988	64.9	964	590	-	nd	
ILO_ND_4b	27										
NH <sub>4</sub> Cl		40.2	146.2	-	-	4.4	16.0	2.1	-	-1.32	3.2
HAc		52.6	169.4	231	82.3	-	13.2	-	41.2	nd	4.2
HF-HNO <sub>3</sub>		1174	1990	2085	2020	63.5	929	572	-	-1.08	
ILO_ND_4c	37										
NH <sub>4</sub> Cl		34.1	99.2	-	-	1.3	12.6	2.0	-	-1.17	2.6
HAc		57.7	148	209	72.3	-	13.7	-	31.8	nd	4.3
HF-HNO <sub>3</sub>		1243	2553	2485	1320	124	862	788	-	-1.00	
ILO_ND_4d	45										
NH <sub>4</sub> Cl		30.1	98.4	-	-	1.2	14.0	1.9	-	-1.15	2.0
HAc		46.0	136	145	51.4	-	12.4	-	25.7	nd	3.0
HF-HNO <sub>3</sub>		1433	2429	2607	1511	84.1	1051	708	-	-1.01	
ILO_HR_5a	15										
NH <sub>4</sub> Cl		69.0	113.3	-	-	2.2	32.8	5.8	-	nd	4.8
HAc		80.3	163.9	370	251	-	35.4	-	16.7	nd	5.5
HF-HNO <sub>3</sub>		1303	2125	2005	1372	74.9	966	575	-	nd	
ILO_HR_5b	24										
NH <sub>4</sub> Cl		72.6	115.8	-	-	3.0	36.4	6.4	-	-0.91	5.6

		HAc	90.5	179.1	505	306	-	36.9	-	16.9	nd	6.9
		HF-HNO <sub>3</sub>	1141	1295	1904	1301	59.4	866	499	-	nd	
ILO_HR_5c	30											
		NH <sub>4</sub> Cl	19.8	27.3	-	-	2.0	-	2.4	-	-0.93	4.5
		HAc	25.4	30.8	162	71.4	-	8.6	-	24.0	nd	5.7
		HF-HNO <sub>3</sub>	400	1791	2202	561	359	102	1144	-	nd	
ILO_HR_5d	40											
		NH <sub>4</sub> Cl	51.9	163	-	-	5.0	28.0	5.0	-	-1.08	3.3
		HAc	44.0	205	275	167	-	49.9	4.1	11.0	nd	2.8
		HF-HNO <sub>3</sub>	1457	1550	2514	1532	56.3	1243	539	-	nd	
ILO_SV_6a	47											
		NH <sub>4</sub> Cl	39.1	73.7	-	-	-	17.2	11.7	-	-1.02	4.9
		HAc	51.9	97.5	310	203	-	-	-	56.4	nd	6.5
		HF-HNO <sub>3</sub>	704	1304	1310	910	56.9	538	367	-	-1.02	
ILO_SV_6b	80											
		NH <sub>4</sub> Cl	2.7	-	-	-	-	-	0.1	-	-1.35	0.7
		HAc	11.4	15.2	91.2	29.1	-	-	-	36.9	-1.28	3.0
		HF-HNO <sub>3</sub>	371	1880	2098	424	333	58.4	1103	-	-0.98	
ILO_SV_6c	100											
		NH <sub>4</sub> Cl	36.6	58.0	-	-	-	-	5.0	-	-1.37	24.0
		HAc	45.8	70.9	179	171	-	-	-	52.2	-1.55	30.0
		HF-HNO <sub>3</sub>	70.4	154	331	476	4.3	50.4	35.6	-	-1.11 (-1.08)	
ILO_SV_6d	115											
		NH <sub>4</sub> Cl	3.2	11.6	-	-	-	-	1.8	-	-1.41	0.8
		HAc	11.2	28.3	89.3	21.7	-	8.0	-	18.1	nd	2.7
		HF-HNO <sub>3</sub>	395	1612	2325	479	450	140	1220	-	-0.99 (-0.99)	
ILO_SV_6e	147											
		NH <sub>4</sub> Cl	67.6	76.3	-	-	-	-	3.4	1.7	-1.20 (-1.20)	21.2
		HAc	78.4	82.6	173	83.9	-	-	-	37.2	-1.43	24.5
		HF-HNO <sub>3</sub>	174	228	517	464	6.1	131	65.0	-	-1.08 (-1.10)	

*Vegetation*

ILV_BG_1	80.0	96.5	6.4	3.9	70.6	37.3	3.3	17.6	-2.12	nd
ILV_BG_2	132	317	27.4	20.1	164	106	4.5	17.4	-1.47	nd
ILV_BNG_3	68.6	87.1	22.3	21.5	169	46.3	12.3	29.8	-1.57	nd
ILV_BNG_4	51.8	178	8.6	10.5	14.5	38.0	6.0	44.0	nd	nd
ILV_SV_5	61.4	47.6	0.9	1.0	493	69.1	5.0	7.7	nd	nd
ILV_HR_7	232	64.9	4.8	2.7	638	140	3.7	6.3	-1.61	nd
ILV_HR_9	53.6	62.4	25.4	18.6	206	47.1	10.1	19.6	nd	nd
ILV_SV_10	311	781	221	184	205	214	25.4	19.1	-1.52	nd

---

The HAc step leached an average of  $7.2\% \pm 7.5\%$  ( $1\sigma_{SD}$ ,  $n = 18$ ) of the total Ca and yielded an average  $\delta^{44/40}\text{Ca}$  value of  $-1.33 \pm 0.14\text{‰}$  ( $1\sigma_{SD}$ ,  $n = 6$ ). Although intended to dissolve carbonate, high concentrations of Si, Al, and Fe in the acetic acid leachates clearly indicate contributions from non-carbonate material (Table 3.3), and the overall low Ca concentrations are consistent with absence of pedogenic carbonate. The average  $\delta^{44/40}\text{Ca}$  value for the residual HF-HNO<sub>3</sub> digests of  $-1.04 \pm 0.04\text{‰}$  ( $1\sigma_{SD}$ ,  $n = 12$ ) is identical to the average for bulk basalt. Elemental ratios for the HF-HNO<sub>3</sub> digests (i.e., Sr/Ca, Mg/Ca, Na/Ca, and K/Ca ratios) also overlap with those for bulk basalt. Vegetation produced the lowest average  $\delta^{44/40}\text{Ca}$  value ( $-1.66 \pm 0.24\text{‰}$ ,  $1\sigma_{SD}$ ,  $n = 5$ ) of all samples from the Skagafjörður valley measured in this study.

### 3.5 Discussion

Similar to previously reported data (Hindshaw et al., 2013; Jacobson et al., 2015), basalts show minor geochemical variability, and the range of  $\delta^{44/40}\text{Ca}$  and molar ratios for basalt brackets the values observed for primary minerals from Iceland (Nelson et al., 2021). Of all water samples, only the non-glacial, tributary-type rivers show an average  $\delta^{44/40}\text{Ca}$  that is similar to the values of basalt (Figure 3.2). River samples agree well with previously reported  $\delta^{44/40}\text{Ca}$  for glacial and non-glacial rivers throughout Iceland, and identical to previous studies (Hindshaw et al., 2013; Jacobson et al., 2015), rivers and groundwaters analyzed here have much higher  $\delta^{44/40}\text{Ca}$  values than bulk basalt (Figure 3.2). Selective primary mineral dissolution cannot explain this pattern, as unlike granite (e.g. Ryu et al., 2011), primary minerals composing basalt have a narrow range of  $\delta^{44/40}\text{Ca}$  values, on the order of only  $\sim 0.20\text{‰}$  (Nelson et al., 2021). The data point to one or more mechanisms that fractionate Ca isotopes. I also consider possible sources of heavy Ca isotopes to surface waters that may explain elevated river  $\delta^{44/40}\text{Ca}$  values.

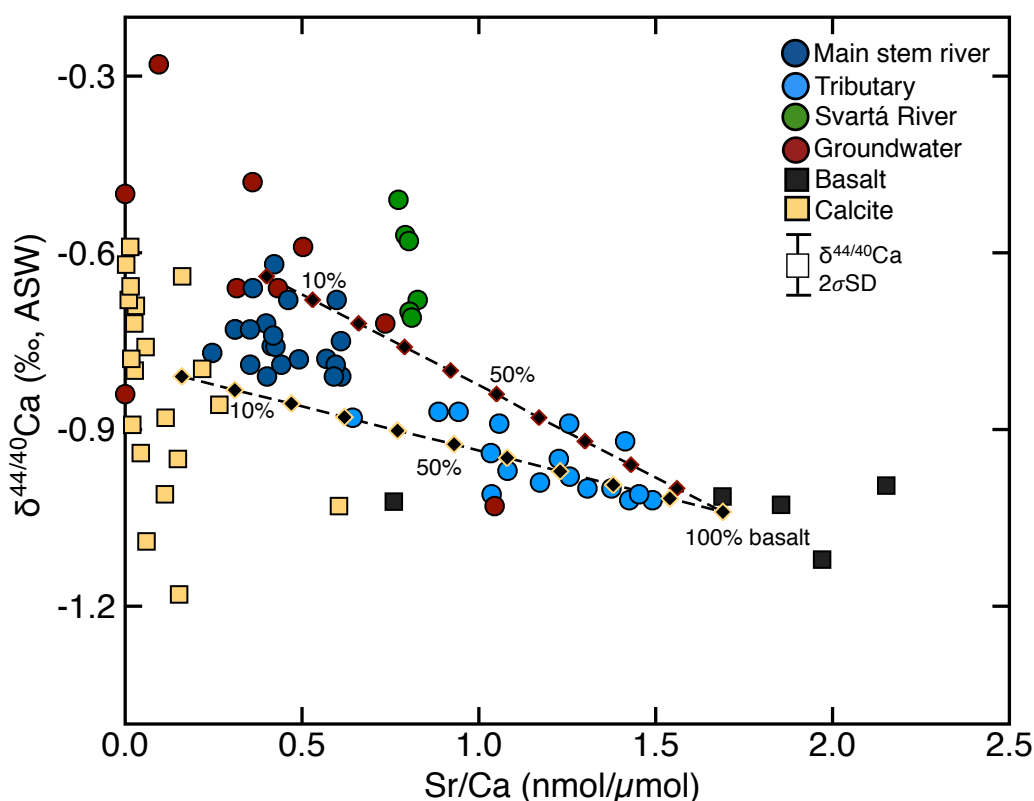


**Figure 3.2:**  $\delta^{44/40}\text{Ca}$  versus Sr/Ca for all river water, groundwater, and basalt samples from this study. Data points for calcite include all reported values from Icelandic samples (Jacobson et al., 2015; Nelson et al., 2021). Theoretical mixing lines were calculated using average values for groundwater, calcite, and basalt (see section 3.5.6).

### 3.5.1 Atmospheric Deposition

Atmospheric deposition in Iceland is compositionally similar to seawater (Gislason and Eugster, 1987b; Gislason et al., 1996), and seawater has a higher  $\delta^{44/40}\text{Ca}$  value (0‰) than rivers. It follows that atmospheric deposition of Ca could elevate riverine  $\delta^{44/40}\text{Ca}$  values. To assess the importance of atmospheric deposition, I estimated proportions of riverine Ca, Mg, Na, and K from atmospheric deposition using a standard equation (e.g., Moore et al., 2013; Andrews et al., 2016).

$$[i]_{riv}^* = [i]_{riv} - [Cl]_{riv} \times \left(\frac{i}{Cl}\right)_{atm} \quad (3.1)$$

Where  $[i]_{riv}^*$  is the corrected concentration of element  $i$  in river water,  $[i]_{riv}$  is the measured concentration of element  $i$  in river water ( $\mu\text{mol/L}$ ),  $[Cl]_{riv}$  is the measured concentration of Cl in river water ( $\mu\text{mol/L}$ ), and  $(i/Cl)_{atm}$  is the molar ratio of element  $i$  to Cl in atmospheric deposition, here assumed to be equivalent to rainwater (Gislason and Eugster, 1987b). Results from this calculation indicated that atmospheric inputs account for only ~10% of riverine Ca, on average. Unmixing this contribution does not substantially change riverine  $\delta^{44/40}\text{Ca}$  values, nor does atmospheric deposition of Ca and other cations affect correlations between riverine  $\delta^{44/40}\text{Ca}$  values and other parameters, such as Sr/Ca, Na/Ca, K/Ca, and Mg/Ca molar ratios.

Moreover, the correction equation assumes that all riverine  $\text{Cl}^-$  derives from precipitation, but in the Skagafjörður valley and many other locations throughout Iceland (Gislason et al., 1996), rivers receive inputs from Cl-rich hot springs, which have very different ion/Cl ratios compared to seawater and rain (Table 3.1; Gislason and Eugster, 1987b). For this reason, no riverine data reported here are corrected for atmospheric contributions. Tributaries draining the eastern drainage divide of the Skagafjörður valley likely receive the least groundwater inputs (Figure 3.1). Here, the correction equation suggests atmospheric deposition could supply up to ~30% of the Ca and relatively higher proportions of other cations, but even at this level, neither  $\delta^{44/40}\text{Ca}$  values nor elemental ratios are substantially impacted. These tributaries also display among the lowest (most basaltic)  $\delta^{44/40}\text{Ca}$  values, which further confirms atmospheric deposition is not a major factor.

### 3.5.2 *Calcite precipitation*

Calcite precipitation, in general, represents an obvious candidate mechanism for elevating riverine  $\delta^{44/40}\text{Ca}$  values (Tipper et al., 2006b, 2008, 2010; Fantle and Tipper, 2014), as most calcite forms kinetically and therefore preferentially incorporates lighter Ca isotopes (Lemarchand et al., 2004; Tang et al., 2008a; DePaolo, 2011). However, for multiple reasons, calcite precipitation is an unlikely explanation for the elemental and isotopic patterns observed in this study. Nearly all Icelandic calcite has  $\delta^{44/40}\text{Ca}$  values higher than basalt (Figure 3.2; Jacobson et al., 2015, Nelson et al., 2021), surface waters are highly undersaturated with respect to calcite (Figure 3.3), and Icelandic soils examined here and elsewhere do not contain pedogenic carbonate (Arnalds, 2015b). In addition, while calcite precipitation could theoretically explain the positive correlation between riverine  $\delta^{44/40}\text{Ca}$  and Na/Ca (Figure 3.4), it less satisfactorily explains the negative correlation between riverine  $\delta^{44/40}\text{Ca}$  and Sr/Ca, as calcite discriminates against Sr during formation (Tang et al., 2008b).

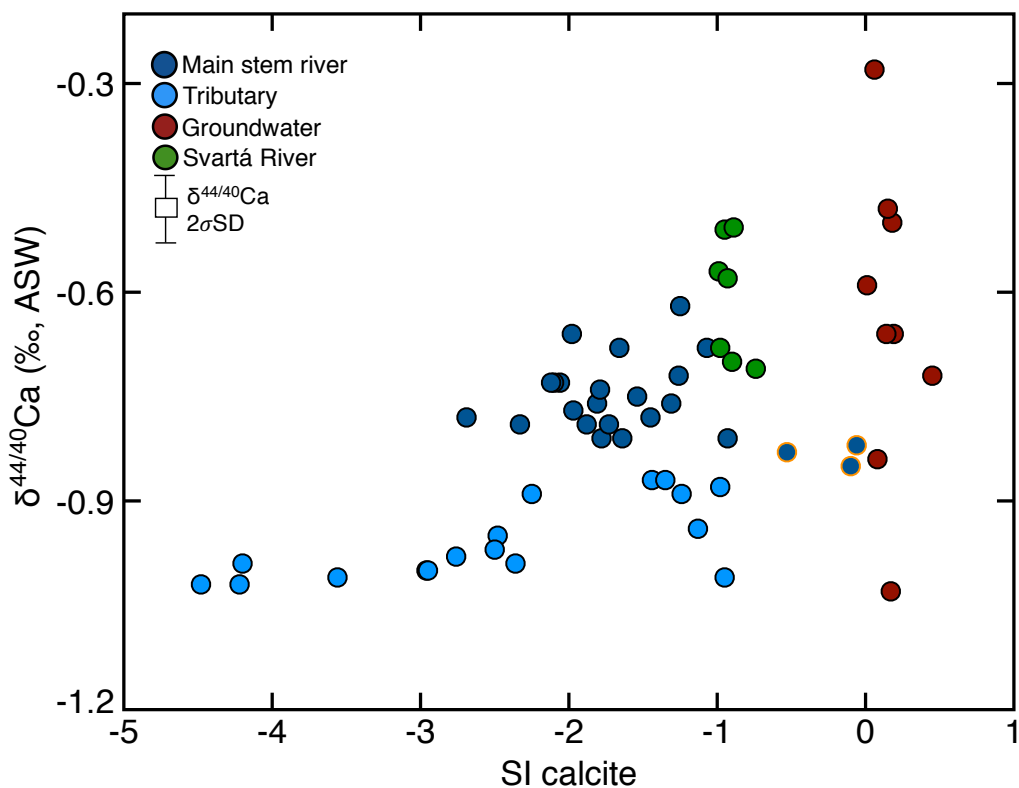


**Figure 3.3:** River and groundwater  $\delta^{44/40}\text{Ca}$  versus the saturation index (SI) of calcite. All rivers are highly undersaturated, with the exception of samples from the CO<sub>2</sub>-rich Hvanná river in southern Iceland (outlined in orange).

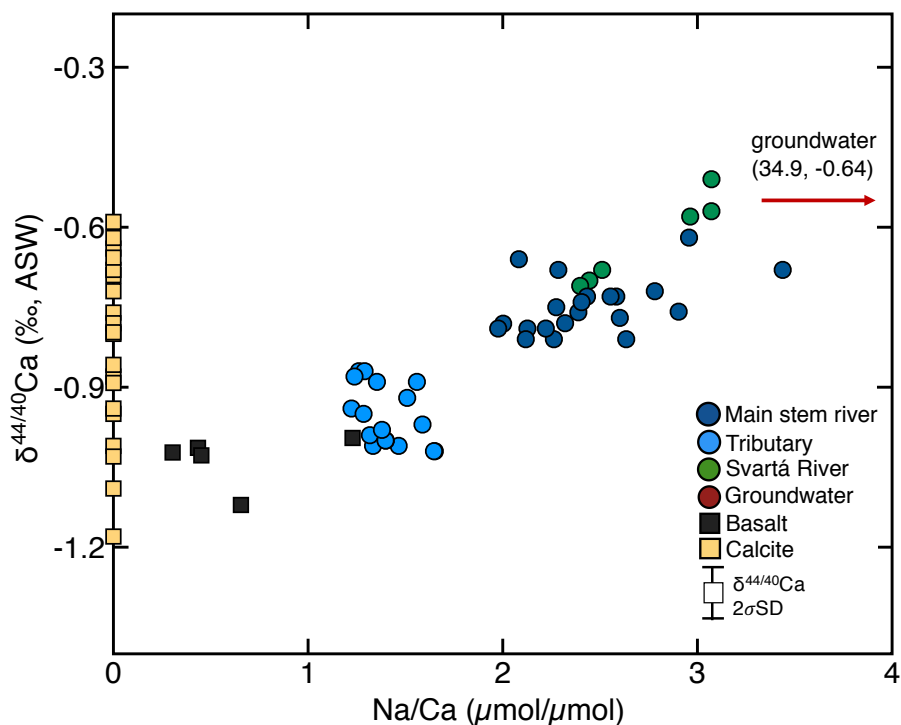


**Figure 3.4:**  $\delta^{44/40}\text{Ca}$  versus Na/Ca for all river water, groundwater, and basalt samples from this study. Data points for calcite include all reported values from Icelandic samples (Jacobson et al., 2015; Nelson et al., 2021). Arrow indicates average values for Skagafjörður groundwater.

In Iceland, most calcite precipitates from hydrothermal waters circulating in the subsurface and is later exposed via erosion (Walker, 1960, 1964; Kristmannsdóttir and Tómasson, 1978; Mehegan et al., 1982; Neuhoff et al., 2000), although in select high-temperature geothermally active areas, carbonate crusts also form where water discharges at the surface. The Hvanná river in southern Iceland offers a prime example. Here, recent eruption of the Eyjafjallajökull volcano has generated a  $\text{CO}_2$ -charged spring that degasses upon emergence from beneath the lava flow, leading to supersaturation with respect to calcite and production of travertine deposits that are up to several centimeters thick (Olsson et al., 2014; Pogge von Strandmann et al., 2019c). Hvanná river travertines are the only Icelandic calcites measured to

date with low  $\delta^{44/40}\text{Ca}$  values (Table 3.2) consistent with kinetic isotope fractionation arising from rapid precipitation. Nonetheless, coexisting water samples from the Hvanná river show intermediate  $\delta^{44/40}\text{Ca}$  values, which are lower than those from the adjacent Krossá river (Table 3.1), where no travertine forms. Thus, in the one river where in-situ calcite precipitation clearly occurs, the mechanism only introduces second-order effects on riverine  $\delta^{44/40}\text{Ca}$  values. Moreover, the low  $\delta^{44/40}\text{Ca}$  values observed for the rapidly precipitated Hvanná travertines further confirms previous interpretations that the high  $\delta^{44/40}\text{Ca}$  values observed for all other Icelandic calcite reflects slower precipitation and possibly isotopic equilibrium between calcite and groundwater (Nelson et al., 2021).

### 3.5.3 Zeolites

The overall negative correlation between riverine  $\delta^{44/40}\text{Ca}$  values and Sr/Ca ratios supports a hypothesis where any sink for lighter Ca isotopes is also a more efficient sink for Sr than Ca. Zeolites are known to be a major sink for Sr in Skagafjörður groundwaters (Fridriksson et al., 2009) and many incorporate light Ca isotopes (Jacobson et al., 2015; Nelson et al., 2021). However, zeolitization is not likely to directly affect surface waters, as zeolite ion-exchange mainly occurs at elevated temperatures (Kristmannsdóttir and Tómasson, 1978; Neuhoff et al., 1999, 2000; Chipera and Apps, 2001; Fridriksson et al., 2001; Fridriksson, 2004). Zeolites form in the subsurface during the hydrothermal alteration of basalt at temperatures  $>30^\circ\text{C}$  (Chipera and Apps, 2001), and zeolites are not common in Skagafjörður rocks exposed above the valley floor that were never deeply buried (Saemundsson et al., 1980; Arnórsson et al., 2002; Fridriksson et al., 2009). No evidence exists that zeolites form authigenically in Icelandic soils. Therefore, fractionation by zeolites is unlikely to directly affect river  $\delta^{44/40}\text{Ca}$  values.

### 3.5.4 Soils

Soil forming processes could play a role in increasing riverine  $\delta^{44/40}\text{Ca}$  values in lower elevation regions of the Skagafjörður valley draining crystalline basalt. To investigate this hypothesis, I analyzed the Ca isotope geochemistry of Icelandic vegetation and soils, as no studies have reported data for these materials. Uptake of light Ca by vegetation or clay minerals in soils could contribute to elevated river  $\delta^{44/40}\text{Ca}$  due to mixing of the residual pool of isotopically enriched soil pore water, as has been observed elsewhere with stable Sr isotopes (Bouchez et al., 2013; Andrews et al., 2016; Oeser and von Blanckenburg, 2020).

#### 5.4.3.1 Vegetation

In other settings, uptake of lighter Ca isotopes by plants has been implicated as a mechanism to elevate soil solution  $\delta^{44/40}\text{Ca}$  values and riverine  $\delta^{44/40}\text{Ca}$  values by extension (Cenki-Tok et al., 2009; Lehn et al., 2017; Schmitt et al., 2012). Related efforts have also shown that degradation of isotopically light plant matter can lower soil solution  $\delta^{44/40}\text{Ca}$  and potentially decrease riverine  $\delta^{44/40}\text{Ca}$  values (Bagard et al., 2013; Fantle and Tipper, 2014; Bullen and Chadwick, 2016; Griffith et al., 2020). Vegetation, which is ubiquitous in the Skagafjörður valley compared to the rest of Iceland, shows the lowest  $\delta^{44/40}\text{Ca}$  values of all samples measured in this study (Table 3.3). Nonetheless, similar to previous Ca isotope studies conducted in Iceland (Hindshaw et al., 2013; Jacobson et al., 2015), I do not find that plant growth and decay can satisfactorily explain regional-scale trends among tributary and main stem rivers, but I infer it could potentially contribute second-order heterogeneity in select locations exhibiting the densest coverage. Vegetation shows a strong preference for K and Mg relative to Ca (Table 3.3);

however, with exception of the Svartá river, riverine  $\delta^{44/40}\text{Ca}$  values do not correlate with either Mg/Ca or K/Ca ratios (Figure 3.5).

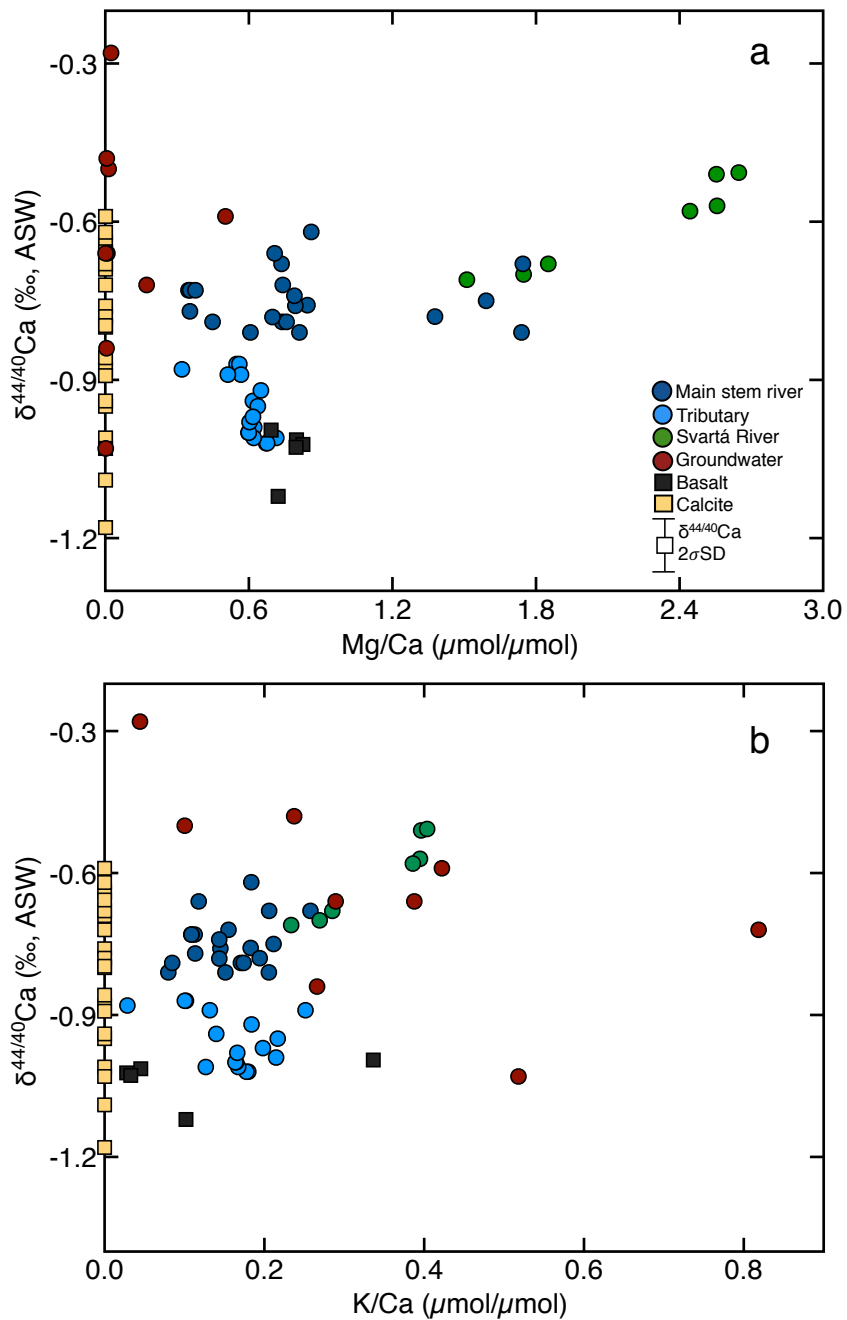


**Figure 3.5:**  $\delta^{44/40}\text{Ca}$  of water, basalt, and calcite versus Mg/Ca (a) and K/Ca (b). In these plots, only water samples from the Svartá river show positive trends.

More significantly, non-glacial tributaries draining vegetated catchments show basaltic  $\delta^{44/40}\text{Ca}$  values, whereas main stem rivers entering the Skagafjörður valley from the non-vegetated highlands show higher  $\delta^{44/40}\text{Ca}$  values. The Austari-Jökulsá and Vestari-Jökulsá rivers show high  $\delta^{44/40}\text{Ca}$  values, and these rivers drain the Icelandic highland region, which is devoid of vegetation and soil. As these rivers flow directly into main stem Skagafjörður rivers, it is unlikely that the primary mechanism elevating Skagafjörður river  $\delta^{44/40}\text{Ca}$  values is related to soil or vegetation processes.

#### 3.5.4.2 *Clays*

Clay minerals are widely expected to either adsorb or structurally bind lighter Ca isotopes (Hindshaw et al., 2011; Fantle et al., 2012; Ockert et al., 2013), although direct measurements of natural samples are lacking. Calcium uptake by phyllosilicates has been documented to fractionate Ca isotopes (Ockert et al., 2013; Brazier et al., 2019); however, Ca-bearing phyllosilicates, such as smectite and kaolinite, are generally absent from Icelandic soils (Crovisier and Daux, 1990; Crovisier et al., 1992; Wada et al., 1992; Stefansson and Gislason, 2001; Arnalds, 2015b; Paque et al., 2016). In Iceland, smectite is largely produced during high-temperature basalt alteration, for example, during burial metamorphism (Walker, 1960; Neuhoff et al., 1999; Weisenberger and Selbekk, 2009). Smectite and kaolinite observed in soils and sediments do not imply authigenic formation in surficial systems, as the clays could derive from hydrothermally altered rocks that were eroded and deposited as glacial till or aeolian material (Crovisier et al., 1992; Wada et al., 1992; Gudmundsson, 1997; Arnalds, 2000; Moulton et al.,

2000; Arnalds and Kimble, 2001; Gísladóttir et al., 2005; Gennadiev et al., 2007; Fridriksson et al., 2009; Franzson et al., 2011; Thorpe et al., 2019).

Icelandic soils mostly comprise poorly ordered allophane and ferrihydrite clays (Wada et al., 1992; Arnalds, 2004, 2015a), which do not efficiently retain Ca (Óskarsson et al., 2012), but it is possible that the adsorption of  $\text{Ca}^{2+}$  onto soil particle surfaces and organic matter could induce a fractionation. Indeed, the soil  $\text{NH}_4\text{Cl}$  leachates generally show lower  $\delta^{44/40}\text{Ca}$  values than bulk basalt (Table 3.3). With two exceptions discussed below for the Svartá river, the reagent leached <6% of the Ca relative to the corresponding HF- $\text{HNO}_3$  digests (Table 3.3), and  $\text{NH}_4\text{Cl}$  leachate  $\delta^{44/40}\text{Ca}$  values positively correlate the amounts of Ca leached (Figure 3.6).

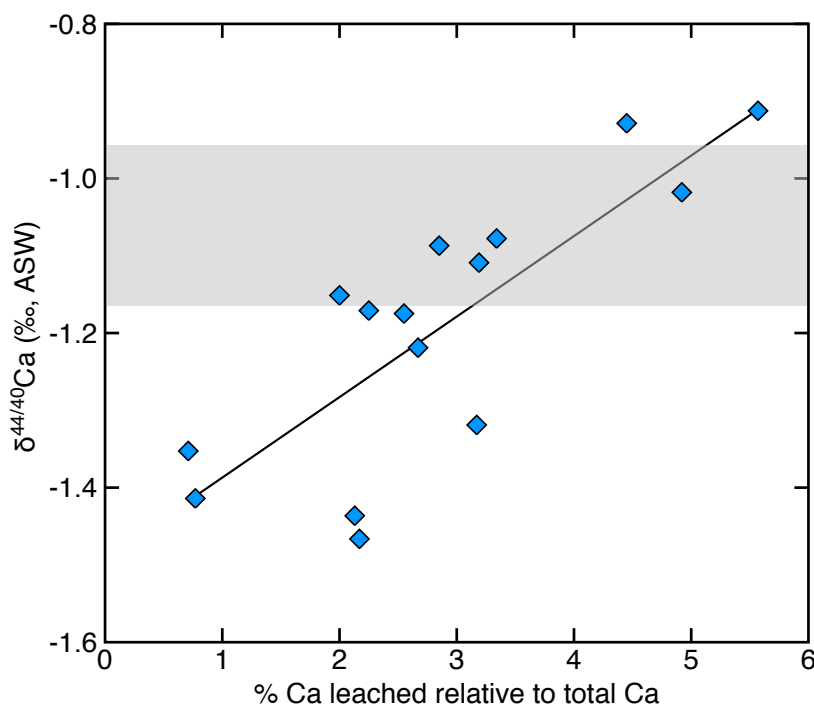


**Figure 3.6:** Soil  $\text{NH}_4\text{Cl}$  leachate  $\delta^{44/40}\text{Ca}$  versus the mol percent of Ca leached by  $\text{NH}_4\text{Cl}$  relative to total soil Ca. The operationally-defined soil “exchangeable” fraction shows low  $\delta^{44/40}\text{Ca}$  values when the leachate extracts less Ca, possibly suggesting a fractionation induced by the leaching procedure. The exchangeable  $\delta^{44/40}\text{Ca}$  value approaches the range for primary minerals (grey shading) when ~3% of Ca is leached.

Relatively low  $\delta^{44/40}\text{Ca}$  values correlate with very small amounts of leached Ca (<1%), while  $\delta^{44/40}\text{Ca}$  values converge on the range for bulk basalt and primary minerals when only 3% of the Ca is leached. These results could indicate that Icelandic soils support a very small exchangeable pool of lighter Ca isotopes, although I cannot eliminate the possibility that  $\text{NH}_4^+$  preferentially exchanges with lighter Ca isotopes (Teichert et al., 2009; Nelson et al., 2021). In either scenario, the adsorbed reservoir of Ca appears to represent a minor fraction of soil Ca. It is unclear how fractionation of Ca isotopes during adsorption could contribute to riverine trends with Sr/Ca and  $\delta^{44/40}\text{Ca}$ , as uptake onto volcanic soil exchange sites does not generally discriminate between Sr and Ca (Bullen and Chadwick, 2016). Similarly, fractionation by soils could not explain the observed riverine  $\delta^{44/40}\text{Ca}$  trends with molar ratios and SI calcite (Figures 3.2 to 3.5).

The soil data presented here generally point toward other processes as primary determinants of Skagafjörður river Ca isotope geochemistry. Future studies that include soil pore water measurements are necessary to more completely resolve the impact of soil processes on riverine  $\delta^{44/40}\text{Ca}$  values, but with the possible exception of the Svartá river discussed below, fractionation of Ca isotopes by plants and clays does not adequately explain first-order patterns observed for Skagafjörður valley surface waters.

#### 3.5.4.3 *Svartá exception*

As mentioned, two soil samples do not conform to the above interpretations, as they had anomalously high amounts of leached Ca (Table 3.3). Both of these samples came from a single pit that was part of a ~2 m thick soil sequence in the Svartá river valley on the western side of Skagafjörður. For these two samples, collected from the deepest horizon representing the glacial

till layer, about half of the total Ca was leached, compared to < 12% in the other pits (Table 3.3). These leachates also correspond to the lowest  $\delta^{44/40}\text{Ca}$  values of all soil leachates. Thus, a mineralogical reservoir of light Ca not identified in other samples may be present in Svartá soils. The Svartá river also has clearly distinct geochemistry compared to other rivers (Figure 3.2). It is possible that the geochemistry of these two samples reflects the presence of Ca-bearing minerals with low  $\delta^{44/40}\text{Ca}$  deep in the soil profile deposited by glacial activity. Zeolites and smectite-variety clays form during the alteration of basalt at elevated subsurface temperatures (Kristmannsdóttir and Tómasson, 1978; Saemundsson et al., 1980; Franzson, 2000; Thien et al., 2015), and altered rock containing zeolites and/or smectite exposed during glacial incision could be present in the glacial till (Crovisier et al., 1992; Wada et al., 1992; Gudmundsson, 1997; Arnalds, 2000; Arnalds and Kimble, 2001; Gisladóttir et al., 2005; Franzson et al., 2011). The soil leachates here have virtually no Mg (Table 3.3), whereas the Svartá river draining these soils has the highest Mg/Ca ratios of all water samples. Unlike all other Skagafjörður rivers, in the Svartá river, Mg/Ca ratios and  $\delta^{44/40}\text{Ca}$  positively correlate (Figure 3.5), inconsistent with a smectite-related fractionation mechanism, as smectite shows an equal preference for  $\text{Mg}^{2+}$  and  $\text{Ca}^{2+}$  (Crovisier and Daux, 1990; Crovisier et al., 1992; Wada et al., 1992; Stefansson and Gislason, 2001; Paque et al., 2016). It is unclear what is contributing to the low  $\delta^{44/40}\text{Ca}$  and high percentages of Ca leached in the Svartá soil samples, however, the soil data presented here from Svartá samples indicate that, of all samples analyzed, the Svartá samples are the most likely to reflect a soil-related fractionation mechanism. Considering the Svartá river samples are geochemically distinct from other Skagafjörður rivers, this generally points to an absence of soil

fractionation processes in other rivers. While soil fractionation mechanisms may contribute to the unique geochemistry of the Svartá river, another possible explanation is presented below.

### 3.5.5 *Sediments*

Bedload sediments show basaltic  $\delta^{44/40}\text{Ca}$ , and little to no exchangeable Ca (Table 3.3), consistent with small proportions of secondary minerals in bedload sediments, as had been observed elsewhere in Iceland (Thorpe et al., 2019). However, adsorption of light Ca isotopes to suspended material could elevate  $\delta^{44/40}\text{Ca}$  (Hindshaw et al., 2013), as adsorption of  $\text{Ca}^{2+}$  generally results in the fractionation of light isotopes to the adsorbed material (Ockert et al., 2013; Brazier et al., 2019). Rivers with the highest concentrations of suspended material correspond to the most available exchange sites. River  $\delta^{44/40}\text{Ca}$  values do not correlate with suspended sediment concentration, suggesting negligible adsorption control on dissolved  $\delta^{44/40}\text{Ca}$ . In parallel, adsorption or precipitation of colloidal material does not contribute to riverine  $\delta^{44/40}\text{Ca}$  (Appendix C).

### 3.5.6 *Groundwater and calcite*

Skagafjörður groundwaters show considerable geochemical variability relative to surface waters (Figures 3.2 to 3.5). Groundwater  $\delta^{44/40}\text{Ca}$  values correlate with Sr/Ca ratios, temperature, pH, and distance from the coast (Figure 3.7). Groundwater in the study region primarily originates from meteoric sources and geochemically evolves during progressive basalt-water interactions, which raises pH and results in the precipitation of secondary minerals, which mainly include zeolites and calcite (Arnórsson and Sveinbjörnsdóttir, 2000, 2004; Arnórsson et al., 2002; Fridriksson et al., 2009). Trends with distance from coast arise because, relative to

inland groundwaters, those closer to the coast have longer residence times and flow through older and more extensively altered basalt, consistent with their overall lower temperatures and lower degrees of undersaturation with respect to primary minerals (Arnórsson et al., 2002). Coastal groundwater are estimated to be thousands of years old, whereas inland waters have ages on the order of decades (Arnórsson and Sveinbjörnsdóttir, 2000; Arnórsson et al., 2002). High  $\delta^{44/40}\text{Ca}$  values and pH, as well as low Sr/Ca ratios, observed for coastal groundwaters, are consistent with higher degrees of geochemical evolution and extensive interaction with zeolites, which are expected to elevate dissolved  $\delta^{44/40}\text{Ca}$  values while lowering Sr/Ca ratios (Fridriksson et al., 2009; Jacobson et al., 2015; Nelson et al., 2021). Groundwaters in the southern region of the Skagafjörður valley (i.e., the highlands) originate from glacial meltwater infiltration in the highlands, and show higher temperatures, lower pH, and basaltic  $\delta^{44/40}\text{Ca}$  values, likely reflecting less geochemical evolution and minimal interaction with zeolites (Arnórsson et al., 2002). Unlike rivers, groundwaters are either at equilibrium or oversaturated with respect to calcite but show no trends between  $\delta^{44/40}\text{Ca}$  and SI calcite (Figure 3.3), confirming previous assertions that calcite precipitation does not contribute to groundwater  $\delta^{44/40}\text{Ca}$  variability (Jacobson et al., 2015; Andrews and Jacobson, 2017; Nelson et al., 2021). However, low  $\delta^{13}\text{C}$  values observed for Skagafjörður groundwaters are due to C isotope fractionation during subsurface calcite precipitation (Barry et al., 2014; Stefánsson et al., 2016; Sveinbjörnsdóttir et al., 2020) .

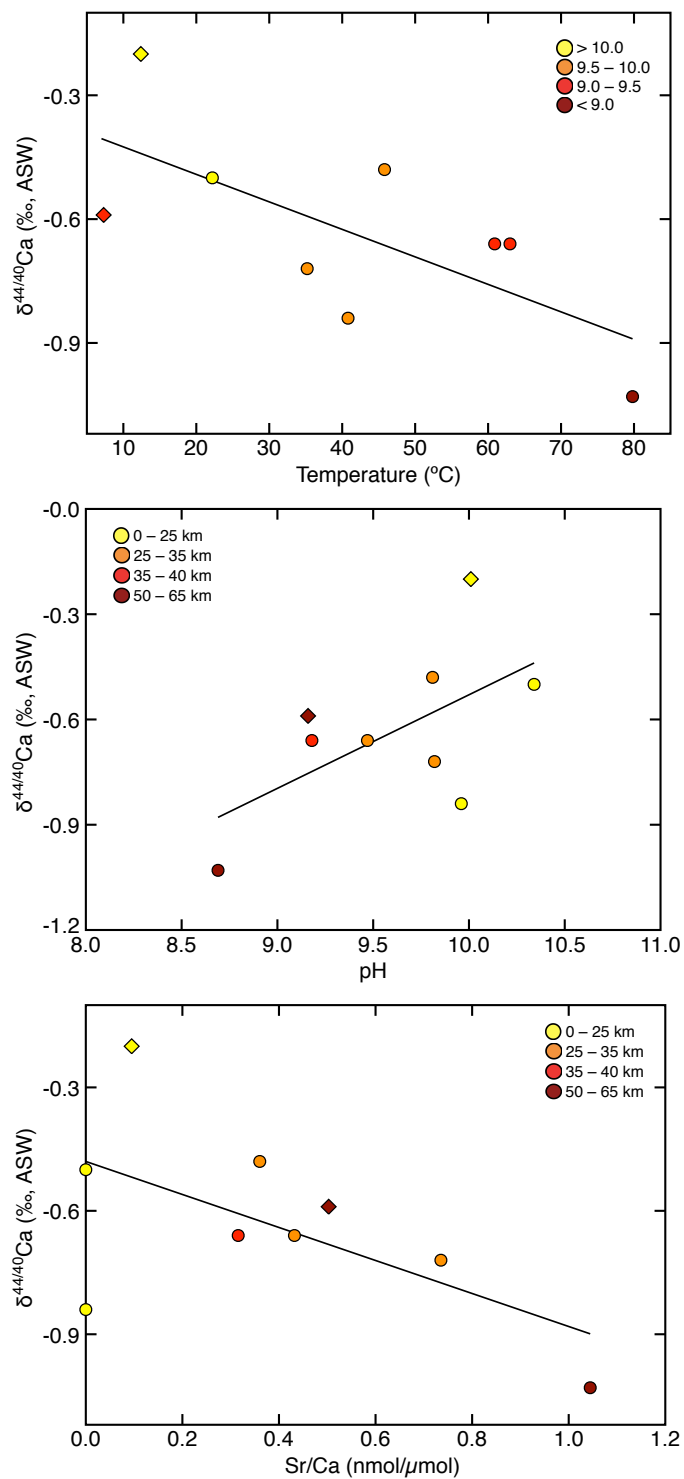


**Figure 3.7:** Geochemistry of Skagafjörður thermal (circles) and non-thermal (diamonds) groundwater springs. Trends are observed between  $\delta^{44/40}\text{Ca}$  and temperature, pH, Sr/Ca, and distance from coast.

Geochemical evolution of groundwater also explains the high  $\delta^{44/40}\text{Ca}$  of hydrothermal calcite (Jacobson et al., 2015; Nelson et al., 2021), as the travertines rapidly precipitated from surface waters show low  $\delta^{44/40}\text{Ca}$  values (Table 3.2). Previous studies have demonstrated the significance of trace calcite weathering in controlling Icelandic river geochemistry (Jacobson et al., 2015; Andrews and Jacobson, 2017); however, because of the similar geochemistry of calcite and groundwater, it is difficult to disentangle the impacts of calcite weathering and groundwater inputs on river chemistry. The reservoirs together can explain the trends observed for river  $\delta^{44/40}\text{Ca}$ , Sr/Ca, and SI calcite. Moreover, groundwater inputs are the best explanation of the observed correlation for  $\delta^{44/40}\text{Ca}$  and Na/Ca, as no fractionation mechanism offered a satisfactory explanation. Although carbon isotopes behave non-conservatively, river  $\delta^{13}\text{C}$  values can elucidate relative impact of each Ca source because Icelandic calcite has high  $\delta^{13}\text{C}$  values (-3.86‰ to -1.22‰, VPDB) and Skagafjörður groundwater has low  $\delta^{13}\text{C}$  values (Figure 3.8). As shown in Figure 3.8,  $\delta^{13}\text{C}$  values and SI calcite of most Skagafjörður rivers generally correlate. I interpret this to reflect some degree of calcite weathering control, where rivers with higher SI calcite and higher  $\delta^{13}\text{C}$  values represent greater calcite weathering influence.

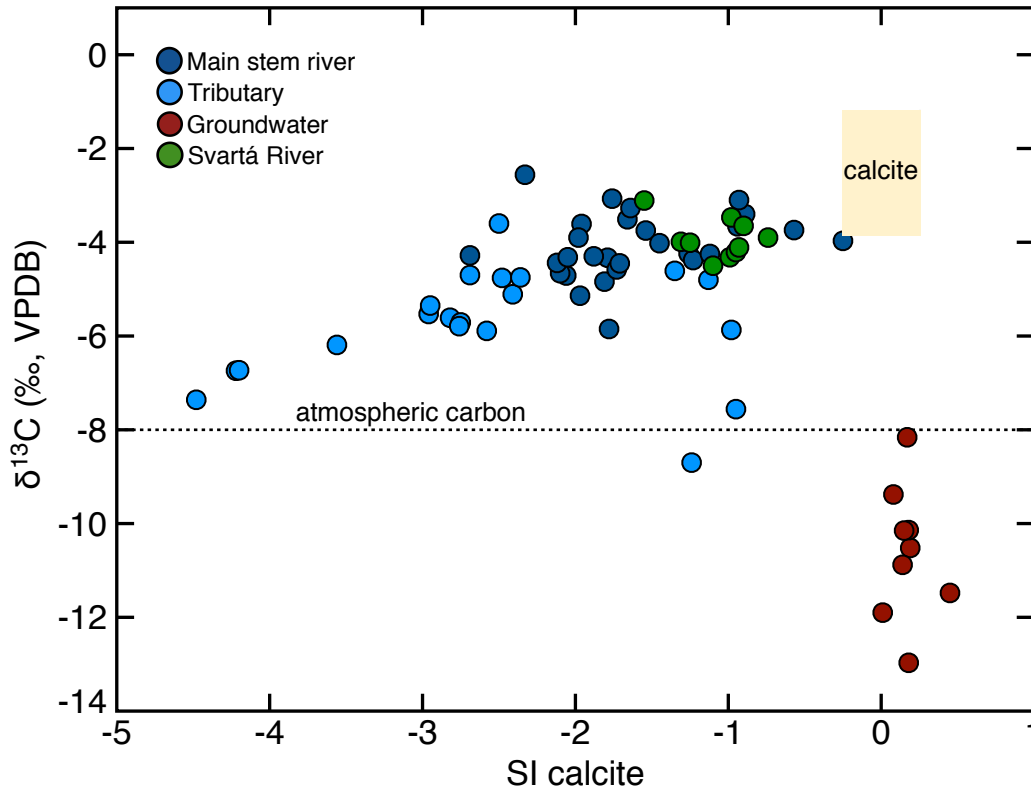


**Figure 3.8:** River and groundwater  $\delta^{13}\text{C}$  versus the saturation index of calcite. The height of the calcite region reflects the  $\delta^{13}\text{C}$  range of calcites measured in this study. The box is centered at an SI value of 0 (equilibrium) with a width of  $\pm 0.25$ , which represents the uncertainty of the index.

While I cannot apportion heavy Ca isotopes to either calcite weathering or groundwater from the present dataset, I can nevertheless approximate the influence of basalt weathering on river  $\delta^{44/40}\text{Ca}$  values. In Figure 3.2, I plot two mixing lines using the average values of basalt and each heavy end member, calcite and groundwater. The theoretical percentages were calculated using the following standard, two-component mixing equations:

$$(\text{Sr}/\text{Ca})_m = f_b \times (\text{Sr}/\text{Ca})_b + (1 - f_b) \times (\text{Sr}/\text{Ca})_h \quad (3.2)$$

$$\delta^{44/40}\text{Ca}_m = f_b \times \delta^{44/40}\text{Ca}_b + (1 - f_b) \times \delta^{44/40}\text{Ca}_h \quad (3.3)$$

where  $f$  is the mole fraction of Ca, and subscripts  $m$ ,  $b$ , and  $h$  refer to the mixture, basalt, and the “heavy” endmember, respectively. With the exception of the Svartá river discussed below, mixing between basalt, calcite, and groundwater provides a good explanation of the present dataset (Figure 3.2). Basalt weathering contributes a maximum of ~25% to 30% of Ca to main stem rivers, and up to 90% of Ca to direct-runoff tributaries. As basalt weathering dynamics in the subsurface differ from surficial silicate weathering, riverine elemental fluxes in main stem basalt-draining rivers do not reflect basalt weathering rates by atmospheric CO<sub>2</sub>. Similarly, calcite weathering proceeds orders of magnitude faster than basalt, and theoretically could supply a significant portion of Ca<sup>2+</sup> and HCO<sub>3</sub><sup>-</sup> to rivers. These results indicate that quantifications of basalt weathering rates by atmospheric CO<sub>2</sub> and constraints on parameters influencing these rates are only applicable to direct-runoff, tributary type rivers.

As shown in Figures 3.2 to 3.5, the Svartá river shows geochemical trends that are unlike those observed for other Skagafjörður rivers. While a fractionation mechanism unique to the Svartá watershed could explain these observations (see section 3.5.4.3), another possibility exists. One early investigation of Skagafjörður reported permeability, δ<sup>18</sup>O, and δ<sup>2</sup>H anomalies in several western groundwaters (the Svartá watershed) indicative of a pre-Holocene water source that is distinct from all other Skagafjörður groundwaters (Arnórsson and Sveinbjörnsdóttir, 2004). The authors also reported that these waters showed high Cl<sup>-</sup> concentrations, possibly indicative of either compositionally different, pre-Holocene precipitation, or a “tiny seawater component” isolated to the groundwater springs along the Svartá river. Svartá river samples in this study show high Mg/Ca and K/Ca, whereas all other river samples show ratios that overlap with those of bulk basalt (Figure 3.5). Svartá river Mg/Ca and K/Ca correlate weakly with

$\delta^{44/40}\text{Ca}$ , consistent with a small seawater component (Lebrato et al., 2020). The Svartá is the only river where  $\delta^{44/40}\text{Ca}$  do not correlate with Sr/Ca (Figure 3.2), indicating mixing with a water source that is compositionally different from most Skagafjörður groundwaters, possibly consistent with a pre-Holocene seawater component. The Svartá river, soil, and groundwater samples are unlike all other Skagafjörður samples (Arnórsson and Sveinbjörnsdóttir, 2004), indicating that the mechanism contributing to elevated  $\delta^{44/40}\text{Ca}$  in this river is not a factor in any other Skagafjörður river. More work is needed to resolve whether soil-related fractionation, seawater mixing, or another mechanism is controlling Svartá river geochemistry. However, the clear distinction between the Svartá river and other Skagafjörður rivers further underscores our interpretation that river  $\delta^{44/40}\text{Ca}$  primarily reflects mixing with groundwater and calcite weathering.

### 3.6 Conclusions

Rivers draining the Skagafjörður region of Iceland generally show higher  $\delta^{44/40}\text{Ca}$  values than basalt, and the values correlate with Sr/Ca and Na/Ca ratios, as well as the saturation index of calcite. Additionally, riverine  $\delta^{13}\text{C}$  values correlate with the saturation index of calcite. Vegetation and soil leachates show lower  $\delta^{44/40}\text{Ca}$  values, indicating that Ca isotopes are fractionated during vegetation uptake and adsorption. However, fractionation appears to have, at most, second order controls on riverine  $\delta^{44/40}\text{Ca}$  values and overall does not provide an adequate explanation of the present dataset. Groundwaters show the highest  $\delta^{44/40}\text{Ca}$  values of all Icelandic samples. The values correlate with other indicators of geochemical evolution, including pH, temperature, and Sr/Ca ratios, confirming previous interpretations that progressive ion-exchange

with zeolites is the primary control on groundwater Ca isotope geochemistry (Jacobson et al., 2015; Nelson et al., 2021). The results largely indicate that the majority of solutes in main-stem glacial rivers in the Skagafjörður valley are sourced from a combination of calcite weathering and groundwater inputs. A simple, two-component mixing model indicates that a maximum of ~20% of dissolved Ca in main-stem rivers is sourced from primary minerals that compose basalt. Only tributaries draining Tertiary basalt that are isolated from groundwater inputs show geochemistry indicative of basalt weathering by atmospheric CO<sub>2</sub>. Thus, future studies aiming to quantify parameters that influence basalt weathering rates and estimate atmospheric CO<sub>2</sub> drawdown should focus solely on direct-runoff tributaries that drain unaltered basalt.

## Chapter 4

### **Basalt weathering in the Icelandic highlands: reassessing the role of basalt weathering on long term climate regulation with Ca isotope geochemistry**

#### **4.1 Introduction**

The chemical weathering of basalt and granite regulates Earth's climate over geologic timescales by removing atmospheric CO<sub>2</sub> (Urey, 1952; Berner et al., 1983). However, basalt is widely accepted to do so at faster rates. Given that the proportions of basalt and granite composing crustal rocks have changed through time, quantifying the relative weatherability of basalt and granite has key implications for understanding the habitability of Earth and likely other planets that cycle carbon between their endo- and exo-genic reservoirs.

The hypothesis that basalt weathers faster than granite largely traces to an early study, which concluded that mafic rocks weather faster than felsic rocks at the Earth's surface due to the higher susceptibility of mafic minerals to chemical breakdown (Goldich, 1938). In more recent times, the geochemistry of rivers has been interpreted as direct confirmation of the relative “mineral stability” paradigm. Basalt-draining rivers globally show much higher HCO<sub>3</sub><sup>-</sup> export fluxes than granite-draining rivers, which has led to the assertion that basaltic regions are atmospheric CO<sub>2</sub> consumption “hot spots” (Gaillardet et al., 1999; Dessert et al., 2001, 2003; Hartmann et al., 2014; Li et al., 2016; Ibarra et al., 2016). Rapid weathering of basalt and other mafic rocks has been invoked to explain changes in global climate throughout geologic history (Dessert et al., 2001; Cox et al., 2016; Macdonald et al., 2019) and also forms the basis for burgeoning geoengineering strategies to mitigate the effects of anthropogenic climate change (Snæbjörnsdóttir et al., 2020; Beerling et al., 2020).

Nonetheless, broader consideration of the mineral stability paradigm raises challenging questions. If basalt weathers faster than granite, then rivers draining carbonate bedrock should yield higher  $\text{HCO}_3^-$  export fluxes than those draining basalt, as carbonate minerals dissolve several orders of magnitude faster than mafic minerals (Chou et al., 1989; Arvidson et al., 2003). However, rivers draining basalt and carbonate curiously display similar  $\text{HCO}_3^-$  fluxes (Dessert et al., 2001; Suchet et al., 2003). Thus, a key paradox arises: does basalt weathering occur as quickly as carbonate weathering, or alternatively, does carbonate weathering pervasively occur in basaltic landscapes, despite absence of sedimentary carbonate rocks?

To address this paradox, this study investigates the calcium and carbon isotope ( $\delta^{44/40}\text{Ca}$  and  $\delta^{13}\text{C}$ ) geochemistry of rivers draining the highlands of central Iceland. Here, large and sediment-laden rivers drain ice caps that have formed on top of young, glassy basalt. The region is devoid of soils and vegetation, which yield unique chemical weathering signatures (Moulton et al., 2000) compared to glaciated landscapes that simply comprise ice, water, and rock. The rivers are hypothesized to consume large amounts of atmospheric  $\text{CO}_2$  due to the combined effects of rapid glass weathering (Gislason and Eugster, 1987a; Gislason and Arnórsson, 1993; Gislason et al., 1996; Oelkers and Gislason, 2001; Gislason and Oelkers, 2003) and accelerated mechanical erosion by glacial activity (Anderson et al., 1997; Gislason et al., 2009). The highlands also experience vigorous hydrothermal activity leading to the precipitation of hydrothermal calcite (Gíslason et al., 2002; Warner and Farmer, 2010; Galeczka et al., 2014), as well as widespread hot spring discharge that contributes to river geochemistry (Gislason and Eugster, 1987b; Sigurdsson, 1990; Gislason et al., 1996; Lawler and Bjornsson, 1996; Oskarsdottir et al., 2011;

Barry et al., 2014; Galeczka et al., 2015; Ármannsson, 2016), as has been documented in other locations of basaltic volcanism (Rad et al., 2007; Rivé et al., 2013).

Two previous Ca isotope studies have reported that Icelandic rivers have much higher  $\delta^{44/40}\text{Ca}$  values than basalt (Hindshaw et al., 2013; Jacobson et al., 2015). However, the origin of the signal remains controversial, and no studies have specifically targeted the highlands. Clays and other silicate weathering byproducts are widely expected to preferentially incorporate lighter Ca isotopes and thereby elevate riverine  $\delta^{44/40}\text{Ca}$  values. However, hydrothermal calcite dispersed throughout Iceland has higher  $\delta^{44/40}\text{Ca}$  values than rivers (Jacobson et al., 2015; Nelson et al., 2021), and numerous studies have demonstrated that trace calcite weathering can dominate riverine  $\text{Ca}^{2+}$  and  $\text{HCO}_3^-$  fluxes due to the mineral's high solubility and fast reaction kinetics (Blum et al., 1998; Anderson et al., 2002; Anderson, 2005; Moore et al., 2013). The carbon isotope composition of dissolved inorganic carbon ( $\delta^{13}\text{C}_{\text{DIC}}$ ) can help resolve the origin of  $\delta^{44/40}\text{Ca}$  values in Icelandic rivers, as the proxy sensitively traces DIC inputs from silicate versus carbonate weathering (Telmer and Veizer, 1999; Das et al., 2005a; Spence and Telmer, 2005; Li et al., 2008; Jin et al., 2009; Schulte et al., 2011; Rivé et al., 2013; Lehn et al., 2017) but is insensitive to clay formation, ion-exchange, and other phenomena hypothesized to fractionate Ca isotopes.

## 4.2 Geologic Setting

Iceland is an exposed section of the Atlantic mid-ocean ridge overlying a mantle plume that has caused extensive rifting and volcanism over the past 50-60 Myr (White and McKenzie, 1989). Rocks increase in age away from the active rift zone, with the oldest rocks at the edges of

Iceland dating to ~16 Ma (Moorbath et al., 1968). This study focuses on the central Icelandic highlands, where rocks effectively have zero ages (Figure 4.1). The central rift zone comprises one main axis in the north and two legs in the south, where the European and North American plates actively diverge. Intraplate volcanic activity occurring along these axes has supplied lava that presently piles to a maximum height of ~2000 m. Three major ice caps (the Hofsjökull, Langjökull, and Vatnajökull) overlie the active rift zone and collectively cover ~11% of Iceland's total land area (Björnsson and Pálsson, 2008). Runoff from the highlands accounts for 33% of Iceland's total runoff (Björnsson and Pálsson, 2008). The mean annual temperature in the highlands is ~0°C. Most samples were collected from the Northern desert region of the highlands (Figure 4.1), where mean annual precipitation (300-1000 mm/year) is lowest in all of Iceland (Arnalds, 2004; Rögnvaldsson et al., 2007). The region is devoid of soils and vegetation (Arnalds, 2004; Mankasingh and Gísladóttir, 2019). Highland rocks are mainly hyaloclastites, which are a breccia of primary basaltic minerals, volcanic glass, and varying amounts of secondary minerals. Rapid quenching of basaltic magma during subglacial eruptions causes vitrification, such that hyaloclastites can contain up to 90% glass (Watton et al., 2013). Hydrous alteration occurring syn-eruption or soon thereafter produces secondary alteration products, such as palagonite, clay minerals, zeolites, and calcite, which together generally comprise 0-40% of volume of solid rock, although some samples can contain up to 90% alteration minerals (Stroncik and Schmincke, 2002; Franzson et al., 2011). The rivers examined here are fed mostly by the Hofsjökull ice cap; however, some samples are fed by the Langjökull and Vatnajökull ice caps (Figure 4.1).

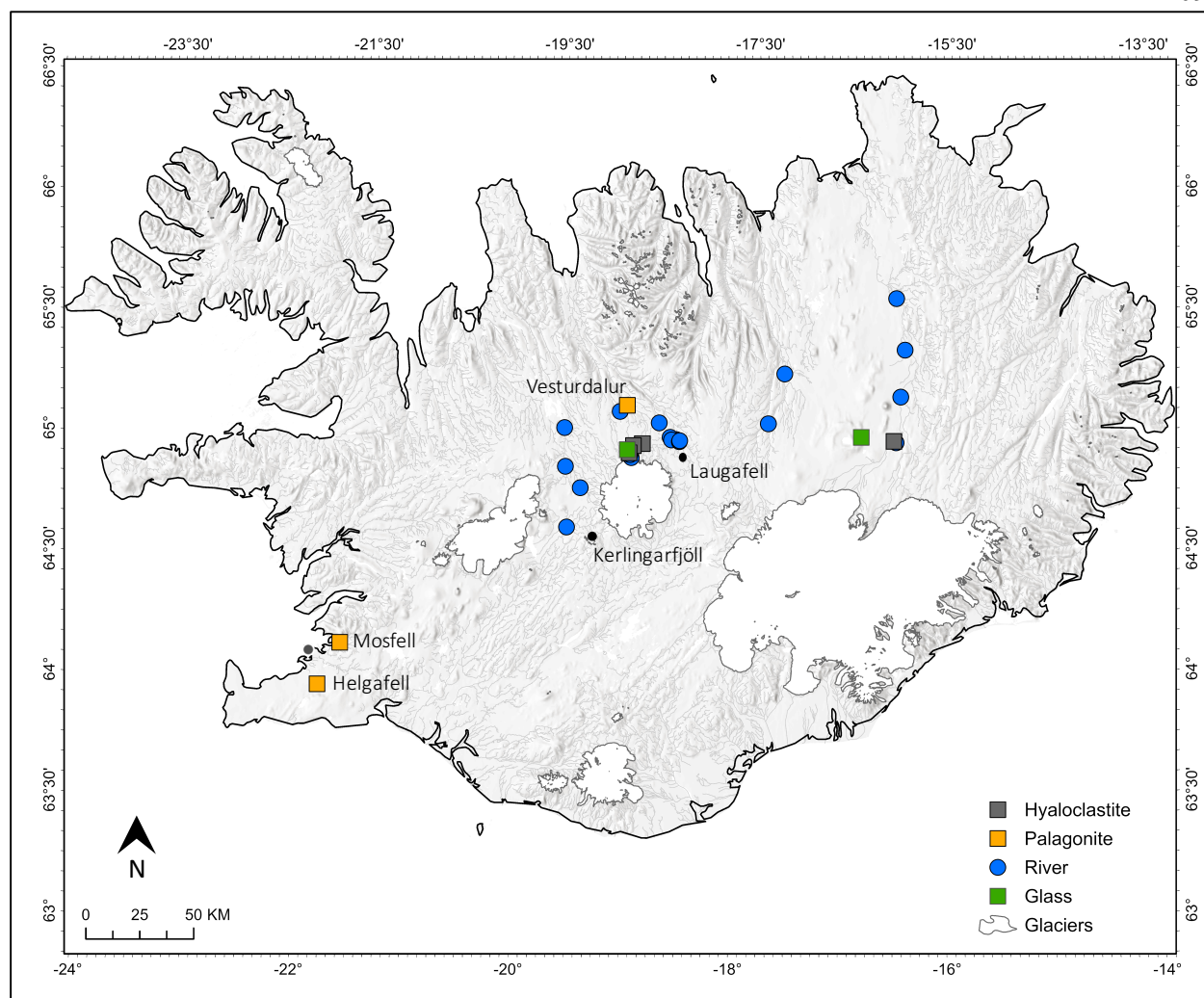


**Figure 4.1:** Map of Iceland showing highland river sample locations. Palagonite sample locations are labeled. Black points indicate the high-temperature volcanic center at Kerlingarfjöll and the hydrothermal spring at Laugafell.

## 4.3 Methods

### 4.3.1 Field Collection

River water samples ( $n=25$ ) were collected in July of 2017 and 2019. Some samples were collected as close as  $\sim 100$  m from a terminal lobe of the Hofsjökull ice cap. At each sample site, geographic data were documented with a Garmin 60CSx handheld GPS receiver (Appendix B).

Water pH and temperature data were recorded on site using a Thermo-Scientific Orion 3-Star Portable pH Meter equipped with a temperature probe and an Orion 8104BNUWP ROSS glass body rugged bulb pH electrode. The electrode was calibrated daily with pH 4, 7, and 10 buffers. Water samples were collected using a peristaltic pump and filtered through Geotech 0.45  $\mu\text{m}$  filter capsules containing a Versapor membrane. Samples for cation and Si concentrations, as well as Ca isotope ratios, were collected into I-CHEM HDPE bottles and acidified to pH <2 with ultrapure, concentrated  $\text{HNO}_3$ . Samples for anion and alkalinity analyses were collected into LDPE bottles. One snow sample, collected from the terminus of the Hofsjökull glacier, was collected in an LDPE bag, melted, and filtered into HDPE bottles. Total carbonate alkalinity ( $A_T = [\text{HCO}_3^-] + 2[\text{CO}_3^{2-}]$ ) in  $\mu\text{eq/L}$  was measured by Gran Titration with 0.02N HCl. Uncertainty of this method was determined to be  $\pm 5\%$  by repeatedly measuring a gravimetric  $\text{Na}_2\text{CO}_3$  standard. Considering the pH range of water samples,  $A_T \approx [\text{HCO}_3^-]$ . Water samples for the carbon isotope composition of total dissolved inorganic carbon ( $\delta^{13}\text{C}_{\text{DIC}}$ ) were collected using a BD 5 mL sterile syringe equipped with a BD Precision Glide 23-gauge needle. Samples were filtered through Whatman Puradisc 25 mm polypropylene 0.45  $\mu\text{m}$  filters into white-cap 12 mL round-bottom Exetainers.

Suspended sediment samples were collected on pre-weighed glass-microfiber filters by vacuum-pumping water through a porcelain Buchner funnel into an Erlenmeyer flask. Water collected in the flask was then poured into a graduated cylinder, and total volume of water passed through the filter was recorded. Filters saturated with sediment were later dried and weighed to estimate suspended sediment concentrations in rivers.

Highland rocks were sampled from outcrops and stored in LDPE bags. Rocks from two palagonite ridges outside of the highlands, Helgafell and Mosfell (Figure 4.1), were sampled at elevation intervals of approximately ~120 m. In addition, samples were taken from another palagonitized outcrop in the Vesturdalur valley along the Hofsa river (Appendix D).

#### *4.3.2 Sample Preparation*

Whole rock samples were cut with a rock saw to remove any weathering rinds, and the inner portions were powdered in a shatterbox with a tungsten-carbide grinding container. Basaltic glass was subsampled from hyaloclastite rocks and powdered in a Diamonite mortar and pestle. Filters containing suspended sediment samples were dried and weighed, and sediment was recovered from filters and collected into pre-weighed LDPE centrifuge tubes. Sediment powders were processed through a sequential leaching and digestion procedure to isolate exchangeable, carbonate, and silicate fractions. Sediment powder (~1 g) was weighed into LDPE centrifuge tubes and reacted with ~10 mL of 1M NH<sub>4</sub>Cl (adjusted to pH 8) on a rocker table for ~6 hours. Samples were centrifuged, and the supernatants were filtered through Whatman Puradisc 25 mm polypropylene 0.45 μm filters into Teflon vials. These samples, defined here as the “exchangeable fraction”, were dried and redissolved in 5% HNO<sub>3</sub>. The remaining residue was then reacted with ~10 mL of 0.2 M acetic acid on a rocker table for 6~8 hours. The mixture was centrifuged, and the supernatants were collected by the same procedure. The acetic acid step was repeated until the supernatant reached a constant pH of < 2. For each repetition, the supernatant was collected into the same Teflon vial, and the total solution was dried and redissolved in 5% HNO<sub>3</sub>. Finally, the remaining residues, assumed to represent the “silicate fraction,” were dried in an oven at 50°C, and ~0.8 g subsamples were weighed into

Teflon vials and digested with a combined HF-HNO<sub>3</sub> mixture at 130°C for several days until no visible material remained. Samples were dried, refluxed in concentrated HNO<sub>3</sub>, dried again, and refluxed in 6N HCl to ensure complete dissolution. Samples were dried and redissolved in 5% HNO<sub>3</sub>. Bulk rock powders were digested using the same procedure.

#### *4.3.3 Elemental Analysis*

All solutions were analyzed for cation and Si concentrations using a Thermo Scientific iCAP 6500 inductively coupled plasma-optical emission spectrometer (ICP-OES) at Northwestern University. For select samples with low [Al], [Al] was measured using a Thermo iCapQ quadrupole ICP-MS at the Quantitative Bio-element Imaging Center at Northwestern University. All concentrations have an uncertainty of ±10% (RSD), as determined by repeated analyses of NIST SRM 1643f. Anion concentrations in river water samples were analyzed using a Dionex DX-120 Ion Chromatograph equipped with an AS15 exchange column and an ASRS-300 suppressor. Repeated analyses of a NIST-traceable standard were within ±10% (RSD) of reported concentrations. The average charge balance error [CBE = (TZ<sup>+</sup> - TZ<sup>-</sup>)/(TZ<sup>+</sup> + TZ<sup>-</sup>)], where TZ<sup>+</sup> is the sum of all cations and TZ<sup>-</sup> is the sum of all anions (in equivalents), for all river samples is 6% (n=25). Ion activities were computed using PHREEQC (Parkhurst and Appelo, 1999) implemented with the llnl.dat database. Calcite saturation indices were calculated using the ion activity output and the temperature-dependent equilibrium constants from Plummer and Busenberg (1982).

#### *4.3.4 Carbon Isotope Ratios*

The carbon isotope composition of total dissolved inorganic carbon ( $\delta^{13}\text{C}_{\text{DIC}}$ ) was analyzed using a Thermo Gasbench II mated to a Delta V Plus Isotope Ratio Mass Spectrometer (IRMS) at the Northwestern University Stable Isotope Biogeochemistry Laboratory. Filtered samples (0.45  $\mu\text{m}$ ), collected in airtight glass Exetainers, were acidified using 103%  $\text{H}_3\text{PO}_4$  so that all of the DIC was converted to  $\text{CO}_2$  for measurement by IRMS.  $\delta^{13}\text{C}_{\text{DIC}}$  values are reported relative to VPDB. Replicates of in-house standards ( $\text{NaHCO}_3$ ) indicate a precision of  $\pm 0.09\text{‰}$  ( $1\sigma_{\text{SD}}$ ) for  $\delta^{13}\text{C}$ .

#### 4.3.5 Calcium Isotope Ratios

Calcium isotope ratios ( $^{44}\text{Ca}/^{40}\text{Ca}$ ) were measured with a Thermo-Fisher Triton MC-TIMS at Northwestern University, using an optimized  $^{43}\text{Ca}$ - $^{42}\text{Ca}$  double-spike procedure (Lehn et al., 2013). Samples containing 50  $\mu\text{g}$  of Ca were equilibrated with the spike, and the solutions were eluted through Teflon columns packed with Bio-Rad AG MP-50 cation exchange resin. Approximately 12.5  $\mu\text{g}$  of purified Ca was loaded onto outgassed, single Ta filament assemblies together with 0.5  $\mu\text{L}$  of 10%  $\text{H}_3\text{PO}_4$ . Total procedural blanks ( $n = 4$ ) determined with a  $^{42}\text{Ca}$  isotope dilution method were negligible (65 – 117 ng). Reported  $\delta^{44/40}\text{Ca}$  have an internal precision of  $\pm 0.02$ - $0.03\text{‰}$  ( $2\sigma_{\text{SEM}}$ ). The double-spike was frequently recalibrated by analyzing at least 8 OSIL ASW standards and 2 NIST 915b standards every 30 or fewer samples. During the period of study, repeated analyses of the standards yielded  $\delta^{44/40}\text{Ca}_{\text{ASW}} = 0.000 \pm 0.005\text{‰}$  ( $2\sigma_{\text{SEM}}$ ,  $n = 68$ ) and  $\delta^{44/40}\text{Ca}_{915\text{b}} = -1.147 \pm 0.012\text{‰}$  ( $2\sigma_{\text{SEM}}$ ,  $n = 17$ ). These data correspond to a short-term external reproducibility ( $2\sigma_{\text{SD}}$ ) of  $\pm 0.045\text{‰}$  for OSIL ASW and  $\pm 0.049\text{‰}$  for NIST 915b. Long-term records for the laboratory yield  $\delta^{44/40}\text{Ca}_{\text{ASW}} = 0.000 \pm 0.002\text{‰}$  ( $2\sigma_{\text{SEM}}$ ,  $n = 661$ )

and  $\delta^{44/40}\text{Ca}_{915b} = -1.135 \pm 0.003\text{‰}$  ( $2\sigma_{\text{SEM}}$ ,  $n = 263$ ). These data point to a  $2\sigma_{\text{SD}}$  of  $\pm 0.044\text{‰}$  for OSIL ASW and  $\pm 0.048\text{‰}$  for NIST 915b. Based on all standard measurements, I adopt an uncertainty of  $\pm 0.05\text{‰}$  for all  $\delta^{44/40}\text{Ca}$  values reported in the present dataset. Duplicate analyses of sample unknowns are better than  $\pm 0.04\text{‰}$ .

## 4.4 Results

### 4.4.1 Major Ion, Ca Isotope, and C Isotope Geochemistry of Rivers

Table 4.1 presents the elemental and isotope geochemistry of water samples. For most river samples,  $\text{Na}^+$  and  $\text{K}^+$  dominate the cationic charge ( $\sim 30\% - 65\%$ ), followed by  $\text{Ca}^{2+}$  ( $\sim 26\% - 43\%$ ), with a smaller contribution from  $\text{Mg}^{2+}$  ( $\sim 8\% - 28\%$ ). For all rivers, on average,  $\text{HCO}_3^-$  dominates the anionic charge ( $>75\%$ ), with roughly equal contributions from  $\text{Cl}^-$  ( $\sim 13\%$ ) and  $\text{SO}_4^{2-}$  ( $\sim 11\%$ ). All water samples are undersaturated with respect to calcite. The charge contributions differ slightly for samples collected in closest proximity to the Hofsjökull glacial terminus ( $\sim 5000 - 100$  m from ice). Here, rivers show roughly equal proportions of cationic charge from  $\text{Ca}^{2+}$ ,  $\text{Mg}^{2+}$ , and  $\text{Na}^+$  and  $\text{K}^+$ , as well as greater contributions of  $\text{Cl}^-$  to the anionic charge ( $\sim 15\% - 25\%$ ) relative to  $\text{HCO}_3^-$  ( $\sim 62\% - 75\%$ ).

Measured  $\delta^{44/40}\text{Ca}$  values for highland rivers range from  $-0.85\text{‰}$  to  $-0.62\text{‰}$ , with an average of  $-0.77 \pm 0.06\text{‰}$  ( $1\sigma_{\text{SD}}$ ,  $n = 23$ ), which is similar to averages for Icelandic glacial rivers previously reported in Hindshaw et al. (2013) and Jacobson et al. (2015). Complementary  $\delta^{13}\text{C}$  values range from  $-8.02\text{‰}$  to  $-0.16\text{‰}$ , with an average of  $-5.43\text{‰} \pm 1.85\text{‰}$  ( $1\sigma_{\text{SD}}$ ,  $n = 24$ ).

**Table 4.1.** Geochemical and isotopic data of river water samples from the highlands, as well as ice from the Hofsjökull glacier. Duplicate analyses are given in parentheses. “-” indicates below detection limit, and “nm” indicates not measured.

Sample ID	T (°C)	pH	Ca (μmol/L)	K (μmol/L)	Mg (μmol/L)	Na (μmol/L)	Al (nmol/L)	Si (μmol/L)	Sr (nmol/L)	Cl (μmol/L)	SO <sub>4</sub> (μmol/L)	HCO <sub>3</sub> <sup>-</sup> (μmol/L)	logΩ <sub>cal</sub>	δ <sup>44/40</sup> Ca (‰, ASW)	Suspended Sediments (mg/L)	δ <sup>13</sup> C <sub>DIC</sub> (‰, VPDB)
AJ_e	6.3	7.78	81.1	11.0	42.8	329	5012	183	26.2	56.5	12	564	-1.74	-0.62 (-0.65)	142.28	-8.02
AJ_i	12.0	7.87	80.1	7.52	23.6	219	4688	184	19.4	75.5	15	365	-1.72	-0.75	nm	-6.43
AJt_f	7.0	7.66	87.6	10.7	31.6	247	1165	229	36.5	59.1	15	447	-1.91	-0.72	nm	-6.34
VJ_g	0.3	7.33	41.5	4.02	32.6	74.7	7900	61	21.7	38.8	14	197	-3.03	-0.79	756.09	-6.42
VJ_h	0.9	7.27	40.5	3.54	31.8	71.7	8308	58	22.8	38.6	14	163	-3.18	-0.80 (-0.85)	nm	-6.76
VJ_i	1.4	7.3	41.9	3.09	32.7	72.9	9140	63	22.8	38.8	14	199	-3.04	-0.80 (-0.83)	624.66	-6.61
VJ_j	1.3	7.33	40.2	3.57	31.5	71.9	7481	57	20.5	36.9	13	193	-3.03	-0.83	nm	-6.38
VJ_k	5	7.44	21.1	1.08	18.0	37.3	4476	58	13.7	30.9	10	81.6	-3.51	-0.80 (-0.84)	685.99	-6.98
VJ_l	5.1	7.59	20.7	1.69	17.5	33.8	6628	59	13.7	30.3	9.4	81.8	-3.40	nm	nm	-6.90
FS_1	3.8	7.25	26.3	1.76	17.9	47.0	929	41	4.6	25.5	5.7	80.5	-3.60	-0.75	nm	-6.97
FS_2	3.8	7.23	24.1	1.95	17.3	49.0	1499	41	6.9	26.0	4.6	98.1	-3.57	-0.81	nm	-6.91
BL_1	7.0	7.53	93.8	5.20	59.3	125	3394	138	27.4	56.6	33	323	-2.16	-0.79	372.29	-3.29
BL_2	10.7	8.00	91.5	12.8	40.2	395	-	242	37.7	104	31	530	-1.47	-0.80	nm	-7.00
BL_3	10.0	7.58	89.7	9.37	65.9	169	6550	193	48.0	65.1	32	393	-2.01	-0.85	238.51	-4.56
JF_1	7.9	8.02	256	13.9	141	515	10936	253	99.4	138	129	1042	-0.78	-0.80	771.51	-3.41
JF_2	9.7	8.00	207	13.0	114	485	866	213	80.0	123	113	876	-0.92	-0.82	nm	-3.29
JF_3	9.8	7.69	138	11.9	78.9	365	10241	180	64.0	98.2	71	631	-1.54	-0.73	981.52	-4.48
JF_4	9.4	7.89	131	11.9	75.7	368	3595	172	56.0	100	66	606	-1.37	-0.73 (-0.72)	nm	-4.14
SK_1	10.8	7.97	112	8.26	68.2	321	617	248	30.8	71.1	45	543	-1.37	-0.80	38.17	-4.03
SK_2	15.2	8.04	106	9.01	66.4	353	2929	246	35.4	70.0	52	573	-1.25	-0.82	nm	-2.98
HT_1	5.7	7.70	144	7.63	78.9	180	12211	188	46.8	76.0	55	474	-1.70	-0.83 (-0.78)	nm	-0.16
HF_h	6.8	8.17	101	20.4	81.1	494	592	259	42.2	66.0	16	822	-1.10	-0.67	nm	-6.58
HJ_1	6.7	7.60	73.4	5.68	27.5	215	7304	172	14.8	56.6	11	418	-2.13	-0.68	nm	-5.84
HJ_2	13.6	8.08	81.9	10.2	24.7	385	974	235	13.7	73.4	18	523	-1.40	-0.64	nm	-5.87
Ice	0	nm	2.35	0.75	0.79	3.51	-	-	-	19.1	4.53	nm	nm	nm	nm	nm

#### 4.4.2 Ca Isotope Geochemistry of Rock, Glass, and Sediment Samples

Table 4.2 reports elemental concentrations and Ca isotope ratios of rock, glass, and sediment samples. Hyaloclastites show an average  $\delta^{44/40}\text{Ca}$  value of  $-1.11 \pm 0.10\text{‰}$  ( $1\sigma_{\text{SD}}$ ,  $n = 5$ ). One sample yielded a relatively low value of  $-1.28\text{‰}$ . Excluding this sample, the average  $\delta^{44/40}\text{Ca}$  value of hyaloclastites ( $-1.07 \pm 0.03\text{‰}$ ,  $1\sigma_{\text{SD}}$ ,  $n = 4$ ) is nearly identical to that of bulk Icelandic basalt ( $-1.06 \pm 0.01\text{‰}$ ,  $1\sigma_{\text{SD}}$ ,  $n = 6$ ; Jacobson et al., 2015). Bulk palagonites from the southern region (Helgafell and Mosfell) have average  $\delta^{44/40}\text{Ca}$  value of  $-1.09 \pm 0.02\text{‰}$  ( $1\sigma_{\text{SD}}$ ,  $n = 7$ ), which is similar to the averages for bulk hyaloclastites and basalts. Other palagonite samples from an outcrop in the Vesturdalur valley north of the highlands (Figure 4.1) produced the lowest average  $\delta^{44/40}\text{Ca}$  value ( $-1.23 \pm 0.03\text{‰}$ ,  $1\sigma_{\text{SD}}$ ,  $n = 4$ ). One volcanic glass sample yielded the highest  $\delta^{44/40}\text{Ca}$  value ( $-0.93\text{‰}$ ) of all rock samples analyzed, but the value is lower than those observed for rivers.

**Table 4.2.** Geochemical and isotopic data of rock samples presented in this study. Duplicate analyses are given in parentheses.

Sample ID	Rock type	Ca ( $\mu\text{mol/g}$ )	K ( $\mu\text{mol/g}$ )	Mg ( $\mu\text{mol/g}$ )	Na ( $\mu\text{mol/g}$ )	Sr (nmol/g)	$\delta^{44/40}\text{Ca}$ (‰, ASW)
FS_17	highland hyaloclastite	2250	1771	22	663	1634	-1.04
YG_14	highland hyaloclastite	2006	2012	37	524	1955	-1.09
HL_16.5	highland hyaloclastite	1829	1884	56	497	2156	-1.28
JF_8	highland hyaloclastite	1835	1503	126	822	2802	-1.04 (-1.08)
VJ_13b	highland hyaloclastite	2140	1415	22	584	2197	-1.10

MSf_22a	Mosfell palagonite	2024	2338	6.6	501	1692	-1.07
MSf_22b	Mosfell palagonite	2048	2180	7.6	563	1437	-1.10
MSf_22c	Mosfell palagonite	1848	2158	17	555	1898	-1.06
HGf_21a	Helgafell palagonite	1743	2121	24	524	1975	-1.09
HGf_21b	Helgafell palagonite	1699	2068	29	485	1851	-1.13
HGf_21c	Helgafell palagonite	1305	1577	16	404	1420	-1.08
HF_2a	Vesturdalur palagonite	949	1335	140	155	1500	-1.25
HF_2b	Vesturdalur palagonite	847	921	170	475	1915	-1.25 (-1.23)
HF_3a	Vesturdalur palagonite	1316	1187	68	441	2018	-1.21
HF_3b	Vesturdalur palagonite	958	723	178	656	2000	-1.20
HN_1	Vesturdalur palagonite	1260	1547	46	433	2118	-1.10
VJ_13a	highland glass	171	27	644	1339	650	-0.95 (-0.98)
JF_10a	highland glass	443	433	210	858	868	-0.93

Table 4.3 presents elemental concentrations and Ca isotope ratios of suspended sediment leachates and digests. Of the three suspended sediments fractions, the exchangeable ( $\text{NH}_4\text{Cl}$ ) leachates produced the lowest average  $\delta^{44/40}\text{Ca}$  value ( $-1.34 \pm 0.03\text{‰}$ ,  $1\sigma_{\text{SD}}$ ,  $n = 6$ ). The acetic acid leachates and silicate digests yielded similar average  $\delta^{44/40}\text{Ca}$  values ( $-1.05 \pm 0.24\text{‰}$ ,  $1\sigma_{\text{SD}}$ ,  $n = 5$  and  $-1.08 \pm 0.02\text{‰}$ ,  $1\sigma_{\text{SD}}$ ,  $n = 5$ ), although the acetic acid leachates span a much larger range ( $-1.28\text{‰}$  to  $-0.75\text{‰}$ ).

**Table 4.3.** Suspended sediment elemental and isotopic data for exchangeable leachate ( $\text{NH}_4\text{Cl}$ ), acetic acid leachate, and the residual digest. Duplicate analyses are given in parentheses. “-” indicates values below detection limit.

Sample	Ca ( $\mu\text{mol/g}$ )	Na ( $\mu\text{mol/g}$ )	Sr ( $\text{nmol/g}$ )	Mg ( $\mu\text{mol/g}$ )	K ( $\mu\text{mol/g}$ )	$\delta^{44/40}\text{Ca}$ (‰, ASW)
<i>Exchangeable Leachate</i>						
BL_1	132	22.0	247	41.9	15.2	-1.35
BL_3	128	48.5	303	47.6	17.9	-1.33
JF_1	22.4	5.2	36.0	5.0	2.2	-1.36

JF_3	61.9	13.5	149	17.1	6.2	-1.33 (-1.35)
VJ_k	33.6	9.5	84.9	14.0	2.9	-1.29
VJ_m	26.1	6.9	62.8	17.1	4.5	
HR_12	66.9	16.2	87.5	19.2	8.7	-1.35
<i>Acetic Acid Leachate</i>						
BL_1	20.7	7.3	23.9	20.3	-	-0.75
BL_3	30.2	9.0	39.6	24.2	-	-0.83 (-0.86)
JF_1	10.0	3.2	23.0	5.6	-	-1.18
JF_3	22.3	7.2	40.5	16.6	-	
VJ_k	11.7	2.9	27.3	7.1	-	
VJ_m	15.0	4.1	28.6	8.2	-	-1.28
HR_12	25.1	3.8	48.1	16.4	-	-1.21
<i>Silicate Digest</i>						
BL_1	1414	446	1174	1145	61.2	-1.09
BL_3	1334	449	1211	1038	63.9	-1.10
JF_1	1852	584	1702	1451	51.2	-1.06 (-1.04)
VJ_k	2044	319	830	780	19.4	-1.08
HR_12	1786	494	1367	1405	48.8	-1.06

To assess whether fractionation during Ca adsorption onto suspended sediment surfaces affects riverine  $\delta^{44/40}\text{Ca}$  values, the ratio of dissolved Ca to adsorbed Ca ( $R$ ) was calculated using the following equation:

$$R = \frac{[\text{Ca}]_w}{[\text{Ca}]_{ex}/SS}, \quad (4.1)$$

where  $\text{Ca}_w$  is the concentration of Ca in river water ( $\mu\text{mol/L}$ ),  $\text{Ca}_{ex}$  is the concentration of Ca in the exchangeable leachate ( $\mu\text{mol/g}$ ), and SS is the concentration of suspended sediment in river water ( $\text{g/L}$ ). Table 4.4 provides measured values for these variables for each sampling location where suspended sediment was collected.

**Table 4.4.** Summary of suspended sediment leachate molar percentages and isotopic composition of calculated bulk value, as well as calculated molar ratio of dissolved riverine Ca to exchangeable, or adsorbed Ca (see methods).

Sample	Mole percent Ca leached, exchangeable (%)	Exchangeable leachate $\delta^{44/40}\text{Ca}$ (‰)	Mole percent Ca leached, acetic (%)	Acetic leachate $\delta^{44/40}\text{Ca}$ (‰)	Silicate Digest $\delta^{44/40}\text{Ca}$ (‰)	Calculated Bulk $\delta^{44/40}\text{Ca}$ (‰)	Water Sample $\delta^{44/40}\text{Ca}$ (‰)	R ( $\text{Ca}_w:\text{Ca}_{ad}$ , moles/moles)
BL_1	8.4	-1.35	1.3	-0.75	-1.09	-1.11	-0.79	1.9
BL_3	8.6	-1.33	2.0	-0.83	-1.10	-1.11	-0.85	2.9
JF_1	1.2	-1.36	0.5	-1.18	-1.06	-1.06	-0.80	14.8
VJ_k	1.6	-1.29	0.6		-1.08	-1.08	-0.80	0.9
HR_12	3.6	-1.35	1.3	-1.21	-1.06	-1.07		4.5

## 4.5 Discussion

Riverine solute data presented here are not corrected for atmospheric inputs because the correction assumes all  $\text{Cl}^-$  in rivers derives from atmospheric deposition. However, Icelandic groundwater systems also supply  $\text{Cl}^-$  to rivers (Arnórsson and Andrésdóttir, 1995; Oskarsdóttir et al., 2011), and subglacial geothermal water discharge pervasively occurs throughout the highlands (Gislason and Eugster, 1987b; Gudmundsson et al., 1995; Lawler and Björnsson, 1996; Björnsson, 2003; Warner and Farmer, 2010; Barry et al., 2014). Additionally, atmospheric deposition in Iceland mostly derives from seawater (Gislason and Eugster, 1987b; Gislason et al., 1996), but the study region is far from the coast and receives little annual rainfall (Figure 4.1). Nonetheless, to assess the importance of atmospheric deposition, I estimated proportions of riverine Ca, Mg, Na, and K from atmospheric deposition using a standard equation (Chapter 3, Section 3.5.1). The correction was implemented with two different proxies for the composition of atmospheric deposition, including Icelandic rainfall (Gislason and Eugster, 1987b) and a sample of snow collected from the Hofsjökull glacier (Table 4.1) (Gannoun et al., 2006). For all scenarios, atmospheric contributions are negligible, and correcting riverine solute concentrations does not change the observed trends. The same applies to riverine  $\delta^{44/40}\text{Ca}$  values, assuming seawater has a  $\delta^{44/40}\text{Ca}$  value of 0%.

Rivers draining the central highlands have the highest  $\delta^{44/40}\text{Ca}$  values of nearly all Icelandic rivers measured to date (Hindshaw et al., 2013; Jacobson et al., 2015). Previous studies have interpreted elevated riverine  $\delta^{44/40}\text{Ca}$  relative to basalt to reflect either fractionation (Hindshaw et al., 2013) or mixing between carbonate and silicate weathering sources (Jacobson et al., 2015; Andrews and Jacobson, 2017). A major limitation to the previously proposed

“fractionation hypothesis” (Hindshaw et al., 2013) is that no candidate reservoirs with low  $\delta^{44/40}\text{Ca}$  were identified. The present study identifies two isotopically light reservoirs of Ca – suspended sediment leachates and altered rocks (Figure 4.2). I discuss possible effects of these materials on riverine  $\delta^{44/40}\text{Ca}$  values in the following two sections.

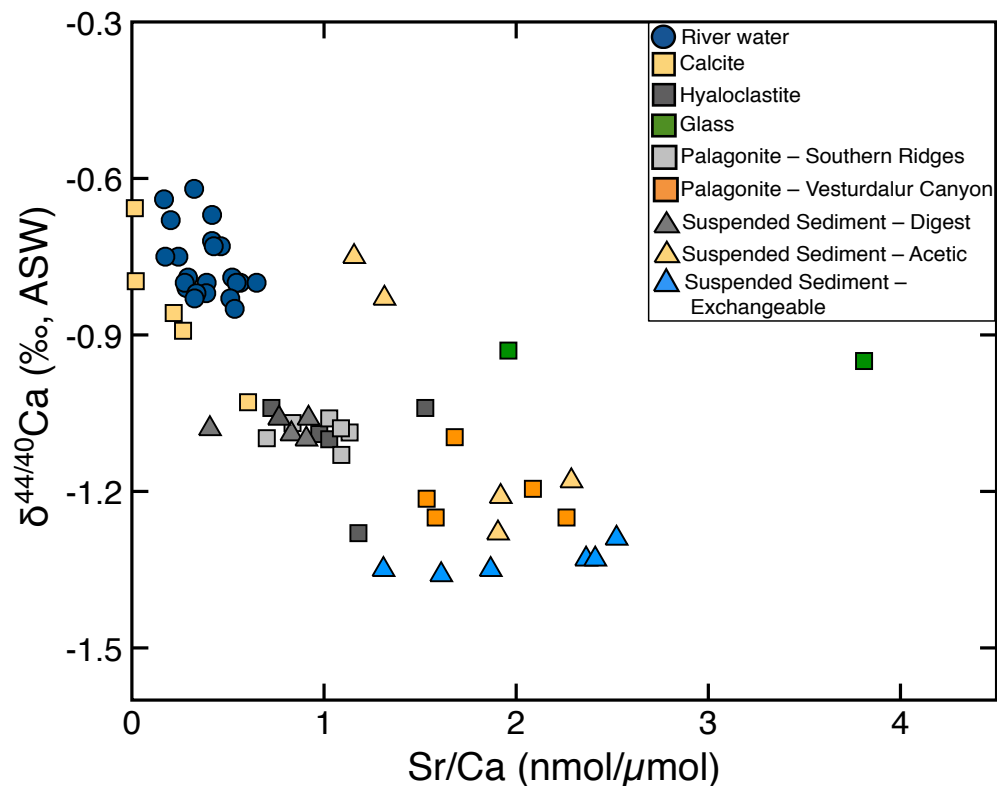


**Figure 4.2.**  $\delta^{44/40}\text{Ca}$  versus Sr/Ca of all highland samples, non-highland palagonite samples, and calcite samples from Nelson et al. (2021).

#### 4.5.1 Fractionation Control

##### 4.5.1.1 In-Stream Processes

In-stream processes, such as clay formation or adsorption onto suspended material, could fractionate Ca isotopes and elevate  $\delta^{44/40}\text{Ca}$  values (Hindshaw et al., 2013; Ockert et al., 2013; Brazier et al., 2019). In Iceland, glacial and non-glacial rivers exhibit different isotope

geochemistry with respect to Ca, stable Sr, Li, Mg, and Si isotopes (Georg et al., 2007; Pogge von Strandmann et al., 2008; Vigier et al., 2009; Hindshaw et al., 2013; Jacobson et al., 2015). Li, Mg, and Si isotope ratios are similar to basalt in glacial rivers, which points to *less fractionation by clay formation* in glacial rivers compared to non-glacial rivers (Georg et al., 2007; Pogge von Strandmann et al., 2008; Vigier et al., 2009). The opposite trend is observed for Ca and stable Sr isotopes, where glacial rivers are more distinct from basalt, suggesting *more fractionation* is occurring in glacial rivers relative to non-glacial rivers (Hindshaw et al., 2013; Jacobson et al., 2015; Andrews and Jacobson, 2017). This discrepancy generally indicates that in-stream clay formation, which controls Li, Mg, and Si isotope ratios, is not the primary control on Ca and stable Sr isotope ratios. Thus, the elevated  $\delta^{44/40}\text{Ca}$  values of highland rivers are most likely unrelated to fractionation during in-stream clay formation.

Many of the highland rivers contain high concentrations of suspended material (Table 4.1). Suspended sediment in these rivers mostly derives from glacially-ground hyaloclastites and represents a significant fraction of the total export flux of weathered material (Gislason et al., 2006; Louvat et al., 2008). While the suspended sediment leachates have low  $\delta^{44/40}\text{Ca}$  values (Figure 2), less than 10% of the total suspended sediment Ca is exchangeable (Table 4.4). Two of the acetic acid leachates intended to isolate the carbonate fraction of suspended sediment produced higher  $\delta^{44/40}\text{Ca}$  than bulk rocks, consistent with values for hydrothermal calcites throughout Iceland (Jacobson et al., 2015); however, others produced low  $\delta^{44/40}\text{Ca}$  values (Table 4.3). These leachates with low  $\delta^{44/40}\text{Ca}$  have Sr/Ca and K/Ca ratios similar to the clay-rich rock samples (Figures 4.2 and 4.3), likely indicating that these sediments are carbonate-free and/or that the reagent dissolved small amounts of zeolites or poorly crystalline clay.

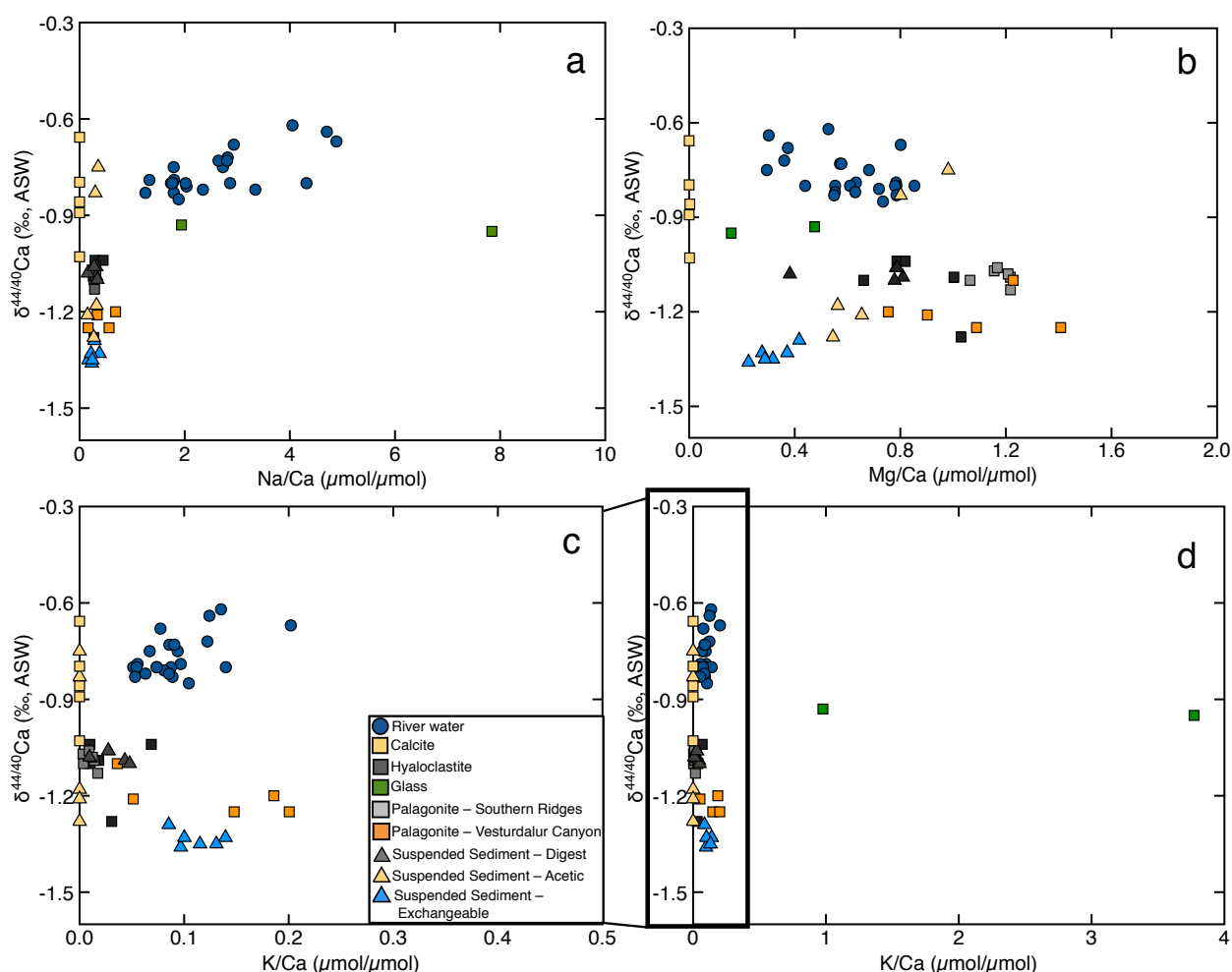


**Figure 4.3.**  $\delta^{44/40}\text{Ca}$  versus Na/Ca (a), Mg/Ca (b), and K/Ca (c and d) of all highland samples, non-highland palagonite samples, and calcite samples from Nelson et al. (2021). Panel (c) shows inset from panel (d)

The exchangeable leachates of the suspended sediment have consistently lower  $\delta^{44/40}\text{Ca}$  than bulk rocks. Because hyaloclastites can contain zeolites and clays, the low  $\delta^{44/40}\text{Ca}$  values measured for the exchangeable fraction could reflect Ca sourced from these minerals, however this is unlikely, as secondary mineral inclusion in hyaloclastites is highly heterogeneous and the suspended sediment exchangeable fraction produced uniform  $\delta^{44/40}\text{Ca}$  values (Figure 4.2). Alternatively, the exchangeable fraction of suspended sediment could represent adsorbed

riverine  $\text{Ca}^{2+}$ . Lighter Ca isotopes appear to preferentially adsorb to particulate surfaces (Ockert et al., 2013; Brazier et al., 2019), and the exchangeable fraction of suspended material can contribute to elemental fluxes (Gislason et al., 2006; Tipper et al., 2021). Therefore, adsorbed  $\text{Ca}^{2+}$  may represent a sufficient reservoir of lighter Ca isotopes to influence riverine  $\delta^{44/40}\text{Ca}$  values. The assumption that all exchangeable  $\text{Ca}^{2+}$  was adsorbed from the dissolved fraction offers the most generous assessment of whether in-stream fractionation can elevate riverine  $\delta^{44/40}\text{Ca}$  values. Based on this assumption, I used a simple mass balance model to estimate the relative amounts of Ca in the dissolved versus exchange pools (see results). Taking into account the concentration of suspended sediment in water, and the concentration of [Ca] in the corresponding water sample (Table 4.1), I calculated ratios of dissolved [Ca] to adsorbed  $\text{Ca}^{2+}$  ( $\text{Ca}_w:\text{Ca}_{ad} = R$ ), where R ranges from 0.91 to 14.8 (Table 4.4). If  $\text{Ca}^{2+}$  adsorption onto suspended material controls riverine  $\delta^{44/40}\text{Ca}$ , I would expect to observe a correlation between R and riverine  $\delta^{44/40}\text{Ca}$ , but no such correlation exists. In fact, water samples with the most adsorbed Ca ( $R = 0.91$ ) and the least adsorbed Ca ( $R=14.8$ ) have identical  $\delta^{44/40}\text{Ca}$  values of  $-0.80\text{‰}$ , which is on the low end of the range for all rivers (Table 4.1). This indicates that any fractionation of Ca isotopes during adsorption onto suspended material unlikely elevates riverine  $\delta^{44/40}\text{Ca}$ . Furthermore, no rivers have basaltic  $\delta^{44/40}\text{Ca}$ , and the lowest  $\delta^{44/40}\text{Ca}$  of all river samples is  $-0.85\text{‰}$  (Figure 4.2). A direct in-stream fractionation unlikely explains this “gap” in  $\delta^{44/40}\text{Ca}$  space between silicate rocks and rivers, as no fractionation mechanism is expected to affect all rivers uniformly. Rather, in the absence of any other controls, I would expect at least some rivers to display basaltic  $\delta^{44/40}\text{Ca}$  values.

#### 4.5.1.2 Rock Alteration Processes

Hyaloclastites are a heterogeneous breccia that usually contain up to 40% by volume of alteration minerals, including clays, zeolites, and calcite (Franzson et al., 2011), as well as up to 90% glass (sideromelane) (Watton et al., 2013). Highland hyaloclastites have elemental ratios and  $\delta^{44/40}\text{Ca}$  values similar to those previously reported for primary minerals and bulk basalt (Jacobson et al., 2015; Nelson et al., 2021). Glass samples show higher Na/Ca and K/Ca ratios than bulk hyaloclastites (Figure 4.3), consistent with the incompatibility of Na and K in primary basaltic minerals. While the hyaloclastites analyzed here could have high glass contents by volume, glass does not significantly affect bulk hyaloclastite  $\delta^{44/40}\text{Ca}$  values because Ca is more concentrated in primary minerals. In addition, while glass is generally expected to dissolve rapidly (Gislason and Eugster, 1987a; Oelkers and Gislason, 2001; Gislason and Oelkers, 2003), no evidence exists that glass weathering directly contributes to the Ca isotope composition of rivers (Figures 4.2 and 4.3). At high temperatures, glass readily alters to secondary minerals, such as clays, zeolites, and calcite (Gislason and Eugster, 1987b; Crovisier and Daux, 1990; Crovisier et al., 1992; Warner and Farmer, 2010; Franzson et al., 2011; Aradóttir et al., 2013), thus the possibility exists that an alteration pathway could represent a fractionation mechanism that may affect river Ca isotope geochemistry.

Clay minerals, which are present in many hyaloclastites throughout Iceland (Gislason and Eugster, 1987a; Crovisier and Daux, 1990; Crovisier et al., 1992; Franzson et al., 2011), are widely expected to incorporate lighter Ca isotopes (Hindshaw et al., 2011, 2013; Fantle et al., 2012; Ockert et al., 2013; Brazier et al., 2019). Clays in Icelandic rocks generally form in the subsurface under higher temperature conditions ( $\sim 30^\circ\text{C}$  to  $\sim 200^\circ\text{C}$ ) characteristic of burial

metamorphism that also produces zeolite zones (Neuhoff et al., 1999; Weisenberger and Selbekk, 2009; Thien et al., 2015; Weisenberger et al., 2020). Poorly crystalline clays can also be produced in surface environments during “palagonitization”, which describes the hydrous alteration of hyaloclastite where intergranular glass is replaced with secondary clay-like material (Bonatti, 1965; Crovisier and Daux, 1990; Jercinovic et al., 1990; Stroncik and Schmincke, 2002). While palagonitization occurs on microscopic-to-submicroscopic scales (Thorseth et al., 1991; Gysi and Stefánsson, 2012a), the term “palagonite” in Iceland has been used to characterize hyaloclastites that contain hydrated or altered glasses, which are generally either yellow or orange-brown colored rocks (Appendix D). Palagonitization happens either during eruptions, when meteoric water from glaciers quenches and hydrates glasses during cooling (Bonatti, 1965; Schiffman et al., 2000; Warner and Farmer, 2010), or after eruptions cease, due to meteoric or hydrothermal water circulation at temperatures ranging from ambient to  $\sim 140^{\circ}\text{C}$  (Jakobsson, 1978; Warner and Farmer, 2010; Jakobsson and Moore).

I analyzed altered hyaloclastites from regions in Iceland representing various formation conditions, including samples from two well-characterized “palagonite ridges” in Southern Iceland, as well as from an outcrop in Vesturdalur canyon (Figure 4.1). The palagonites analyzed in this study were altered subaerially at Mosfell (Furnes, 1978, 1984; Thorseth et al., 1991) and subglacially at Helgafell (Schopka et al., 2006). Water-rock ratios, temperature, original sideromelane composition and grain size, fluid chemistry, duration of alteration, and other factors can impact the geochemistry of palagonites on scales ranging from microns to kilometers (Jakobsson, 1978; Stroncik and Schmincke, 2002; Warner and Farmer, 2010; Pauly et al., 2011; Aradóttir et al., 2013). Therefore, I analyzed samples spanning a range of elevations at Mosfell

and Helgafell to account for heterogeneity (Figure D2). Despite the differing palagonitization mechanisms and varying degrees of alteration at these two locations, all samples show a narrow range of  $\delta^{44/40}\text{Ca}$  values identical to basalt (Table 4.2), indicating that hyaloclastite alteration during subglacial or subaerial palagonitization, both syn- and post- eruption, is not a sufficient mechanism to explain the Ca isotope composition of rivers.

I also analyzed additional clay-rich samples from a small (~8 m thick) palagonitized outcrop in the Vesturdalur canyon north of the Hofsjökull glacier (see Appendix D). Rocks from this outcrop have a soft, clayey texture and are brightly colored, likely indicating that this was a tephra unit altered under high-temperature conditions. Moreover, the outcrop is capped by a post-depositional basaltic lava flow with a fundamentally different appearance (Figure D3), thus these samples are interpreted to represent the high-temperature end member of all rocks in this study. Bulk samples from this outcrop show low  $\delta^{44/40}\text{Ca}$  values, indicating that only the highest temperature alteration can produce rocks with low  $\delta^{44/40}\text{Ca}$  relative to basalt. Crystalline smectite and kaolinite were both detected in this outcrop by qualitative XRD; however, their Mg/Ca ratios are similar to those for clay-poor hyaloclastites (Figure 4.3). It is unclear if clay controls bulk rock  $\delta^{44/40}\text{Ca}$ , as it is also possible that these rocks contain other secondary minerals, such as zeolites, which can have very low  $\delta^{44/40}\text{Ca}$  (Jacobson et al., 2015; Nelson et al., 2021).

Aside from the clay-rich rock samples discussed above, one of the highland hyaloclastite samples (HL\_16) produced a lower  $\delta^{44/40}\text{Ca}$  relative to all other bulk hyaloclastites (Table 4.2). Zeolites and calcite commonly form in subglacial hyaloclastites (Stefánsdóttir and Gíslason, 2005; Warner and Farmer, 2010; Franzson et al., 2011; Galeczka et al., 2014), however hydrothermal calcite from Iceland uniformly has higher  $\delta^{44/40}\text{Ca}$  than basalt (Jacobson et al.,

2015; Nelson et al., 2021); therefore, any calcite in this particular sample cannot explain its low  $\delta^{44/40}\text{Ca}$  value. Because primary minerals and bulk basalts have a narrow range of  $\delta^{44/40}\text{Ca}$  values (Nelson et al., 2021), sample HL\_16 likely contains a small amount of zeolite. Zeolites, such as heulandite and mesolite, have very low  $\delta^{44/40}\text{Ca}$  values relative to basalt (Nelson et al., 2021), and highland hyaloclastites are heterogeneous by nature; therefore, zeolite-bearing amygdules in the rock sample could result in lower bulk  $\delta^{44/40}\text{Ca}$  values. As only one highland rock sample shows low  $\delta^{44/40}\text{Ca}$ , it is unlikely that the formation of zeolites within highland hyaloclastites is widespread enough to fractionate Ca isotopes to a degree that would directly elevate riverine  $\delta^{44/40}\text{Ca}$  on a regional scale.

Of all the palagonitized, clay-rich rocks analyzed here, only the ones altered under the highest temperatures show low  $\delta^{44/40}\text{Ca}$  values relative to basalt and primary minerals. It appears that clays produced during alteration of hyaloclastites either have small fractionation factors and/or contain little Ca. While zeolites represent a reservoir of isotopically light Ca, the fact that most bulk rocks analyzed have basaltic  $\delta^{44/40}\text{Ca}$  values, despite spanning a range of alteration conditions, indicates that fractionation of Ca isotopes during highland rock alteration is not the primary control on riverine  $\delta^{44/40}\text{Ca}$  values.

#### *4.5.2 Mixing Control*

Previous studies have estimated that hydrothermal activity contributes minimally to river geochemistry, supplying less than 1% of solutes (Vigier et al., 2009; Hindshaw et al., 2013). However, in the highlands, groundwater discharge heavily influences many of the rivers, due to their close proximity to volcanic centers. Subglacial volcanic activity affects river chemistry in

several ways. Young and porous subglacial rock permits high infiltration rates and continuous groundwater recharge, resulting in the emergence of springs that have geochemically evolved in the subsurface (Gislason and Eugster, 1987b; Sigurdsson, 1990; Gislason et al., 1996; Lawler and Bjornsson, 1996; Jónsdóttir, 2008; Galeczka et al., 2014). Moreover, volcanic heat fluxes cause substantial subglacial melting, and floods of subglacial discharge and rock fragments periodically emerge from beneath glaciers in acute outburst events, termed “jökulhlaups” (Gudmundsson et al., 1995; Lawler and Bjornsson, 1996; Flowers et al., 2003; Björnsson, 2003). Groundwater discharge readily explains the high Na/Ca and K/Ca ratios and low Sr/Ca ratios observed for highland rivers, as well as the correlations observed between molar ratios and  $\delta^{44/40}\text{Ca}$  values (Figures 4.2 and 4.3), as groundwaters have the highest  $\delta^{44/40}\text{Ca}$  values of all Icelandic samples thus far measured (Hindshaw et al., 2013; Jacobson et al., 2015; Pogge von Strandmann et al., 2019a; Nelson et al., 2021). Ion-exchange with zeolites offers the best explanation why groundwaters have high  $\delta^{44/40}\text{Ca}$  values, as well as low Sr/Ca ratios (Fridriksson et al., 2009; Jacobson et al., 2015; Nelson et al., 2021). River samples with the highest  $\delta^{44/40}\text{Ca}$  values, highest Na/Ca and K/Ca, and lowest Sr/Ca ratios were collected in closest proximity to Laugafell, an active geothermal spring in the study region (Figure 4.1).

Previous studies have proposed that the chemical weathering of hydrothermal carbonate significantly affects the geochemistry of Icelandic rivers (Jacobson et al., 2015; Andrews and Jacobson, 2017). Calcite is commonly produced during subglacial volcanic eruptions and is prevalent in Icelandic hyaloclastites (Franzson et al., 2011); although, no calcite was detected in the hyaloclastites analyzed here. Assuming highland calcite has similar  $\delta^{44/40}\text{Ca}$  values to previously measured calcites collected throughout Iceland (Jacobson et al., 2015; Nelson et al.,

2021), river samples plot in a three-component mixing space defined by bulk hyaloclastites, glass, and hydrothermal calcite (Figure 4.2). It is difficult to distinguish between calcite weathering and groundwater inputs to rivers, as both sources have elevated riverine  $\delta^{44/40}\text{Ca}$  values and low Sr/Ca ratios, but their relative impacts can be constrained with the aid of  $\delta^{13}\text{C}_{\text{DIC}}$  values. Icelandic calcite and groundwater generally show distinct  $\delta^{13}\text{C}_{\text{DIC}}$  values (Chapter 3). Moreover, fractionation processes that could potentially impact Ca isotopes, such as clay formation or adsorption, do not affect C isotopes. Although the carbon isotope composition of riverine DIC is subject to other fractionation processes, such as biologic activity, evasion, and atmospheric equilibration (Telmer and Veizer, 1999; Spence and Telmer, 2005; Schulte et al., 2011), rivers here show an average  $\text{HCO}_3^-/\text{DIC}$  ratio of  $\sim 0.85$ , indicating that river C isotopes meet the criteria for conservative behavior. Calcite precipitation strongly influences the  $\delta^{13}\text{C}_{\text{DIC}}$  of groundwater (Sveinbjörnsdóttir et al., 2020) but is not a factor for surface waters, which are highly undersaturated with respect to calcite.

With the exception of rivers draining glacial outlets ( $< 5$  km away from ice), riverine  $\delta^{44/40}\text{Ca}$  and  $\delta^{13}\text{C}$  generally correlate (Figure 4;  $R^2 = 0.48$ ,  $p = 0.003$ ). Therefore, a common mechanism must affect both tracers. Plotting lowland hot spring and calcite data (Chapter 3) together with data for highland waters, I observe that most rivers display two-component mixing between calcite and groundwater (Figure 4.4). In this space, rivers with the highest  $\delta^{44/40}\text{Ca}$  values reflect the most groundwater inputs, consistent with elemental ratio trends shown in Figures 4.2 and 4.3. Highland rivers distinctly differ from the end-member expected for the weathering of basalt and glass by atmospheric  $\text{CO}_2$ .

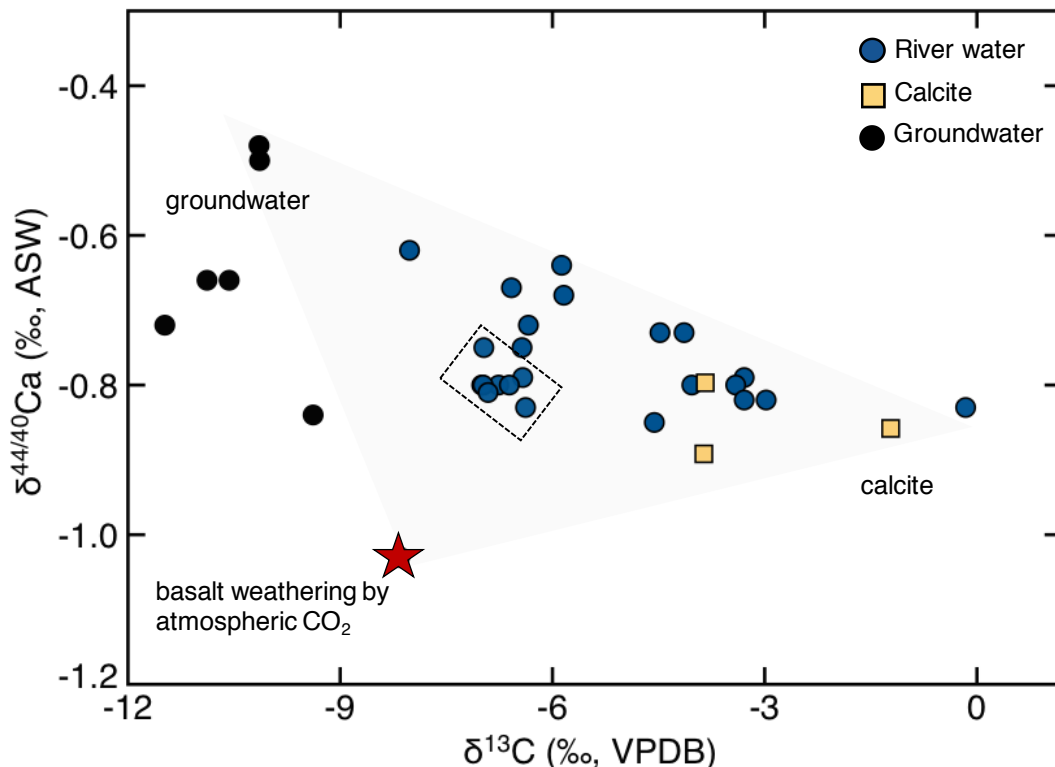


**Figure 4.4.**  $\delta^{44/40}\text{Ca}$  versus  $\delta^{13}\text{C}$  of highland river water, Skagafjörður hot spring water (Nelson Skaga) and Berufjörður-Breiðdalur calcite samples from Nelson et al., (2021). Red star indicates values for basalt weathering by atmospheric  $\text{CO}_2$ . Most rivers generate a significant correlation ( $R^2 = 0.48$ ,  $p = 0.003$ ), and plot in two-component mixing space between calcite and hydrothermal water. Box outlines river samples closest to glacial terminus (<5km) that are excluded from the regression and trend towards the basalt weathering end member.

In addition to a correlation with  $\delta^{44/40}\text{Ca}$  values,  $\delta^{13}\text{C}$  values also correlate with the saturation index of calcite (Figure 4.5), which provides further evidence that calcite weathering, to some degree, contributes to  $\delta^{13}\text{C}$  variations. Less undersaturated rivers have higher  $\delta^{13}\text{C}$  values, consistent with greater DIC contributions from calcite weathering, while more undersaturated rivers show greater contributions from DIC derived from basalt weathering by atmospheric  $\text{CO}_2$  (Figure 4.5). Groundwater-fed rivers are shifted towards lower  $\delta^{13}\text{C}$  values as

well as higher  $\delta^{44/40}\text{Ca}$  values (Figure 4.5). One apparent outlier, a sample from the Hvítá river, has the highest  $\delta^{13}\text{C}$  value. Such high  $\delta^{13}\text{C}$  values have been observed in some axial rift zone groundwaters in Iceland (Barry et al., 2014; Stefánsson et al., 2016, 2017; Thomas et al., 2016), and the Hvítá river is close to the active Kerlingarfjöll volcano (Figure 4.1). The trend between SI calcite and  $\delta^{13}\text{C}$  implies that for rivers not heavily influenced by hydrothermal inputs, calcite weathering elevates  $\delta^{13}\text{C}$  to values higher than atmospheric  $\text{CO}_2$ . Even river samples with atmospheric-like  $\delta^{13}\text{C}$  values do not have basaltic  $\delta^{44/40}\text{Ca}$  values, which indicates that calcite weathering elevates riverine values to at least  $-0.85\text{‰}$  from an initially basaltic reservoir having a  $\delta^{44/40}\text{Ca}$  value of  $\sim -1\text{‰}$ . Rivers with  $\delta^{44/40}\text{Ca}$  values higher than  $-0.85\text{‰}$  most likely reflect mixing between calcite weathering and groundwater.

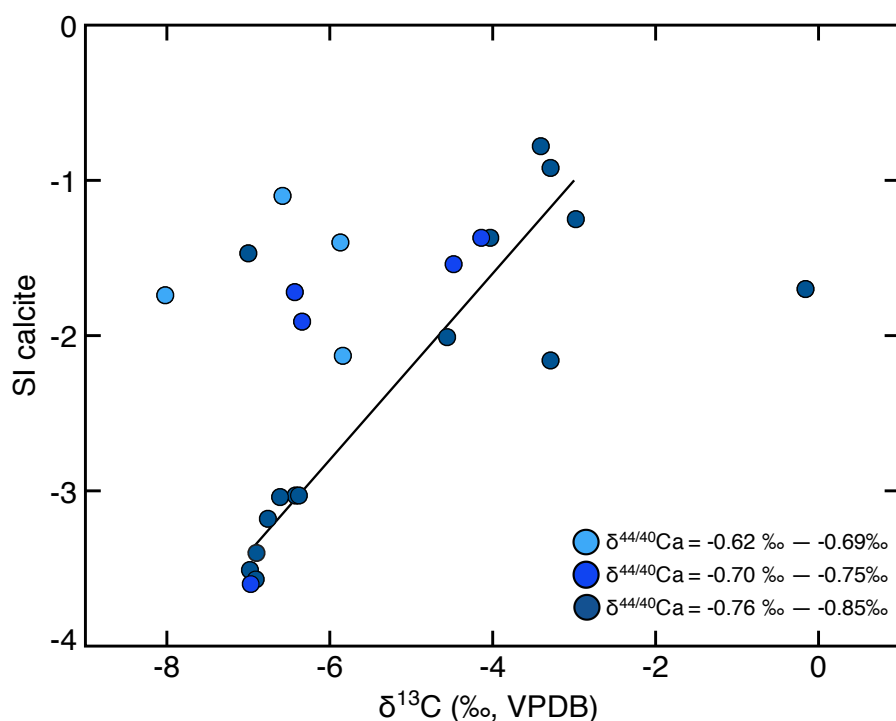


**Figure 4.5.**  $\delta^{13}\text{C}$  versus the saturation index of calcite of all rivers. Points are shaded according to Ca isotope ratios. Most rivers generate a highly significant correlation ( $R^2 = 0.89$ ,  $p < 0.0001$ ), indicating that, where groundwater inputs are minimal, carbon isotopes are controlled by calcite weathering

The trend in Figure 4.4 clearly indicates that  $\text{HCO}_3^-$  fluxes from Icelandic glacial rivers do not reflect basalt weathering by atmospheric  $\text{CO}_2$ . Since highland rocks are young, it is possible that highland calcite is forming and weathering on timescales less than that of the long-term carbon cycle ( $< 1$  Myr), thus calcite can be thought of as an “intermediate reservoir” for silicate weathering products. If calcite were formed from basalt weathering by atmospheric  $\text{CO}_2$ , then  $\text{HCO}_3^-$  fluxes from the weathering of young calcite could represent atmospheric  $\text{CO}_2$  drawdown. However, the weathering of calcite formed with mantle  $\text{CO}_2$  would result in non-atmospheric  $\text{HCO}_3^-$  fluxes, even if calcite is less than 1 Ma. In either scenario, riverine solute fluxes do not reflect basalt weathering, as the weathering dynamics of calcite are extremely different from silicate minerals. The same logic applies solute fluxes from groundwater. Even if groundwater solutes are sourced directly from the weathering of silicate minerals by atmospheric  $\text{CO}_2$ , river solute fluxes are not representative of basalt weathering rates, as elevated subsurface temperatures can lead to faster dissolution rates (Stefansson, 2001; Stefansson et al., 2001; Gislason and Oelkers, 2003; Dessert et al., 2009).

#### 4.6 Conclusions

Rivers draining the highlands region of central Iceland have  $\delta^{44/40}\text{Ca}$  values that are at least 0.20‰ higher than the value for bulk basalt and primary basaltic minerals (Figure 4.2). Using the mixing model from Jacobson et al. (2015), these values suggest that *an absolute maximum* of 20% of the Ca in highland rivers is supplied from basalt weathering by atmospheric  $\text{CO}_2$ . No river show evidence for rapid volcanic glass weathering. In  $\delta^{44/40}\text{Ca}$  and  $\delta^{13}\text{C}_{\text{DIC}}$  space, almost all rivers plot on a mixing line defined by calcite weathering and groundwater inputs

(Figure 4.4). Rivers nearest the glacial terminus (<5 km) show the greatest contributions from basalt weathering by atmospheric CO<sub>2</sub>, but the contributions are minor by comparison to those from calcite weathering and groundwater inputs. Hence, the vast majority of solutes in rivers draining the young, glassy volcanic rock of Iceland do not represent basalt weathering by atmospheric CO<sub>2</sub>, and for most samples, none of the solutes are supplied by surficial silicate weathering.

Many studies have interpreted high solute fluxes in rivers draining young volcanic provinces as evidence for the rapid weathering of volcanic glass. The data presented here show that volcanic glass weathering plays a negligible role on riverine Ca fluxes and that high solute fluxes previously thought to indicate rapid basalt weathering more likely reflect carbonate mineral weathering and hydrothermal inputs. Riverine solute fluxes cannot be used to quantify the parameters that influence basalt weathering rates, and solute fluxes used to calculate atmospheric CO<sub>2</sub> drawdown or approximate the strength of the silicate weathering feedback will significantly overestimate of the role of basalt weathering in long-term climate regulation.

## Chapter 5

### Conclusions

Prior to this dissertation, only three works have studied the Ca isotope geochemistry of Icelandic materials (Hindshaw et al., 2013; Jacobson et al., 2015; Pogge von Strandmann et al., 2019a). Through the research presented here, I offer novel isotopic measurements of key Ca-bearing reservoirs, including the first ever measurements of primary minerals, secondary zeolites, travertine, soil, and vegetation. The combined work demonstrates the largely untapped potential of the Ca isotope proxy as a tool for investigating basalt chemical weathering. By characterizing the  $\delta^{44/40}\text{Ca}$  values of mineral reservoirs (Chapter 2) and analyzing mechanisms hypothesized to fractionate and mix Ca isotopes (Chapter 3), this dissertation greatly advances the applicability of the Ca isotope tracer to future weathering studies. Furthermore, the striking results presented in Chapter 2 provide new perspectives on fundamental atomic-scale mechanisms governing equilibrium versus kinetic fractionation, which are potentially applicable to other novel stable metal isotope systems. The results presented for zeolite minerals point to development of the Ca isotope tracer as an entirely new “geothermometer” for examining low-grade basalt metamorphism. Additionally, the findings in Chapter 2 shed new light on application of the proxy in paleoenvironmental and paleoclimate studies (Gussone et al., 2020a).

The most recent Ca isotope study in Iceland measured  $\delta^{44/40}\text{Ca}$  values of pre- and post-injection waters from the CarbFix site, where groundwater charged with anthropogenic  $\text{CO}_2$  is injected into a basaltic aquifer, to quantify the magnitude and rate of engineered calcite mineralization (Pogge von Strandmann et al., 2019a). Termed “mineral carbonation of basalt”, this is a promising method for sequestering carbon that has the potential to play a crucial role

mitigating the effects of anthropogenic climate change (Snæbjörnsdóttir et al., 2020). Pogge von Strandman et al. (2019) implicated Ca isotopes as a unique and possibly essential tool for the quantifying the of mineral carbonation of basalt. Through filling data gaps with direct measurements of the  $\delta^{44/40}\text{Ca}$  values of alteration products, and elucidating processes that affect Ca isotopes in the basaltic subsurface, this dissertation has wide-ranging implications for realizing the development and application of Ca isotopes as a novel tracer of mineral carbonation.

This dissertation also demonstrates that many aspects of basalt weathering remain incompletely understood and require more attention. For example, efforts to parameterize the strength of the basalt weathering climate feedback as a function of  $\text{CO}_2$ , temperature, runoff, vegetation, glacial activity, and other variables should account for hydrothermal and calcite weathering inputs to rivers draining basaltic regions. The work presented in Chapter 3 positions Ca isotope ratios as an ideal tracer for achieving this goal. Correlations between riverine  $\delta^{44/40}\text{Ca}$  and  $\delta^{13}\text{C}$  values presented in Chapter 4 provide strong evidence that solute fluxes in basalt-draining rivers are controlled by processes other than surficial silicate mineral weathering by atmospheric  $\text{CO}_2$ . Contrary to the long-standing hypothesis that basalt weathers significantly faster than granite at the Earth's surface, the results presented in this dissertation suggest that riverine  $\text{HCO}_3^-$  fluxes derived from the weathering of mafic and felsic minerals are more similar than widely appreciated. The exact role of basalt weathering in long-term regulation deserves more research, and is yet to be fully understood.

## References

- Alberti, A., Galli, E., Vezzalini, G., Passaglia, E., and Zanazzi, P.F., 1982, Position of cations and water molecules in hydrated chabazite. Natural and Na-, Ca-, Sr- and K-exchanged chabazites: *Zeolites*, v. 2, p. 303–309, doi:10.1016/S0144-2449(82)80075-4.
- Alfredsson, H.A., Oelkers, E.H., Hardarsson, B.S., Franzson, H., Gunnlaugsson, E., and Gislason, S.R., 2013, The geology and water chemistry of the Hellisheidi, SW-Iceland carbon storage site: *International Journal of Greenhouse Gas Control*, v. 12, p. 399–418, doi:10.1016/j.ijggc.2012.11.019.
- AlKhatib, M., and Eisenhauer, A., 2017, Calcium and strontium isotope fractionation in aqueous solutions as a function of temperature and reaction rate; I. Calcite: *Geochimica et Cosmochimica Acta*, v. 209, p. 296–319, doi:10.1016/j.gca.2016.09.035.
- Amini, M., Eisenhauer, A., Böhm, F., Fietzke, J., Bach, W., Garbe-Schönberg, D., Rosner, M., Bock, B., Lackschewitz, K.S., and Hauff, F., 2008, Calcium isotope ( $\delta^{44}/^{40}\text{Ca}$ ) fractionation along hydrothermal pathways, Logatchev field (Mid-Atlantic Ridge, 14°45'N): *Geochimica et Cosmochimica Acta*, v. 72, p. 4107–4122, doi:10.1016/j.gca.2008.05.055.
- Anderson, S.P., 2005, Glaciers show direct linkage between erosion rate and chemical weathering fluxes: *Geomorphology*, v. 67, p. 147–157, doi:10.1016/j.geomorph.2004.07.010.
- Anderson, S.P., Dietrich, W.E., and Jr, G.H.B., 2002, Weathering profiles, mass-balance analysis, and rates of solute loss: Linkages between weathering and erosion in a small, steep catchment: *Geological Society of America Bulletin*, p. 16.
- Anderson, S.P., Drever, J.I., and Humphrey, N.F., 1997, Chemical weathering in glacial environments: , p. 4.
- Andrews, M.G., and Jacobson, A.D., 2017, The radiogenic and stable Sr isotope geochemistry of basalt weathering in Iceland: Role of hydrothermal calcite and implications for long-term climate regulation: *Geochimica et Cosmochimica Acta*, v. 215, p. 247–262, doi:10.1016/j.gca.2017.08.012.
- Andrews, M.G., Jacobson, A.D., Lehn, G.O., Horton, T.W., and Craw, D., 2016, Radiogenic and stable Sr isotope ratios ( $^{87}\text{Sr}/^{86}\text{Sr}$ ,  $\delta^{88}/^{86}\text{Sr}$ ) as tracers of riverine cation sources and biogeochemical cycling in the Milford Sound region of Fiordland, New Zealand: *Geochimica et Cosmochimica Acta*, v. 173, p. 284–303, doi:10.1016/j.gca.2015.10.005.
- Antonelli, M.A., Mittal, T., McCarthy, A., Tripoli, B., Watkins, J.M., and DePaolo, D.J., 2019a, Ca isotopes record rapid crystal growth in volcanic and subvolcanic systems: *Proceedings of the National Academy of Sciences*, v. 116, p. 20315–20321, doi:10.1073/pnas.1908921116.

- Antonelli, M.A., Schiller, M., Schauble, E.A., Mittal, T., DePaolo, D.J., Chacko, T., Grew, E.S., and Tripoli, B., 2019b, Kinetic and equilibrium Ca isotope effects in high-T rocks and minerals: *Earth and Planetary Science Letters*, v. 517, p. 71–82, doi:10.1016/j.epsl.2019.04.013.
- Antonelli, M.A., and Simon, J.I., 2020, Calcium isotopes in high-temperature terrestrial processes: *Chemical Geology*, v. 548, p. 119651, doi:10.1016/j.chemgeo.2020.119651.
- Aradóttir, E.S.P., Sigfússon, B., Sonnenthal, E.L., Björnsson, G., and Jónsson, H., 2013, Dynamics of basaltic glass dissolution – Capturing microscopic effects in continuum scale models: *Geochimica et Cosmochimica Acta*, v. 121, p. 311–327, doi:10.1016/j.gca.2013.04.031.
- Aradóttir, E.S.P., Sonnenthal, E.L., Björnsson, G., and Jónsson, H., 2012, Multidimensional reactive transport modeling of CO<sub>2</sub> mineral sequestration in basalts at the Hellisheidi geothermal field, Iceland: *International Journal of Greenhouse Gas Control*, v. 9, p. 24–40, doi:10.1016/j.ijggc.2012.02.006.
- Ármannsson, H., 2016, The fluid geochemistry of Icelandic high temperature geothermal areas: *Applied Geochemistry*, v. 66, p. 14–64, doi:10.1016/j.apgeochem.2015.10.008.
- Armbruster, T., 1993, Dehydration mechanism of clinoptilolite and heulandite: Single-crystal X-ray study of Na-poor, Ca-, K-, Mg-rich clinoptilolite at 100 K: *American Mineralogist*, v. 78, p. 260–264.
- Armbruster, T., and Gunter, M.E., 2001, Crystal Structures of Natural Zeolites: Reviews in Mineralogy and Geochemistry, v. 45, p. 1–67, doi:10.2138/rmg.2001.45.1.
- Arnalds, O., 2015a, Classification and the Main Soil Types, *in* *The Soils of Iceland*, Dordrecht, Springer Netherlands, World Soils Book Series, p. 55–70, doi:10.1007/978-94-017-9621-7\_6.
- Arnalds, O., 2000, The Icelandic ‘rofabard’ soil erosion features: *Earth Surface Processes and Landforms*, v. 25, p. 17–28, doi:10.1002/(SICI)1096-9837(200001)25:1<17::AID-ESP33>3.0.CO;2-M.
- Arnalds, O., 2015b, *The Soils of Iceland*: Dordrecht, Springer Netherlands, World Soils Book Series, doi:10.1007/978-94-017-9621-7.
- Arnalds, O., 2004, Volcanic soils of Iceland: *CATENA*, v. 56, p. 3–20, doi:10.1016/j.catena.2003.10.002.
- Arnalds, O., and Kimble, J., 2001, Andisols of Deserts in Iceland: *Soil Science Society of America Journal*, v. 65, p. 1778–1786, doi:https://doi.org/10.2136/sssaj2001.1778.

- Arnórsson, S., and Andrésdóttir, A., 1995, Processes controlling the distribution of boron and chlorine in natural waters in Iceland: *Geochimica et Cosmochimica Acta*, v. 59, p. 4125–4146, doi:10.1016/0016-7037(95)00278-8.
- Arnórsson, S., Gunnarsson, I., Stefansson, A., Andresdottir, A., and Sveinbjörnsdóttir, A.E., 2002, Major element chemistry of surface- and ground waters in basaltic terrain, N-Iceland. I. Primary mineral saturation: *Geochimica et Cosmochimica Acta*, v. 66, p. 4015–4046.
- Arnórsson, S., and Sveinbjörnsdóttir, Á.E., 2000, Age and chemical evolution of groundwaters in Skagafjörður, Iceland: *Journal of Geochemical Exploration*, v. 69–70, p. 459–463, doi:10.1016/S0375-6742(00)00129-1.
- Arnórsson, S., and Sveinbjörnsdóttir, A.E., 2004, The source and relative age of non-thermal and up to 90 C ground waters in the Skagafjörður tholeiite flood basalt province, N-Iceland., *in* *Water-Rock Interaction, Two Volume Set: Proceedings of the Eleventh International Symposium on Water-Rock Interaction*, Saratoga Springs, New York, USA, CRC Press, p. 69–73.
- Artioli, G., Smith, J.V., and Pluth, J.J., 1986, X-ray structure refinement of mesolite: *Acta Crystallographica Section C Crystal Structure Communications*, v. 42, p. 937–942, doi:10.1107/S0108270186093939.
- Arvidson, R.S., Ertan, I.E., Amonette, J.E., and Luttge, A., 2003, Variation in calcite dissolution rates: *Geochimica et Cosmochimica Acta*, v. 67, p. 1623–1634, doi:10.1016/S0016-7037(02)01177-8.
- Aufort, J., Ségalen, L., Gervais, C., Paulatto, L., Blanchard, M., and Balan, E., 2017, Site-specific equilibrium isotopic fractionation of oxygen, carbon and calcium in apatite: *Geochimica et Cosmochimica Acta*, v. 219, p. 57–73, doi:10.1016/j.gca.2017.09.020.
- Babechuk, M.G., Widdowson, M., and Kamber, B.S., 2014, Quantifying chemical weathering intensity and trace element release from two contrasting basalt profiles, Deccan Traps, India: *Chemical Geology*, v. 363, p. 56–75, doi:10.1016/j.chemgeo.2013.10.027.
- Bacakova, L., Vandrovцова, M., Kopova, I., and Jirka, I., 2018, Applications of zeolites in biotechnology and medicine – a review: *Biomaterials Science*, v. 6, p. 974–989, doi:10.1039/C8BM00028J.
- Baek, W., Ha, S., Hong, S., Kim, S., and Kim, Y., 2018, Cation exchange of cesium and cation selectivity of natural zeolites: Chabazite, stilbite, and heulandite: *Microporous and Mesoporous Materials*, v. 264, p. 159–166, doi:10.1016/j.micromeso.2018.01.025.
- Bagard, M.-L., Schmitt, A.-D., Chabaux, F., Pokrovsky, O.S., Viers, J., Stille, P., Labolle, F., and Prokushkin, A.S., 2013, Biogeochemistry of stable Ca and radiogenic Sr isotopes in a

- larch-covered permafrost-dominated watershed of Central Siberia: *Geochimica et Cosmochimica Acta*, v. 114, p. 169–187, doi:10.1016/j.gca.2013.03.038.
- Barrer, R.M., and Klinowski, J., 1972, Influence of framework charge density on ion-exchange properties of zeolites: *Journal of the Chemical Society, Faraday Transactions 1: Physical Chemistry in Condensed Phases*, v. 68, p. 1956, doi:10.1039/f19726801956.
- Barry, P.H., Hilton, D.R., Furi, E., Halldórsson, S.A., and Grönvold, K., 2014, Carbon isotope and abundance systematics of Icelandic geothermal gases, fluids and subglacial basalts with implications for mantle plume-related CO<sub>2</sub> fluxes: *Geochimica et Cosmochimica Acta*, v. 134, p. 74–99, doi:10.1016/j.gca.2014.02.038.
- Beerling, D.J. et al., 2020, Potential for large-scale CO<sub>2</sub> removal via enhanced rock weathering with croplands: *Nature*, v. 583, p. 242–248, doi:10.1038/s41586-020-2448-9.
- Berner, R.A., 1992, Weathering, plants, and the long-term carbon cycle: *Geochimica et Cosmochimica Acta*, v. 56, p. 3225–3231, doi:10.1016/0016-7037(92)90300-8.
- Berner, R.A., Lasaga, A.C., and Garrels, R.M., 1983, The carbonate-silicate geochemical cycle and its effect on atmospheric carbon dioxide over the past 100 million years: *American Journal of Science*, v. 283, p. 641–683, doi:10.2475/ajs.283.7.641.
- Bigeleisen, J., and Mayer, M.G., 1947, Calculation of Equilibrium Constants for Isotopic Exchange Reactions: *The Journal of Chemical Physics*, v. 15, p. 261–267, doi:10.1063/1.1746492.
- Björnsson, H., 2003, Subglacial lakes and jökulhlaups in Iceland: *Global and Planetary Change*, v. 35, p. 255–271, doi:10.1016/S0921-8181(02)00130-3.
- Björnsson, H., and Pálsson, F., 2008, Icelandic glaciers: *Jokull*, v. 58, p. 365–386.
- Blättler, C.L., Hong, W.-L., Kirsimäe, K., Higgins, J.A., and Lepland, A., 2021, Small calcium isotope fractionation at slow precipitation rates in methane seep authigenic carbonates: *Geochimica et Cosmochimica Acta*, v. 298, p. 227–239, doi:10.1016/j.gca.2021.01.001.
- Blum, J.D., Gazis, C.A., Jacobson, A.D., and Chamberlain, C.P., 1998, Carbonate versus silicate weathering in the Raikhot watershed within the High Himalayan Crystalline Series: , p. 4.
- Bluth, G.J.S., and Kump, L.R., 1994, Lithologic and climatologic controls of river chemistry: *Geochimica et Cosmochimica Acta*, v. 58, p. 2341–2359, doi:10.1016/0016-7037(94)90015-9.
- Bonatti, E., 1965, Palagonite, hyaloclastites and alteration of volcanic glass in the ocean: *Bulletin Volcanologique*, v. 28, p. 257–269, doi:10.1007/BF02596930.

- Borai, E.H., Harjula, R., malinen, L., and Paajanen, A., 2009, Efficient removal of cesium from low-level radioactive liquid waste using natural and impregnated zeolite minerals: *Journal of Hazardous Materials*, v. 172, p. 416–422, doi:10.1016/j.jhazmat.2009.07.033.
- Bouchez, J., von Blanckenburg, F., and Schuessler, J.A., 2013, Modeling novel stable isotope ratios in the weathering zone: *American Journal of Science*, v. 313, p. 267–308, doi:10.2475/04.2013.01.
- Bourg, I.C., Richter, F.M., Christensen, J.N., and Sposito, G., 2010, Isotopic mass dependence of metal cation diffusion coefficients in liquid water: *Geochimica et Cosmochimica Acta*, v. 74, p. 2249–2256, doi:10.1016/j.gca.2010.01.024.
- Brazier, J.-M., Schmitt, A.-D., Gangloff, S., Pelt, E., Chabaux, F., and Tertre, E., 2019, Calcium isotopic fractionation during adsorption onto and desorption from soil phyllosilicates (kaolinite, montmorillonite and muscovite): *Geochimica et Cosmochimica Acta*, v. 250, p. 324–347, doi:10.1016/j.gca.2019.02.017.
- Brown, S.T., Kennedy, B.M., DePaolo, D.J., Hurwitz, S., and Evans, W.C., 2013, Ca, Sr, O and D isotope approach to defining the chemical evolution of hydrothermal fluids: Example from Long Valley, CA, USA: *Geochimica et Cosmochimica Acta*, v. 122, p. 209–225, doi:10.1016/j.gca.2013.08.011.
- Brown, S.T., Turchyn, A.V., Bickle, M.J., Davis, A.C., Alt, J.C., Bédard, J.H., Skulski, T., and DePaolo, D.J., 2020, High-temperature kinetic isotope fractionation of calcium in epidiosites from modern and ancient seafloor hydrothermal systems: *Earth and Planetary Science Letters*, v. 535, p. 116101, doi:10.1016/j.epsl.2020.116101.
- Bullen, T., and Chadwick, O., 2016, Ca, Sr and Ba stable isotopes reveal the fate of soil nutrients along a tropical climosequence in Hawaii: *Chemical Geology*, v. 422, p. 25–45, doi:10.1016/j.chemgeo.2015.12.008.
- Cai, W.-J., Guo, X., Chen, C.-T.A., Dai, M., Zhang, L., Zhai, W., Lohrenz, S.E., Yin, K., Harrison, P.J., and Wang, Y., 2008, A comparative overview of weathering intensity and HCO<sub>3</sub><sup>-</sup> flux in the world's major rivers with emphasis on the Changjiang, Huanghe, Zhujiang (Pearl) and Mississippi Rivers: *Continental Shelf Research*, v. 28, p. 1538–1549, doi:10.1016/j.csr.2007.10.014.
- Cenki-Tok, B., Chabaux, F., Lemarchand, D., Schmitt, A.-D., Pierret, M.-C., Viville, D., Bagard, M.-L., and Stille, P., 2009, The impact of water–rock interaction and vegetation on calcium isotope fractionation in soil- and stream waters of a small, forested catchment (the Strengbach case): *Geochimica et Cosmochimica Acta*, v. 73, p. 2215–2228, doi:10.1016/j.gca.2009.01.023.
- Chacko, T., Cole, D.R., and Horita, J., 2001, Equilibrium Oxygen, Hydrogen and Carbon Isotope Fractionation Factors Applicable to Geologic Systems: *Reviews in Mineralogy & Geochemistry*, v. 43, p. 1–81.

- Chen, C., Huang, J.X., Foley, S.F., Wang, Z., Moynier, F., Liu, Y., Wei, D., and Ming, L., 2020, Compositional and pressure controls on calcium and magnesium isotope fractionation in magmatic systems: *Geochimica et Cosmochimica Acta*, v. 290, p. 257–270.
- Chipera, S.J., and Apps, J.A., 2001, *Geochemical Stability of Natural Zeolites*: Mineralogical Society of America, v. 45, p. 117–161.
- Chou, L., Garrels, R.M., and Wollast, R., 1989, Comparative study of the kinetics and mechanisms of dissolution of carbonate minerals: *Chemical Geology*, v. 78, p. 269–282, doi:10.1016/0009-2541(89)90063-6.
- Clark, D.E., Galeczka, I.M., Dideriksen, K., Voigt, M.J., Wolff-Boenisch, D., and Gislason, S.R., 2019, Experimental observations of CO<sub>2</sub>-water-basaltic glass interaction in a large column reactor experiment at 50 °C: *International Journal of Greenhouse Gas Control*, v. 89, p. 9–19, doi:10.1016/j.ijggc.2019.07.007.
- Colla, C.A., Wimpenny, J., Yin, Q.-Z., Rustad, J.R., and Casey, W.H., 2013, Calcium-isotope fractionation between solution and solids with six, seven or eight oxygens bound to Ca(II): *Geochimica et Cosmochimica Acta*, v. 121, p. 363–373, doi:10.1016/j.gca.2013.07.041.
- Coombs, D.S., Ellis, A.J., Fyfe, W.S., and Taylor, A.M., 1959, The zeolite facies, with comments on the interpretation of hydrothermal syntheses: *Geochimica et Cosmochimica Acta*, v. 17, p. 53–107.
- Cox, G.M., Halverson, G.P., Stevenson, R.K., Vokaty, M., Poirier, A., Kunzmann, M., Li, Z.-X., Denyszyn, S.W., Strauss, J.V., and Macdonald, F.A., 2016, Continental flood basalt weathering as a trigger for Neoproterozoic Snowball Earth: *Earth and Planetary Science Letters*, v. 446, p. 89–99, doi:10.1016/j.epsl.2016.04.016.
- Crovisier, J.L., and Daux, V., 1990, Populations of clays formed by alteration of subglacial hyaloclastites from Iceland: *Chemical Geology*, v. 84, p. 261–263, doi:10.1016/0009-2541(90)90232-V.
- Crovisier, J.-L., Honnorez, J., Fritz, B., and Petit, J.-C., 1992, Dissolution of subglacial volcanic glasses from Iceland: laboratory study and modelling: *Applied Geochemistry*, v. 7, p. 55–81, doi:10.1016/S0883-2927(09)80064-4.
- Das, A., Krishnaswami, S., and Bhattacharya, S.K., 2005a, Carbon isotope ratio of dissolved inorganic carbon (DIC) in rivers draining the Deccan Traps, India: Sources of DIC and their magnitudes: *Earth and Planetary Science Letters*, v. 236, p. 419–429, doi:10.1016/j.epsl.2005.05.009.
- Das, A., Krishnaswami, S., and Kumar, A., 2006, Sr and <sup>87</sup>Sr/<sup>86</sup>Sr in rivers draining the Deccan Traps (India): Implications to weathering, Sr fluxes, and the marine <sup>87</sup>Sr/<sup>86</sup>Sr record around K/T: *Geochemistry, Geophysics, Geosystems*, v. 7, doi:10.1029/2005GC001081.

- Das, A., Krishnaswami, S., Sarin, M.M., and Pande, K., 2005b, Chemical weathering in the Krishna Basin and Western Ghats of the Deccan Traps, India: Rates of basalt weathering and their controls: *Geochimica et Cosmochimica Acta*, v. 69, p. 2067–2084, doi:10.1016/j.gca.2004.10.014.
- DePaolo, D.J., 2004, Calcium Isotopic Variations Produced by Biological, Kinetic, Radiogenic and Nucleosynthetic Processes: *Reviews in Mineralogy and Geochemistry*, v. 55, p. 255–288.
- DePaolo, D.J., 2011, Surface kinetic model for isotopic and trace element fractionation during precipitation of calcite from aqueous solution: *Geochimica et Cosmochimica Acta*, v. 75, p. 1039–1056.
- Dessert, C., Dupré, B., François, L.M., Schott, J., Gaillardet, J., Chakrapani, G., and Bajpai, S., 2001, Erosion of Deccan Traps determined by river geochemistry: impact on the global climate and the  $^{87}\text{Sr}/^{86}\text{Sr}$  ratio of seawater: *Earth and Planetary Science Letters*, v. 188, p. 459–474, doi:10.1016/S0012-821X(01)00317-X.
- Dessert, C., Dupré, B., Gaillardet, J., François, L.M., and Allègre, C.J., 2003, Basalt weathering laws and the impact of basalt weathering on the global carbon cycle: *Chemical Geology*, v. 202, p. 257–273, doi:10.1016/j.chemgeo.2002.10.001.
- Dessert, C., Gaillardet, J., Dupre, B., Schott, J., and Pokrovsky, O.S., 2009, Fluxes of high- versus low-temperature water–rock interactions in aerial volcanic areas: Example from the Kamchatka Peninsula, Russia: *Geochimica et Cosmochimica Acta*, v. 73, p. 148–169, doi:10.1016/j.gca.2008.09.012.
- Donahoe, R.J., and Liou, J.G., 1985, An experimental study on the process of zeolite formation: *Geochimica et Cosmochimica Acta*, v. 49, p. 2349–2360, doi:10.1016/0016-7037(85)90235-2.
- Druhan, J.L., Steefel, C.I., Williams, K.H., and DePaolo, D.J., 2013, Calcium isotope fractionation in groundwater: Molecular scale processes influencing field scale behavior: *Geochimica et Cosmochimica Acta*, v. 119, p. 93–116, doi:10.1016/j.gca.2013.05.022.
- Eiriksdottir, E.S., Gislason, S.R., and Oelkers, E.H., 2013, Does temperature or runoff control the feedback between chemical denudation and climate? Insights from NE Iceland: *Geochimica et Cosmochimica Acta*, v. 107, p. 65–81, doi:10.1016/j.gca.2012.12.034.
- Fantle, M.S., and DePaolo, D.J., 2007, Ca isotopes in carbonate sediment and pore fluid from ODP Site 807A: The  $\text{Ca}^{2+}(\text{aq})$ –calcite equilibrium fractionation factor and calcite recrystallization rates in Pleistocene sediments: *Geochimica et Cosmochimica Acta*, v. 71, p. 2524–2546, doi:10.1016/j.gca.2007.03.006.

- Fantle, M.S., and Tipper, E.T., 2014, Calcium isotopes in the global biogeochemical Ca cycle: Implications for development of a Ca isotope proxy: *Earth-Science Reviews*, v. 129, p. 148–177, doi:10.1016/j.earscirev.2013.10.004.
- Fantle, M.S., Tollerud, H., Eisenhauer, A., and Holmden, C., 2012, The Ca isotopic composition of dust-producing regions: Measurements of surface sediments in the Black Rock Desert, Nevada: *Geochimica et Cosmochimica Acta*, v. 87, p. 178–193, doi:10.1016/j.gca.2012.03.037.
- Feng, C., Qin, T., Huang, S., Wu, Z., and Huang, F., 2014, First-principles investigations of equilibrium calcium isotope fractionation between clinopyroxene and Ca-doped orthopyroxene: *Geochimica et Cosmochimica Acta*, v. 143, p. 132–142, doi:10.1016/j.gca.2014.06.002.
- Flaathen, T.K., Gislason, S.R., Oelkers, E.H., and Sveinbjörnsdóttir, Á.E., 2009, Chemical evolution of the Mt. Hekla, Iceland, groundwaters: A natural analogue for CO<sub>2</sub> sequestration in basaltic rocks: *Applied Geochemistry*, v. 24, p. 463–474, doi:10.1016/j.apgeochem.2008.12.031.
- Fleischer, M., 1954, The abundance and distribution of the chemical elements in the earth's crust: *Journal of Chemical Education*, v. 31, p. 446, doi:10.1021/ed031p446.
- Flowers, G.E., Björnsson, H., and Pálsson, F., 2003, New insights into the subglacial and periglacial hydrology of Vatnajökull, Iceland, from a distributed physical model: *Journal of Glaciology*, v. 49, p. 257–270, doi:10.3189/172756503781830827.
- Franzson, H., 2000, Hydrothermal Evolution of the Nesjavellir High-Temperature System, Iceland: *Proceedings of the World Geothermal Congress*, v. May 28, p. 2075–2080.
- Franzson, H., Gudfinnsson, G.H., Frolova, J., Helgadóttir, H.M., Pauly, B., Mortensen, A.K., and Jakobsson, S.P., 2011, Icelandic Hyaloclastite Tuffs: Report prepared for National Energy Authority and Reykjavík Energy. ISOR, p. 1–105.
- Fridriksson, T., 2004, Experimental determination of thermodynamic properties of ion-exchange in heulandite: Binary ion-exchange experiments at 55 and 85 C involving Ca<sup>2+</sup>, Sr<sup>2+</sup>, Na<sup>+</sup>, and K<sup>+</sup>: *American Journal of Science*, v. 304, p. 287–332, doi:10.2475/ajs.304.4.287.
- Fridriksson, T., Arnórsson, S., and Bird, D.K., 2009, Processes controlling Sr in surface and ground waters of Tertiary tholeiitic flood basalts in Northern Iceland: *Geochimica et Cosmochimica Acta*, v. 73, p. 6727–6746, doi:10.1016/j.gca.2009.08.025.
- Fridriksson, T., Neuhoﬀ, P.S., Arnórsson, S., and Bird, D.K., 2001, Geological constraints on the thermodynamic properties of the stilbite—stellerite solid solution in low-grade metabasalts: *Geochimica et Cosmochimica Acta*, v. 65, p. 3993–4008, doi:10.1016/S0016-7037(01)00629-9.

- Furnes, H., 1984, Chemical changes during progressive subaerial palagonitization of a subglacial olivine tholeiite hyaloclastite: A microprobe study: *Chemical Geology*, v. 43, p. 271–285, doi:10.1016/0009-2541(84)90054-8.
- Furnes, H., 1978, Element mobility during palagonitization of a subglacial hyaloclastite in Iceland: *Chemical Geology*, v. 22, p. 249–264, doi:10.1016/0009-2541(78)90034-7.
- Gaillardet, J., Dupré, B., Louvat, P., and Allègre, C.J., 1999, Global silicate weathering and CO<sub>2</sub> consumption rates deduced from the chemistry of large rivers: *Chemical Geology*, v. 159, p. 3–30, doi:10.1016/S0009-2541(99)00031-5.
- Galeczka, I., Eiriksdottir, E.S., Hardardottir, J., Oelkers, E.H., Torssander, P., and Gislason, S.R., 2015, The effect of the 2002 glacial flood on dissolved and suspended chemical fluxes in the Skaftá river, Iceland: *Journal of Volcanology and Geothermal Research*, v. 301, p. 253–276, doi:10.1016/j.jvolgeores.2015.05.008.
- Galeczka, I., Oelkers, E.H., and Gislason, S.R., 2014, The chemistry and element fluxes of the July 2011 Múlakvísl and Kaldakvísl glacial floods, Iceland: *Journal of Volcanology and Geothermal Research*, v. 273, p. 41–57, doi:10.1016/j.jvolgeores.2013.12.004.
- Gannoun, A., Burton, K.W., Vigier, N., Gislason, S.R., Rogers, N., Mokadem, F., and Sigfússon, B., 2006, The influence of weathering process on riverine osmium isotopes in a basaltic terrain: *Earth and Planetary Science Letters*, v. 243, p. 732–748, doi:10.1016/j.epsl.2006.01.024.
- Gennadiev, A.N., Geptner, A.R., Zhidkin, A.P., Chernyanskii, S.S., and Pikovskii, Yu.I., 2007, Exothermic and endothermic soils of Iceland: *Eurasian Soil Science*, v. 40, p. 595–607, doi:10.1134/S1064229307060014.
- Georg, R.B., Reynolds, B.C., West, A.J., Burton, K.W., and Halliday, A.N., 2007, Silicon isotope variations accompanying basalt weathering in Iceland: *Earth and Planetary Science Letters*, v. 261, p. 476–490, doi:10.1016/j.epsl.2007.07.004.
- Gisladottir, F.O., Arnalds, O., and Gisladottir, G., 2005, The effect of landscape and retreating glaciers on wind erosion in South Iceland: *Land Degradation & Development*, v. 16, p. 177–187, doi:10.1002/ldr.645.
- Gislason, S.R. et al., 2009, Direct evidence of the feedback between climate and weathering: *Earth and Planetary Science Letters*, v. 277, p. 213–222, doi:10.1016/j.epsl.2008.10.018.
- Gislason, S.R., and Arnórsson, S., 1993, Dissolution of primary basaltic minerals in natural waters: saturation state and kinetics: *Chemical Geology*, v. 105, p. 117–135, doi:10.1016/0009-2541(93)90122-Y.

- Gislason, S.R., Arnorsson, S., and Armannsson, H., 1996, Chemical weathering of basalt in Southwest Iceland; effects of runoff, age of rocks and vegetative/glacial cover: *American Journal of Science*, v. 296, p. 837–907, doi:10.2475/ajs.296.8.837.
- Gislason, S.R., and Eugster, H.P., 1987a, Meteoric water-basalt interactions. I: A laboratory study: *Geochimica et Cosmochimica Acta*, v. 51, p. 2827–2840, doi:10.1016/0016-7037(87)90161-X.
- Gislason, S.R., and Eugster, H.P., 1987b, Meteoric water-basalt interactions. II: A field study in N.E. Iceland: *Geochimica et Cosmochimica Acta*, v. 51, p. 2841–2855, doi:10.1016/0016-7037(87)90162-1.
- Gislason, S.R., and Oelkers, E.H., 2003, Mechanism, rates, and consequences of basaltic glass dissolution: II. An experimental study of the dissolution rates of basaltic glass as a function of pH and temperature: *Geochimica et Cosmochimica Acta*, v. 67, p. 3817–3832, doi:10.1016/S0016-7037(03)00176-5.
- Gislason, S.R., Oelkers, E.H., and Snorrason, Á., 2006, Role of river-suspended material in the global carbon cycle: *Geology*, v. 34, p. 49, doi:10.1130/G22045.1.
- Gislason, S.R., Snorrason, Á., Kristmannsdóttir, H.K., Sveinbjörnsdóttir, Á.E., Torsander, P., Ólafsson, J., Castet, S., and Dupré, B., 2002, Effects of volcanic eruptions on the CO<sub>2</sub> content of the atmosphere and the oceans: the 1996 eruption and flood within the Vatnajökull Glacier, Iceland: *Chemical Geology*, v. 190, p. 181–205, doi:10.1016/S0009-2541(02)00116-X.
- Goldich, S.S., 1938, A Study in Rock-Weathering: *The Journal of Geology*, v. 46, p. 17–58.
- Griffith, E.M., and Fantle, M.S., 2020, Introduction to calcium isotope geochemistry: Past lessons and future directions: *Chemical Geology*, v. 537, p. 119470, doi:10.1016/j.chemgeo.2020.119470.
- Griffith, E.M., Schauble, E.A., Bullen, T.D., and Paytan, A., 2008, Characterization of calcium isotopes in natural and synthetic barite: *Geochimica et Cosmochimica Acta*, v. 72, p. 5641–5658, doi:10.1016/j.gca.2008.08.010.
- Griffith, E.M., Schmitt, A.-D., Andrews, M.G., and Fantle, M.S., 2020, Elucidating modern geochemical cycles at local, regional, and global scales using calcium isotopes: *Chemical Geology*, v. 534, p. 119445, doi:10.1016/j.chemgeo.2019.119445.
- Gudmundsson, H.J., 1997, A review of the holocene environmental history of Iceland: *Quaternary Science Reviews*, v. 16, p. 81–92, doi:10.1016/S0277-3791(96)00043-1.
- Gudmundsson, M.T., Björnsson, H., and Pálsson, F., 1995, Changes in jökulhlaup sizes in Grímsvötn, Vatnajökull, Iceland, 1934–91, deduced from in-situ measurements of

- subglacial lake volume: *Journal of Glaciology*, v. 41, p. 263–272, doi:10.3189/S0022143000016166.
- Gunter, M.E., Armbruster, T., Kohler, T., and Knowles, C.R., 1994, Crystal structure and optical properties of Na- and Pb- exchanged heulandite-group zeolites: *American Mineralogist*, v. 79, p. 675–682.
- Gupta, H., Chakrapani, G.J., Selvaraj, K., and Kao, S.-J., 2011, The fluvial geochemistry, contributions of silicate, carbonate and saline–alkaline components to chemical weathering flux and controlling parameters: Narmada River (Deccan Traps), India: *Geochimica et Cosmochimica Acta*, v. 75, p. 800–824, doi:10.1016/j.gca.2010.11.010.
- Gussone, N., Ahm, A.-S.C., Lau, K.V., and Bradbury, H.J., 2020a, Calcium isotopes in deep time: Potential and limitations: *Chemical Geology*, v. 544, p. 119601, doi:10.1016/j.chemgeo.2020.119601.
- Gussone, N., Austrheim, H., Westhues, A., and Mezger, K., 2020b, Origin of Rodingite Forming Fluids Constrained by Calcium and Strontium Isotope Ratios in the Leka Ophiolite Complex: *Chemical Geology*, v. 542, p. 119598, doi:10.1016/j.chemgeo.2020.119598.
- Gussone, N., Böhm, F., Eisenhauer, A., Dietzel, M., Heuser, A., Teichert, B.M.A., Reitner, J., Wörheide, G., and Dullo, W.-C., 2005, Calcium isotope fractionation in calcite and aragonite: *Geochimica et Cosmochimica Acta*, v. 69, p. 4485–4494, doi:10.1016/j.gca.2005.06.003.
- Gussone, N., Schmitt, A.-D., Heuser, A., Wombacher, F., Dietzel, M., Tipper, E., and Schiller, M., 2016, *Calcium Stable Isotope Geochemistry*: Berlin, Heidelberg, Springer, *Advances in Isotope Geochemistry*, doi:10.1007/978-3-540-68953-9.
- Gysi, A.P., and Stefánsson, A., 2012a, CO<sub>2</sub>-water–basalt interaction. Low temperature experiments and implications for CO<sub>2</sub> sequestration into basalts: *Geochimica et Cosmochimica Acta*, v. 81, p. 129–152, doi:10.1016/j.gca.2011.12.012.
- Gysi, A.P., and Stefánsson, A., 2012b, Experiments and geochemical modeling of CO<sub>2</sub> sequestration during hydrothermal basalt alteration: *Chemical Geology*, v. 306–307, p. 10–28, doi:10.1016/j.chemgeo.2012.02.016.
- Gysi, A.P., and Stefánsson, A., 2012c, Mineralogical aspects of CO<sub>2</sub> sequestration during hydrothermal basalt alteration — An experimental study at 75 to 250°C and elevated pCO<sub>2</sub>: *Chemical Geology*, v. 306–307, p. 146–159, doi:10.1016/j.chemgeo.2012.03.006.
- Gysi, A.P., and Stefánsson, A., 2008, Numerical modelling of CO<sub>2</sub>-water-basalt interaction: *Mineralogical Magazine*, v. 72, p. 55–59, doi:10.1180/minmag.2008.072.1.55.

- Hartmann, J., Moosdorf, N., Lauerwald, R., Hinderer, M., and West, A.J., 2014, Global chemical weathering and associated P-release — The role of lithology, temperature and soil properties: *Chemical Geology*, v. 363, p. 145–163, doi:10.1016/j.chemgeo.2013.10.025.
- Hay, R.L., and Sheppard, R.A., 2001, Occurrence of Zeolites in Sedimentary Rocks: An Overview: *Reviews in Mineralogy and Geochemistry*, v. 45, p. 217–234, doi:10.2138/rmg.2001.45.6.
- Hewish, N.A., Neilson, G.W., and Enderby, J.E., 1982, Environment of Ca<sup>2+</sup> ions in aqueous solvent: *Nature*, v. 297, p. 138–139, doi:10.1038/297138a0.
- Hindshaw, R.S., Bourdon, B., Pogge von Strandmann, P.A.E., Vigier, N., and Burton, K.W., 2013, The stable calcium isotopic composition of rivers draining basaltic catchments in Iceland: *Earth and Planetary Science Letters*, v. 374, p. 173–184, doi:10.1016/j.epsl.2013.05.038.
- Hindshaw, R.S., Reynolds, B.C., Wiederhold, J.G., Kretzschmar, R., and Bourdon, B., 2011, Calcium isotopes in a proglacial weathering environment: Damma glacier, Switzerland: *Geochimica et Cosmochimica Acta*, v. 75, p. 106–118, doi:10.1016/j.gca.2010.09.038.
- Hjartarson, A., and Saemundsson, K., 2014, Geological Map of Iceland. Bedrock. 1:600 000: Iceland Geosurvey,.
- Hofmann, A.E., Bourg, I.C., and DePaolo, D.J., 2012, Ion desolvation as a mechanism for kinetic isotope fractionation in aqueous systems: *Proceedings of the National Academy of Sciences*, v. 109, p. 18689–18694, doi:10.1073/pnas.1208184109.
- Huang, S., Farkaš, J., and Jacobsen, S.B., 2010, Calcium isotopic fractionation between clinopyroxene and orthopyroxene from mantle peridotites: *Earth and Planetary Science Letters*, v. 292, p. 337–344.
- Ibarra, D.E., Caves, J.K., Moon, S., Thomas, D.L., Hartmann, J., Chamberlain, C.P., and Maher, K., 2016, Differential weathering of basaltic and granitic catchments from concentration–discharge relationships: *Geochimica et Cosmochimica Acta*, v. 190, p. 265–293, doi:10.1016/j.gca.2016.07.006.
- Iijima, A., 1980, Geology of natural zeolites and zeolitic rocks: *Pure and Applied Chemistry*, v. 52, p. 2115–2130.
- Jacobson, A.D., Grace Andrews, M., Lehn, G.O., and Holmden, C., 2015, Silicate versus carbonate weathering in Iceland: New insights from Ca isotopes: *Earth and Planetary Science Letters*, v. 416, p. 132–142, doi:10.1016/j.epsl.2015.01.030.
- Jacobson, A.D., and Holmden, C., 2008,  $\delta^{44}\text{Ca}$  evolution in a carbonate aquifer and its bearing on the equilibrium isotope fractionation factor for calcite: *Earth and Planetary Science Letters*, v. 270, p. 349–353, doi:10.1016/j.epsl.2008.03.039.

- Jagoutz, O., Macdonald, F.A., and Royden, L., 2016, Low-latitude arc–continent collision as a driver for global cooling: *Proceedings of the National Academy of Sciences*, v. 113, p. 4935–4940, doi:10.1073/pnas.1523667113.
- Jakobsson, S.P., 1978, Environmental factors controlling the palagonitization of the Surtsey tephra, Iceland: *Bulletin of the Geological Society of Denmark*, v. 27, p. 15.
- Jakobsson, S.P., and Moore, J.G. Hydrothermal minerals and alteration rates at Surtsey volcano, Iceland: , p. 12.
- Jercinovic, M.J., Keil, K., Smith, M.R., and Schmitt, R.A., 1990, Alteration of basaltic glasses from north-central British Columbia, Canada: *Geochimica et Cosmochimica Acta*, v. 54, p. 2679–2696, doi:10.1016/0016-7037(90)90004-5.
- Jiang, N., Shang, R., Heijman, S.G.J., and Rietveld, L.C., 2018, High-silica zeolites for adsorption of organic micro-pollutants in water treatment: A review: *Water Research*, v. 144, p. 145–161, doi:10.1016/j.watres.2018.07.017.
- Jin, L., Ogrinc, N., Hamilton, S.K., Szramek, K., Kanduc, T., and Walter, L.M., 2009, Inorganic carbon isotope systematics in soil profiles undergoing silicate and carbonate weathering (Southern Michigan, USA): *Chemical Geology*, v. 264, p. 139–153, doi:10.1016/j.chemgeo.2009.03.002.
- John, T., Gussone, N., Podladchikov, Y.Y., Bebout, G.E., Dohmen, R., Halama, R., Klemd, R., Magna, T., and Seitz, H.-M., 2012, Volcanic arcs fed by rapid pulsed fluid flow through subducting slabs: *Nature Geoscience*, v. 5, p. 489–492, doi:10.1038/ngeo1482.
- Jónsdóttir, J.F., 2008, A runoff map based on numerically simulated precipitation and a projection of future runoff in Iceland / Une carte d'écoulement basée sur la précipitation numériquement simulée et un scénario du futur écoulement en Islande: *Hydrological Sciences Journal*, v. 53, p. 100–111, doi:10.1623/hysj.53.1.100.
- Kallo, D., 2001, Applications of Natural Zeolites in Water and Wastewater Treatment: *Reviews in Mineralogy and Geochemistry*, v. 45, p. 519–550, doi:10.2138/rmg.2001.45.15.
- Katz, A.K., Glusker, J.P., Beebe, S.A., and Bock, C.W., 1996, Calcium Ion Coordination: A Comparison with That of Beryllium, Magnesium, and Zinc: *Journal of the American Chemical Society*, v. 118, p. 5752–5763, doi:10.1021/ja953943i.
- Kirfel, A., and Gibbs, G.V., 2000, Electron density distributions and bonded interactions for the fibrous zeolites natrolite, mesolite and scolecite and related materials: *Physics and Chemistry of Minerals*, v. 27, p. 270–284.
- Kirov, G., and Filizova, L., 2012, Cationic hydration impact on zeolite formation and properties: A review and discussion: *Geochemistry, Mineralogy and Petrology*, v. 49, p. 65–82.

- Kiseleva, I., Navrotsky, A., Belitsky, I., and Fursenko, B., 2001, Thermochemical study of calcium zeolites—heulandite and stilbite: *American Mineralogist*, v. 86, p. 448–455, doi:10.2138/am-2001-0408.
- Kol'tsova, T.N., 2010, Scolecite-mesolite transition in relation to sodium substitution for calcium: *Inorganic Materials*, v. 46, p. 187–195, doi:10.1134/S0020168510020184.
- Kousehlar, M., Weisenberger, T.B., Tutti, F., and Mirnejad, H., 2012, Fluid control on low-temperature mineral formation in volcanic rocks of Kahrizak, Iran: Fluid control on low-temperature mineral formation: *Geofluids*, v. 12, p. 295–311, doi:10.1111/gfl.12001.
- Kristmannsdóttir, H., and Tómasson, J., 1978, Zeolite zones in geothermal areas in Iceland: *Natural Zeolites*, p. 227–284.
- Lammers, L.N., Kulasinski, K., Zarzycki, P., and DePaolo, D.J., 2020, Molecular simulations of kinetic stable calcium isotope fractionation at the calcite-aqueous interface: *Chemical Geology*, v. 532, p. 119315, doi:10.1016/j.chemgeo.2019.119315.
- Lawler, D.M., and Bjornsson, H., 1996, IMPACT OF SUBGLACIAL GEOTHERMAL ACTIVITY ON MELTWATER QUALITY IN THE JÖKULSÁ Á SÓLHEIMASANDI SYSTEM, SOUTHERN ICELAND: *Hydrological Processes*, v. 10, p. 557–578.
- Lebrato, M. et al., 2020, Global variability in seawater Mg:Ca and Sr:Ca ratios in the modern ocean: *Proceedings of the National Academy of Sciences*, v. 117, p. 22281–22292, doi:10.1073/pnas.1918943117.
- Lehn, G.O., Jacobson, A.D., Douglas, T.A., McClelland, J.W., Barker, A.J., and Khosh, M.S., 2017, Constraining seasonal active layer dynamics and chemical weathering reactions occurring in North Slope Alaskan watersheds with major ion and isotope ( $\delta^{34}\text{S}$   $\text{SO}_4$ ,  $\delta^{13}\text{C}$   $\text{DIC}$ ,  $\delta^{87}\text{Sr}/\delta^{86}\text{Sr}$ ,  $\delta^{44}/\delta^{40}\text{Ca}$ , and  $\delta^{44}/\delta^{42}\text{Ca}$ ) measurements: *Geochimica et Cosmochimica Acta*, v. 217, p. 399–420, doi:10.1016/j.gca.2017.07.042.
- Lehn, G.O., Jacobson, A.D., and Holmden, C., 2013, Precise analysis of Ca isotope ratios ( $\delta^{44}/\delta^{40}\text{Ca}$ ) using an optimized  $^{43}\text{Ca}$ – $^{42}\text{Ca}$  double-spike MC-TIMS method: *International Journal of Mass Spectrometry*, v. 351, p. 69–75, doi:10.1016/j.ijms.2013.06.013.
- Lemarchand, D., Wasserburg, G.J., and Papanastassiou, D.A., 2004, Rate-controlled calcium isotope fractionation in synthetic calcite: *Geochimica et Cosmochimica Acta*, v. 68, p. 4665–4678, doi:10.1016/j.gca.2004.05.029.
- Leyva-Ramos, R., Monsivais-Rocha, J.E., Aragon-Piña, A., Berber-Mendoza, M.S., Guerrero-Coronado, R.M., Alonso-Davila, P., and Mendoza-Barron, J., 2010, Removal of ammonium from aqueous solution by ion exchange on natural and modified chabazite: *Journal of Environmental Management*, v. 91, p. 2662–2668, doi:10.1016/j.jenvman.2010.07.035.

- Li, G. et al., 2016, Temperature dependence of basalt weathering: Earth and Planetary Science Letters, v. 443, p. 59–69, doi:10.1016/j.epsl.2016.03.015.
- Li, S.-L., Calmels, D., Han, G., Gaillardet, J., and Liu, C.-Q., 2008, Sulfuric acid as an agent of carbonate weathering constrained by  $\delta^{13}\text{C}_{\text{DIC}}$ : Examples from Southwest China: Earth and Planetary Science Letters, v. 270, p. 189–199, doi:10.1016/j.epsl.2008.02.039.
- Li, J., Chang, H., Ma, L., Hao, J., and Yang, R.T., 2011, Low-temperature selective catalytic reduction of  $\text{NO}_x$  with  $\text{NH}_3$  over metal oxide and zeolite catalysts—A review: Catalysis Today, v. 175, p. 147–156, doi:10.1016/j.cattod.2011.03.034.
- Li, Y., Li, L., and Yu, J., 2017, Applications of Zeolites in Sustainable Chemistry: Chem, v. 3, p. 928–949, doi:10.1016/j.chempr.2017.10.009.
- Lim, L.H.V., Pribil, A.B., Ellmerer, A.E., Randolph, B.R., and Rode, B.M., 2009, Temperature dependence of structure and dynamics of the hydrated  $\text{Ca}^{2+}$  ion according to *ab initio* quantum mechanical charge field and classical molecular dynamics: Journal of Computational Chemistry, v. 31, p. 1195–1200, doi:10.1002/jcc.21405.
- Liou, J.G., de Capitani, C., and Frey, M., 1991, Zeolite equilibria in the system  $\text{CaAl}_2\text{Si}_2\text{O}_8$  -  $\text{NaAlSi}_3\text{O}_8$  -  $\text{SiO}_2$  -  $\text{H}_2\text{O}$ : New Zealand Journal of Geology and Geophysics, v. 34, p. 293–301, doi:10.1080/00288306.1991.9514467.
- Liou, J., Maruyama, S., and Cho, A., 1985, Phase Equilibria and Mineral Parageneses of Metabasites in Low-Grade Metamorphism: Mineralogical Magazine, v. 49, doi:10.1180/minmag.1985.049.352.03.
- Lisitzina, N.A., and Butuzova, G.Yu., 1982, Authigenic zeolites in the sedimentary mantle of the world ocean: Sedimentary Geology, v. 31, p. 33–41, doi:10.1016/0037-0738(82)90005-7.
- Lonin, A.Y., Levenets, V.V., Neklyudov, I.M., and Shchur, A.O., 2015, The usage of zeolites for dynamic sorption of cesium from waste waters of nuclear power plants: Journal of Radioanalytical and Nuclear Chemistry, v. 303, p. 831–836, doi:10.1007/s10967-014-3597-9.
- Louvat, P., and Allègre, C.J., 1997, Present denudation rates on the island of Réunion determined by river geochemistry: Basalt weathering and mass budget between chemical and mechanical erosions: Geochimica et Cosmochimica Acta, v. 61, p. 3645–3669, doi:10.1016/S0016-7037(97)00180-4.
- Louvat, P., Gislason, S.R., and Allegre, C.J., 2008, Chemical and mechanical erosion rates in Iceland as deduced from river dissolved and solid material: American Journal of Science, v. 308, p. 679–726, doi:10.2475/05.2008.02.

- Macdonald, F.A., Swanson-Hysell, N.L., Park, Y., Lisiecki, L., and Jagoutz, O., 2019, Arc-continent collisions in the tropics set Earth's climate state: *Science*, p. eaav5300, doi:10.1126/science.aav5300.
- Mackenzie, F., and Garrels, R.M., 1966, Chemical mass balance between rivers and oceans.: *American Journal of Science*, v. 264, p. 507–525, doi:https://doi.org/10.2475/ajs.264.7.507.
- Mankasingh, U., and Gísladóttir, G., 2019, Early indicators of soil formation in the Icelandic sub-arctic highlands: *Geoderma*, v. 337, p. 152–163, doi:10.1016/j.geoderma.2018.09.002.
- Marriott, C.S., Henderson, G.M., Belshaw, N.S., and Tudhope, A.W., 2004, Temperature dependence of  $\delta^7\text{Li}$ ,  $\delta^{44}\text{Ca}$  and Li/Ca during growth of calcium carbonate: *Earth and Planetary Science Letters*, v. 222, p. 615–624, doi:10.1016/j.epsl.2004.02.031.
- Matter, J.M. et al., 2016, Rapid carbon mineralization for permanent disposal of anthropogenic carbon dioxide emissions: *Science*, v. 352, p. 1312–1314, doi:10.1126/science.aad8132.
- Mayfield, K.K. et al., 2021, Groundwater discharge impacts marine isotope budgets of Li, Mg, Ca, Sr, and Ba: *Nature Communications*, v. 12, p. 148, doi:10.1038/s41467-020-20248-3.
- Mehegan, J.M., Robinson, P.T., and Delaney, J.R., 1982, Secondary mineralization and hydrothermal alteration in the Reydarfjordur drill core, eastern Iceland: *Journal of Geophysical Research: Solid Earth*, v. 87, p. 6511–6524, doi:10.1029/JB087iB08p06511.
- Meybeck, M., 1987, Global chemical weathering of surficial rocks estimated from river dissolved loads: *American Journal of Science*, v. 287, p. 401–428.
- Mills, J.V., DePaolo, D.J., and Lammers, L.N., 2021, The influence of Ca:CO<sub>3</sub> stoichiometry on Ca isotope fractionation: Implications for process-based models of calcite growth: *Geochimica et Cosmochimica Acta*, v. 298, p. 87–111, doi:10.1016/j.gca.2021.01.016.
- Moon, S., Chamberlain, C.P., and Hilley, G.E., 2014, New estimates of silicate weathering rates and their uncertainties in global rivers: *Geochimica et Cosmochimica Acta*, v. 134, p. 257–274, doi:10.1016/j.gca.2014.02.033.
- Moorbath, S., Sigurdsson, H., and Goodwin, R., 1968, KAr ages of the oldest exposed rocks in Iceland: *Earth and Planetary Science Letters*, v. 4, p. 197–205, doi:10.1016/0012-821X(68)90035-6.
- Moore, J., Jacobson, A.D., Holmden, C., and Craw, D., 2013, Tracking the relationship between mountain uplift, silicate weathering, and long-term CO<sub>2</sub> consumption with Ca isotopes: *Southern Alps, New Zealand: Chemical Geology*, v. 341, p. 110–127, doi:10.1016/j.chemgeo.2013.01.005.

- Moulton, K.L., West, J., and Berner, R.A., 2000, Solute flux and mineral mass balance approaches to the quantification of plant effects on silicate weathering: *American Journal of Science*, v. 300, p. 539–570, doi:10.2475/ajs.300.7.539.
- Moynier, F., and Fujii, T., 2017, Calcium isotope fractionation between aqueous compounds relevant to low-temperature geochemistry, biology and medicine: *Scientific Reports*, v. 7, p. 44255, doi:10.1038/srep44255.
- Mumpton, F.A., 1999, La roca magica: Uses of natural zeolites in agriculture and industry: *Proceedings of the National Academy of Sciences*, v. 96, p. 3463–3470, doi:10.1073/pnas.96.7.3463.
- Nakamura, H., Okumura, M., and Machida, M., 2014, Monte Carlo simulation studies of cation selectivity in ion exchange of zeolites: *RSC Adv.*, v. 4, p. 52757–52761, doi:10.1039/C4RA09460C.
- Nelson, C., Jacobson, A., Kitch, G., and Weisenberger, T.B., 2021, Large calcium isotope fractionations by zeolite minerals from Iceland: *Communications Earth and Environment*.
- Nesbitt, H.W., and Wilson, R.E., 1992, Recent Chemical Weathering of Basalts: *American Journal of Science*, v. 292, p. 740–777.
- Neuhoff, P.S., Fridriksson, T., and Arnorsson, S., 1999, Porosity evolution and mineral paragenesis during low-grade metamorphism of basaltic lavas at Teigarhorn, eastern Iceland: *American Journal of Science*, v. 299, p. 467–501, doi:10.2475/ajs.299.6.467.
- Neuhoff, P.S., Fridriksson, T., and Bird, D.K., 2000, Zeolite Parageneses in the North Atlantic Igneous Province: Implications for Geotectonics and Groundwater Quality of Basaltic Crust: *International Geology Review*, v. 42, p. 15–44, doi:10.1080/00206810009465068.
- Nielsen, L.C., DePaolo, D.J., and De Yoreo, J.J., 2012, Self-consistent ion-by-ion growth model for kinetic isotopic fractionation during calcite precipitation: *Geochimica et Cosmochimica Acta*, v. 86, p. 166–181, doi:10.1016/j.gca.2012.02.009.
- Ockert, C., Gussone, N., Kaufhold, S., and Teichert, B.M.A., 2013, Isotope fractionation during Ca exchange on clay minerals in a marine environment: *Geochimica et Cosmochimica Acta*, v. 112, p. 374–388, doi:10.1016/j.gca.2012.09.041.
- Oelkers, E.H., and Gislason, S.R., 2001, The mechanism, rates and consequences of basaltic glass dissolution: I. An experimental study of the dissolution rates of basaltic glass as a function of aqueous Al, Si and oxalic acid concentration at 25°C and pH = 3 and 11: *Geochimica et Cosmochimica Acta*, v. 65, p. 3671–3681, doi:10.1016/S0016-7037(01)00664-0.

- Oelkers, E.H., Pogge von Strandmann, P.A.E., and Mavromatis, V., 2019, The rapid resetting of the Ca isotopic signatures of calcite at ambient temperature during its congruent dissolution, precipitation, and at equilibrium: *Chemical Geology*, v. 512, p. 1–10, doi:10.1016/j.chemgeo.2019.02.035.
- Oeser, R.A., and von Blanckenburg, F., 2020, Strontium isotopes trace biological activity in the Critical Zone along a climate and vegetation gradient: *Chemical Geology*, v. 558, p. 119861, doi:10.1016/j.chemgeo.2020.119861.
- Olsson, J., Stipp, S.L.S., Makovicky, E., and Gislason, S.R., 2014, Metal scavenging by calcium carbonate at the Eyjafjallajökull volcano: A carbon capture and storage analogue: *Chemical Geology*, v. 384, p. 135–148, doi:10.1016/j.chemgeo.2014.06.025.
- Oskarsdottir, S.M., Gislason, S.R., Snorrason, A., Halldorsdottir, S.G., and Gisladottir, G., 2011, Spatial distribution of dissolved constituents in Icelandic river waters: *Journal of Hydrology*, v. 397, p. 175–190, doi:10.1016/j.jhydrol.2010.11.028.
- Óskarsson, B.V., Riishuus, M.S., and Arnalds, Ó., 2012, Climate-dependent chemical weathering of volcanic soils in Iceland: *Geoderma*, v. 189–190, p. 635–651, doi:10.1016/j.geoderma.2012.05.030.
- Pabalan, R.T., and Bertetti, F.P., 2001, Cation-Exchange Properties of Natural Zeolites: *Reviews in Mineralogy and Geochemistry*, v. 45, p. 453–518, doi:10.2138/rmg.2001.45.14.
- Paque, M., Detienne, M., Maters, E.C., and Delmelle, P., 2016, Smectites and zeolites in ash from the 2010 summit eruption of Eyjafjallajökull volcano, Iceland: *Bulletin of Volcanology*, v. 78, p. 61, doi:10.1007/s00445-016-1056-x.
- Parkhurst, D., and Appelo, C.A.J., 1999, User's guide to PHREEQC (Version 2): A computer program for speciation, batch-reaction, one-dimensional transport, and inverse geochemical calculations: *Water-resources investigations report*, v. 99, p. 312, doi:10.3133/wri994259.
- Passaglia, E., and Sheppard, R.A., 2001, *The Crystal Chemistry of Zeolites*: Mineralogical Society of America, v. 45, p. 69–116.
- Pauly, B.D., Schiffman, P., Zierenberg, R.A., and Clague, D.A., 2011, Environmental and chemical controls on palagonitization: *Geochemistry, Geophysics, Geosystems*, v. 12, doi:https://doi.org/10.1029/2011GC003639.
- Plummer, L.N., and Busenberg, E., 1982, The solubilities of calcite, aragonite and vaterite in CO<sub>2</sub>-H<sub>2</sub>O solutions between 0 and 90°C, and an evaluation of the aqueous model for the system CaCO<sub>3</sub>-CO<sub>2</sub>-H<sub>2</sub>O: *Geochimica et Cosmochimica Acta*, v. 46, p. 1011–1040, doi:10.1016/0016-7037(82)90056-4.

- Pogge von Strandmann, P.A.E., Burton, K.W., James, R.H., van Calsteren, P., Gislason, S.R., and Sigfússon, B., 2008, The influence of weathering processes on riverine magnesium isotopes in a basaltic terrain: *Earth and Planetary Science Letters*, v. 276, p. 187–197, doi:10.1016/j.epsl.2008.09.020.
- Pogge von Strandmann, P.A.E., Burton, K.W., Opfergelt, S., Eiríksdóttir, E.S., Murphy, M.J., Einarsson, A., and Gislason, S.R., 2016, The effect of hydrothermal spring weathering processes and primary productivity on lithium isotopes: Lake Myvatn, Iceland: *Chemical Geology*, v. 445, p. 4–13, doi:10.1016/j.chemgeo.2016.02.026.
- Pogge von Strandmann, P.A.E., Burton, K.W., Porcelli, D., James, R.H., van Calsteren, P., and Gislason, S.R., 2011, Transport and exchange of U-series nuclides between suspended material, dissolved load and colloids in rivers draining basaltic terrains: *Earth and Planetary Science Letters*, v. 301, p. 125–136, doi:10.1016/j.epsl.2010.10.029.
- Pogge von Strandmann, P.A.E., Burton, K.W., Snæbjörnsdóttir, S.O., Sigfússon, B., Aradóttir, E.S., Gunnarsson, I., Alfredsson, H.A., Mesfin, K.G., Oelkers, E.H., and Gislason, S.R., 2019a, Rapid CO<sub>2</sub> mineralisation into calcite at the CarbFix storage site quantified using calcium isotopes: *Nature Communications*, v. 10, p. 1–7, doi:10.1038/s41467-019-10003-8.
- Pogge von Strandmann, P.A.E., Hatton, J.E., and Robinson, L.F., 2019b, The Response of Magnesium, Silicon, and Calcium Isotopes to Rapidly Uplifting and Weathering Terrains: South Island, New Zealand: *Frontiers in Earth Science*, v. 7, p. 240, doi:10.3389/feart.2019.00240.
- Pogge von Strandmann, P.A.E., Olsson, J., Luu, T.-H., Gislason, S.R., and Burton, K.W., 2019c, Using Mg Isotopes to Estimate Natural Calcite Compositions and Precipitation Rates During the 2010 Eyjafjallajökull Eruption: *Frontiers in Earth Science*, v. 7, p. 6, doi:10.3389/feart.2019.00006.
- Rad, S., Allegre, C., and Louvat, P., 2007, Hidden erosion on volcanic islands: *Earth and Planetary Science Letters*, v. 262, p. 109–124, doi:10.1016/j.epsl.2007.07.019.
- Reeder, R.J., 1983, Carbonates: mineralogy and chemistry: Washington DC, Mineralogical Society of America, v. 11, doi:10.1515/9781501508134-toc.
- Richter, F.M., Dauphas, N., and Teng, F.-Z., 2009, Non-traditional fractionation of non-traditional isotopes: Evaporation, chemical diffusion and Soret diffusion: *Chemical Geology*, v. 258, p. 92–103, doi:10.1016/j.chemgeo.2008.06.011.
- Ridgwell, A.J., 2003, Carbonate Deposition, Climate Stability, and Neoproterozoic Ice Ages: *Science*, v. 302, p. 859–862, doi:10.1126/science.1088342.
- Rivé, K., Gaillardet, J., Agrinier, P., and Rad, S., 2013, Carbon isotopes in the rivers from the Lesser Antilles: origin of the carbonic acid consumed by weathering reactions in the

- Lesser Antilles: CARBON ISOTOPES IN THE RIVERS FROM THE LESSER ANTILLES: *Earth Surface Processes and Landforms*, v. 38, p. 1020–1035, doi:10.1002/esp.3385.
- Robinson, P.T., Mehegan, J., Gibson, I.L., and Schmincke, H.-U., 1982, Lithology and structure of the volcanic sequence in eastern Iceland: *Journal of Geophysical Research: Solid Earth*, v. 87, p. 6429–6436, doi:10.1029/JB087iB08p06429.
- Rögnvaldsson, Ó., Jónsdóttir, J.F., and Ólafsson, H., 2007, Numerical simulations of precipitation in the complex terrain of Iceland Comparison with glaciological and hydrological data: *Meteorologische Zeitschrift*, v. 16, p. 71–85, doi:10.1127/0941-2948/2007/0174.
- Rustad, J.R., Casey, W.H., Yin, Q.-Z., Bylaska, E.J., Felmy, A.R., Bogatko, S.A., Jackson, V.E., and Dixon, D.A., 2010, Isotopic fractionation of Mg<sup>2+</sup>(aq), Ca<sup>2+</sup>(aq), and Fe<sup>2+</sup>(aq) with carbonate minerals: *Geochimica et Cosmochimica Acta*, v. 74, p. 6301–6323, doi:10.1016/j.gca.2010.08.018.
- Ryu, J.-S., Jacobson, A.D., Holmden, C., Lundstrom, C., and Zhang, Z., 2011, The major ion,  $\delta^{44}/^{40}\text{Ca}$ ,  $\delta^{44}/^{42}\text{Ca}$ , and  $\delta^{26}/^{24}\text{Mg}$  geochemistry of granite weathering at pH=1 and T=25°C: power-law processes and the relative reactivity of minerals: *Geochimica et Cosmochimica Acta*, v. 75, p. 6004–6026, doi:10.1016/j.gca.2011.07.025.
- Saemundsson, K., Kristjansson, L., McDougall, I., and Watkins, N.D., 1980, K-Ar dating, geological and paleomagnetic study of a 5-km lava succession in northern Iceland: *Journal of Geophysical Research: Solid Earth*, v. 85, p. 3628–3646, doi:10.1029/JB085iB07p03628.
- Sarshar, Z., Zahedi-Niaki, M.H., Huang, Q., Eic, M., and Kaliaguine, S., 2009, MTW zeolites for reducing cold-start emissions of automotive exhaust: *Applied Catalysis B: Environmental*, v. 87, p. 37–45, doi:10.1016/j.apcatb.2008.08.025.
- Schauble, E.A., 2004, Applying Stable Isotope Fractionation Theory to New Systems: *Reviews in Mineralogy & Geochemistry*, v. 55, p. 65–111.
- Schiffman, P., Spero, H.J., Southard, R.J., and Swanson, D.A., 2000, Controls on palagonitization versus pedogenic weathering of basaltic tephra: Evidence from the consolidation and geochemistry of the Keanakako'i Ash Member, Kilauea Volcano: *Geochemistry, Geophysics, Geosystems*, v. 1, doi:https://doi.org/10.1029/2000GC000068.
- Schmitt, A.-D., Vigier, N., Lemarchand, D., Millot, R., Stille, P., and Chabaux, F., 2012, Processes controlling the stable isotope compositions of Li, B, Mg and Ca in plants, soils and waters: A review: *Comptes Rendus Geoscience*, v. 344, p. 704–722, doi:10.1016/j.crte.2012.10.002.

- Schopka, H.H., Derry, L.A., and Arcilla, C.A., 2011, Chemical weathering, river geochemistry and atmospheric carbon fluxes from volcanic and ultramafic regions on Luzon Island, the Philippines: *Geochimica et Cosmochimica Acta*, v. 75, p. 978–1002, doi:10.1016/j.gca.2010.11.014.
- Schopka, H.H., Gudmundsson, M.T., and Tuffen, H., 2006, The formation of Helgafell, southwest Iceland, a monogenetic subglacial hyaloclastite ridge: Sedimentology, hydrology and volcano–ice interaction: *Journal of Volcanology and Geothermal Research*, v. 152, p. 359–377, doi:10.1016/j.jvolgeores.2005.11.010.
- Schulte, P. et al., 2011, Applications of stable water and carbon isotopes in watershed research: Weathering, carbon cycling, and water balances: *Earth-Science Reviews*, v. 109, p. 20–31, doi:10.1016/j.earscirev.2011.07.003.
- Sigurdsson, F., 1990, Groundwater from glacial areas in Iceland: *Jokull*, v. 40, p. 119–146.
- Skinner, J., and Jansen, H., 1994, Structure and bonding of calcite: A theoretical study: *American Mineralogist*, v. 79, p. 205–214.
- Smyth, J.R., and Ahrens, T.J., 1997, The crystal structure of calcite III: *Geophysical Research Letters*, v. 24, p. 1595–1598, doi:10.1029/97GL01603.
- Snæbjörnsdóttir, S.Ó., Oelkers, E.H., Mesfin, K., Aradóttir, E.S., Dideriksen, K., Gunnarsson, I., Gunnlaugsson, E., Matter, J.M., Stute, M., and Gíslason, S.R., 2017, The chemistry and saturation states of subsurface fluids during the in situ mineralisation of CO<sub>2</sub> and H<sub>2</sub>S at the CarbFix site in SW-Iceland: *International Journal of Greenhouse Gas Control*, v. 58, p. 87–102, doi:10.1016/j.ijggc.2017.01.007.
- Snæbjörnsdóttir, S.Ó., Sigfússon, B., Marieni, C., Goldberg, D., Gíslason, S.R., and Oelkers, E.H., 2020, Carbon dioxide storage through mineral carbonation: *Nature Reviews Earth & Environment*, doi:10.1038/s43017-019-0011-8.
- Spence, J., and Telmer, K., 2005, The role of sulfur in chemical weathering and atmospheric CO<sub>2</sub> fluxes: Evidence from major ions,  $\delta^{13}\text{CDIC}$ , and  $\delta^{34}\text{SSO}_4$  in rivers of the Canadian Cordillera: *Geochimica et Cosmochimica Acta*, v. 69, p. 5441–5458, doi:10.1016/j.gca.2005.07.011.
- Ståhl, K., and Thomasson, R., 1994, The dehydration and rehydration processes in the natural zeolite mesolite studied by conventional and synchrotron X-ray powder diffraction: *Zeolites*, v. 14, p. 12–17, doi:10.1016/0144-2449(94)90048-5.
- Stefánsdóttir, M.B., and Gíslason, S.R., 2005, The erosion and suspended matter/seawater interaction during and after the 1996 outburst flood from the Vatnajökull Glacier, Iceland: *Earth and Planetary Science Letters*, v. 237, p. 433–452, doi:10.1016/j.epsl.2005.07.002.

- Stefansson, A., 2001, Dissolution of primary minerals of basalt in natural waters I. Calculation of mineral solubilities from 0°C to 350°C: *Chemical Geology*, v. 172, p. 225–250.
- Stefansson, A., and Gislason, S.R., 2001, Chemical weathering of basalts, southwest Iceland: effect of rock crystallinity and secondary minerals on chemical fluxes to the ocean: *American Journal of Science*, v. 301, p. 513–556, doi:10.2475/ajs.301.6.513.
- Stefansson, A., Gislason, S.R., and Arnórsson, S., 2001, Dissolution of primary minerals in natural waters: *Chemical Geology*, v. 172, p. 251–276, doi:10.1016/S0009-2541(00)00262-X.
- Stefansson, A., Hilton, D.R., Sveinbjörnsdóttir, Á.E., Torssander, P., Heinemeier, J., Barnes, J.D., Ono, S., Halldórsson, S.A., Fiebig, J., and Arnórsson, S., 2017, Isotope systematics of Icelandic thermal fluids: *Journal of Volcanology and Geothermal Research*, v. 337, p. 146–164, doi:10.1016/j.jvolgeores.2017.02.006.
- Stefansson, A., Sveinbjörnsdóttir, Á.E., Heinemeier, J., Arnórsson, S., Kjartansdóttir, R., and Kristmannsdóttir, H., 2016, Mantle CO<sub>2</sub> degassing through the Icelandic crust: Evidence from carbon isotopes in groundwater: *Geochimica et Cosmochimica Acta*, v. 191, p. 300–319, doi:10.1016/j.gca.2016.06.038.
- Stroncik, N.A., and Schmincke, H.-U., 2002, Palagonite – a review: *International Journal of Earth Sciences*, v. 91, p. 680–697, doi:10.1007/s00531-001-0238-7.
- Suchet, P.A., Probst, J.-L., and Ludwig, W., 2003, Worldwide distribution of continental rock lithology: Implications for the atmospheric/soil CO<sub>2</sub> uptake by continental weathering and alkalinity river transport to the oceans: *Global Biogeochemical Cycles*, v. 17, doi:10.1029/2002GB001891.
- Sveinbjörnsdóttir, Á.E., Stefansson, A., Heinemeier, J., Arnórsson, S., Eiríksdóttir, E.S., and Ólafsdóttir, R., 2020, Assessing the sources of inorganic carbon in surface-, soil- and non-thermal groundwater in Iceland by  $\delta^{13}\text{C}$  and  $^{14}\text{C}$ : *Geochimica et Cosmochimica Acta*, v. 279, p. 165–188, doi:10.1016/j.gca.2020.03.021.
- Syverson, D.D., Scheuermann, P., Higgins, J.A., Pester, N.J., and Seyfried, W.E., 2018, Experimental partitioning of Ca isotopes and Sr into anhydrite: Consequences for the cycling of Ca and Sr in seafloor mid-ocean ridge hydrothermal systems: *Geochimica et Cosmochimica Acta*, v. 236, p. 160–178, doi:10.1016/j.gca.2018.03.018.
- Tang, J., Dietzel, M., Böhm, F., Köhler, S.J., and Eisenhauer, A., 2008a, Sr<sup>2+</sup>/Ca<sup>2+</sup> and <sup>44</sup>Ca/<sup>40</sup>Ca fractionation during inorganic calcite formation: II. Ca isotopes: *Geochimica et Cosmochimica Acta*, v. 72, p. 3733–3745, doi:10.1016/j.gca.2008.05.033.
- Tang, J., Köhler, S.J., and Dietzel, M., 2008b, Sr<sup>2+</sup>/Ca<sup>2+</sup> and <sup>44</sup>Ca/<sup>40</sup>Ca fractionation during inorganic calcite formation: I. Sr incorporation: *Geochimica et Cosmochimica Acta*, v. 72, p. 3718–3732, doi:10.1016/j.gca.2008.05.031.

- Taylor, T.I., and Urey, H.C., 1938, Fractionation of the Lithium and Potassium Isotopes by Chemical Exchange with Zeolites: *The Journal of Chemical Physics*, v. 6, p. 429–438, doi:10.1063/1.1750288.
- Teichert, B.M.A., Gussone, N., and Torres, M.E., 2009, Controls on calcium isotope fractionation in sedimentary porewaters: *Earth and Planetary Science Letters*, v. 279, p. 373–382, doi:10.1016/j.epsl.2009.01.011.
- Telmer, K., and Veizer, J., 1999, Carbon fluxes, pCO<sub>2</sub> and substrate weathering in a large northern river basin, Canada: carbon isotope perspectives: *Chemical Geology*, v. 159, p. 61–86, doi:10.1016/S0009-2541(99)00034-0.
- Thien, B.M.J., Kosakowski, G., and Kulik, D.A., 2015, Differential alteration of basaltic lava flows and hyaloclastites in Icelandic hydrothermal systems: *Geothermal Energy*, v. 3, p. 11, doi:10.1186/s40517-015-0031-7.
- Thomas, D.L., Bird, D.K., Arnórsson, S., and Maher, K., 2016, Geochemistry of CO<sub>2</sub>-rich waters in Iceland: *Chemical Geology*, v. 444, p. 158–179, doi:10.1016/j.chemgeo.2016.09.002.
- Thorpe, M.T., Hurowitz, J.A., and Dehouck, E., 2019, Sediment geochemistry and mineralogy from a glacial terrain river system in southwest Iceland: *Geochimica et Cosmochimica Acta*, v. 263, p. 140–166, doi:10.1016/j.gca.2019.08.003.
- Thorseth, I.H., Furnes, H., and Tumyr, O., 1991, A textural and chemical study of Icelandic palagonite of varied composition and its bearing on the mechanism of the glass-palagonite transformation: *Geochimica et Cosmochimica Acta*, v. 55, p. 731–749, doi:10.1016/0016-7037(91)90337-5.
- Tipper, E.T. et al., 2021, Global silicate weathering flux overestimated because of sediment–water cation exchange: *Proceedings of the National Academy of Sciences*, v. 118, p. e2016430118, doi:10.1073/pnas.2016430118.
- Tipper, E.T., Bickle, M.J., Galy, A., West, A.J., Pomiès, C., and Chapman, H.J., 2006a, The short term climatic sensitivity of carbonate and silicate weathering fluxes: Insight from seasonal variations in river chemistry: *Geochimica et Cosmochimica Acta*, v. 70, p. 2737–2754, doi:10.1016/j.gca.2006.03.005.
- Tipper, E.T., Gaillardet, J., Galy, A., Louvat, P., Bickle, M.J., and Capmas, F., 2010, Calcium isotope ratios in the world’s largest rivers: A constraint on the maximum imbalance of oceanic calcium fluxes: *RIVERINE Ca ISOTOPES: Global Biogeochemical Cycles*, v. 24, p. n/a-n/a, doi:10.1029/2009GB003574.
- Tipper, E.T., Galy, A., and Bickle, M.J., 2008, Calcium and magnesium isotope systematics in rivers draining the Himalaya-Tibetan-Plateau region: Lithological or fractionation

- control? *Geochimica et Cosmochimica Acta*, v. 72, p. 1057–1075, doi:10.1016/j.gca.2007.11.029.
- Tipper, E., Galy, A., and Bickle, M., 2006b, Riverine evidence for a fractionated reservoir of Ca and Mg on the continents: Implications for the oceanic Ca cycle: *Earth and Planetary Science Letters*, v. 247, p. 267–279, doi:10.1016/j.epsl.2006.04.033.
- Todorova, T., Hünenberger, P.H., and Hutter, J., 2008, Car–Parrinello Molecular Dynamics Simulations of CaCl<sub>2</sub> Aqueous Solutions: *Journal of Chemical Theory and Computation*, v. 4, p. 779–789, doi:10.1021/ct700302m.
- Torres, M.A., Moosdorf, N., Hartmann, J., Adkins, J.F., and West, A.J., 2017, Glacial weathering, sulfide oxidation, and global carbon cycle feedbacks: *Proceedings of the National Academy of Sciences*, v. 114, p. 8716–8721, doi:10.1073/pnas.1702953114.
- Urey, H.C., 1952, On the Early Chemical History of the Earth and the Origin of Life: *Proceedings of the National Academy of Sciences of the United States of America*, v. 38, p. 351–363.
- Urey, H.C., 1947, The Thermodynamic properties of isotopic substances: *Journal of the Chemical Society*, v. 4, p. 562–581.
- Utada, M., 2001, Zeolites in Burial Diagenesis and Low-grade Metamorphic rocks: *Reviews in Mineralogy and Geochemistry*, v. 45, p. 277–304, doi:10.2138/rmg.2001.45.9.
- Vigier, N., Gislason, S.R., Burton, K.W., Millot, R., and Mokadem, F., 2009, The relationship between riverine lithium isotope composition and silicate weathering rates in Iceland: *Earth and Planetary Science Letters*, v. 287, p. 434–441, doi:10.1016/j.epsl.2009.08.026.
- Wada, K., Arnalds, O., Kakuto, Y., Wilding, L.P., and Hallmark, C.T., 1992, Clay minerals of four soils formed in eolian and tephra materials in Iceland: *Geoderma*, v. 52, p. 351–365, doi:10.1016/0016-7061(92)90046-A.
- Walker, G.P.L., 1964, Geological investigations in eastern Iceland: *Bulletin Volcanologique*, v. 27, p. 351–363, doi:10.1007/BF02597532.
- Walker, G.P.L., 1960, Zeolite Zones and Dike Distribution in Relation to the Structure of the Basalts of Eastern Iceland: *The Journal of Geology*, v. 68, p. 515–528.
- Walker, J., Hays, P.B., and Kasting, J.F., 1981, A negative feedback mechanism for the long-term stabilization of Earth's surface temperature: *Journal of Geophysical Research: Oceans*, v. 86, p. 9776–9782, doi:10.1029/JC086iC10p09776.
- Wang, J., Jacobson, A.D., Sageman, B.B., and Hurtgen, M.T., 2021, Stable Ca and Sr isotopes support volcanically triggered biocalcification crisis during Oceanic Anoxic Event 1a: *Geology*, v. 49, doi:10.1130/G47945.1.

- Warner, N.H., and Farmer, J.D., 2010, Subglacial Hydrothermal Alteration Minerals in Jökulhlaup Deposits of Southern Iceland, with Implications for Detecting Past or Present Habitable Environments on Mars: *Astrobiology*, v. 10, p. 523–547, doi:10.1089/ast.2009.0425.
- Watton, T.J., Jerram, D.A., Thordarson, T., and Davies, R.J., 2013, Three-dimensional lithofacies variations in hyaloclastite deposits: *Journal of Volcanology and Geothermal Research*, v. 250, p. 19–33, doi:10.1016/j.jvolgeores.2012.10.011.
- Weisenberger, T., and Bucher, K., 2011, Mass transfer and porosity evolution during low temperature water–rock interaction in gneisses of the simano nappe: Arvigo, Val Calanca, Swiss Alps: *Contributions to Mineralogy and Petrology*, v. 162, p. 61–81, doi:10.1007/s00410-010-0583-2.
- Weisenberger, T.B., Ingimarsson, H., Hersir, G.P., and Flóvenz, Ó.G., 2020, Cation-Exchange Capacity Distribution within Hydrothermal Systems and Its Relation to the Alteration Mineralogy and Electrical Resistivity: *Energies*, v. 13, p. 5730, doi:10.3390/en13215730.
- Weisenberger, T., and Selbekk, R.S., 2009, Multi-stage zeolite facies mineralization in the Hvalfjörður area, Iceland: *International Journal of Earth Sciences*, v. 98, p. 985–999, doi:10.1007/s00531-007-0296-6.
- Weisenberger, T.B., Spürgin, S., and Lahaye, Y., 2014, Hydrothermal alteration and zeolitization of the Fohberg phonolite, Kaiserstuhl Volcanic Complex, Germany: *International Journal of Earth Sciences*, v. 103, p. 2273–2300, doi:10.1007/s00531-014-1046-1.
- Wenzhong, W., Qin, T., Zhou, C., Huang, S., Wu, Z., and Huang, F., 2017, Concentration effect on equilibrium fractionation of Mg-Ca isotopes in carbonate minerals: Insights from first-principles calculations: *Geochimica et Cosmochimica Acta*, v. 208, p. 185–197, doi:10.1016/j.gca.2017.03.023.
- West, A., Galy, A., and Bickle, M., 2005, Tectonic and climatic controls on silicate weathering: *Earth and Planetary Science Letters*, v. 235, p. 211–228, doi:10.1016/j.epsl.2005.03.020.
- White, R., and McKenzie, D., 1989, Magmatism at rift zones: The generation of volcanic continental margins and flood basalts: *Journal of Geophysical Research*, v. 94, p. 7685, doi:10.1029/JB094iB06p07685.
- Wood, D.A., Gibson, I.L., and Thompson, R.N., 1976, Elemental mobility during zeolite facies metamorphism of the Tertiary basalts of eastern Iceland: *Contributions to Mineralogy and Petrology*, v. 55, p. 241–254, doi:10.1007/BF00371335.
- Yan, H., Schmitt, A.-D., Liu, Z., Gangloff, S., Sun, H., Chen, J., and Chabaux, F., 2016, Calcium isotopic fractionation during travertine deposition under different hydrodynamic conditions: Examples from Baishuitai (Yunnan, SW China): *Chemical Geology*, v. 426, p. 60–70, doi:10.1016/j.chemgeo.2016.02.002.

- Zeebe, R.E., and Caldeira, K., 2008, Close mass balance of long-term carbon fluxes from ice-core CO<sub>2</sub> and ocean chemistry records: *Nature Geoscience*, v. 1, p. 312–315, doi:10.1038/ngeo185.
- Zhang, R., Nash, C.P., and Rock, P.A., 1988, Thermodynamics of calcium-isotope-exchange reactions. I. Exchange between isotopic calcium carbonates and aqueous calcium ions: *The Journal of Physical Chemistry*, v. 92, p. 3989–3993, doi:10.1021/j100324a060.
- Zhao, X., Zhang, Z., Huang, S., Liu, Y., Li, X., and Zhang, H., 2017, Coupled extremely light Ca and Fe isotopes in peridotites: *Geochimica et Cosmochimica Acta*, v. 208, p. 368–380, doi:10.1016/j.gca.2017.03.024.

## Appendix A

### A.1 Zeolite statistical analyses

Bond length data were compiled from structure refinement studies using single-crystal X-ray diffraction methods. To the best of my ability, I selected studies of natural zeolites that formed at relatively low temperatures and pressures consistent with those of the hydrothermal system examined here. As bond length data are estimates only, uncertainties were omitted from Figure 4 in the main text. Details of the compiled bond length data used in the statistical regression are presented in Table A1.

Regression analysis was utilized to examine covariance between the variables of Ca-O bond length and zeolite  $\delta^{44/40}\text{Ca}$  values (Figure 2.4), as well as Si/Al ratios and  $\delta^{44/40}\text{Ca}$  values (Figure A1). Perhaps due to the small sample size, the Cook's distance plot for evaluating the regression between bulk zeolite  $\delta^{44/40}\text{Ca}$  values and average bond length indicates that several points have high influence. Thus, five alternate linear models were constructed in which each high influence point was sequentially removed from the model according to its leverage. The results for each alternative model suggest that points with high leverage do not influence the  $R^2$  value nor the significance of the correlation produced by the original model, which excludes the values for mesolite (Table A2). The bulk zeolite  $\delta^{44/40}\text{Ca}$  values exhibit heteroscedasticity when regressed against Si/Al ratios (Figure A1).

**Table A1**  
Ca-O bond length data and sources.

Mineral Type	Site	Average Ca-O <sub>w</sub> bond length (Å)	Standard Deviation Ca-O <sub>w</sub> (2σ <sub>SD</sub> )	Average Ca-O <sub>fmwk</sub> bond length (Å)	Standard Deviation Ca-O <sub>fmwk</sub> (2σ <sub>SD</sub> )	Number of zeolite samples (n)
<i>Stilbite</i> <sup>1,2,3,4</sup>	Ca-only	2.45	0.08	-	-	8
<i>Mesolite</i> <sup>5,6</sup>	Ca-only channel	2.34	0.00	2.51	0.00	2
	Na-only channel	-	-	-	-	
<i>Scolecite</i> <sup>6,7,8</sup>	Ca-only channel	2.34	0.00	2.53	0.02	3
<i>Thomsonite</i> <sup>9,10,11</sup>	Ca-only	2.39	0.16	2.52	0.02	3
	Ca or Na	2.56	0.10	2.57	0.02	
<i>Chabazite</i> <sup>12</sup>	C1- Ca-only			3.05		1
	C2			2.80		
	C3	2.362		2.82		
	C4- Ca-only			2.67		
<i>Heulandite</i> <sup>13,14,15,16</sup>	Ca2	2.63	0.10	2.85	0.22	4

<sup>1</sup> Alberti, A. et al. (1999). *Proc. 12th Int. Zeolite Conference* (Vol. 2345, p. 2354)

<sup>2</sup> Gómez-Hortigüela, L., et al. (2014). *Micropor. and Mesopor. Materials*, 193, 93-102.

<sup>3</sup> Slaughter, M. (1970). *Am. Mineralogist: Journ. of Earth and Plan. Materials*, 55, 387-397.

<sup>4</sup> Quartieri, S., & Vezzalini, G. (1987). *Zeolites*, 7(2), 163-170.

<sup>5</sup> Kirfel, A., & Gibbs, G. V. (2000). *Physics and Chemistry of Minerals*, 27(4), 270-284.

<sup>6</sup> Artioli, G. et al. (1986). *Acta Crystallographica: Crystal Structure Comm.*, 42(8), 937-942.

<sup>7</sup> Kvik, Å., et al. (1985). *Crystalline Materials*, 171(1-2), 141-154.

<sup>8</sup> Cametti, G., et al. (2015). *Micropor. and mesopor. materials*, 208, 171-180.

<sup>9</sup> Gatta, G. D., et al. (2010). *Am. Mineralogist*, 95(4), 495-502.

<sup>10</sup> Likhacheva, A. Y., et al. (2007). *Am. Mineralogist*, 92(10), 1610-1615.

<sup>11</sup> Ståhl, K., et al. (1990). *Acta Crystallographica: Crystal Structure Comm.*, 46(8), 1370-1373.

<sup>12</sup> Alberti, A., et al. (1982). *Zeolites*, 2(4), 303-309.

<sup>13</sup> Armbruster, T. (1993). *Am. Mineralogist*, 78(3-4), 260-264.

<sup>14</sup> Merkle, A. & Slaughter, M. (1968). *Am. Mineralogist: Journ. of Earth and Plan. Materials*, 53(7-8), 1120-1138.

<sup>15</sup> Seryotkin, Y. V. (2015). *Micropor. and Mesopor. Materials*, 214, 127-135.

<sup>16</sup> Sacerdoti, M., & Lucchetti, G. (2010). *Micropor. and Mesopor. Materials*, 131(1-3), 310-313.

**Table A2**

Results of alternate linear regression models used to assess the relationship between zeolite  $\delta^{44/40}\text{Ca}$  values and average bond length.

Model	Excluded data (x,y; mineral)	R <sup>2</sup>	p-value
Original	(2.44, -1.78); Mesolite	0.93	<0.001
Alternate 1	(2.78, -1.41); Chabazite	0.94	<0.001
Alternate 2	(2.79, -2.00); Heulandite	0.96	<0.001
Alternate 3	(2.45, -0.62); Stilbite	0.96	<0.001
Alternate 4	(2.45, -0.85); Stilbite	0.96	<0.001
Alternate 5	(2.45, -0.84); Scolecite	0.96	<0.001

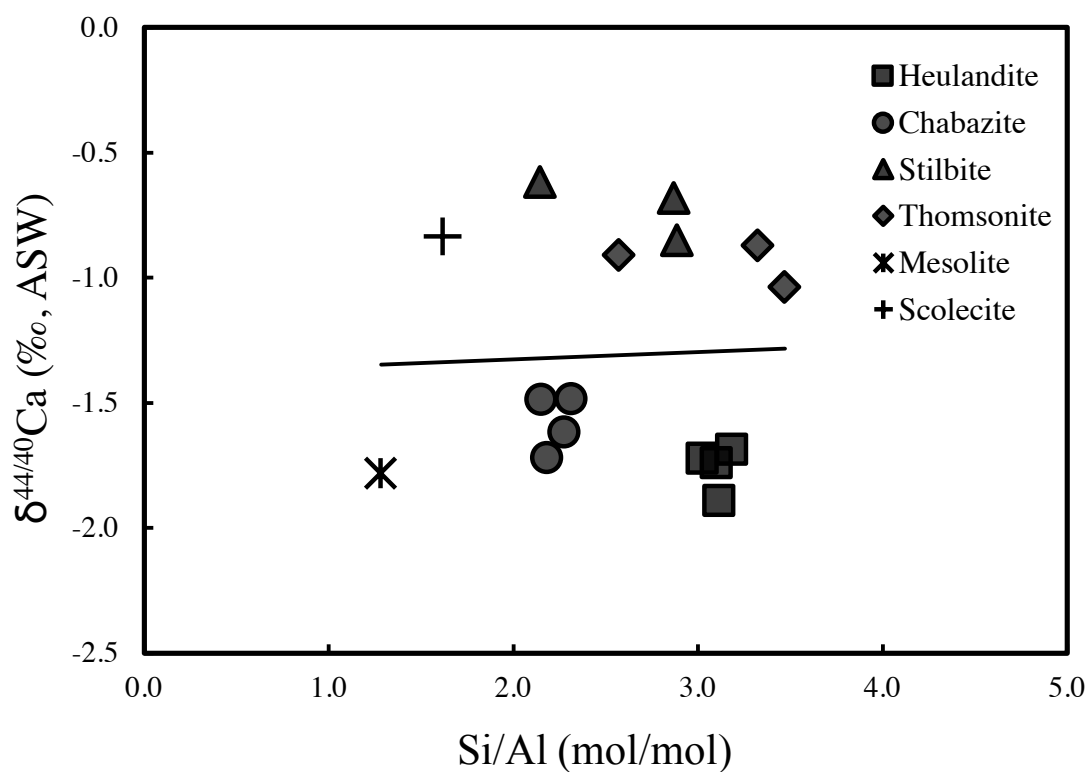


**Figure A1:**  $\delta^{44/40}\text{Ca}$  versus Si/Al molar ratio for bulk zeolites ( $R^2 = 0.08$ ,  $p = 0.30$ ,  $n = 16$ ).

## A.2 Zeolite sequential leaching and digestion experiment

### *Methods*

An attempt was made to examine operationally defined “exchangeable” and “silicate” fractions of the zeolites using a sequential leaching and digestion procedure. It is important to note that all Ca in zeolites is exchangeable because their frameworks only comprise Al, Si, and O. Therefore, the “silicate” fractions analyzed here are more appropriately categorized as “exchangeable” fraction residues. Powdered samples weighing ~1 g were transferred into LDPE centrifuge tubes and reacted with 10 mL of 1M NH<sub>4</sub>Cl (adjusted to pH 8) on a rocker table for 6-8 hours. The mixtures were centrifuged and filtered through 0.45 μm syringe filters into Teflon vials. The supernatants were dried on a hot plate and re-dissolved in 5% HNO<sub>3</sub>. The remaining residues were dried, and ~0.08 g subsamples were completely digested using HF and HNO<sub>3</sub> acids. Elemental and isotopic analyses followed the methods outlined in the main text.

### *Results*

Table A3 reports elemental and Ca isotope data for the experiments. Exchangeable  $\delta^{44/40}\text{Ca}$  range from -1.55‰ to -2.68‰. Scolecite has the highest exchangeable  $\delta^{44/40}\text{Ca}$  (-1.55‰, n = 1), followed by stilbite ( $-1.73 \pm 0.16\%$ ,  $2\sigma_{\text{SD}}$ , n = 3), thomsonite ( $-1.93 \pm 0.20\%$ ,  $2\sigma_{\text{SD}}$ , n = 3), chabazite ( $-2.41 \pm 0.06\%$ ,  $2\sigma_{\text{SD}}$ , n = 4), then heulandite ( $-2.44 \pm 0.34\%$ ,  $2\sigma_{\text{SD}}$ , n = 5). Residue  $\delta^{44/40}\text{Ca}$  range from -0.48‰ to -2.00‰. Stilbite has the highest average residue  $\delta^{44/40}\text{Ca}$  ( $-0.55 \pm 0.14\%$ ,  $2\sigma_{\text{SD}}$ , n=4), followed by thomsonite ( $-0.69 \pm 0.20\%$ ,  $2\sigma_{\text{SD}}$ , n=3), scolecite (-0.79‰, n=1), chabazite ( $-1.25 \pm 0.42\%$ ,  $2\sigma_{\text{SD}}$ , n=4), heulandite ( $-1.76 \pm 0.34\%$ ,  $2\sigma_{\text{SD}}$ , n=5), then mesolite (-1.72‰, n=1). For all zeolites, the exchangeable leachates produced lower

$\delta^{44/40}\text{Ca}$  values than the corresponding residues. The  $\text{NH}_4\text{Cl}$  solution leached between  $\sim 1\%$  and  $20\%$  of bulk zeolite Ca.

As shown in Figure A2, all leachate and residue  $\delta^{44/40}\text{Ca}$  values are lower and higher, respectively, than the corresponding bulk values. These results provide good evidence that the  $\text{NH}_4\text{Cl}$  exchange solution selectively leached  $^{40}\text{Ca}$ . Other studies have reported very similar findings (Teichert et al., 2009). Additionally, most leachate  $\delta^{44/40}\text{Ca}$  values correlate with Na/Ca ratios, which further indicates that the  $\text{NH}_4\text{Cl}$  solution produced artifacts not representative of bulk zeolite geochemistry (Figure A3). No correlation exists between leachate  $\delta^{44/40}\text{Ca}$  values and mole fraction of Ca leached; however, a weak correlation exists between residue  $\delta^{44/40}\text{Ca}$  and mole fraction of Ca leached, which is also consistent with fractionation during leaching (Figure A4). While the results offer limited environmental meaning, evidence for fractionation during ion-exchange broadly supports the main conclusions of the study.

**Table A3**

Elemental and Ca isotope data for zeolite leachate and residual digests. Duplicate analyses are shown in “()”. Analyses not made due to limited sample sizes are marked with “-”.

Sample ID	$\text{NH}_4\text{Cl}$ leachate				Residual Digest			
	Ca	Na	Sr	$\delta^{44/40}\text{Ca}$	Ca	Na	Sr	$\delta^{44/40}\text{Ca}$
	( $\mu\text{mol/g}$ )	( $\mu\text{mol/g}$ )	( $\text{nmol/g}$ )	( $\text{‰}$ )	( $\mu\text{mol/g}$ )	( $\mu\text{mol/g}$ )	( $\text{nmol/g}$ )	( $\text{‰}$ )
<i>Heulandite</i>								
HD_1	63.2	70.1	751	-2.21	1197	364	23253	-1.67 (-1.67)
HD_11	44.7	64.2	482	-2.42	1248	667	21663	-1.61
HD_18	46.4	74.3	562	-2.42	1201	788	25165	-1.63

HD_23	62.1	71.0	848	-2.46	1224	351	25534	-1.88
HD_28	64.4	124	862	-2.68	1221	242	20164	-2.00
<i>Chabazite</i>								
CZ_54	359	65.1	1416	-2.43 (-2.43)	1435	80.5	17678	-1.44
CZ_56b	355	106	1250	-2.41	1194	201	9915	-1.09
CZ_61	353	110	894	-2.38	1191	539	9829	-1.04 (-1.08)
CZ_62	367	74.6	1318	-2.43	1335	102	16465	-1.43
<i>Thomsonite</i>								
TM_57	285	166	17.7	-1.96	1065	555	48.7	-0.60
TM_58	270	150	7.97	-1.82	1141	298	26.7	-0.68
TM_63	263	181	26.1	-2.01	1092	1010	94.6	-0.79
<i>Stilbite</i>								
SB_17	188	55.8	7.13	-1.70	1252	266	34.7	-0.48
SB_69	181	51.0	17.4	-1.66	1216	100	68.3	-0.57
SB_73	269	103	28.3	-1.82	1252	317	242	-0.61
<i>Mesolite</i>								
MS_50	-	-	-	-	1702	3472	3646	-1.72
<i>Scolecite</i>								
SC_3	26.0	11.7	2.51	-1.55 (-1.53)	2292	105	45.7	-0.80

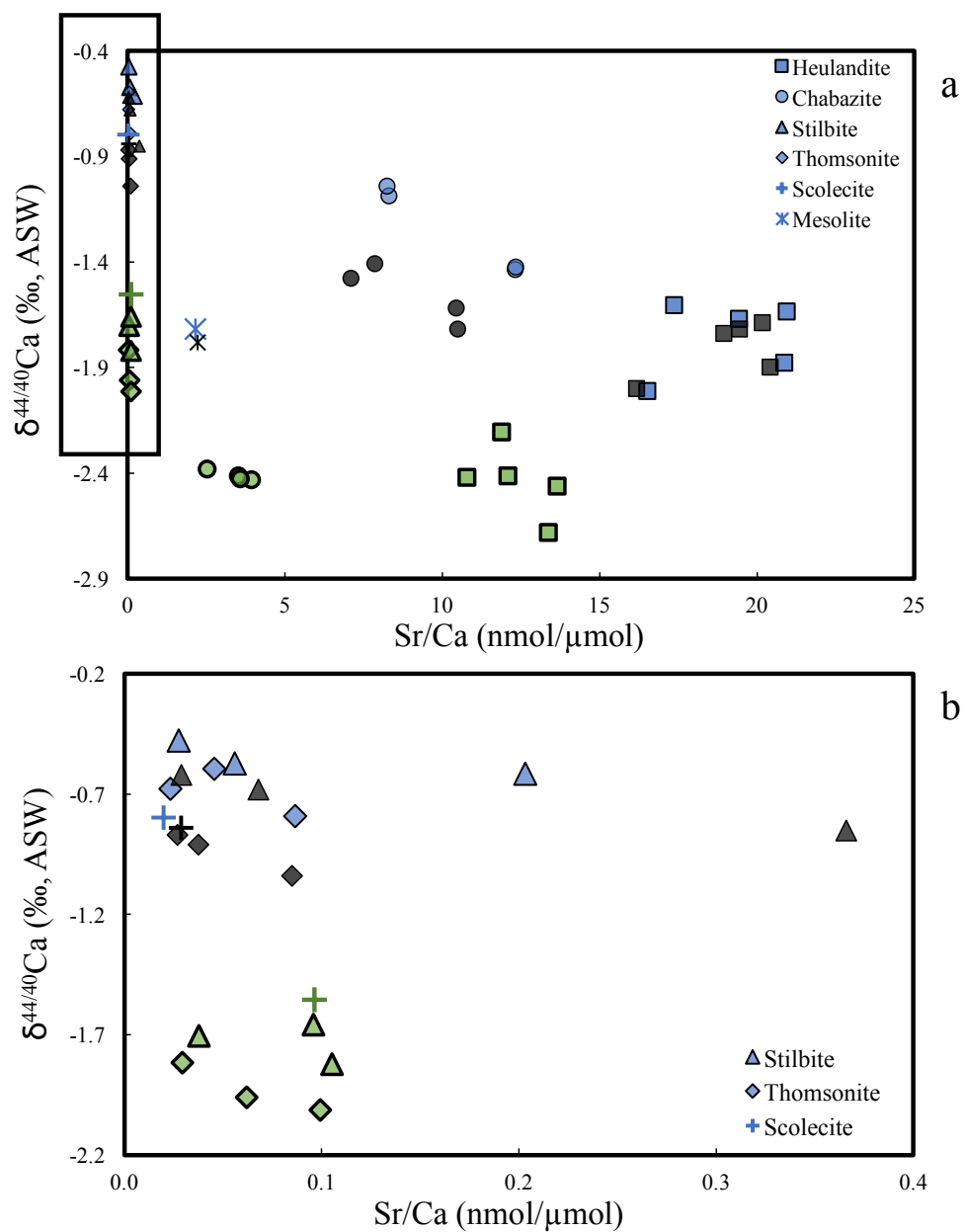


**Figure A2:**  $\delta^{44/40}\text{Ca}$  versus Sr/Ca for zeolite leachate (green), residual digest (blue), and bulk (black). Panel (b) shows inset from panel (a).

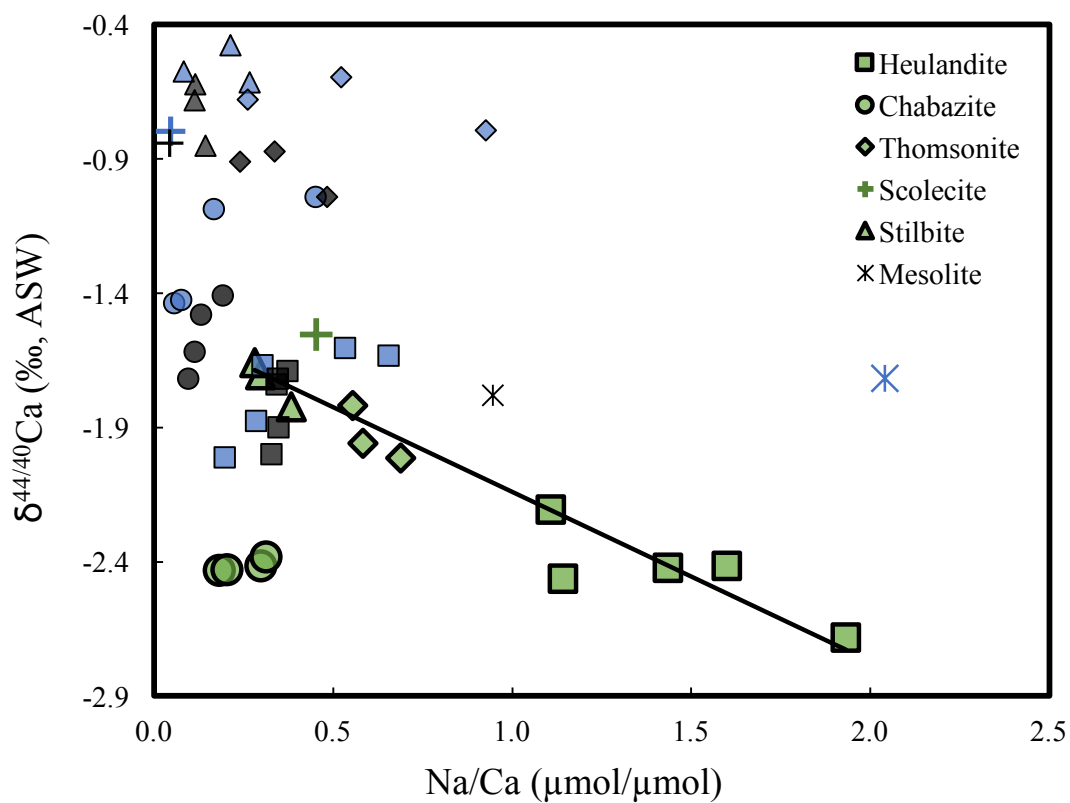


**Figure A3:**  $\delta^{44/40}\text{Ca}$  of leachate (green), residual digest (blue), and bulk mineral (black) versus Na/Ca. With the exception of chabazite, leachate  $\delta^{44/40}\text{Ca}$  and Na/Ca strongly correlate ( $R^2 = 0.90$ ,  $p < 0.0001$ ,  $n = 12$ ). No correlation exists for bulk and residual data.

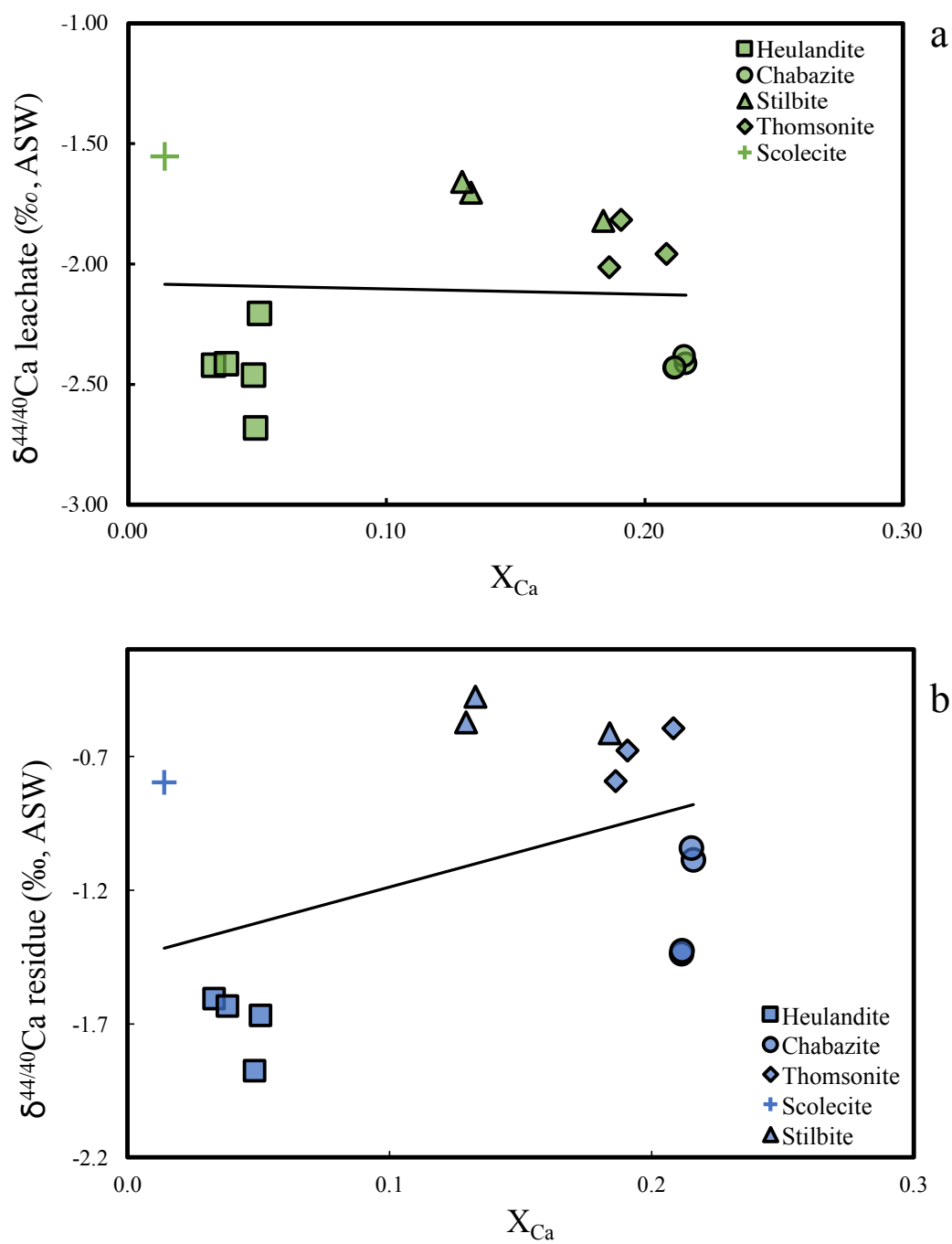


**Figure A4:**  $\delta^{44/40}\text{Ca}$  versus mole fraction of Ca leached ( $X_{\text{Ca}}$ ) for (a) leachates ( $R^2 = 0.09$ ,  $p = 0.37$ ,  $n = 16$ ) and (b) residues ( $R^2 = 0.20$ ,  $p = 0.05$ ,  $n = 15$ ).

## Appendix B

## Sample location and field data

Table B1. Locations and dates collected of samples included in Chapter 3.

Sample ID	Sample Location	Latitude (°)	Longitude (°)	Date collected (m/d/yr)
<i>Tributaries</i>				
ILW_BNG_1	Hrolleifsdalsá	65.97290	-19.25868	7/3/2017
ILW_BNG_2	Hrolleifsdalsá	65.98199	-19.28006	7/3/2017
ILW_BNG_3	Hrolleifsdalsá	65.98670	-19.29087	7/3/2017
ILW_BNG_5	Hrolleifsdalsá	65.99655	-19.32623	7/3/2017
ILW_Y_1	Hrútagil	65.27231	-18.98411	7/11/2017
ILW_MF_1	Mælifellsá	65.42474	-19.39739	7/14/2017
ILW_MF_2	Mælifellsá	65.44915	-19.38364	7/11/2017
ILW_VT_1	Vatnsskarðsá	65.51447	-19.59153	7/11/2017
ILW_VT_2	Vatnsskarðsá	65.52505	-19.54796	7/14/2017
ILW_ND_1	Norðurá	65.45149	-18.98120	7/13/2017
ILW_ND_2	Norðurá	65.44164	-19.01973	7/13/2017
ILW_ND_3	Norðurá	65.43034	-19.13264	7/13/2017
ILW_BT_1	Djúpadalsá	65.55404	-19.28560	7/14/2017
ILW_BG_1	Viðinesá	65.72371	-18.95690	6/28/2017
ILW_BG_2	Viðinesá	65.73189	-18.96240	6/28/2017
ILW_BG_3	Viðinesá	65.73866	-18.96720	6/28/2017
ILW_BG_4	Viðinesá	65.75023	-19.00085	7/1/2017
ILW_BG_5	Viðinesá	65.75150	-19.03141	7/1/2017
ILW_BG_6	Viðinesá	65.75093	-19.06230	7/1/2017
ILW_BG_7	Viðinesá	65.74388	-19.11106	7/1/2017
ILW_BG_8	Hólar	65.67677	-19.09309	7/6/2019
ILW_WT_1	Gönguskarðsá	65.73684	-19.73700	7/16/2019
ILW_MF_3	Mælifellsá	65.33935	-19.41051	7/12/2019
ILW_HG_1		65.68962	-18.41334	7/2/2019
<i>Main Stem</i>				
<i>Rivers</i>				
ILW_HF_a	Hofsá	65.18946	-18.87657	7/11/2017
ILW_HF_b	Hofsá	65.20307	-18.92232	7/11/2017
ILW_HF_d	Hofsá	65.21328	-18.94592	7/11/2017
ILW_HF_e	Hofsá	65.23361	-18.96394	7/11/2017
ILW_HF_g	Hofsá	65.28399	-19.02832	7/11/2017
ILW_SV_1	Svartá	65.26392	-19.16393	7/5/2017
ILW_SV_2	Svartá	65.27135	-19.17251	7/5/2017
ILW_SV_3	Svartá	65.27796	-19.17315	7/5/2017
ILW_SV_4	Svartá	65.38722	-19.24450	7/14/2017
ILW_SV_5	Svartá	65.44078	-19.32460	7/11/2017
ILW_SV_6	Svartá	65.46881	-19.35898	7/14/2017
ILW_SV_7	Svartá	65.25092	-19.15211	7/8/2019
ILW_SV_8	Svartá	65.26040	-19.15978	7/8/2019

ILW_SV_9	Svartá	65.50899	-19.38926	7/12/2019
ILW_SV_10	Svartá	65.49328	-19.38310	7/14/2019
ILW_AJ_a	Austari-Jökulsá	65.26690	-18.76808	7/7/2017
ILW_AJ_b	Austari-Jökulsá	65.28241	-18.80928	7/7/2017
ILW_AJ_c	Austari-Jökulsá	65.30365	-18.86833	7/7/2017
ILW_AJ_d	Austari-Jökulsá	65.31329	-18.90686	7/7/2017
ILW_AJ_j	Austari-Jökulsá	65.27530	-18.79049	7/14/2019
ILW_VJ_a	Vestari-Jökulsá	65.29762	-19.07020	7/9/2017
ILW_VJ_b	Vestari-Jökulsá	65.30544	-19.07278	7/9/2017
ILW_VJ_c	Vestari-Jökulsá	65.31885	-19.08737	7/9/2017
ILW_VJ_d	Vestari-Jökulsá	65.32845	-19.08574	7/9/2017
ILW_VJ_e	Vestari-Jökulsá	65.34503	-19.10275	7/9/2017
ILW_VJ_m	Vestari-Jökulsá	65.32880	-19.08502	7/14/2019
ILW_HR_1	Héraðsvötn	65.38294	-19.12524	7/13/2017
ILW_HR_2	Héraðsvötn	65.38732	-19.13140	7/13/2017
ILW_HR_3	Héraðsvötn	65.41750	-19.18744	7/13/2017
ILW_HR_4	Héraðsvötn	65.43837	-19.22144	7/13/2017
ILW_HR_5	Héraðsvötn	65.47096	-19.26849	7/13/2017
ILW_HR_6	Héraðsvötn	65.52480	-19.31748	7/13/2017
ILW_HR_7	Héraðsvötn	65.56392	-19.36323	7/13/2017
ILW_HR_8	Héraðsvötn	65.61752	-19.44914	7/13/2017
ILW_HR_9	Héraðsvötn	65.66195	-19.49480	7/13/2017
ILW_HR_10	Héraðsvötn	65.71442	-19.40640	7/14/2017
ILW_HR_11	Héraðsvötn	65.45564	-19.23728	6/29/2019
ILW_HR_12	Héraðsvötn	65.38051	-19.12418	7/14/2019
ILW_HT_2	Hvítá	64.44610	-19.95807	7/21/2019
ILW_HT_3	Hvítá	64.26920	-20.20648	7/21/2019
ILW_TH_1	Þjórsá	63.91770	-20.68072	7/22/2019
ILW_HF_i	Hofsá	65.19507	-18.90523	7/1/2019
ILW_SK_3	Skjálfandafljót	65.50760	-17.45637	7/10/2019
ILW_EY_1	Eyjafljót	65.27091	-18.23957	7/9/2019
<i>Groundwater</i>				
ILW_HS_1	Hofsvellir	65.28539	-19.04025	7/9/2017
ILW_HS_2	Hverhólar	65.34724	-19.10260	7/10/2017
ILW_HS_3	Réttarholt	65.57787	-19.35550	7/14/2017
ILW_HS_4	Vindheimar	65.50097	-19.34664	7/14/2017
ILW_HS_5	Reykir	65.47144	-19.35653	7/14/2017
ILW_HS_6	Starrastaðir	65.43200	-19.32143	7/14/2017
ILW_HS_7	Þormóðsholt	65.52718	-19.31469	7/14/2017
ILW_HS_8	Hofsvellir	65.28539	-19.04025	7/9/2017
ILW_GW_1	Hrolleifsdalsá	65.98883	-19.30031	7/3/2017
ILW_GW_2	Hofsá	65.20104	-18.91498	7/11/2017
ILW_GW_3	Djúpadalsá	65.55421	-19.28255	7/14/2017
<i>Þórsmörk, Southern Iceland</i>				
ILW_HV_1	Hvanná	63.65157	-19.44823	7/20/2017
ILW_HV_2	Hvanná	63.65224	-19.45248	7/20/2017
ILW_HV_3	Hvanná	63.65468	-19.45161	7/20/2017
ILW_HV_4	Hvanná	63.65598	-19.45289	7/20/2017

ILW_HV_5	Hvanná	63.65688	-19.45767	7/20/2017
ILW_KR_1	Krossá	63.67799	-19.41857	7/23/2019
ILW_KR_2	Krossá	63.67964	-19.47971	7/23/2019
<i>Basalt</i>				
ILR_BG_1	Hólar	65.72371	-18.95690	7/1/2017
ILR_SV_2	Svartá	65.29633	-19.16702	7/5/2017
ILR_AJ_3a	Austari-Jökulsá	65.28054	-18.80481	7/7/2017
ILR_SV_16a	Svartá	65.28972	-19.20861	7/8/2019
ILR_x_19	Hofsá	65.23701	-18.95920	7/16/2017
<i>Calcite</i>				
WT	Gönguskarðsá	65.73684	-19.73700	7/16/2019
AK	Vaðlaheiði	65.68885	-18.05198	7/10/2019
<i>Stream Sediment</i>				
ILS_BG_1	Hólar	65.73147	-18.96789	7/1/2017
ILS_BG_2	Hólar	65.75122	-19.02488	7/1/2017
ILS_BNG_3	Hrolleifsdalsá	65.99065	-19.29508	7/3/2017
ILS_SV_4	Svartá	65.27078	-19.16839	7/5/2017
ILS_AJ_5	Austari-Jökulsá	65.30580	-18.87382	7/7/2017
ILS_HR_6	Héraðsvötn	65.38294	-19.12524	7/13/2017
ILS_HR_7	Héraðsvötn	65.67581	-19.51034	7/13/2017
ILS_FS_8	Fossá	65.01973	-18.84026	7/16/2017
<i>Soil</i>				
ILO_BG_1		65.74755	-19.10179	7/1/2017
ILO_AJ_3	Austari-Jökulsá	65.26748	-18.77220	7/7/2017
ILO_ND_4	Norðurá	65.45312	-18.97132	7/13/2017
ILO_HR_5	Héraðsvötn	65.41773	-19.18212	7/13/2017
ILO_SV_6	Svartá	65.31270	-19.16104	7/18/2017
<i>Vegetation/other</i>				
	<i>Sample Type</i>			
ILV_1	<i>Vaccinium uliginosum</i>	65.75249	-19.03793	7/1/2017
ILV_2	<i>Alchemilla alpina</i>	65.74487	-19.11552	7/1/2017
ILV_3	<i>Deschampsia alpina</i>	65.99707	-19.31945	7/3/2017
ILV_4	horse manure	65.99903	-19.33113	7/3/2017
ILV_5	unidentified grass	65.44114	-19.32083	7/11/2017
ILV_7	<i>Thymus praecox arcticus</i>	65.43914	-19.21371	7/13/2017
ILV_9	<i>Carex lyngbyei</i>	65.56392	-19.36323	7/13/2017
ILV_10	sheep manure	65.28869	-19.16589	7/18/2017

**Table B2.** Locations and dates collected of samples included in Chapter 4. “\*” denotes river sample where suspended sediment was collected.

Sample ID	Sample Type	Sample location	Latitude (°)	Longitude (°)	Date collected (m/d/yr)
AJ_e	River water	Austari-Jökulsá	65.06102	-18.48402	7/16/2017
AJ_i	River water	Austari-Jökulsá	65.05189	-18.42455	7/4/2019
AJt_f	River water	Strangilækur	65.05038	-18.46985	7/16/2017
VJ_g	River water	Vestari-Jökulsá	64.97724	-18.86591	7/16/2017
VJ_h	River water	Vestari-Jökulsá	64.98987	-18.87896	7/16/2017
VJ_i	River water	Vestari-Jökulsá	64.99908	-18.88894	7/16/2017
VJ_j	River water	Vestari-Jökulsá	65.00710	-18.8987	7/16/2017
VJ_k*	River water	Vestari-Jökulsá	65.00097	-18.89305	7/4/2019
VJ_l*	River water	Vestari-Jökulsá	65.16972	-18.97472	7/4/2019
FS_1	River water	Fossá	65.02060	-18.8408	7/16/2017
FS_2	River water	Fossá	65.02773	-18.84353	7/16/2017
BL_1*	River water	Blönduós	64.85211	-19.36723	6/30/2019
BL_2	River water	Blönduós	64.94123	-19.51244	6/30/2019
BL_3*	River water	Blönduós	65.10181	-19.52441	6/30/2019
JF_1*	River water	Jökulsá á Fjöllum	65.01437	-16.2594	7/3/2019
JF_2	River water	Jökulsá á Fjöllum	65.20301	-16.19370	7/3/2019
JF_3*	River water	Jökulsá á Fjöllum	65.39749	-16.13038	7/3/2019
JF_4	River water	Jökulsá á Fjöllum	65.61242	-16.19113	7/3/2019
SK_1	River water	Skjálfandafljót	65.11092	-17.51203	7/10/2019
SK_2	River water	Skjálfandafljót	65.31598	-17.33619	7/10/2019
HT_1	River water	Hvítá	64.68834	-19.49705	7/21/2019
HF_h	River water	Hofsá	65.12160	-18.58986	7/16/2017
HJ_1	River water	Hnjúskvísl	65.04284	-18.39274	7/16/2017
HJ_2	River water	Hnjúskvísl	65.04657	-18.38914	7/4/2019
Ice	Glacial Ice	Hofsjökull	64.97394	-18.86185	7/16/2017

FS_17	hyaloclastite	Hofsafrétt	65.02761	-18.84510	7/16/2017
YG_14	hyaloclastite	Hofsafrétt	65.03596	-18.75738	7/16/2017
HL_16.5	hyaloclastite	Hofsafrétt	64.99781	-18.88780	7/16/2017
JF_8	hyaloclastite	Upptyppingar	65.02053	-16.28091	7/3/2019
VJ_13b	hyaloclastite	Hofsafrétt	65.01095	-18.90661	7/4/2019
MSf_22a	palagonite	Mosfell	64.195278	-21.62388	7/20/2019
MSf_22b	palagonite	Mosfell	64.193210	-21.62168	7/20/2019
MSf_22c	palagonite	Mosfell	64.187778	-21.62055	7/20/2019
HGf_21a	palagonite	Helgafell	64.01312	-21.84367	7/19/2019
HGf_21b	palagonite	Helgafell	64.01510	-21.84658	7/19/2019
HGf_21c	palagonite	Helgafell	64.01361	-21.84666	7/19/2019
HF_2a	palagonite				
HF_2b	palagonite				
HF_3a	palagonite	Vesturdalur Canyon – along Hofsá river	65.19508	-18.90476	7/1/2019
HF_3b	palagonite				
HN_1	palagonite				
VJ_13a	glass	Hofsafrétt	65.01095	-18.90661	7/4/2019
JF_10a	glass	Askja	65.04264	-16.60100	7/3/2019
HS_1	Hot spring water	Hofsvellir	65.28539	-19.04025	7/9/2017
HS_2	Hot spring water	Hverhólar	65.34724	-19.10260	7/10/2017
HS_3	Hot spring water	Réttarholt	65.57787	-19.35550	7/14/2017
HS_4	Hot spring water	Vindheimar	65.50097	-19.34664	7/14/2017
HS_6	Hot spring water	Reykir	65.47144	-19.35653	7/14/2017
HS_7	Hot spring water	Starrastaðir	65.43200	-19.32143	7/14/2017
HS_8	Hot spring water	Þormóðsholt	65.52718	-19.31469	7/14/2017

---

## Appendix C

### Colloid separation methods and experiments

#### C.1 Methods

River water samples (~2 L) were collected and filtered through Geotech 0.45  $\mu\text{m}$  filters with a Versapor membrane during the summer of 2017 and 2019. On the day of collection, aliquots of sample were sequentially passed through a Sartorius tangential flow filtration (TFF) system with a Sartocon polyethersulfone membrane cassette, similar to methods used for other isotope systems (Pogge von Strandmann et al., 2011). In short, water flows through the pressurized system tangentially along the membrane, where the “colloidal” size fraction is recirculated and the “ultrafiltered” size fraction passes through the membrane and exits the system. The “colloidal” size fraction is thus gradually concentrated as the volume of the ultrafiltered portion increases. Mass of the total water passed through the system and mass of the concentrated “colloidal” fraction were recorded in order to calculate a “concentration factor” for the colloidal fraction (Table C1). Samples were acidified with concentrated  $\text{HNO}_3$  and elemental concentrations for each fraction (dissolved, colloidal, ultrafiltered) were measured at Northwestern University using a Thermo Scientific iCAP 6500 ICP-OES, and the concentration factor was used to correct the measured colloidal Ca concentrations.

Two methods were employed for colloid separation and ultrafiltration. Method #1 (2017 field season) used a 5 kD cassette, and Method #2 (2019 field season) used a 10 kD cassette, as well as a multi-step cleaning procedure. For both methods, the cassette was flushed with Milli-Q water and “pre-contaminated” with ~10 mL of the <0.45  $\mu\text{m}$  sample, which was discarded. An additional ~20 mL of the <0.45  $\mu\text{m}$  sample was then passed through the system in order to triple

rinse I-CHEM HDPE collection bottles with the fraction being collected, i.e., either colloidal or ultrafiltered. Aliquots of known mass of the  $<0.45 \mu\text{m}$  sample were introduced into the filtration system and passed through the cassette at 2.5 bar pressure until sufficient volume of the colloid-rich fraction was collected. In general,  $\sim 2\text{-}4 \text{ L}$  of the  $<0.45 \mu\text{m}$  sample was needed to collect  $\sim 125 \text{ mL}$  of the colloidal fraction and  $\sim 500 \text{ mL}$  of the ultrafiltered fraction, with the remainder being discarded. Because of the large volume demand of initial sample, the colloidal fraction was collected for only a subset of samples. The cassette was then flushed with Milli-Q water at 5 bar for 10 minutes and stored in a refrigerator. Method #1 defines the size fractions as follows:  $<0.45 \mu\text{m}$  is dissolved,  $0.45 \mu\text{m} >$  colloidal  $> 5 \text{ kD}$ , and  $<5 \text{ kD}$  is ultrafiltered.

Method #2 employed the same steps as Method #1 but used a 10 kD cassette and included a multi-step cleaning procedure. After each sample and initial Milli-Q water flush as described above, the cassette was washed with  $\sim 15 \text{ mL}$  of 0.5 N NaOH. The NaOH was flushed through the cassette at 5 bar for 10 minutes and discarded as waste. The cassette was then flushed again with Milli-Q water. At the end of each day ( $\sim 3$  samples/day), the cassette was cleaned with 1 N HCl, then 10 mM NaEDTA, and finally, 1 N HCl. The cassette was then rinsed with Milli-Q water and stored in a refrigerator. Blanks, which were collected between samples to monitor the effectiveness of the cleaning procedure, showed an average Ca concentration of  $1.92 \mu\text{mol/L}$  ( $\pm 1.26 \mu\text{mol/L}$ ,  $1\sigma_{\text{SD}}$ ,  $n = 8$ ), which is significantly lower than sample Ca concentrations. Method #2 defines the size fractions as follows:  $<0.45 \mu\text{m}$  is dissolved,  $0.45 \mu\text{m} >$  colloidal  $> 10 \text{ kD}$ , and ultrafiltered is  $<10 \text{ kD}$ .

Ca isotope and Ca concentration data for dissolved, ultrafiltered and colloidal water samples are summarized in Table C1.

**Table C1**

Summary of relevant Ca concentration and isotope data for samples and standards processed by TFF methods.

Sample	Concentration Factor	Ca (μmol/L)	$\delta^{44/40}\text{Ca}$ (‰, ASW)	$\Delta^{44/40}\text{Ca}_{\text{col-dissolved}}$	$\Delta^{44/40}\text{Ca}_{\text{col-UF}}$	$\Delta^{44/40}\text{Ca}_{\text{UF-dissolved}}$
<b>Method #1</b>						
BG_3		31.5	-0.99	-0.36		
		22.1				
		10.2	-1.35			
BG_4	10.6	10.2	-1.35	-0.4	-0.67	0.27
		25.1	-0.74			
		9.8	-1.41			
BG_5	12.2	9.8	-1.41	-0.37	-0.63	0.26
		43.2	-1.00			
		32.2	-0.74			
		10.7	-1.37			
BG_6	12.4	10.7	-1.37	-0.38	-0.63	0.25
		46.2	-1.00			
		32.3	-0.75			
		11.8	-1.38			
BG_7	11.7	11.8	-1.38	-0.41	-0.64	0.23
		50	-0.98			
		37.4	-0.75			
		11.6	-1.39			
AJ_a	12.8	11.6	-1.39			0.28
		78.8	-0.77			
		57.4	-0.49			
AJ_c		73.6	-0.73			0.21
		56.5	-0.52			
AJ_d		71.1	-0.73			0.17
		56.2	-0.56			
AJ_e		81.1	-0.62			0.20
		58.5	-0.42			
VJ_a		87.8	-0.68			0.10
		75.5	-0.58			
VJ_d		95.4	-0.75			0.15
		83.3	-0.60			
VJ_e		104.3	-0.78			0.20
		88.5	-0.58			
HF_b		119	-0.68			0.13
		90.7	-0.55			
HF_e		114	-0.62			0.08
		98	-0.54			

<b>Method #2</b>							
AJ_j	<i>dissolved</i>		78.6			-0.83	
	<i>ultrafiltered</i>		69.8	-0.40			
	<i>colloid</i>	7.9	15.3	-1.23			
EY_1	<i>dissolved</i>		61.4	-0.79	-0.77	-0.98	0.21
	<i>ultrafiltered</i>		52.2	-0.58			
	<i>colloid</i>	12.5	9.6	-1.56			
SK_3	<i>dissolved</i>		128.1	-0.81			0.06
	<i>ultrafiltered</i>		118.7	-0.75			
	<i>colloid</i>	13.6	14.9				
SV_8	<i>dissolved</i>		120	-0.51	-0.36	-0.36	0
	<i>ultrafiltered</i>		114.9	-0.51			
	<i>colloid</i>	15.3	10.4	-0.87			
HR_11	<i>dissolved</i>		65.1	-0.78	-0.58	-0.73	0.15
	<i>ultrafiltered</i>		55.5	-0.63			
	<i>colloid</i>	9.22	11	-1.36			
	<i>colloid</i>						
	<i>free- 0.02</i>						
	<i>filtered</i>		61.8	-0.74			
<b>Standards</b>							
<b>Method #1</b>							
ASW	<i>dissolved</i>		83.7	0.01	-0.18	-0.28	0.10
	<i>ultrafiltered</i>		71.6	0.11			
	<i>colloid</i>		12.1	-0.17			
Ultrafiltered	<i>"dissolved"</i>		74.1	0.08	-0.12	-0.28	0.16
ASW	<i>double</i>		57.5	0.24			
	<i>ultrafiltered</i>						
	<i>colloid</i>		16.6	-0.04			
<b>Method #2</b>							
Ca-only	<i>dissolved</i>		63.7	-0.80	0.00	-0.02	0.02
standard	<i>ultrafiltered</i>		62.7	-0.78			
	<i>colloid</i>		0.97	-0.80			

The uniform magnitude of isotopic offset between the colloidal and dissolved fraction ( $\Delta^{44/40}\text{Ca}_{\text{col-dissolved}}$ ) as well as the colloidal and ultrafiltered fraction ( $\Delta^{44/40}\text{Ca}_{\text{col-UF}}$ ) warranted further inquiry of the validity of Method #1. Experiments using the OSIL Atlantic Seawater (ASW) standard were performed to test if Method #1 introduced any analytical artifacts to the

data. The results are summarized in Figure C1. Similar trends were observed for ASW, where the colloidal fraction showed lower  $\delta^{44/40}\text{Ca}$  than the dissolved, and the residual ultrafiltered fraction showed higher  $\delta^{44/40}\text{Ca}$ . This result indicated that, either ASW has colloids, or Method #1 introduces an artifact. To further test this, the ASW standard was passed through a brand new 5 kD cassette and the ultrafiltered portion was collected. The ultrafiltered ASW (theoretically, colloid-free) was then reintroduced to the system as the initial sample, resulting in three ultrafiltered fractions: the initially ultrafiltered fraction (analogous to “dissolved”), an ultrafiltered “colloid” fraction, and a doubly ultrafiltered fraction. Isotopic offsets for this experiment with “colloid-free” ASW were similar to those observed for regular ASW, providing good evidence that the 5 kD membrane fractionates Ca isotopes (Table C1).

Prior to the 2019 field season, Method #2 was designed and tested using a Ca-only standard. This standard was prepared gravimetrically by diluting SRM 3109a Ca standard solution with Milli-Q. This standard was used to test the hypothesis that concentrated solutions, like ASW, may contribute to filter clogging and thus analytical artifacts. Results of this experiment show negligible isotopic offsets between the three fractions, either due to the dilute nature of the solution or the 10 kD membrane. Because of limited time to further experiment with more concentrated solutions, Method #2 was employed during the 2019 field season in the hope that the larger membrane size and cleaning procedures would minimize analytical artifacts affecting Ca isotope ratios of the solutions.

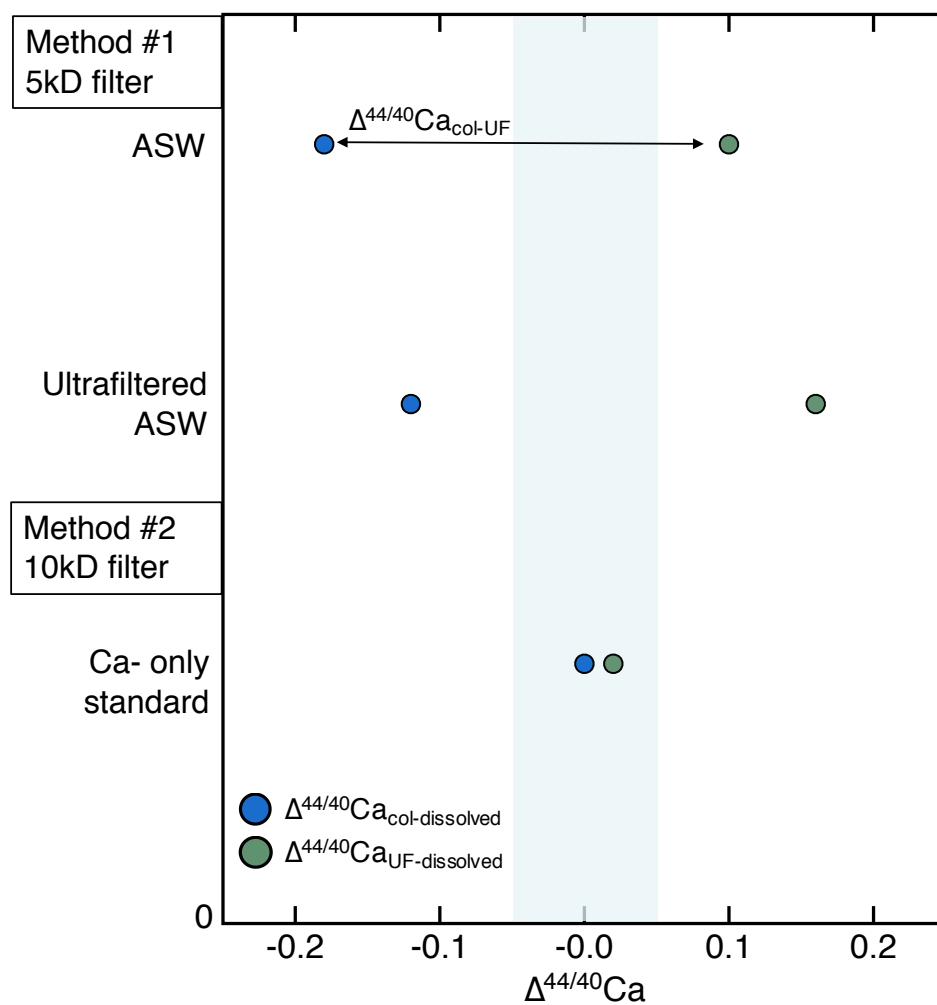


**Figure C1:** Results of the experiments performed with each method using standards. Blue shading represents analytical uncertainty of  $\pm 0.05$  ‰.

## C.2 Results and discussion

For one sample from the 2019 field campaign (HR\_11), the solution was passed through a Whatman Anotop 0.02  $\mu\text{m}$  syringe filter, creating a “colloid-free” sample in addition to the colloid-free ultrafiltered fraction from the TFF method. Although the size fractions are not identical, this gives a first-order constraint on the accuracy of the TFF method. As shown in Table C1, the methods of generating “colloid-free” water for sample HR\_11 did not produce

solutions with the same  $\delta^{44/40}\text{Ca}$  value. The  $\delta^{44/40}\text{Ca}$  value of the 0.02  $\mu\text{m}$  filtered sample matched, within analytical uncertainty, the  $\delta^{44/40}\text{Ca}$  value observed for the dissolved fraction. Although this is only one sample, this result suggests that the TFF method may produce analytical artifacts.

Because of the results from the Method #2 experiments, I cannot rule out that the isotopic offsets observed between fractions is due to a fractionation by colloids, where colloidal material is taking up light Ca, resulting in a heavier residual ultrafiltered fraction. Thus, it is worth discussing our preliminary observations for the behavior of Ca isotopes during interactions with “colloids”. The amount of Ca by mass balance in the “colloidal” fraction was greater for more dilute samples, inconsistent with our experiments, which suggested that more concentrated solutions led to filter clogging and analytical artifacts. From Method #1 (5 kD), an average of 22.9% ( $\pm 6.5\%$ ,  $1\sigma_{\text{SD}}$ ,  $n = 14$ ) of Ca was in the “colloidal” fraction, compared to an average of 10.5% ( $\pm 4.7\%$ ,  $1\sigma_{\text{SD}}$ ,  $n = 5$ ) of Ca for Method #2 (10 kD). The proportion of Ca in the colloidal fraction from Method #2 is somewhat higher than the a previously reported estimate for Ca (<7%) using the same size filter (Pogge von Strandmann et al., 2008). This study indicated that Icelandic colloids generally precipitate directly from solution, or originate as small particles that precipitate from soil solutions and are later transported to rivers. The discrepancy between the mass balance estimates of colloidal Ca could be due to the different size fraction used to define the “dissolved load”. Method #2 defines  $0.45 \mu\text{m} > x < 10 \text{ kD}$  as “colloidal” material, whereas Pogge von Strandmann et al. (2008) defines colloidal material as  $0.2 \mu\text{m} > x < 10 \text{ kD}$ . The greater particulate size incorporated into our “colloidal” fraction likely led to higher percentages of Ca in

the colloidal fraction. The larger initial filter size could also contribute to analytical artifacts possibly observed in our dataset compared to those of Pogge von Strandmann et al. (2008, 2011).

Despite not being able to constrain or rule out analytical artifacts, I can assume the “colloidal” fraction data here represents fractionation by colloids to generate a first-order estimate for the effect of colloids on river chemistry. One interesting observation is the isotopic offset between the ultrafiltered and dissolved fraction ( $\Delta^{44/40}\text{Ca}_{\text{UF-Dissolved}}$ ) varies inversely with Ca concentration (Figure C2) and the dissolved fraction  $\delta^{44/40}\text{Ca}$ , where rivers with more Ca are heavier and show larger  $\Delta^{44/40}\text{Ca}_{\text{UF-Dissolved}}$ .

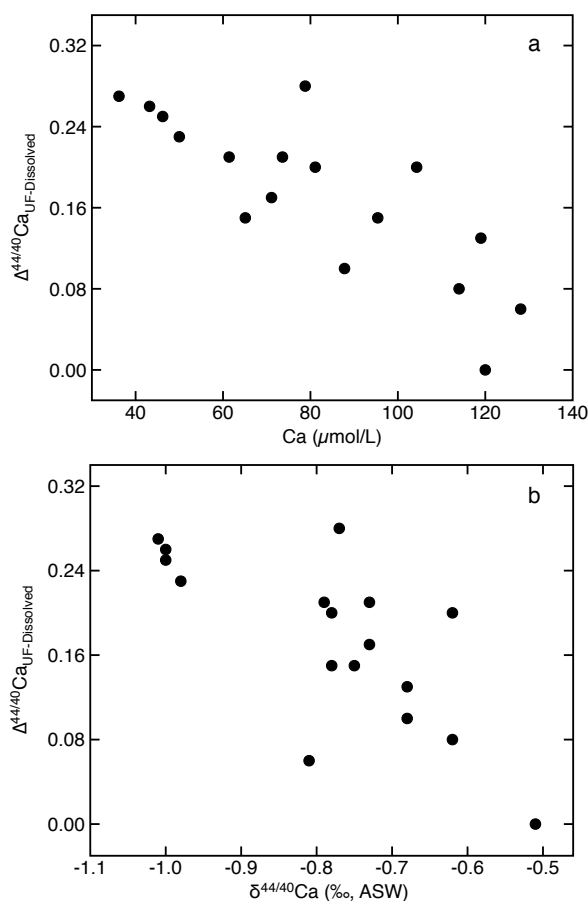


**Figure C2:** Isotopic offsets between ultrafiltered and dissolved fraction of samples processed by TFF methods versus Ca concentration (a) and dissolved fraction  $\delta^{44/40}\text{Ca}$  value (b).

To give context, in a sample with no fractionation by colloids,  $\Delta^{44/40}\text{Ca}_{\text{UF-dissolved}} = 0$ . Thus, for natural samples, the “fractionation by colloids” is *more pronounced* in overall more dilute samples, which is the opposite of what I observed for the ASW and Ca-standards experiments. As shown in Figure C2,  $\Delta^{44/40}\text{Ca}_{\text{UF-dissolved}}$  converges on the analytical uncertainty of the TIMS method ( $\sim 0.08\%$ ) at Ca concentrations of greater than  $\sim 115 \mu\text{mol/L}$  Ca. The elemental compositions of the dissolved, ultrafiltered, and colloid rich samples is summarized in Table C2. Colloids show nearly identical molar ratios to dissolved samples, but appear to discriminate against Na and Si relative to Ca (Figure C3). Furthermore, the dissolved fraction for rivers with greater  $\Delta^{44/40}\text{Ca}_{\text{UF-dissolved}}$  (which can be assumed to represent more fractionation by colloids) is elevated relative to basalt, and this fraction inherently incorporates colloids. Thus, even if light Ca isotopes were removed from solution with large fractionation factors, the observation that the “bulk” dissolved samples have high  $\delta^{44/40}\text{Ca}$  values immediately indicate that colloid formation cannot be fractionating Ca isotopes to any significant degree. Moreover, colloids show identical Sr/Ca to the dissolved and ultrafiltered fractions (Figure C4), whereas riverine  $\delta^{44/40}\text{Ca}$  and Sr/Ca correlate, suggesting a similar mechanism controlling both variables. Additionally, heavy rivers show small  $\Delta^{44/40}\text{Ca}_{\text{UF-dissolved}}$ , indicating that colloids are a negligible reservoir of light riverine Ca. And finally, rivers where apparent offsets are large (BG\_3 to BG\_7) show dissolved fraction  $\delta^{44/40}\text{Ca}$  values similar to basalt ( $\sim -1.05\%$ ), further indicating that fractionation by colloids does not affect river Ca isotope geochemistry (Table C1). More work is needed to better constrain methods for analyzing colloidal Ca, however our results likely indicate that colloids are not a factor in Ca cycling in Icelandic rivers.

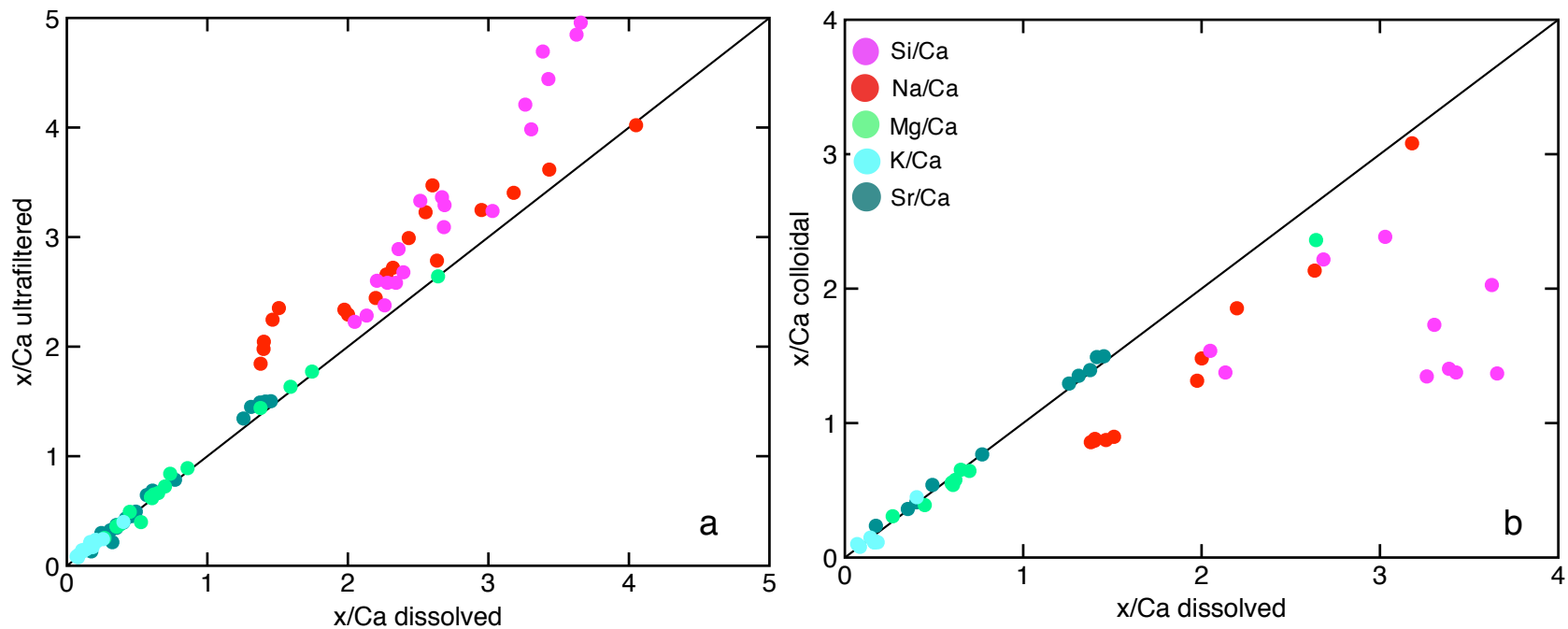


**Figure C3:** Ca-normalized elemental ratios of ultrafiltered (a) and colloid (b) fractions versus the dissolved fraction. Trends indicate that the colloids discriminate against Na and Si relative to Ca, while the other molar ratios are identical between all three fractions.

**Table C2.** Major cation and Si concentrations for samples processed through the ultrafiltration and colloidal separation method. “nd” indicates no data measured.

Sample ID	Dissolved					Ultrafiltered					Colloidal				
	K (µmol/L)	Mg (µmol/L)	Na (µmol/L)	Si (µmol/L)	Sr (nmol/L)	K (µmol/L)	Mg (µmol/L)	Na (µmol/L)	Si (µmol/L)	Sr (nmol/L)	K (µmol/L)	Mg (µmol/L)	Na (µmol/L)	Si (µmol/L)	Sr (nmol/L)
BG_3	5.8	20.5	47.5	114.3	44.5	3.8	14.7	52.0	107.1	33.1	1.2	6.7	9.2	20.7	15.2
BG_4	6.0	22.4	53.0	132.4	52.6	5.4	16.3	56.4	124.4	37.7	1.1	5.7	8.6	13.4	14.7
BG_5	7.1	25.9	60.5	148.0	59.4	6.3	20.1	63.7	143.0	48.0	1.3	5.9	9.3	14.7	14.9
BG_6	7.6	27.8	64.8	156.5	60.5	6.2	20.3	66.1	151.6	46.8	1.3	6.6	10.4	16.6	16.0
BG_7	8.3	30.1	69.0	163.1	62.8	6.4	23.3	69.0	157.4	50.3	1.4	6.4	10.0	15.6	15.0
AJ_a	8.9	27.9	205.0	198.2	19.4	7.5	20.7	199.3	191.2	17.1	nd	nd	nd	nd	nd
AJ_c	8.0	26.1	187.9	196.5	22.8	7.5	20.1	182.3	190.1	18.3	nd	nd	nd	nd	nd
AJ_d	7.7	26.8	173.0	191.1	25.1	8.0	21.1	168.1	185.0	19.4	nd	nd	nd	nd	nd
AJ_e	11.0	42.8	328.5	183.4	26.2	8.7	23.3	235.2	139.1	12.6	nd	nd	nd	nd	nd
VJ_a	18.1	153.2	200.7	210.3	52.5	17.9	133.8	195.9	202.2	49.1	nd	nd	nd	nd	nd
VJ_d	20.2	151.9	217.0	223.5	58.2	18.5	136.1	221.5	215.1	57.1	nd	nd	nd	nd	nd
VJ_e	20.3	143.8	242.1	237.9	59.3	19.2	127.4	240.7	228.6	57.1	nd	nd	nd	nd	nd
HF_b	30.6	87.5	408.5	280.9	54.8	22.0	76.2	328.0	262.2	41.1	nd	nd	nd	nd	nd
HF_e	20.9	97.9	336.4	251.6	47.9	20.4	87.3	318.2	254.9	42.3	nd	nd	nd	nd	nd
AJ_j	5.4	21.1	172.8	161.0	13.7	5.9	17.7	170.6	155.4	9.1	1.5	4.7	28.4	23.5	3.6
EY_1	5.2	27.5	121.3	202.9	21.7	5.2	25.7	122.0	207.9	19.4	0.8	3.7	12.6	16.6	3.5
SK_3	10.2	77.7	337.4	273.3	51.4	9.1	73.2	330.5	271.1	46.8	1.3	8.0	31.8	20.5	6.1
SV_8	48.3	317.0	381.6	363.5	92.4	46.0	303.5	391.1	372.1	90.2	4.7	24.6	32.0	24.8	8.0
HR_11	9.3	45.5	130.3	174.7	32.0	8.7	40.2	127.2	171.5	27.4	1.6	7.1	16.3	24.4	5.9

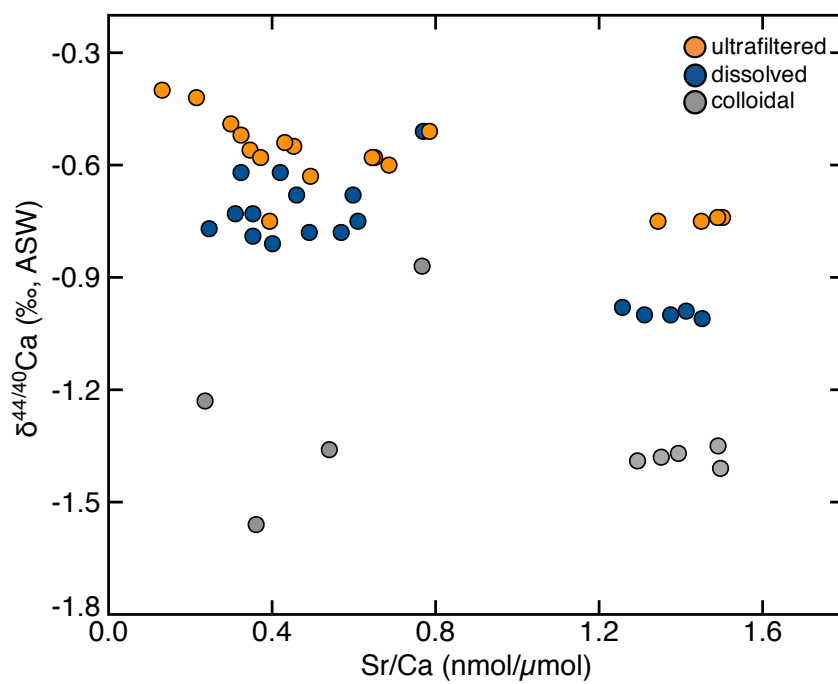


**Figure C4:**  $\delta^{44/40}\text{Ca}$  versus Sr/Ca ratio of riverine dissolved, ultrafiltered, and colloidal fractions isolated using both Method #1 and #2. Sr/Ca molar ratios are identical between the three fraction.

## Appendix D

## Field photos of palagonites and hyaloclastites



**Figure D1.** Typical highland hyaloclastite and glass. Left photo shows that hyaloclastites are highly heterogeneous breccias of primary minerals, glass, and alteration products. Photo on the right shows glass samples physically separated from the outcrop seen on the left.

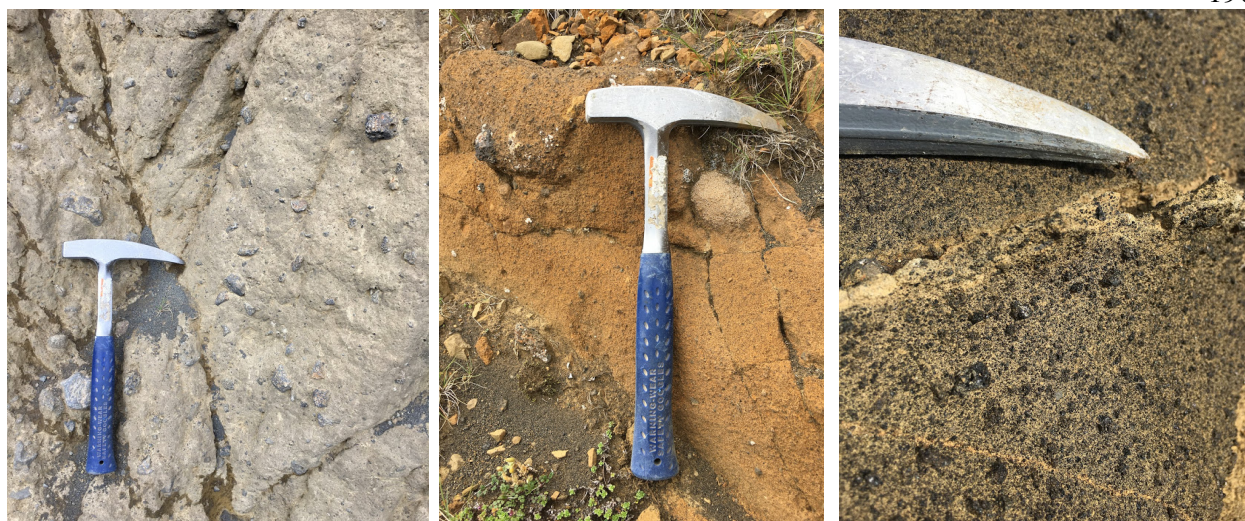


**Figure D2.** Photos of rock sampled from Helgafell, a palagonite ridge in Southern Iceland. Samples were collected in intervals of increasing elevation (left to right), where the leftmost sample is the least altered, similar to highland hyaloclastite (Figure D1), and the right most sample is the most palagonitized.

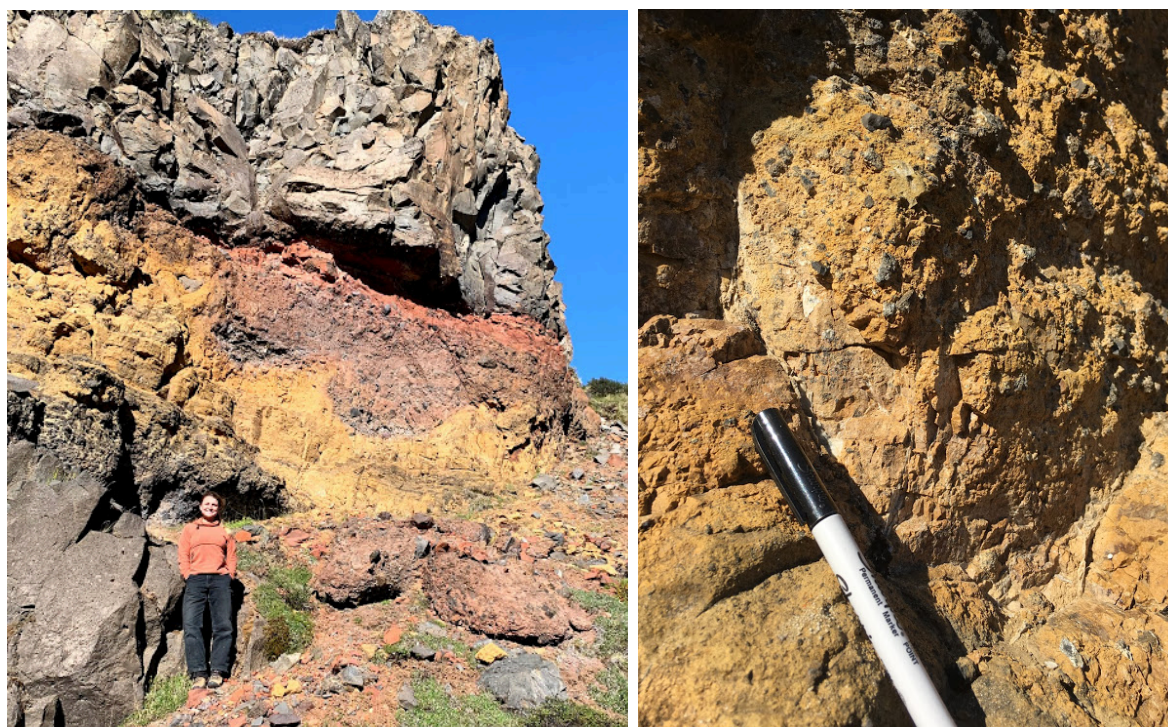


**Figure D3.** Palagonitized outcrop in the Vesturdalur canyon, north of the highlands. Photo on left shows outcrop is overlain by a post-depositional basaltic lava flow. Photo on right is of sample collected from lower layer of outcrop, with a soft, clay-like texture. Outcrop is interpreted to represent the highest temperature of alteration of all rocks in this study.